Study of biomass powders in the context of thermal recovery processes

Clément Vanneste-Ibarcq

THÈSE

En vue de l'obtention du

DOCTORAT DE L'UNIVERSITÉ DE TOULOUSE

Délivré par :

IMT - École Nationale Supérieure des Mines d'Albi-Carmaux

Présentée et soutenue par :
Clément VANNESTE-IBARCQ

le 15 novembre 2018

Titre :
Study of biomass powders in the context of thermal recovery processes

---

École doctorale et discipline ou spécialité :
ED MEGEP : Génie des procédés et de l'Environnement

Unité de recherche :
Centre RAPSODEE, UMR CNRS 5302, IMT Mines Albi

Directeur/trice(s) de Thèse :
Alain DE RYCK, Professeur, IMT Mines Albi

Jury :
Khashayar SALEH, Professeur, Université de Technologie Compiègne, Président
Nouria FATAH, Professeur, Ecole Nationale Supérieure de Chimie Lille, Rapporteur
Sylvia LARSSON, Professeur, Swedish Univ. of Agricultural Sciences, Examinateur
Capucine DUPONT, Associate Professor, IHE Delft, Examinateur
Thierry MELKIOR, Ingénieur de Recherche, CEA Grenoble, Examinateur

Etude de poudres de biomasse dans le cadre de la valorisation thermique de biomasse

Study of biomass powders in the context of thermal recovery processes

Remerciements

Je tiens à remercier de nombreuses personnes pour leur aide dans ce travail. En effet, la thèse a duré trois ans pendant lesquels j'ai évolué, fait des découvertes et appris de nombreuses choses, sur les plans tant personnel que scientifique. Voici une liste des personnes qui m'ont accompagné dans cette aventure, je l'espère la plus exhaustive possible !

Tout d'abord, un immense merci à Thierry, mon encadrant. Tu as su me guider dans les méandres du doctorat, depuis mon stage et jusqu'à la fin de la thèse. Merci d'avoir gardé courage jusqu'au bout !

Je tiens à remercier mon directeur de thèse Alain de Ryck pour ses nombreux conseils et son accompagnement tout au long de la thèse. La distance entre Grenoble et Albi n'a pas aidé à ce que nous nous voyions très souvent, mais je tiens à souligner votre disponibilité par mail ou téléphone.

Merci aux membres du jury, Mme Fatah, Mme Larsson, Capucine et M. Saleh. Vos remarques ont été très constructives et me permettront, en plus des corrections au manuscrit de thèse, d'améliorer ma démarche scientifique.

J'aimerais ensuite remercier tous les membres de l'équipe biomasse du CEA. En particulier Muriel, toujours à l'écoute ; mes voisins du M30, Thierry, Maguelone, Guillaume (encore merci pour ton aide pour l'évaluation économique), Françoise, Geert, André et Julien ; mais aussi Sylvie (merci pour la verveine), Pierre, Hélène, Seb, Philippe, Snoop, Mickael, Anne, Marine, Gilles, Isabelle, merci à tous pour cette agréable ambiance au laboratoire ! Je n'oublie pas ceux dont le passage a été plus rapide, Hary, Faizal (merci pour les manips !), Rafael…

Cette expérience a aussi été l'occasion de me faire de très bons amis, Maria, Morgane (A cane non magno sæpe tenetur aper), Tilia (tu voulais un slam ? En voilà un, madame !), Carolina et Oscar (Tengo muchas cosas que decir, pero no puedo escribir lo que quiero aqui… Gracias amigos !), Florent, Lucas, mais aussi les anciennes du labo, Elvira et Marion.

Merci à mes amis grenoblois, en particulier Xavier, camarade de sport inégalable, mais aussi Camille, ma complice de swing, et Natacha, pour les mémorables retours à la maison ! Merci pour tout Eric, continuons ensemble à cheminer sur la voie du zéro déchet.

Je voudrais adresser un souvenir ému à ces personnes qui sont parties trop tôt, Jacques, mon grand-père, Jean-Pascal, mon oncle et Pauline, mon amie. Merci pour tous ces moments partagés.

Enfin, je souhaite dire un grand merci à mes amis de Toulouse, sans qui la vie serait moins douce et à ma famille, bien sûr (je me sens obligé de mentionner Erton et Falko).

Remerciements

TABLE OF CONTENT

List of figures

List of tables

Nomenclature

Latin letters

a: Constant (-)
b: Constant (m)
C: Cohesion (Pa)
C_G: Constant parameter (-)
g: Acceleration of gravity (m/s²)
H: Powder moisture content (wet basis) (-)
I: Inertial bond number (-)
K: Ratio of normal stress over shear stress (-)
l: Cohesion length
m_D: Mass of dry powder (kg)
m_H: Mass of humid powder (kg)
m_w: Mass of water in the humid powder (kg)
n: Warren-Spring index (-)
P/P_0: Relative vapor water pressure (-)
R: Silo diameter (m)
T : Tensile strength (Pa)
V_D: Volume of the dry powder (m^3)
V_H: Volume of the humid powder (m^3)
W_M: Mass of water taken up per gram of solid equivalent to monomolecular coverage (-)
wt%: mass percentage

Greek letters

α: Constant (°/m)
β: constant (°)
ε: Void fraction (-)
μ: Static friction coefficient (-)
ρ: Powder density (kg/m^3)
ρ_{bulk}: Bulk density (kg/m^3)
ρ_D: Density of the dry powder (kg/m^3)
ρ_H: Density of the humid powder (kg/m^3)
ρ_p: Particle density (kg/m^3)
ρ_{packed}: Packed density (kg/m^3)
σ: Normal stress (Pa)
σ_f: Abscissa of the contact point between Mohr circle and yield locus (Pa)
σ_p: Preconsolidation normal stress (Pa)
σ_{sat}: Maximum stress underwent by the powder (Pa)
σ_1: Major preconsolidation stress (Pa)
τ: Shear stress (Pa)
τ_P : Pre-shear stress (Pa)

Acronyms

EFR: Entrained flow reactor

CI: Carr Index (%)
FF: Flow function (-)
HR: Hausner ratio (-)
UYS: Unconfined yield stress (Pa)

INTRODUCTION

Since the industrial revolution, levels of CO_2 in the atmosphere have increased, leading to climate change (Figure 1). A 0.74°C temperature rise in global mean temperature is observed since pre-industrial period. The consequences are already observable: acidification of the oceans, coral reef bleaching, and mass extinction of amphibians for instance [1]. The climate change prospects according to the Intergovernmental Panel on Climate Change (IPCC) are alarming. If 2°C temperature rise is exceeded, climate change could lead to:

- Loss of natural habitat for 8% of the vertebrate animals, 18% of the insects and 16% of the plants
- Total melting of the ice floe in summer once every decade
- 10 cm rising of the water levels...

This situation is caused by human activities, and the use of fossil resources in particular.

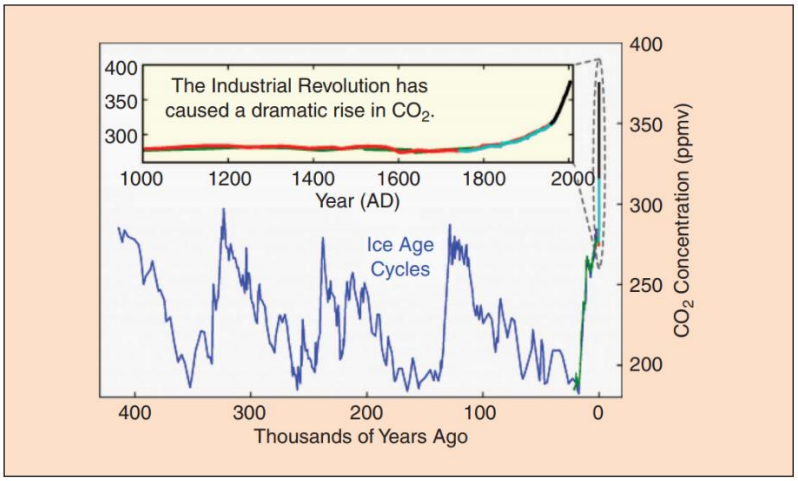

Figure 1: Evolution of the CO2 atmospheric concentration [2].

Solutions have to be found to decrease the use of fossil fuels, while meeting the increasing energy demand which is expected at least to double by 2050 [3]. Energetic sobriety is a first aspect that could be taken in account. It consists of decreasing the energy consumption by an appropriate use of power consuming facilities (for instance by reducing house heating and using smaller cars). Energetic sobriety has to go hand in hand with the improvement of energetic efficiency, to decrease energy losses. Renewable energies are another solution to meet the energy demand.

Biomass is a promising alternative to replace a part of the fossil fuels, as it is abundant, well distributed around the world, neutral with respect to greenhouse gas emissions (in the context of a sustainably managed biomass production) and renewed in the human time scale. Moreover, numerous applications of use are available. It can be directly burnt to produce heat or electricity. It can be transformed into biofuels with biochemical or biological treatments. Finally, from thermochemical processes, electricity, heat and biofuels can be produced.

The entrained flow reactor (EFR) is one of the most promising gasifier technologies. The typical process conditions are high temperature (1300-1500°C), high pressure (20-70 bars) and short residence time of the biomass in the reactor (a few seconds). Its main advantages are the high conversion rate of biomass into a syngas, with low tar and gaseous hydrocarbons content, and the high output (several tons of biomass treated per hour). However, the development of biomass gasification in EFR faces technological barriers. One of them is the use of biomass powders, which is a requirement due to the low residence time. Biomass powders have a poor flowability, and injecting them in the reactor is a challenge.

Powders are ubiquitous in the industry: food, pharmaceutical substances, cement, sand, coal, ore and many others. Around 60 % of the products in the industry are granular media or require a powder processing step during their production [4]. However, despite the prevalence of powders in the industry, their behavior is poorly understood and processing problems are faced by approximately 94% of solid process plants [5]. Biomass powders in particular are cohesive due to several features: low bulk density, polydispersed particle size and elongated particles for example. Thus, flowability problems are frequent as shown in Figure 2, and can lead to production shutdowns.

Figure 2: Ratholing during the discharge of a hopper with a wood powder.

The gasification in EFR process has numerous powder handling steps (storage, conveying, injection…), and biomass powders may block in each one of them. The objective of this thesis is to better understand the flow of biomass powders, and to propose solutions to improve the biomass powder handling in the context of gasification in EFR. Characterization of biomass powder flowability is a recent research subject, and their flow is poorly understood. Therefore, this work includes the study of biomass powder flowability both at lab scale and at pilot scale. Moreover, several preparation methods exist to prepare biomass for its injection in EFR (torrefaction, pyrolysis…). In this work, an innovative granulation process, adapted to EFR gasification is proposed.

The first chapter provides a literature review, divided into three parts. The first part is a description of biomass and its structure. The second part reviews powder behaviors and their characterization. Finally, the third part deals with industrial handling of powders.

The second chapter is dedicated to the description of the material and methods used in the study at lab scale. Characterization methods include powder rheometer and rotating drum tests, density, moisture, and size and shape measurements.

In the third chapter, the experimental results at lab scale are shown and discussed. The link between avalanche angle, shear test parameters and aerated density is put into evidence. Moreover, the effect of moisture content on biomass powders flowability is discussed. Finally the effect of the granulation method on the flowability is presented.

The fourth chapter describes the material and methods used in the study at pilot scale. The injection pilot IRIS is presented as well as the experimental set-up of the tests performed. Moreover, the preparation methods of the different powders are provided, and the granulation method in particular.

The last chapter presents the results obtained at pilot scale. It includes the studies of the screw feeder and hopper filling height, the accumulation of powder in the injector and an energetic evaluation of the granulation process compared with the torrefaction process.

CHAPTER I: LITERATURE REVIEW

1. Biomass and its structure

The powders studied in this work are made of biomass, and wood in particular. In this part, their principal features, their provenance and their structure are presented.

1.1. Biomass

Biomass comes from organic matter, such as trees, plants and agricultural and urban wastes. It is a limited resource, but continuously regenerated. Hence it is renewable. It has been traditionally used for heating, but it can also be used, among others, to produce electricity and fuels.

Lignocellulosic biomass is produced by plants during photosynthesis. It consists of photochemical transformation of water and carbon dioxide in carbohydrates for their subsistence. The absorbed energy during photosynthesis is stored in the formed organic compound and released when the plant is burned or transformed [6]. The carbon dioxide formed during the plant combustion is not accounted for in the carbon footprint, since it has been absorbed by the plant during its growth [7].

1.2. Chemical structure

Structurally, lignocellulosic biomass (such as wood) consists of a network of cellulose micro-fibrils, more or less crystalline. This network is immersed in a hemicellulose and lignin matrix, connecting the cellulose fibrils. The interactions between this three macromolecular components stiffen the structure [8].

Cellulose and hemicellulose are made up of polysaccharides and lignin is made up of phenylpropane units [9]. Thus, biomass composition is mainly carbon, oxygen and hydrogen. Inorganic compounds (ashes) can also be present. The average content in inorganic compounds for a forest biomass is 1.5% (on a dry basis). It can be up to 8% for agricultural biomasses. It ranges from 1.5 to 5% for herbaceous crops.

Thus, biomass structure is very complex, as shown in Figure 3. Composition and proportion of each constituent can strongly vary from a biomass to another.

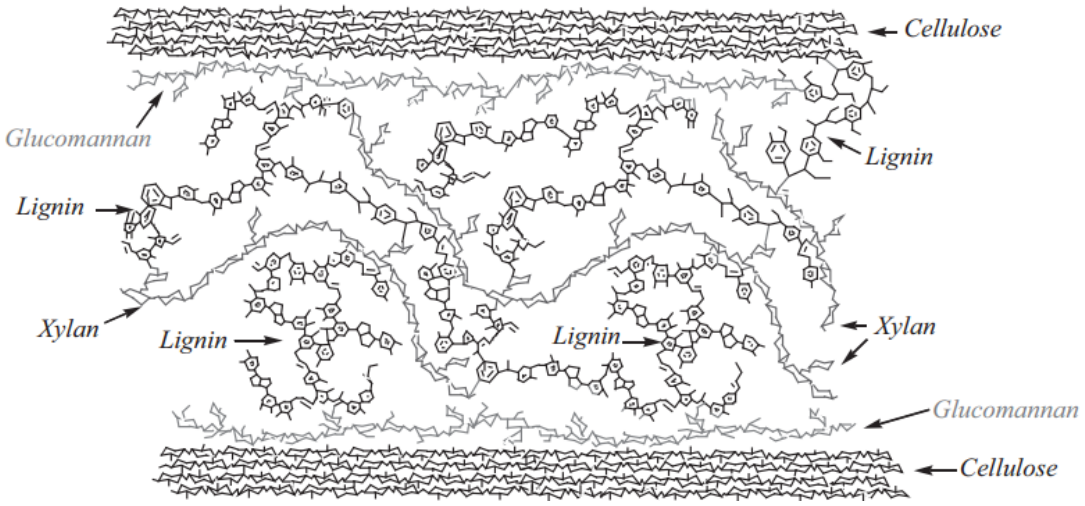

Figure 3: Schematic of the complex network composing biomass. Cellulose and hemicellulose are bounded by lignin [10]

These macromolecules form a protective layer for plant cell walls [11].

1.3. Macroscopic structure of the wood

Wood is composed of elongated cells, directed lengthwise. They give wood its mechanical resistance, transport liquids and store energy. A schematic of a trunk section is presented in Figure 4:

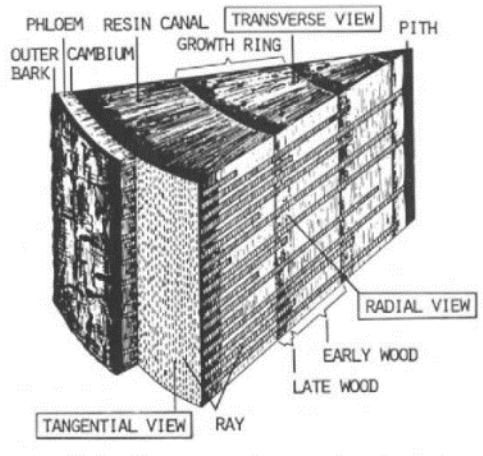

Figure 4: schematic of a trunk section, showing its internal organization [9]

The central part in black corresponds to the tissues formed during the first year. Then, the wood grows by concentric rings. Horizontal rays can be observed, the vessel elements (length 100-160 µm, width 2-50 µm in average. 25-31 units/mm3 for the Scots pine) and the tracheids (2-4 mm length, 20-40 mm width for softwood), which allow water circulation. In the case of softwood, resinous channels are present in the longitudinal direction. The inner part of the trunk in composed of dark wood, and the outer part is composed of the recently form wood, the sapwood. Sapwood is lighter in colour than the core and transports water from the roots to the leaves. The cambium is a thin layer of living cells located between the wood and the inner part of bark. Wood growth occurs in this layer [9].

2. Powder behavior study

In this part are presented the general powder behavior, properties and the measures that can be carried out on them.

2.1. Powders and granular media

A granular medium is a collection of solid particles with a size above 100 microns, while a powder is a collection of solid particles with a size between 1 and 100 microns. This threshold (100 microns) corresponds to the dominating type of interaction between particles. Particles with a size above 100 microns interact with contact forces, whereas particles with a particle size between 1 and 100 microns are submitted to Van der Waals forces, moisture effects and surrounding fluid effects [12].

2.1.1. General properties

Powders are a hybrid state of matter, intermediate between liquids, solids and gas. However, unlike them, their properties are mostly described empirically. To handle such materials can be problematic [12]:

- The large number of particles may impose to describe it as a continuous medium (for example, a tea spoon of powdered sugar contains approximately 10^5 particles).
- Thermal fluctuations are low. Thus, contrary to liquid and gas, it is impossible to derive macroscopic quantities from microscopic ones.
- The grains are observable, unlike liquids and gas. Consequently, the limit between microscopic and macroscopic scales is uncertain.
- Contact interactions between grains are complex.
- The medium is highly dissipative due to friction and collisions between grains.
- Granular media appear under different states depending on the conditions are subjected to. When forming a heap, they behave like a solid (dominated by contact interactions). Highly agitated, it behaves like a gas (dominated by collisions). Flowing in a funnel, the medium behaves like a liquid (dominated by friction and collisions).

2.1.2. Granular friction

Granular medium mechanics is highly influenced by friction. For instance, powders can form heaps, whereas liquids and gas cannot. This is due to friction forces acting at the contact points between grains.

Suppose a powder heap in equilibrium. In 1773, Coulomb showed that a layer of grains in line of slope (see Figure 5) stayed in equilibrium until the weigh component in line of the slope, T, is below a fraction of the its normal component to the surface, N.

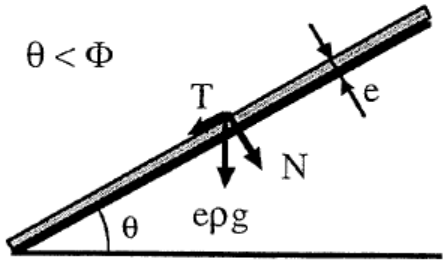

Figure 5: schematic of a layer of powder in equilibrium on the surface of a heap [13] with ρ the density and e the thickness of the layer

The powders stays in equilibrium as long as $T < kN$, k is the coefficient of static friction. The maximum value of θ is Φ. It is the angle of repose or friction angle. k is linked with the angle of repose such that $k = tan(\theta_{max}) = tan(\Phi)$. To this day, it is not possible to calculate k for mechanical properties of the grains [13].

2.1.3. Cohesion

The cohesion of a powder can be interpreted as its shear resistance stress under no load. It is representative of the inter-particle forces (or cohesive forces) acting in the powder. A cohesive powder has a poor flowability (Examples: icing sugar, flour, powdered chocolate). The resistance to flow is due to inter-particle forces [14]–[16] :

- Van der Waals forces: they are attractive forces. For fine enough particles (diameter below 100 microns), these forces become greater than the weight.
- Liquid bridges or capillary forces: these forces appear when the particles are wet. They are bounded by liquid bridges that modify their flow.
- Electrostatic forces: they intervene when dry particles with a diameter between 1 micron and a few millimeters are charged. These forces are attractive or repulsive. This phenomenon is particularly observed during pneumatic conveying. The collisions between particles and with the walls result in accumulation of charges by triboelectrification.
- Magnetic dipole-dipole interaction: does not concern biomass powders which are not magnetic.
- Interlocking: it intervenes for non-spherical particles.

2.1.4. Dilatancy and density

When a volume of powder is deformed, a change in granular stacking is initiated. The sample volume increases because particles have to overlap because they cannot penetrate each other, as shown in Figure 6:

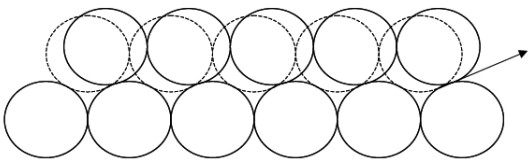

Figure 6: schematic showing the motion of particles during de deformation of a dense powder sample [14]

The sample volume increases until it reaches a critical density. If the initial density is below the critical density, the sample volume decreases during deformation. If the initial density is greater than the critical density, the sample dilates at shearing. It is the so-called dilatancy described by Reynolds [17].

2.1.5. Parameters with an influence on the powder flow

Several parameters have an influence on the powder flow. Among them, particle shape and size, moisture content, ageing and temperature can be mentioned. Other parameters such as the particle material can play a role in the flow, influencing the nature of inter-particle forces.

2.1.5.1. Shape

The particle shape is one the most important parameters driving the flow. Particle shape description can be qualitative or quantitative. Qualitative description is based on terms such as “spherical” or “elongated” for example. There is no standard for the particle shape description [18]. The description can be operated at different scales (Figure 7):

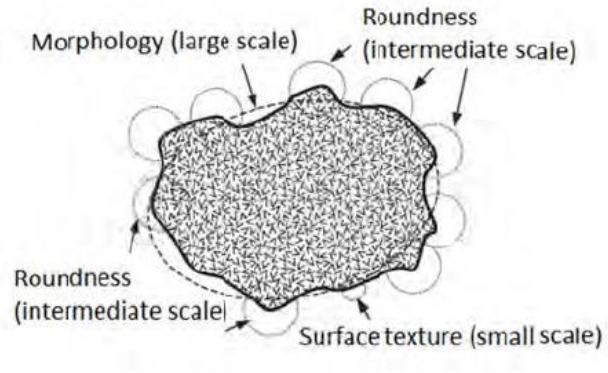

Figure 7: Examples of words describing particle shape at different scales[18]

Description of the shape can also be quantitative by using relations between particle quantities and comparing them with ideal shapes (sphere or disc for example). Quantities such as sphericity and elongation can be defined this way [18].

The present study focuses on the influence of particle size and shape on their dense-phase flow and on a silo discharge. This influence is observed on parameters derived from shear tests.

Influence of the particle shape on the flow: Particle shape has an influence on the unconfined yield stress (UYS) (see 202.4.4.1). UYS varies depending on the number of contact points and the direction of the contacts. It is possible to determine the UYS of a granular media composed of non-spherical particles from the UYS of a granular media composed of spherical particles by applying a correction value. The correction value takes in account the contact number and angle between particles. This study was conducted on beads with different shapes and coated with wax to make them cohesive [19]. Particle shape also has an influence on the medium elasticity. The elastic modulus and yield strength of a medium increase with the imposed confinement stress [20]. Rounded particles (by attrition) form regular arrangements, which decreases inter-particle distance and increases cohesion and UYS [21].

Influence of the particle shape on silo discharge: In the case of a flat bottom silo discharge, a decreased sphericity [22], [23], and an increased elongation [22] make the flow intermittent during the discharge. The study was made on polyhedrons obtained by 3D printing. Rounded edge particles flow better than angular edge particles in terms of output rate and residual solid fraction [23]. This conclusion may appear in contradiction with paper [21], about the increase of UYS for rounder particles. However, output rate and residual fraction do not only depend on the UYS.

2.1.5.2. Size and size distribution

A spherical particle size corresponds to its diameter. However, for non-spherical particles, this definition is not valid, it depends on the powder application. For instance, concerning cylinders, the size can be the diameter or the length. Several particle sizes can be defined, such as the surface equivalent diameter (diameter of a sphere with the same surface as the particle) or the volume equivalent diameter (diameter of a sphere with the same volume as the particle) for example.

A powder with narrow grain size distribution, even with a lower median particle size, has a lower UYS than a powder with a wide grain size distribution [21].

In the case of biomass, there is a link between size and shape of the particles, which depends on the way is the particles have been obtained. For high energy breakage (grinding), breakage is possible in cross-fiber direction. Thus, the lower the diameter, the lower the elongation (major axis over minor axis) [24]. However, for low energy breakage (during manipulation of the powder for example), breakage is easier in the fiber direction. Thus, the lower the diameter, the higher the elongation [25]. The elongation of large particles for different biomasses can be very different, but reaches a limit value obtained around 2.5 when the size decreases. This is due to the decrease of structural differences with the decrease of the size [24].

2.1.5.3. Moisture content

The moisture content of a particle is the mass of water that can be evaporated over the initial mass of the particle. This water can be free water (surround the particle) or bound water (be part of the particle structure). Bound water gives to particles a better deformability and free water has a lubricant effect [26].

Moisture content is the parameter with the strongest influence on the flowability of a powder. Low changes can lead to high modifications of the flowability. Water induces the formation of cohesive forces between particles and adhesive forces between particles and walls. Cohesion, adhesion and likeliness to form arches in a hopper increase with moisture content [21][27]. A higher torque is necessary to convey a wet powder with a screw at a given speed than for a dry powder [27]. Increasing the moisture content of wood powders and pellets increases their density and lowers their elastic modulus. The bulk friction angle and wall friction angle decrease with moisture content for both wood powders, but there is no effect on the cohesion (measured in a shear cell) [26]. Finer particles have a higher specific surface and more contact points per surface unit. Thus, in presence of water, the UYS increases because there are more liquid bridges [21].

2.1.5.4. Storage time

The influence of storage time can be evaluated with the temporal evolution of the yield locus, measured in a shear cell. Greater stresses are necessary to initiate the flow of a stored powder compared with a raw powder [14][28]. For the ageing conditions under stress, it is possible to maintain the powder under a normal stress only or under a normal stress and a shear stress. It has been observed that maintaining the powder under a normal stress only does not allow to describe correctly the storage in silo issues. However, when the powder is maintained under a normal and a shear stress, the time yield locus describes more accurately the issues encountered in silo storage [14].

2.1.5.5. Temperature

Experiments on inorganic powders (corundum and ashes, fine, $d_{50} < 100$ microns) have showed that for temperatures ranging between 20 and 500°C, temperature does not an influence on the results of shear

tests (between 4 and 14 kPa) [29]. For vitreous materials, heating above the temperature of glass transition makes the material to sinter and the building of solid bonds increases the yield strength.

2.2. Qualitative measurements

2.2.1. Size and shape analysis methods

2.2.1.1. Sieving

Sieving is a size analysis method. A sieve is most of the time made of braid wires. Opening in this case are squares. However, the sieve can also be a perforated plate, with circular holes. The space between wires, or the holes, let the particles fall if they are small enough. Opening size ranges from the centimeter to 20 microns (10 microns for wet processing). Sieves are usually stacked, with the largest opening at the top and the smallest at the bottom. The stack is vibrated with chosen frequency, amplitude and duration. The size distribution is then determined by weighing the mass of powder trapped between the sieves [28].

This method gives information on the median dimension of particles only [24], [25]. It is simple and inexpensive, but with inaccuracies:

- Small particles can block in the mesh, decreasing the aperture size [30].
- Particles can agglomerate and not be able to pass the mesh, whereas single particles may have been able to [24]. This problem can be avoided by using the wet process (when it is possible). Moreover, the wet process does not damage the most fragile particles [28].
- Sieve vibrations have a strong influence on the results [30].
- Particles that can pass through the sieve depend on their own shape and the sieve hole shape [30].

2.2.1.2. 2D image analysis

This method give information on the size and shape of the particles. For some technologies, the sample has to be prepared by hand and is therefore adapted to large particles only (straw, pellets…). It is then taken in photo and analyzed thanks to a software. Depending on the technology, this method can analyze a small amount of particles [25], [30], or on the contrary be rapid [31]. It is accurate, easily accessible, and numerous shape factors are available.

3D shape can be derived from the 2D shape using correction values. This correction values take into account that several projections exist for a single object and a projection can correspond to several objects (a 2D disc can be the projection of a cylinder, a disc, a sphere…).

The common image processing is binarization. The area of a particle is then equal to the area of the pixels. The perimeter is more difficult to measure (the angle with the X-axis impose to take in account either the width of a pixel or its diagonal, leading to errors). Moreover, the perimeter can appear as a straight line, but being actually a bent line at a higher resolution. Then, shape factors based on the perimeter must be used with caution [31].

2.2.1.3. 3D image analysis

This method is more costly and time consuming than 2D image analysis. Common technologies are [31]:

- X-ray computed tomography. Particles down to 10 µm can be digitalized. The particle density is mapped.
- 3D optical scanning: User-friendly, less expensive and faster than the X-ray computed tomography. However, resolution is lower, only the surface of the particle is mapped and convex objects are complex to analyze. Moreover, this method do not give information on the internal structure.
- Computer-aided design: This method is based on the use of a few projections of the object. Therefore it is fast and inexpensive compared with other techniques. It is inadequate for some applications, but it is more suitable than 2D analysis for shape factor measurements.

2.2.2. Angular measurements

The flowability of a powder is its ability to flow in a given situation. The flowability can be assessed with angular measurements, which are easy to set up.

2.2.2.1. Methods

Angular measurements consist of measuring angle of repose or dynamic angles. The flowability of different powders are then compared with one another. Some of these methods are compared in Figure 8:

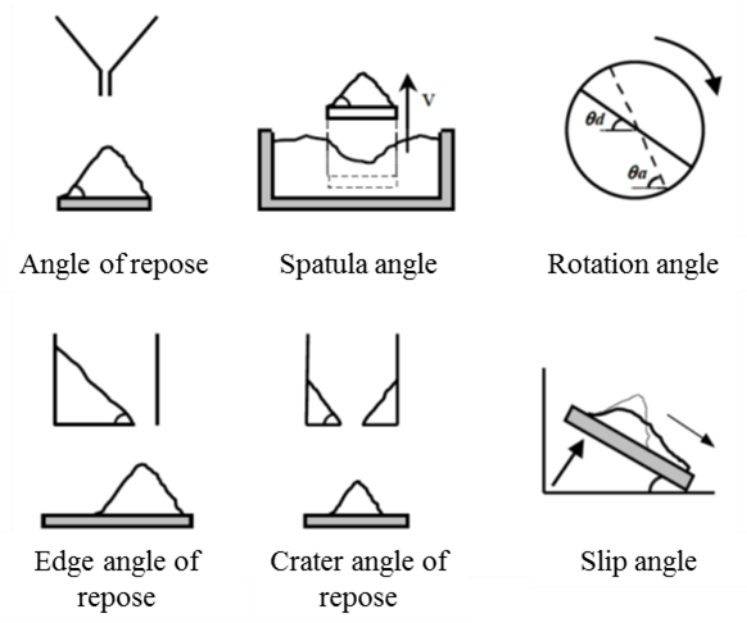

Figure 8: Examples of angular measurements[14].

These different methods are difficult to compare among them. Rotation angle measurement (or avalanche angle) is the only one which results do not depend on the operator. The sample is prepared by a few rotations, erasing the history of the sample preparation by the operator. It is carried out in a rotating drum. The rotating drum Revolution (Mercury Scientifics) is presented in the next part.

2.2.2.2. Revolution powder analyser

A powder flowability under no load can be determined through its avalanche angle. The avalanche angle is a dynamic measurement. It is measured in a rotating drum (Figure 9).

The powder analyzer Revolution (Figure 10) has been developed by Mercury Scientific Inc. It is a drum (10cm diameter, 3.3cm length, see Figure 9) containing 79 mL of powder, rotating in front of a camera.

Figure 9: Drum containing the powder, to be placed in the analyzer [32]

Figure 10: Revolution powder analyzer [32]

The operator chooses the rotation speed and the preparation time of the sample (length of time during which the drum rotates without the angle being measured. This way, the operator effect on the measure is limited). Algorithms determine the angle of avalanche from the images collected by the camera. The angle of avalanche is the angle of the free surface of the powder with the horizontal just before an avalanche (when the powder collapses because of the drum rotation).

2.2.2.3. Parameters influencing the angle of avalanche

The flow of a powder in a rotating drum is governed by [33]:

- Steric repulsion, linked to the particle geometry (shape and size distribution)
- Friction forces, linked to the surface properties and to the chemical nature of the particles
- Inter-particle forces (cohesive forces)
- Interactions with the surrounding fluid
- Interactions with the walls [15], [34]

For particles with a particle size below 50-100 µm, the flowability is mainly directed by the cohesive forces [15], [33].

The majority of studies about rotating drums focused on non-cohesive powders or powders with a low cohesion. The avalanche angle of cohesive powders has been little studied in the literature [15].

2.2.2.4. Relation between cohesion and angle of avalanche

During an avalanche, the force driving the movement of the powder is its weight. The free-surface of the powder and its behavior in the drum depend on a combination of phenomena described above (steric repulsion, friction forces, inter-particle forces and interactions with the surrounding fluid). In such a device, cohesive powders do not flow regularly: time between two avalanches varies. This behavior is different than for non-cohesive powders. Moreover, the flow of non-cohesive powders reaches a steady state when the drum rotation speed increases; they flow continuously, without avalanche. This regime do not exist for cohesive powders, regardless of the rotation speed [16]. Moreover, the free-surface of

cohesive powders is not a straight line [15], [16], [35]. Thus, the determination of the avalanche angle is more complex than with non-cohesive powders.

About the measured properties, there is a relation between the cohesion (measured with a Warren-Spring Bradford Cohesion tester) and the angle of repose (measured with a Mark4 AOR tester) : The higher the cohesion, the higher the angle of repose [36]. This result is valid for fine powders (grain size below 100 µm, the cohesive forces are stronger than the weight).

A way to evaluate the cohesion with a rotating drum is to study the fluctuations of the free-surface around its average position. The standard deviation of these fluctuations is be related to the particle shape (influencing interlocking) [16]. Moreover, the length of time between two avalanches is related to the cohesion: a short and regular time would correspond to a non-cohesive powder; a long and irregular time would correspond to a cohesive behavior [34].

Rotating drums with a low thickness (whose walls are close from each other) can be subject to wall effects, which can lead to distortions in the measurement of the avalanche angle [15], [34]. A way to compensate the wall effects is to use thicker drums (with more distant walls) [15]. Moreover, repeatability can be improved by filling the drum with a low amount of powder [35].

2.2.3. Density and compressibility

2.2.3.1. Density

Density is widely used for in the field of powder characterization: calculation of stresses in a silo, mass flow rate in volumetric feeders or to assess a powder flowability, and more generally when flow is driven by gravity. It is the ratio of the mass of a powder over its apparent volume. Its major issue is that it is not a constant for a given powder, but depends on the way it has been manipulated before the measurement. The definition of the bulk density is presented below:

$$\rho = \frac{mass\ of\ solid + mass\ of\ gas}{total\ volume\ occupied\ by\ the\ powder} \approx \frac{mass\ of\ solid}{total\ volume\ occupied\ by\ the\ powder}$$

It is possible to consider that the mass of gas is negligible compared with the solid. The void fraction ε is the volumetric fraction that is not occupied by solid. Knowing it allows to calculate the particle density, which is a constant:

$$\rho_P = \rho(1 - \varepsilon)$$

ρ_p: particle density
ρ: bulk density
ε: void fraction

The density variations of powders comes from the variability of void fraction, which depends on the particle packing. A powder made of spherical grains in regular packing has a higher density than a powder in random packing. Thus, several definitions of density are proposed such as the tapped density (the powder underwent a given number of standardized taps) or the bulk density [28].

2.2.3.2. Compressibility

Since the particles packing can be modified, the powders are compressible. The compressibility is a good indicator of a powder flowability. Several indicators assess the compressibility. The Hausner ratio is the ratio of packed density over bulk density [28], [37]:

$$H_R = \frac{\rho_{packed}}{\rho_{bulk}}$$

HR: Hausner ratio
ρ_{packed}: packed density
ρ_{bulk}: bulk density

The higher the Hausner ratio, the higher the difference between packed and bulk densities. HR > 1.4 means the powder is considered as a group C powder of Geldart's classification (cohesive powders with poor fluidization properties). HR < 1.25 means the powder is in group A of this classification (slightly cohesive, aeratable). Powders in the range 1.25 - l.4 may exhibit some properties of both groups [38].

The definition of the Carr index is:

$$CI = \left(1 - \frac{\rho_{bulk}}{\rho_{packed}}\right).100$$

CI: Carr Index (%)
ρ_{bulk}: bulk density
ρ_{packed}: packed density

This index ranks the powders from "excellent flowability" (5-15%) to "extremely poor flowability" (>40%) [28].

Carr index and Hausner ratio are easy to determine: they only require to measure densities. However, as presented in the previous section, densities can strongly vary depending on the way it has been measured. Moreover, these indices do not describe the flowability of powders in all conditions. It is necessary to interpret them cautiously.

2.3. Mechanics of granular media

Mechanics of granular media differ from liquids, gas and solids. Indeed, powders possess features from these three states of matter and can be subject to transitions form one to another. For example, they can flow like a liquid and switch to solid behavior.

2.3.1. Stresses

When a granular medium flows densely, the particle bed is considered as a continuous medium at macroscopic scale and continuum mechanics can be applied. Average properties are considered, without taking in account the size and shape of the particles [14].

The slip zone is called shear band. A force applied perpendicular to the shear band is a normal force. The corresponding stress, called normal stress, is the normal force divided by the shear band area. A stress applied in line of the shear band is a shear stress.

2.3.2. Stresses in a silo: Janssen's theory

To determine the stresses in a column of powder, Janssen's theory on mass saturation can be used. It starts from the observation that the poured mass of powder in a cylinder is different than the weighted mass: it reaches a limit value, as presented in Figure 11:

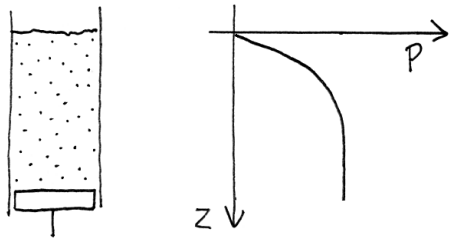

Figure 11: Shape of the stress profile in a column of powder, as a function of depth Z [39]

The presence of arches between the grains distribute the weight on the walls of the silo [28], [39], [40]. The following equation describes the maximum stress (saturation stress) underwent by a powder in a cylinder [28], [40]:

$$\sigma_{sat} = \frac{g.\rho.R}{2.K.\mu}$$

σ_{sat} : Maximum stress underwent by the powder (Pa)
g : Acceleration of gravity (m/s²)
R : Silo diameter (m)
K : Ratio of normal stress over shear stress (-)
μ : Static friction coefficient (-)

K cannot be measured directly. Its typical value ranges between 0.3 and 0.6. A rough estimation can be made using the value 0.4 [40].

The higher the silo diameter and the powder density, the higher the maximum normal stress.

2.3.3. Mohr-Coulomb's failure criterion

An important property of powders is their ability to form heaps when poured from a funnel. The angle formed by the heap is called angle of repose (see Chapter I, 2.1.2). It is presented in Figure 12:

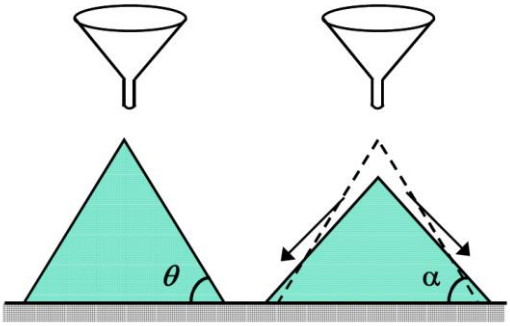

Figure 12: schematic of the heaps formed when powder is poured from a funnel. Left: maximum angle. Right: Angle for which the flow stops when the maximum angle is exceeded [14].

The angle increases until it reaches a critical angle. When this angle is exceeded, the powder flows and stabilizes at a new angle. Coulomb made an analogy between this phenomenon and solid friction. He proposed the "Mohr-Coulomb's failure criterion" [14]:

$$\tau = \mu\sigma$$

τ: Shear stress (Pa)
σ: Normal stress (Pa)
μ: Static friction coefficient (-)

This stands for a non-cohesive power. If there are attractive forces between particles, the yield occurs for:

$$\tau = \mu\sigma + C$$

C: Cohesion (Pa)

The cohesion C is the resistance to shear, without normal stress. It is representative of the attractive phenomena between particles. The $\mu\sigma$ part of the equation is representative of the friction forces between particles.

2.4. Shear test

In the case of silo discharge, several issues can appear (incomplete discharge or sudden discharge for example). In 1964, Jenike established a design method for silos allowing a correct flow from flowing properties [41]. This method is based on the shear test, which gives information on the dense flowing properties of granular media.

2.4.1. Shear test with Jenike's method

Shear test is used to characterize the flowability of a powder. It allows to build the yield locus of the powder, which is the shear stress necessary to initiate the flow of a sample at a given state of consolidation. An example for an alumina powder is shown in Figure 13:

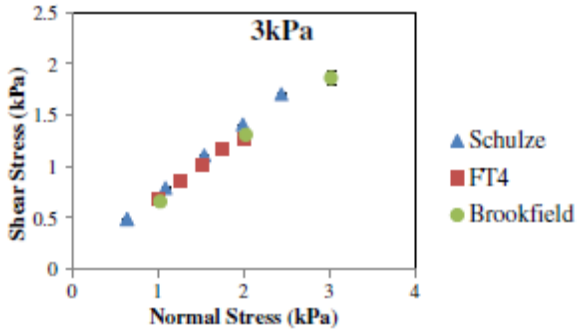

Figure 13: Yield locus of an alumina powder, measured with three shear cells [5]

The yield locus gives access to several parameters such as the static friction coefficient or the cohesion. It is carried out in a device called shear cell. Different types of shear cells exist, they are presented in the next part. The operating mode (Jenike's procedure) is presented below [14], [40], [41]:

- **Cell filling with the powder**. The shear state must be homogeneous.
- **Preconsolidation of the sample**. A preconsolidation normal stress, σ_p, on the surface of the powder. This stress, applied at the beginning of the test, compacts the powder. The powder reaches the consolidation it will keep during the test (and thus its density). During a time yield locus test (simulating storage), the normal stress can be maintained for a specific amount of time. Indeed, the amount of time a powder is kept under a stress can reinforce its mechanical properties (increase of the inter-particle interactions).

- **Pre-shear**. Critic consolidation must be reached during this step (the normal preconsolidation stress is maintained). The critic consolidation is a state of the powder in which results are repeatable (the powder yield depends on the consolidation). This state corresponds to a constant shear stress, τ_P, when the sample is shear at a constant speed under the preconsolidation normal stress. During this step, the sample can be in three consolidation states, as presented in Figure 14:

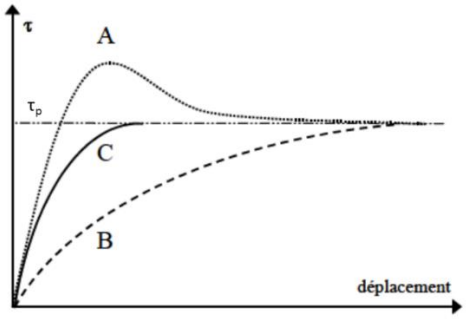

Figure 14: Curves of the shear depending on the consolidation stress. A: Over-consolidated, B: Sub-consolidated, C: Consolidated in critical state [14]

  - Sub-consolidated: After it reached the elastic limit, the sample volume decreases until it reaches the critic consolidation. The shear stress increases until it reaches a constant value.
  - Consolidated in critical state: Le volume of the sample is not modified and the shear stress reaches a constant value quickly.
  - Over-consolidated: an increase of the volume is observed. The shear stress increases until reaches a maximum, and then decreases because of the weakening caused by the dilatation. It then reaches a constant value.
- Shear. The sample is sheared under a normal stress σ_{S1} lower than σ_P until the maximum shear τ_{S1} is reached. This value corresponds to the initiation of the flow under the preconsolidation σ_P. (σ_{S1}; τ_{S1}) is the first point of the yield locus.

The other points of the yield locus are obtained the preconsolidation and pre-shear steps. The shear steps are carried out with $\sigma_{Si} < \sigma_{Si-1}$. Finally, ($\sigma_p$; τ_p) is added to the locus by calculating the average obtained at each step.

The different steps of the shear test are summarized in Figure 15:

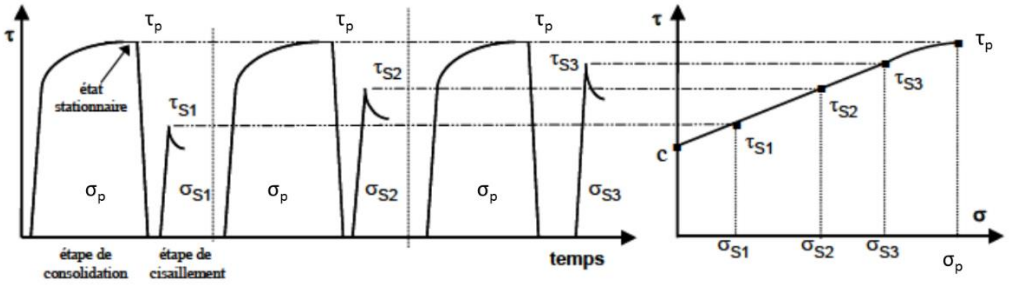

Figure 15: Steps of the shear test [14]

The mechanical characterization devices used to determine the yield locus are presented in the next part.

2.4.2. Standard description methodology

In the standard methodology, the loci are fitted by straight lines which follow the Mohr-Coulomb's failure criterion:

$$\tau = \mu\sigma + c$$

τ: Shear stress (Pa)
σ: Normal stress (Pa)
μ: Static friction coefficient (-)
C: Cohesion (Pa)

Two parameters can be derived from this straight line. They are used to describe the flowability of a powder at a given consolidation. They are:

- The Unconfined Yield Stress (UYS). It represents the normal stress needed to break a cohesive arch within the powder.
- The major consolidation stress. It is the maximum stress applied on the powder to reach its consolidation (there is a plane such as the normal stress vector and the shear stress vector during the preconsolidation a represented by a single vector, orthogonal to this plane. Its norm is σ_1.

These stresses a determined by drawing Mohr circles. Mohr circles are half circles whose diameter is placed on the X-axis. They are representative of the stress state of the powder (cohesive arch, consolidation for example). The stresses UYS and σ_1 are presented in Figure 16:

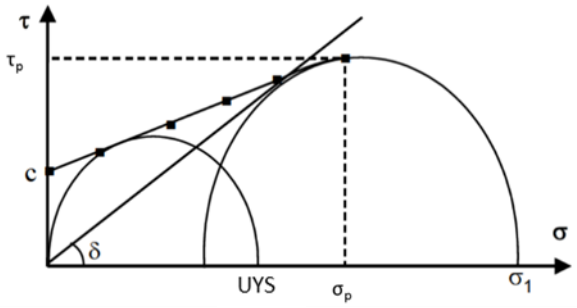

Figure 16: Schematic of a yield locus and associated Mohr circles [14](point names have been modified compared with the original)

Mohr circles must be tangential to the yield locus to be associated with a flow state. When an arch is formed, its free surface is without normal stresses, nor shear stresses, which corresponds to a Mohr circles passing through the origin of the graph. The Mohr circle which represents an arch at the onset of failure is the one passing by the origin and tangential to the locus. Thus, the UYS is the major principal stress (highest normal stress of the circle), as presented in Figure 16. The major preconsolidation stress σ_1 is derived by drawing the circle which passes by (σ_p ; τ_p) and tangential to the locus [14].

A yield locus corresponds to one consolidation. If the sample is consolidated with a bigger normal stress, the yield strength will be greater and the yield locus is in an upper position in the (σ; τ) plane. UYS as a function of σ_1 is called Flow Function (FF). An example is presented in Figure 17:

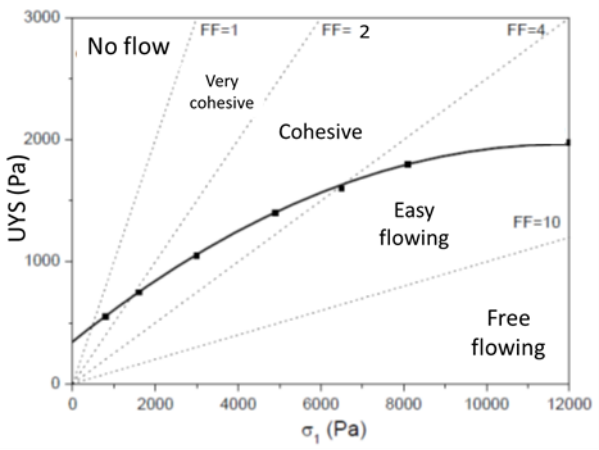

Figure 17: Example of a flow function [14] (translated and point names haves been modified compared with the original)

This diagram ranks powder flow. There are several areas corresponding to values of the flow function [14]. The closer from the X-axis, the better is the flowability. These areas have been defined for yield loci described with a straight line.

2.4.3. Non-linearity of the yield loci for small normal stresses

According to Jenike's method [41], the yield locus is a straight line which is extrapolated towards the Y-axis to get the cohesion. However, the yield locus of cohesive powders is non-linear, which is especially obvious for small stresses [42].

Since there is no theoretical equation for the yield locus, a linear regression (Mohr-Coulomb failure criterion) or a polynomial regression is used to describe it [14], [43]. Industrially, a linear regression is carried out because it is sufficient for silo sizing for example, or because the number of points is often low [43]. Other description methods exist for nonlinear yield loci, as presented below.

2.4.3.1. Best fit (second order polynomial)

There is no theoretical description of the locus. Thus it can be legitimate to use a best-fit description, which best describes the locus (such as a second order polynomial) [43]. The form of the equation is:

$$\boldsymbol{\tau = k\sigma^2 + m\sigma + C}$$

τ: Shear stress (Pa)
k: Constant (Pa^{-1})
m: Constant (-)
C: Cohesion (Pa)

2.4.3.2. Warren-Spring equation

This relation was proposed in 1965. It is the most cited in literature. Ashton obtained this relation by using considerations on the attractive and repulsive forces acting on contact points of particles [44] :

$$\left(\frac{\boldsymbol{\tau}}{\boldsymbol{C}}\right)^{\boldsymbol{n}} = \frac{\boldsymbol{\sigma + T}}{\boldsymbol{T}}$$

τ: Shear stress (Pa)
C: Cohesion (Pa)
n: Warren-Spring index (-)

σ: Normal stress (Pa)
T: Tensile strength (Pa)

n ranges between 1 and 2 and is a flowability index [45]. When n is equal to 1, the Warren-Spring equation becomes the same as the Mohr-Coulomb failure criterion (straight line). T is the point at the intersection of the Locus and the X-axis. Figure 18illustrates the use of this model on cohesive powders:

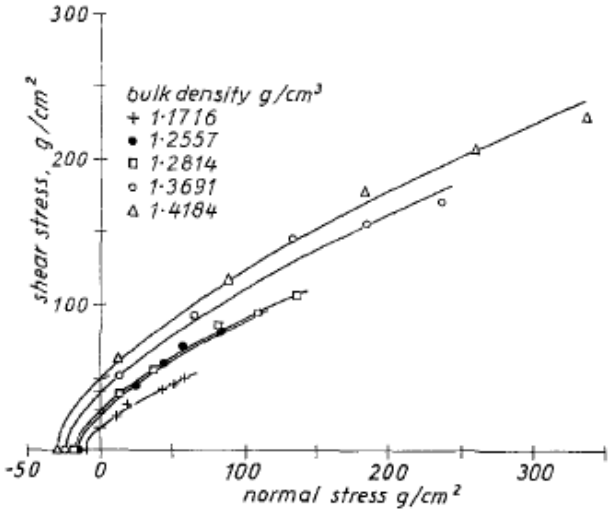

Figure 18: Yield locus of lithopone powder and corresponding Warren-Spring models[44]

This equation is based on a physical approach and correctly describes the experimental data. However, there are uncertainties on the determination of the parameters: several sets of parameters can fit the same experimental data [46], as Figure 19:

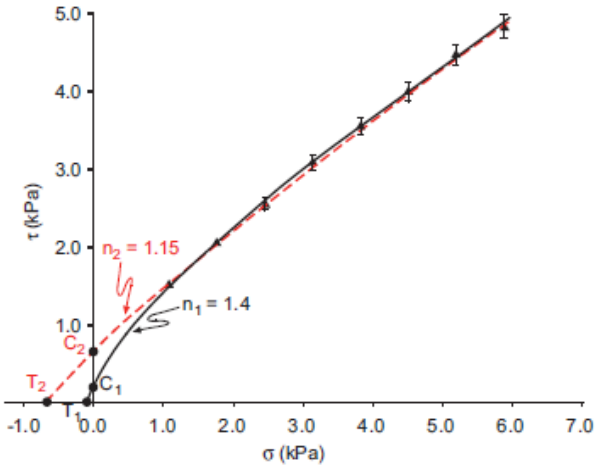

Figure 19: Fittings of the Warren-Spring equation for different values of C, T and n[46]

To use the Warren-Spring equation, it is necessary to know one of the three parameters and then to use a solver to obtain the two others. It is proposed in [44], [47] to measure the tensile strength with a dedicated apparatus and to make the supposition that this value is equal to the intersection between the locus and the X-axis. Indeed, if the logarithm of the equation is considered, the following equation is obtained:

$$\ln(\tau) = \frac{1}{n}\ln\left(\frac{\sigma + T}{T}\right) + ln(C)$$

Then, when $\ln(\tau)$ is plotted versus $\ln\left(\frac{\sigma+T}{T}\right)$, the parameters C and n are easily obtained.

2.4.3.3. Modified Warren-Spring equation

This equation aims at modifying the Warren-Spring equation to determine the parameters with only parameters derived from the shear test [47]. The authors noted that C and T are linked by a powder law as presented below:

$$C = \alpha T^{\beta}$$

C : Cohesion (Pa)
T : Tensile strength (Pa)
α: Constant (-)
β: Constant (-)

The authors supposed that β is a constant for a given material, regardless of its grain size and α depends on the grain size and the material. These two constants are determined by shear tests on the same material with different grain sizes. It is then possible to write the equation in logarithms without C:

$$\boldsymbol{\ln(\tau) = \frac{1}{n}\ln\left(\frac{\sigma + T}{T}\right) + \ln(\alpha) + \beta\ln(T)}$$

τ : Shear stress (Pa)
σ : Normal stress (Pa)
n : Warren-Spring index (-)
T : Tensile strength (Pa)
α: Constant (-)
β: Constant (-)

This method is valid for monodispersed grain size, which is not the case for biomass powders.

2.4.3.4. Model based on the adhesive contact of elastic spheres

Due to the uncertainties on the Warren-Spring parameters, a model based on the adhesive contact of elastic spheres has been proposed. This model has two parameters, C and μ [46]:

$$\boldsymbol{\tau = \frac{C}{2} + \sigma\mu + \left(\frac{C}{2}\right)^{0.5}\left(2\sigma\mu + \frac{C}{2}\right)^{0.5}}$$

τ : Shear stress (Pa)
σ : Normal stress (Pa)
C : Cohesion (Pa)
μ: Static friction coefficient (-)

This equation fits correctly the experimental data, as presented Figure 20:

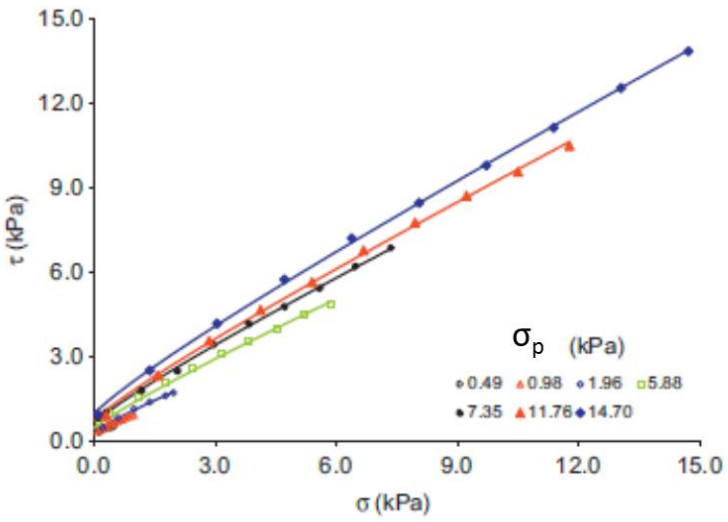

Figure 20: Fitting of the adhesive sphere model for a quartz powder, d50=32.4 µm, for different consolidations [46]

A relation is proposed between T and C:

$$T = \frac{C}{4\mu}$$

From this relation, T can be obtained once C and µ have been adjusted to fit the experimental data.

2.4.4. Mohr circles for Warren-Spring yield loci

The major preconsolidation stress and the unconfined yield stress can be derived from the Mohr circles analysis. Their ratio is the flow function. Using the Warren-Spring equation gives access to a system of equations from which the stresses can be derived.

The idea is that since the circles are tangent to the locus, their equations are equal at the contact point, and also their derivatives [48].

2.4.4.1. Unconfined yield stress

$$C\left(1+\frac{\sigma_f}{T}\right)^{\frac{1}{n}} = \sqrt{(UYS-\sigma_f)\sigma_f}$$

$$\frac{C\left(1+\frac{\sigma_f}{T}\right)^{\frac{1}{n}-1}}{nT} = \frac{UYS-2\sigma_f}{2*\sqrt{(UYS-\sigma_f)\sigma_f}}$$

C: Cohesion (Pa)
T: Tensile strength (Pa)
n: Warren-Spring index (-)
UYS: Unconfined yield stress (Pa)
σ_f: Abscissa of the contact point (Pa)

C, T and n are the Warren-Spring parameters (known). σ_f is the abscissa of the contact point between Mohr circle and locus. UYS and σ_f are unknown.

2.4.4.2. Major preconsolidation stress

$$C\left(1+\frac{\sigma_p}{T}\right)^{\frac{1}{n}} = \sqrt{(\sigma_1 - M)^2 - \left(\sigma_p - M\right)^2}$$

$$\frac{C\left(1+\frac{\sigma_p}{T}\right)^{\frac{1}{n}-1}}{nT} = \frac{M - \sigma_0}{\sqrt{(\sigma_1 - M)^2 - \left(\sigma_p - M\right)^2}}$$

C: Cohesion (Pa)
T: Tensile strength (Pa)
n: Warren-Spring index (-)
σ_p: Normal preconsolidation stress (Pa)
M: Abscissa of the center of the largest Mohr circle (Pa)
σ_1: Major preconsolidation stress (Pa)

C, T and n are the Warren-Spring parameters (known). σ_p is the normal preconsolidation stress (known). M (abscissa of the center of the largest Mohr circle) and σ_1 (major preconsolidation stress) are unknown.

2.5. Apparatuses for mechanical characterization

As presented in the previous part, during a shear test, the powders undergoes a normal stress and a shear stress. The shear stress causes the upper part and the lower part of the sample to move horizontally relatively to each other. If the movement is a translation, the shear apparatus is called translational. If it is a rotation, the apparatus is called rotational. Jenike's cell is the most common translational cell. Rotational cells exist in two technologies: torsional cells and annular cells [40]. There are other technologies called indirect shear cells, but they won't be described in this chapter.

2.5.1. Jenike's shear cell

It is the cell that Jenike built to carry out shear tests. It is often used to make comparisons with other cells. It consists of a fix base on which a ring is put. The device is filled with powder and closed with a lid (see Figure 21). Normal forces are applied on the lid and shear forces are applied on the ring.

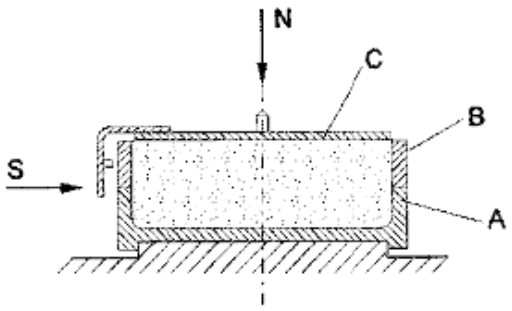

Figure 21: Schematic of Jenike's shear cell. A: Fix base, B: Ring, C: Lid, N: Normal force, S: Shear force [14]

The cell has to be refilled after each shear under a given load due to the short course of displacement, limited to two times the wall thickness (use of different samples for the same test). Another drawback of this cell is that the movement of the ring is limited. Thus, sometimes it is not possible to reach the critic consolidation during the consolidation step [14].

2.5.2. Rotational cells

In this type of cells, a normal stress is applied by a toothed lid on the sample placed in a base. The rotation of the toothed lid generates a shear stress. The resulting torque is measured. There are two types of rotational shear cells (Figure 22):

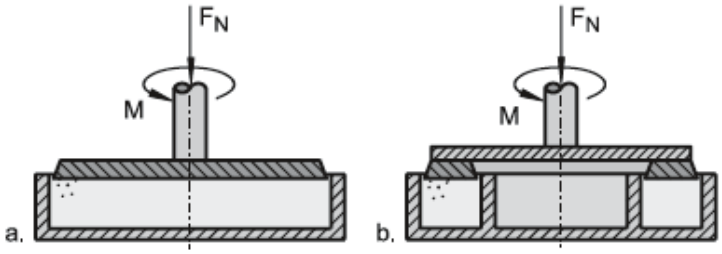

Figure 22: Schematic of rotational shear cells. a: torsional cell, b: annular cell, F_N: Normal force, M: Moment [40]

In the case of a torsional cell, the deformation due to shear varies with the radius. It is also the case with the annular cell, but it can be neglected if the inner diameter is superior to half the outer diameter. An advantage of these cells compared with translational shear cells is that the deformation of the sample is unlimited. Thus, the critic consolidation is always reached. Moreover, the whole experiment can be carried out on the same sample [40].

The most used cells in the literature are Jenike's cell and annular cells (such as Schulze's version) [14].

2.5.3. FT4 powder rheometer (material and methods)

The FT4 powder rheometer was designed by Freeman Tech, UK (see Figure 23). This device can carry out numerous tests, such as the shear test.

Figure 23: From left to right: FT4; shear cell in high position; Shear cell in rotation

The FT4 is a torsional shear cell. It follows the Jenike's shear test method. The instruments needed for the different steps of the test are attached on the machine and the automatically put into motion. The procedure is automated and it is monitored live thanks to a software. The instruments are presented in Figure 24:

Figure 24: Instruments used for shear tests with the FT4. From left to right: propeller, piston, shear cell.

- The propeller: it passes through the cylinder to homogenize the repartition of powder during the filling step.
- The piston: to apply a normal stress on the powder during the consolidation step.
- The shear cell: the device measures the torque necessary to shear the sample by rotating at a constant speed on the sample surface while applying a normal stress.

At the end of the test, an Excel file is created with the shear stress as a function of the normal stress.

2.6. Modeling

In this experimental work, numerical simulation is not planned. However, reviewing the hypothesis established in numerical simulation can provide ideas on the parameters governing the powder flow, and biomass powder flow in particular.

2.6.1. State of the art of powder flow modeling

To this day, there is no robust constitutive equation (relation between two physical parameters, specific to a material, approximating its response to a stimulus, for example the application of a force. Example of a constitutive law: Hooke's law for spring deformation. Some law are empirical, some others are derived from physical principles) about the dense flow that reaches a consensus. Some empirical laws are proposed as functions of the inertial bond number [12] for non-cohesive powders, as presented in the next section.

The powders concerned in this study are cohesive, with non-spherical particles and a fine and polydispersed grain size. However, the main hypothesis numerical simulations are: 2D-studies or 3D studies, with or without gravity, ideal particle shapes (spheres, discs, polygons), slightly dispersed grain size [49]–[52].

2.6.2. Some numbers describing the flow

To model the flow, some numbers have been defined. Form those numbers, constitutive laws (friction, dilatancy) are proposed.

2.6.2.1. Inertial bond number

Definition: Suppose two adjacent layers of grains. The inertial bond number is the ratio of the confinement time related to confinement pressure (time necessary for a particle from the top layer to move from the highest point to the lowest point by passing over the particle from the bottom layer) over

the deformation time related to shear (time for a particle from the top layer to move a distance of one diameter relatively to the bottom layer) [12].

Interpretation: This number defines flow types depending on its value.

- $I \leq 1$ Dense flow [12]
- $I > 1$ Collisional flow (gas-like)[12]
- I approaches 0 means that the flow is close to the equilibrium [52]

In the context of classic modeling of dense flows, constitutive laws have been proposed as functions of I: dilatancy law and friction law [12], [50], [52].

2.6.2.2. Granular bond number

Definition: Ratio of attractive forces over the weight [50], [53].

Interpretation: The granular bond number defines the limit between non-cohesive powder (<1) and cohesive powder (≥1) [53]–[55]. Complex to calculate because it involves numerous parameters such as roughness diameter, Hamaker constant and equilibrium distance [53], [55] or the value of the maximum attractive force reached at a contact [50], [54]. For polydispersed grain sizes it is possible to use the multi-component granular bond number [55].

2.6.3. Quantities qualifying the flow

The following quantities describe quantitatively or qualitatively the flow:

2.6.3.1. Hausner ratio

Definition: It is the ratio of packed density over bulk density.

Interpretation: It is a qualitative quantity. The higher this ratio, the higher the difference between bulk and packed densities. Then, inter-particle forces are intense and the powders has a low flowability. There is a linear relation between the cohesion (derived from a shear test form the Mohr-Coulomb failure criterion, measured in an annular cell and for pre-consolidations below 5 kPa) and this ratio for lactose (cohesive powder) and sand (free flowing) [37].

2.6.3.2. Unconfined yield stress (UYS)

Definition: Derived from a shear test, it is the stress necessary to break a cohesive arch formed by a powder [14].

Interpretation: It is a quantitative quantity and an indicator of the powder tendency to consolidate during storage. It is used to determine the flow function. There is a relation between UYS and cohesion. Indeed, if the yield locus of a powder passes through the origin, the UYS is equal to zero (the smallest Mohr circle is not defined). Moreover, the higher the cohesion, the bigger the smallest Mohr circle, and the higher the UYS.

2.6.3.3. Flow Function

Definition: Derived from a shear test, it is the ratio of the major consolidation stress over the unconfined yield stress.

Interpretation: It is a quantitative quantity. This function ranks powders from “no flow” to “free flowing” [14]. There is a linear relation between the flow function and Hausner’s ratio [37].

2.6.3.4. Cohesion length

Definition: It is a characteristic length. It corresponds to the order of magnitude of the maximum height of a vertical wall that it is possible to build with the powder [14]. Its definition is:

$$l = \frac{c}{\rho g}$$

l: Cohesion length (m)
C: Cohesion derived from a shear test (Pa)
ρ : Powder density (kg/m^3)
g : Acceleration of gravity (m/s^2)

Interpretation: It is a semi-quantitative quantity. This length represents the relative intensity of cohesive forces over the powder weight. A high cohesion length means that cohesive forces become greater than the weight: the powder may present flowability issues.

3. Industrial application and encountered issues

In this part are presented the methods used to handle powders in an industrial context, in the gasification process in particular. In the first part, gasifiers are described. Then, injection in the reactors and storage in silos are presented. Finally, the granulation process is discussed.

3.1. Gasifiers technologies

The biomass gasification process produces a syngas (mostly carbon monoxide and hydrogen) from a resource containing carbon (charcoal, biomass, wastes…) and an oxidant (air, water). The obtained syngas has applications in chemistry and biofuel production for example.

There are mainly three gasifier technologies, each one with advantages and drawbacks. They are here presented from the lowest to the highest reaction time.

3.1.1. Fixed bed reactor

In this type of reactors, biomass forms a dense bed. There are two main types of fixed bed reactors: with co-current or counter-current mass flows [56]–[58], which are presented in Figure 25:

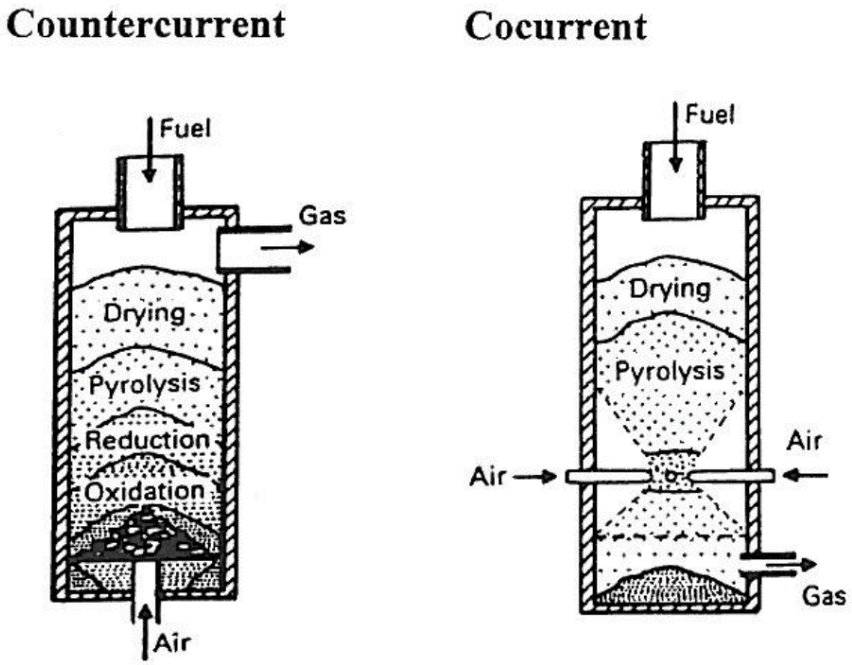

Figure 25: Fixed bed reactors, co-current and counter-current [57]

In the co-current technology, biomass is injected at the top of the reactor and air at mid-height of the reactor. Air injection is made in a narrowing part of the reactor, creating turbulences which improve the oxidation of volatile matter and the cracking of tars. Biomass combustion with air provides heat to the reactor and allows the creation of a pyrolysis area above the injection area and a drying area at the top part of the reactor. This technology provides a tar-less syngas (tar is a complex mix of condensable organic molecules). However, the risk of ash melting requires maintenance [56]. The injected biomass particles are large, around 5mm. The maximum biomass flow rate is around 500 kg/h [58].

In the counter-current technology, biomass is injected at the top of the reactor whereas air is injected at the bottom. The obtained gas contains a lot of tars because it does not cross a high temperature area before to exit the reactor, which would have cracked them [56]. The injected biomass particles are large, the same size and without fine particles. The maximum biomass flow rate is limited to around 4 t/h [58].

3.1.2. Fluidized bed reactor

In this reactor technology, a fluidized bed is suspended by injecting an inert gas at the bottom of the reactor. The advantage of this technology over the fixed bed reactor is the homogeneous repartition of heat. Two main technologies are available, bubbling bed and circulating bed, as presented in Figure 26:

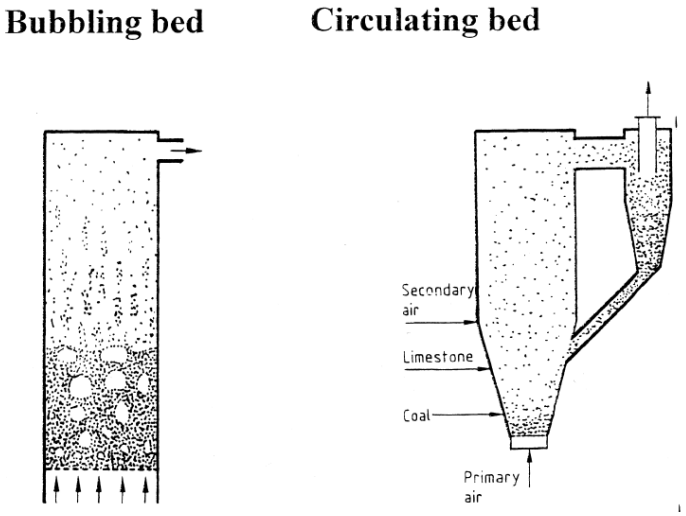

Figure 26: Fluidized bed gasifier technologies [57]

A compromise has to be found for the temperature: a high temperature promotes a clean gas but increases the risk of ash melting, resulting in a de-fluidization of the bed [57], [59]. For bubbling bed reactors, the maximum biomass flow rate is around 10-15 t/h, and above 15 t/h for circulating beds [58].

3.1.3. Entrained flow reactor

Entrained flow gasification is carried out at high temperature (1300-1500 °C) and high pressure (20-70 bars) [60]. In this type of reactor, biomass has to be prepared before its injection: it may be torrefied and must be finely ground [61]. The powder is injected, suspended in the gas, at high speed (6 m/s). Its residence time in the reactor is low, around one second. The obtained gas is clean, with a low tar content [60]. Examples of entrained flow reactors are shown in Figure 27:

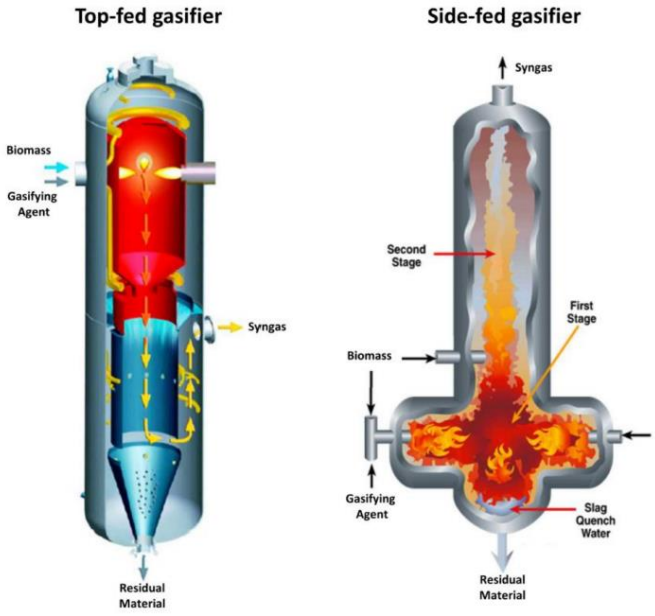

Figure 27: Schematics of entrained flow reactors.[60].

The advantage of this technology are the absence of problems linked to the bed, and the obtained gas is clean. High biomass flow rates are possible. However, powders with a low flowability have to be injected in a pressurized reactor, which may be problematic.

3.2. Injection in pressurized reactors

Conveying and injection are problematic steps in processes using powders. Powders behave neither like liquids, nor like gas. There are numerous conveying and injection technologies adapted to powders. The gravimetric mode is the less expensive, but using it with biomass powders is problematic due to their low flowability. Belt conveying is reliable over long distances, as well as the bucket elevator for short vertical elevations. Screws are used for short distances and often coupled with another conveying technology, such as pneumatic conveying. Vibratory channels can convey powders to a belt conveyor. Finally, powders can be transported over long distances suspended in a liquid [28].

The injection technologies presented in this part concern injection in pressurized reactors. Indeed, the entrained flow gasification, which is the context of this work, is carried out in a pressurized reactor (between 20 and 80 bars).

Pneumatic conveying is a common way to convey powders in the industry (the powder is entrained by a large amount of inert gas) [62]. The issue with this technology in the context of biomass gasification is the introduction of gas in the reactor. Indeed, gases are heated (energetic losses) and have to be separated from syngas after the gasification step (extra steps in the process). Thus, gravity flow must be used rather than pneumatic conveying. However, gravity flow requires special equipment, adapted to cohesive powders features.

3.2.1. Volumetric and gravimetric feeding

3.2.1.1. Volumetric feeding

This feeding is based on the ability of a feeder to deliver a constant volumetric flow rate. For example, in the case of a screw feeder, the engine speed determines the volumetric flow rate. It is an affordable solution for non-critical applications.

The density of numerous powders, and biomass powders in particular, depend on the working conditions (stresses during the storage for example). Thus, for a given volumetric flow rate, the fed mass can vary. This feature results in precision limitations [63].

3.2.1.2. *Gravimetric feeding*

A gravimetric feeder is equipped with a weighing system. The feeder delivers a constant mass. The schematic a gravimetric feeder is presented in Figure 28:

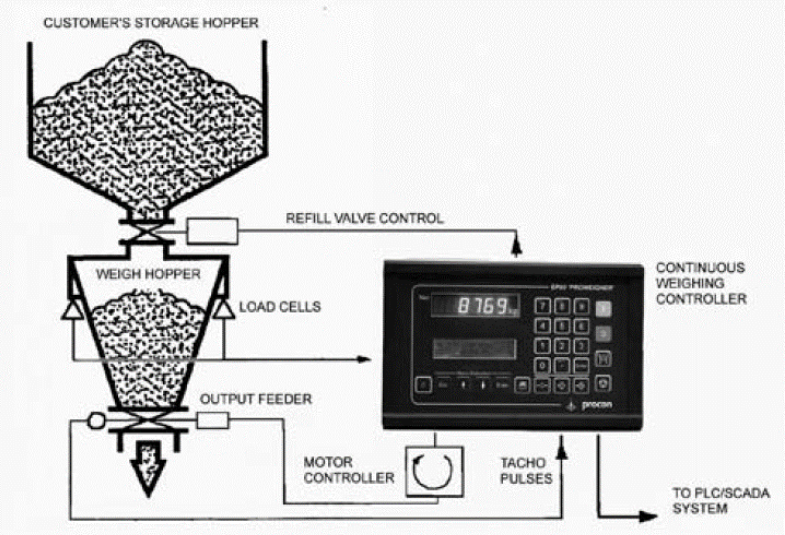

Figure 28: Schematic of a gravimetric feeder [63].

Gravimetric feeding present several issues. Gravimetric feeders have to be turned off during the silo refills (volumetric feeding). They are sensitive to vibrations (the influence of vibrations can be minimized by using dampers, or a screening software). Finally, the hopper closing mechanism can remain open and allow some product to flow, disrupting the weighing [63].

3.2.2. Screw feeding

The powder is compressed in a narrow channel, forming a plug using a screw. The plug forms a barrier, preventing the backflow of gases coming from the reactor. The channel diameter can vary to maintain a stable flow [64], [65]. A schematic of a screw feeder is shown in Figure 29:

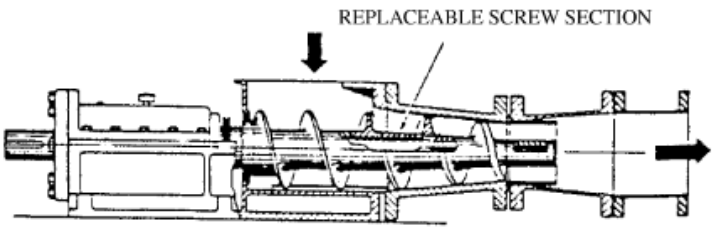

Figure 29: Schematic of a screw feeder [65]

- Screw feeders operates at pressure between 0.5 and 1.5 MPa (5-15 bars) [65].
- Screw feeders can block. Factors influencing the risk of blockage during biomass screw feeding are high levels of powder in the hopper, big particles irregular forms, irregular surfaces, high densities [27].

- In the case of biomass feeding, wider grain size distributions and a higher moisture content require a higher engine torque [27].
- The powders has to form a plug to avoid backflow of gases from the reactor. The plug is easily formed with compressible biomasses. Moreover, compressible biomasses pass faster through the tapered part [27].

Pros and cons of screw feeders are summarized in the table below:

Table 1 : Pros and cons of screw feeders [28]

Advantages	Disadvantages
Economical	Short distances
Low maintenance	Attrition
Totally enclosed	Wear with abrasive materials
Multiple discharge points	Particles must be smaller than the pitch
Easy to install	Small scale testing preferred before usage
Quiet operation	Needs to run full of particles
No return run	As the angle of inclination increases, the allowable capacity decreases
Can operate at inclines	
Volume control	
Can handle bulk materials from sluggish to free-flowing	

3.2.3. Lock-hopper

Lock-hoppers are the most common injection system. Biomass is pressurized by injecting an inert gas after it has been introduced in an airtight hopper. It is then unloaded is a weighted hopper and injected in the reactor thanks to a metering screw followed by an injector screw [65]. The schematic of a lock-hopper is presented in Figure 30:

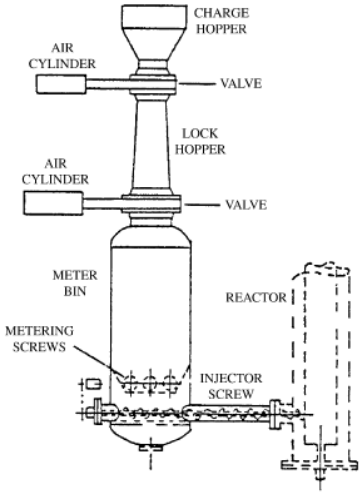

Figure 30: Schematic of a lock-hopper [65]

Lock-hoppers operate at pressures below 3.5 MPa (35 bars). Above 3.5 MPa, excessive gas amounts are necessary for the pressurization. Moreover, the equipment needs more maintenance due to the stresses it is subjected to [64], [65]. To lower the gas and maintenance costs, it is possible to use a double lock-hopper. The number of cycles per equipment is decreased, and the pressure released by a lock-hopper is used to pressurize the other [64]. Craven et al. proposed to use a lock hopper pressurized by hydraulic system. An 81.9% decrease in the energy consumption is observed compared with a classic lock hopper, and no pressurization gas is required [66].

3.2.4. Rotary valve feeder

This equipment works like a revolving door. The powder is conveyed from a non-pressurized area to a pressurized area between the blades of a rotor and the walls. [64], [65]. The schematic of a rotary valve feeder is presented in Figure 31:

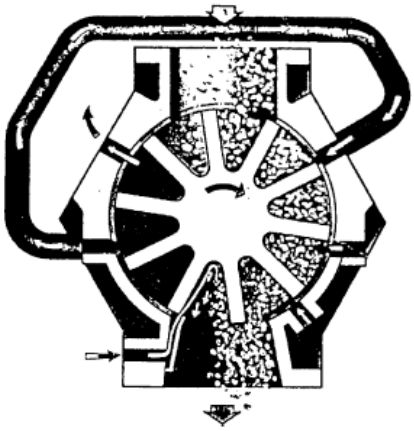

Figure 31: Schematic of a rotary valve feeder [65]

Rotary valve feeders operate at pressure below 1.5 MPa (15 bars) [65]. The rotor may rub the wall, in spite of the steam jet cleaning the pockets [65]. Powder stuck on the walls may lead to problems [64]. This system is subject to pressure drops and backflow of reactor gases [65].

3.3. Storage and discharge

Biomass powders in the gasification process are stored in a silo. Biomass powders face flow issues that can lead to storage and discharge issues (incomplete discharge, arch formation…). In this part flow in silos and stresses in a silo are presented.

3.3.1. Discharge issues

Issues appearing during the silo discharge of granular material are shown in Figure 32:

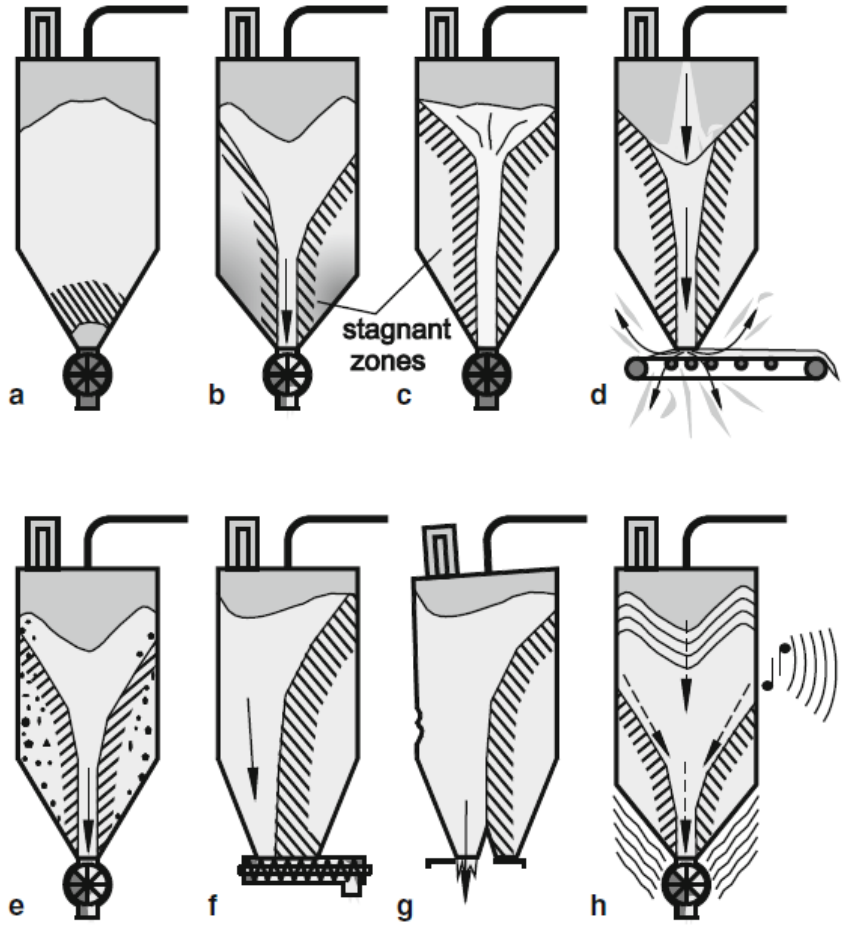

Figure 32: Issues appearing during the silo discharge of granular material; a) arch formation; b) funnel flow (with a large time residence distribution resulting in product deterioration); c) ratholing; d) flooding; e) segregation; f) non-uniform discharge with a screw driver resulting in an eccentric funnel flow; g) buckling caused by an eccentric flow; h) vibrations [28]

Arch formation: if the opening is too small, arching can occur. For particle size close to the opening size, the arch is formed due to particle interlocking. For small particles, the arch is formed due to cohesive forces (schematic a).

Funnel flow: If the silo walls are too rough, powder sticks to them and forms a stagnant area that can consolidate over time. The large residence time distribution may result in product deterioration (schematic b).

Ratholing: The powder can also flow only in a channel in the silo center, which is called funnel flow (schematic c). The funnel flow corresponds to all types of flows where a part of the material remains stationary.

Flooding: The residence time in the channel can be very low. Easily fluidisable material in a funnel flow configuration cannot deaerate, flows like a fluid and floods the feeder (schematic d).

Segregation: it can occur during the silo loading. The fine particles are loaded in the central part, whereas the coarse ones stay near the walls. During the discharge, in case of a funnel flow, the fine particles will be discharged first (schematic e).

Non-uniform discharge: if the silo is not correctly sized, a non-uniform flow can occur. For example with a screw driver at the bottom of the silo (schematic f), the screw conveys the powder from the left

to the right. If the screw is already full on the left it cannot convey powder coming from the right, resulting in an asymmetric discharge.

Buckling: non-uniform discharges result in a non-uniform stress distribution that may cause deformation of the silo, or breakage of the walls (schematic g).

Vibrations: the silo discharge can cause vibrations of the walls (schematic h) [28].

To avoid these issues, Jenike proposed a procedure for silo design. This procedure takes powder properties into account to size the silo. The powders properties are determined with shear tests.

3.3.2. Arching

For biomass powders, the arching tendency seems to be a combined effect of particle shape and particle size [30], [67] moisture content (increasing moisture content causes higher cohesion and adherence, increasing the arching likeliness) [23], consolidation [68], cohesion [28] and tensile strength [25]. However, the arching tendency does not seem to be linked to the angle of repose and bulk density [67].

3.3.3. Silo discharge

Particle shape has an influence on the discharge rate of a silo. Decreasing the sphericity and increasing the particle elongation (larger dimension over smaller dimension) decreases the discharge rate (increase of the shear stress) and makes the flow intermittent for a flat bottom silo [22], [23]. Round-edged particles present a higher discharge rate and a lower residual solid fraction in the silo than sharp-edged particles [23].

The mass flow rate through an orifice can be calculated thanks to different methods. One of the most common for non-cohesive powders is Beverloo's law [40]. It is a relation between the mass flow rate through an orifice and powder parameters:

$$\dot{m} = C.\rho_b.\sqrt{g}.(D_0 - k.d_P)^{2.5}$$

With:
$\dot{m}$: Mass flow rate (kg/s)
C: fitting parameter (0.55-0.65)
ρb: Bulk density (kg/m^3)
g: Acceleration of gravity (m/s^2)
D_0: Diamater of the orifice (m)
k: Fitting parameter (1.5-3)
d_P: Particle diameter (m)

This law is not applicable for fine particles (particle diameter below 200 µm) [28]. For fine particles, the interstitial pressure gradient has to be taken in account [69], but is not easy to establish. The jamming phenomenon will be discussed in Chapter V.

3.4. Granulation

The granulation process increases the particle size by agglomerating particles, for example to improve their flow. There are two processes, the dry process and the wet process, and different technologies.

3.4.1. Dry process

In this process, the powder is compacted using high pressure between two rotating rollers (roller compaction). It is a continuous process, cheaper than the wet process, and well developed [28].

3.4.2. Wet process

In this process, a liquid binder is sprayed, poured or melted on the powder. The liquid binder can be organic or inorganic. Examples of inorganics include alumina, cement, clay, silica and silicates; organics include acrylic, cellulose, gum, polyethylene glycol, starch, sugar and vinyl. It is then granulated. The chosen granulation technology depends on factors such as flow rate, batch or continuous and the acceptable level of dust production.

There are three granule formation mechanisms:

- Nucleation: the binder comes into contact with the powder under agitation.
- Growth: chocks between particles increases the granulate size.
- Breakage and attrition: when the chocks are greater than the granulate resistance, they break or a part of their external layer erodes.

It is possible to calculate dimensionless indicators representing granulation mechanisms such as the powder saturation with the liquid or the particle coating by the binder [28].

The steps of wet granulation are presented in Figure 33:

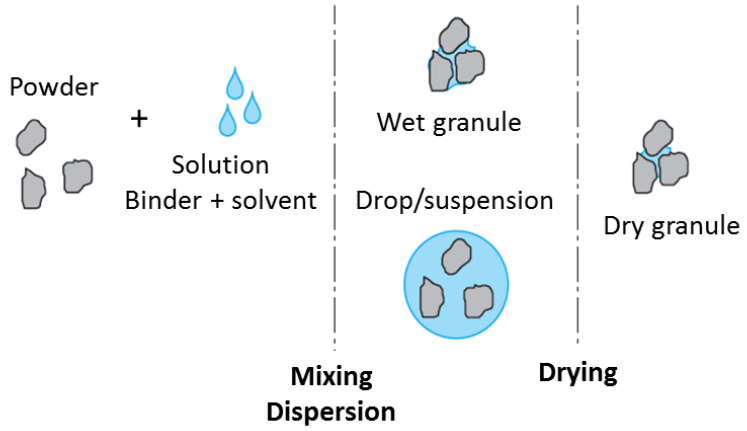

Figure 33: Steps of wet granulation [70](translated)

The granulation steps are [70]:

- Mixing the powders to bring the particles into contact.
- Wetting the powder with the binder.
- The growth of the granules following the granule formation mechanisms.
- The drying of the granules to evaporate the solvent and replace the liquid bridges between particles by solid bridges. This strengthens the granule cohesion.

3.4.3. Wet granulation technologies

The different technologies have in common that they all present a method to mix the powder and a method to inject the binder. The choice of technology has a strong influence on the final product (size distribution, shape, porosity…) [28].

3.4.3.1. Tumbling granulators

In these granulators, particles are set in motion by the centrifugal forces and gravity. There are two main types: the continuous disc and the continuous drum. Flow rate is between 1 and 100 t/h and residence time between 1 and 5 min. The granule size is generally between 1 and 20 mm, never below 250 microns. The granule density is between what is obtained with a fluidized bed (porous) and a mixer granulator (dense).

Important parameters to set are the angle of the granulator with the horizontal and the rotation speed. The powder feeder is either volumetric or gravimetric. A gravimetric feeder prevents fluctuations which could modify the ratio liquid/solid and thus the granule properties. The binder is sprayed by several nozzles distributed on the bed surface, and their positions have an influence on the granulation process [71].

Continuous disc

The continuous disc is a disc with flanges, tilted between 50 and 60° [71]. A schematic of this technology is shown in Figure 34:

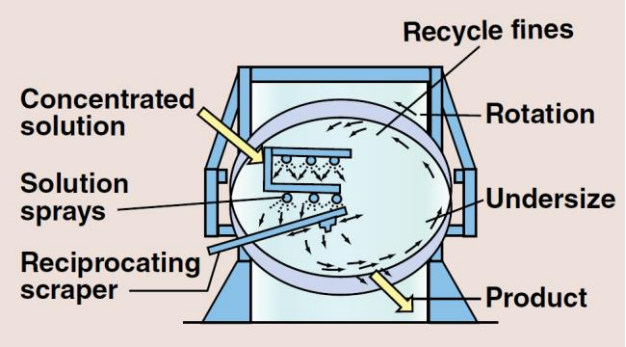

Figure 34: schematic of a continuous disc [71]

An advantage of the continuous disc is that the size classification is operated by natural segregation: large enough particles exit the disc whereas the finer ones stay in the granulator. The size distribution is narrow and the recycling rate is low. On the contrary, continuous drums do not have natural size classification phenomena, and the recycling rate is high [71].

Continuous drum

Continuous drums are cylinders tilted between 3 and 10° [71]. A schematic of a continuous drum is presented below:

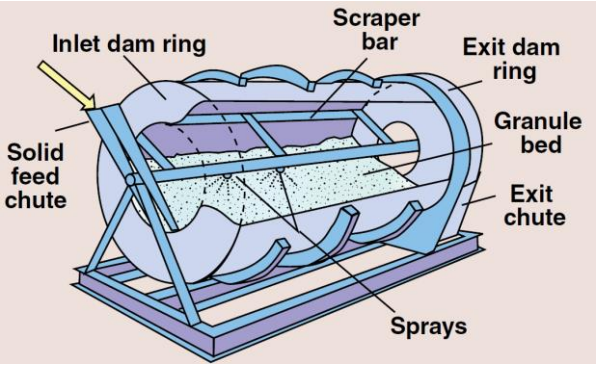

Figure 35: Schematic of a continuous drum [71]

The powder enters the drum and the binder is sprayed over it. The drum rotation leads the powders towards the other end while granulating it. It is sieved at the outlet and too small particles are recycled, whereas too large particles are ground and recycled. A schematic of the recycling system is presented in the figure below:

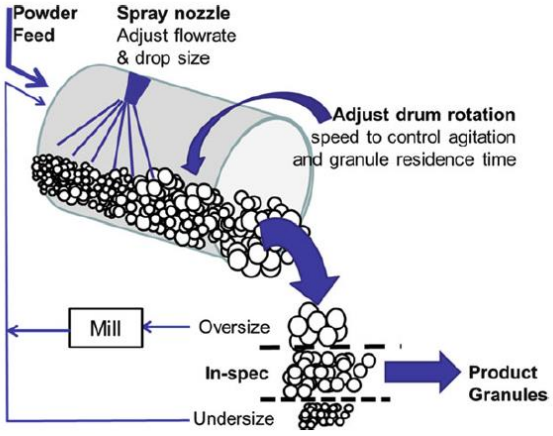

Figure 36: Schematic of a continuous drum with the recycling system [28]

The major drawbacks of this technology are the high energy consumption and poorly controlled operating conditions. The product often do not meet the expected quality, and the recycling rate is high [28].

3.4.3.2. Mixer granulators

In this type of granulator, mechanical agitation granulates the powder. Large ranges of geometries are available. Binder quantity and mixing time influence size and density of the granules. High compactions brought by these granulators produce dense granules, but less spherical than with other technologies, but they require less liquid. Mixer granulators are either low or high shear mixers [71].

Low shear mixers

They operate below 100 rpm, batch or continuous. Residence time are high (between 20 and 40 min). It is used less frequently than high shear mixers [71].

High shear mixers

High shear mixers include continuous shaft mixers and batch mixers.

Shaft mixers have blades or pins fixed on a central shaft, rotating at high speed (generally between 200 and 3500 rpm) [71], as presented in the figure below:

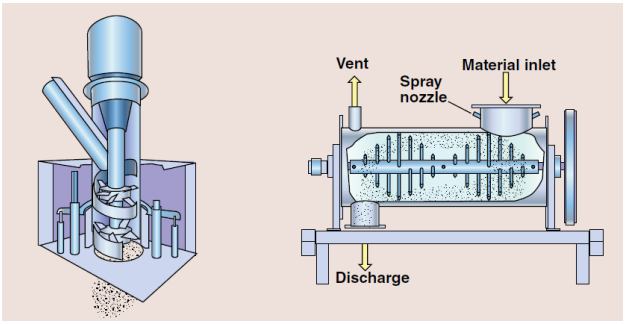

Figure 37: Schematics of high shear mixers with central shafts. On the left, Vertical Schugi Mixer; on the right, Horizontal Pin Mixer [71]

Mixers with a central shaft produce granule size between 0.5 and 1mm. Residence time is around a few seconds and the particles are thoroughly mixed. However, the obtained granules are fine, irregular in shape, fluffy and have a low density. The flow rate ranges between 10 and 200 t/h and the electric consumption can go up to 200 kW. High shear mixers are often followed by granulators with a higher residence time and a lower shear rate for the granulates to continue their growth and densification [71].

Batch technologies can be used with numerous powder types and are easy to clean [71]. Examples of batch granulators are presented in the figure below:

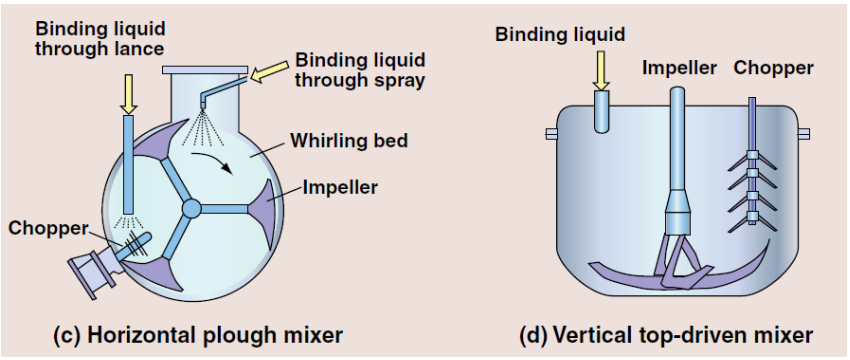

Figure 38: Batch high shear mixers. On the left, Horizontal plough mixer. On the left, Vertical top-driven mixer [71]

The central blade rotates between 60 and 800 rpm. An eccentric chopper rotates between 500 and 3500 rpm to break the oversized aggregates. The volume of batch mixers ranges between 10 and 1200 L and the residence time is 5-10 minutes [71].

High shear mixers produces granules from 200 to 1000 microns. Their quality is hard to predict. It is necessary to test different configurations to get suitable results [28].

Fluidized-bed granulators

The particle motion is due to a gas flow. Powders must be fluidisable to use this technology, and the binder can only be sprayed. The granule size is between 200 and 500 microns, and granules are porous. The air flow dries the aggregates, which allows to eliminate the drying step after the granulation. Numerous geometry are available, the vessel shape and the nozzle orientation a the main parameters [28]. A fluidized bed schematic is shown in the figure below:

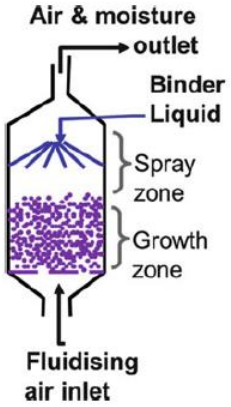

Figure 39: Schematic of a fluidized-bed granulator [28]

This technology is either a batch or a continuous process. The nozzle spraying the binder can be placed above, below or in the powder bed. The batch process exist in numerous shapes and can agglomerate fine powders in porous granules. Another solution is to suspend the powder in a liquid and to spray it on a nucleus bed to produce hard and layered granules [71].

Continuous technologies also produce layered particules. It is often necessaty to recycle out of spec granules (which requires classification and grinding equipment) [71].

During the growth of granules, the minimum fluidization speed is modified, which can result in bed defluidisation [28].

3.4.4. Choice of the granulation technology

The choice of the granulation technology can be made using some powder properties and the expected granulate properties [70]:

Fluidized-bed: This technology dries the granules. The energy consumption is high and the produced granules are porous and have an irregular shape. The powders must be fluidisable to use this technology.

High-shear mixer: This technology produces dense and spherical granules, but wet and with a polydispersed particle size. Sieving and drying steps are necessary.

Continuous drum: The drum produces dense granules (the density is lower than with mixer granulators), but with a very polydispersed particle size. The drying step can be simultaneous with the granulation.

Continuous disc: This technology is easy to set up. The obtained granules are spherical and have an homogeneous size. However, it is complex to obtain both expected size and density. The disc is open, thus it is not suitable for powders producing dusts. The drying step can be simultaneous with the granulation.

3.4.5. Case of biomass granulation

Biomass granulation improves its flow, conveying and storage behaviors. Dry densification presents a high energy consumption. By contrast, wet granulation has a lower energy consumption and is used in different fields: chemical industry, fertilizers, food industry and minerals industry for example [72].

Wet biomass granulation is achieved by grinding the biomass (between 0.5 and 1mm), wetting it with a binder (paper plant wastes, lignin, bentonite, pyrolysis oils, starch) and mixing it to produce granules [72].

The granulator used for biomass granulation depends on the way the granulated biomass will be used and on the granule properties expected. The fluidized bed is used to obtain granule size between 0.07 and 1mm. Continuous disc and continuous drum produce granules between 5 and 15mm [72].

Binder nature plays a critical role in granule properties. If parameters such as binding capacity, thermic properties, ash content and availability are considered, starch seems to be the best alternative to granulate biomass. Binder concentration on a dry basis is generally between 2 and 10% (by mass) [72].

CHAPTER II: MATERIAL AND METHODS FOR THE LAB SCALE STUDIES

Three studies at lab scale have been carried out: a study of the powder parameters (cohesion, density and avalanche angle), a study of the influence of moisture content on flow parameters and a study of a new granulation method. In this chapter, the material and methods used to perform these studies are presented.

1. Material

1.1. Reference powder

During this Ph.D. work, it was necessary to get a powder in large quantities to serve as a reference. This powder should be fine enough to be compatible with the gasification process in entrained flow reactor. Oak from Haute-Marne (France), previously ground to chips, has been ground in an industrial chain mill in the CEA (in Bure). A picture of the chain mill is presented in Figure 40:

Figure 40: Industrial chain mill used to grind the reference powder

The chips are stored in the hopper. They fall in the grinding chamber where chains rotate, crushing the biomass. An air stream drags the particles depending on their size to a sorter. The sorter consists of a cylinder perforated by holes, rotating around its axis. The higher the rotation speed, the smaller the particles that can pass through. Finally, the selected particles are conveyed to the storage bag.

The parameters (air stream intensity and sorter rotation speed) have been chosen to obtain the finest powder. First, an air stream conveys the powder form the grinding chamber to the storage bag. The stronger the stream, the bigger the particles conveyed. Thus, the air stream has been set to its lowest intensity, conveying only the smallest particles. Then, the sorter has been set to its maximum speed. In conclusion, the obtained powder is made of the smallest particles that it was possible to produce. Two cubic meters has been produced. Thus, this powder can be used for small scale applications, but also for pilot scale experiments. It is called “reference powder” and has a 22 µm median particle size. After the production, the powder is stored in a Big Bag and placed in a shelter.

1.2. Link between powder parameters

In this work, experimental data obtained with thirty-four different powders are gathered. Among them, twenty-four are wood powders (deciduous and resinous trees), obtained by grinding wood chips with different grinding technologies (knives, hammer, bar grinders). Some wood powders are sieved. In addition, six other biomass powders are considered: industrial sugar, wheat semolina (two grain sizes), grape grounds and two microalgae (dried and ground). The last four are inorganic powders: talcum from

Fisher Chemicals, beach sand, olivine and alumina. The origin of the different powders is presented in the table below:

Table 2: Origin of the powders used is the study of the link between flow parameters

No.	Supplier	Nature	Comment
A	Canmet	Raw commercial product, Northern white-cedar	Ground in a chain mill. Used in this work and used to make powder A1 and A2
A1	Canmet	Northern white-cedar	Powder A size fraction <50 µm after sieving
A2	Canmet	Northern white-cedar	Powder A size fraction 50-100 µm after sieving
B	Canmet	Raw commercial product, Northern white-cedar	Ground in a chain mill. Different from powder A.
C	Lignex	Raw commercial product, Beech, 0-1000 µm	Not used in the work. Used to make powders C1 to C4
C1	Lignex	Beech	Powder C size fraction <500 µm after sieving
C2	Lignex	Beech	Powder C size fraction >500 µm after sieving
C3	Lignex	Beech	Powder C size fraction 315-500 µm after sieving
C4	Lignex	Beech	Powder C in a mixer with 10 kg of small grinding media, 10 min.
D	Lignex	Raw commercial product, Beech, 0-200 µm	Used in the work and used to make powder D1
D1	Lignex	Beech	Powder D size fraction 0-100 µm after sieving
E	Lignex	Raw commercial product, Beech, 0-75 µm	
F	Lignex	Raw commercial product, Resinous tree, 0-1000 µm, ground in a vibratory mill	
G		Torrefied wood chips	Ground in a vibratory mill
H	SPPS (Société de Participation Parisienne des Sciures)	Raw commercial product, Smocking beech "Savour'Hêtre"	Used in the work and used to make powders H1 to H7
H1	SPPS	Beech	Powder H size fraction 630-900 µm after sieving
H2	SPPS	Beech	Powder H size fraction 500-630 µm after sieving
H3	SPPS	Beech	Powder H size fraction 315-500 µm after sieving
H4	SPPS	Beech	Powder H size fraction <315 µm after sieving
H5	SPPS	Beech	Powder H aerated
H6	SPPS	Beech	Powder H ground in a knife mill with a 200 µm sieve
H7	SPPS	Beech	Powder H ground in a vibratory mill, then sieved 0-200 µm
I	UNGDA (Union nationale de	Grape stalks+peels+pips after pressing and drying	Ground in a vibratory mill, 20 min

	Groupements de Distillateurs d'Alcool)		
J	Commercial product	Sugar	d50 = 419 µm
K	Commercial product	Semolina	d50 = 847 µm
L	Commercial product	Fine semolina	d50 = 487 µm
N	Fisher	Talc general purpose grade	d50 = 49 µm
O	CEA	Chlamidomonas Reinhardtii, dried	Ground with pulverisette 14, Fritsch
P		Dune of Pilat sand	Collected on the dune of Pilat, France. Geographical coordinates : 44°35'36.6"N 1°12'42.2"W. d50 = 338 µm
Q	CEA	Alumina	Made in the cea, Grenoble, France. d50 = 51 µm
R	Alpha-Biotech	Nannochloropsis Oculata after supercritical CO2 extraction of the lipids, 300-500 µm	In the context of the ANR project Shamash
S	CEA	Oak from Haute-Marne, France.	Reference powder. Ground in a chain mill. Used in the work and used to make powder S1. d50 = 22 µm
S1	CEA	Oak from Haute-Marne, France	Powder S size fraction <50 µm after sieving
T	Magnolithe	Olivine	d50 = 530 µm

The objective of this study is to determine the link between flow parameters. Thus, shear tests, avalanche angle measures and density measures are performed to find a link between them. However, the moisture content of powders is not measured. Indeed, moisture content is one of the parameters influencing the parameter cohesion (see chapter I, 2.1.3). Powders were stored in airtight buckets for their moisture content to remain a constant.

1.3. Influence of moisture content on flow parameters

In this study, eight powders are used. They are presented in table below. In the context of the gasification process in entrained flow reactor, the maximum acceptable moisture content of biomass to be injected in the reactor is around 20% (wet basis) [60]. Thus, the study focused on powder moisture contents between 0 and around 20% moisture content (wet basis). The powder 4 has been tested around 30% also.

Table 3: Powders and humidities used in the study on the influence of moisture content on flow parameters

No.	Supplier	Nature	Moisture content (% wet basis)
1a	Lignex	Raw commercial product, Resinous tree (fir or spruce), 0-1000 µm	0; 9; 19.43
1b	Lignex	Resinous tree (fir or spruce)	0.84; 5.08; 18.85
2	Lignex	Raw commercial product, Beech, 0-1000 µm	0; 14.32; 23.78

3	cea	Oak chips from Haute-Marne (France) ground in an industrial chain mill, d50 = 22 µm	0; 10.96; 22.17
4	cea	Oak chips from powder 3, ground in Retsch SK100 comfort with a 1mm sieve	0; 9.91; 19; 29.29
5	cea	Oak chips, ground in Retsch SK100 comfort with a 1mm sieve	0; 10; 20
6	RAGT ENERGIE	Raw powder ground with a 4mm sieve. Ground again in Retsch SK100 comfort with a 0.12 sieve	0; 11.41; 19.51
7	Lignex	Raw commercial product, Beech, 0-200 µm	0; 13.11; 23.19

In this work, the objective is to assess the influence of moisture content on flow parameters by performing shear tests, avalanche angle measures and density measures at different moisture contents.

1.4. New granulation method

Biomass powders may be cohesive. Granulation is a method to improve their flowability [72]. In the context of gasification in entrained flow reactors, the particle size must be around or below 1mm [60]. A new granulation method is proposed to satisfy this condition. It has been subject to a patent [73] (see Appendix). For this study, the reference powder is used to produce granulated powders with different binders. The binders are presented in the table below:

Table 4: Binders used to granulate the reference powder

Binder
Sunflower seed shells
Sorghum
Grape seed cake
Empty fruit bench (palm tree)
Sugar cane
Starch
Seaweed

The interest of theses binders is that they are wastes and this method is a way to valorize them. Moreover, since they are biomass, they do not change the heat properties of the granules compared with the raw powder. The objective of this study is to quantify the benefits of this granulation process on flow parameters, compared with the raw powder. Since granules may be subjected to attrition when sheared, it has been decided to make them flow under their own weight by performing avalanche angle measurements and density measurements only.

2. Methods

2.1. Flowability measurements

2.1.1. FT4

The FT4 powder rheometer was designed by Freeman Tech, UK (Figure 41). This device can carry out numerous tests, such as the shear test. The main advantage of this tester is that the powder is first aerated with a propeller before the actual measurement. Thus, the powder is conditioned, and the results do not depend on the operator manipulations.

Figure 41: From left to right: FT4; shear cell in high position; Shear cell in rotation

The FT4 is an automated torsional shear cell. It follows the Jenike's shear test method. The instruments needed for the different steps of the test are attached on the machine and automatically put into motion. The procedure is automated and it is monitored live thanks to a software. The instruments are presented in the figure below:

Figure 42: Instruments used for shear tests with the FT4. From left to right: propeller, piston, and shear head.

- The propeller: it passes through the cylinder to homogenize the repartition of powder during the filling step.
- The piston: to apply a normal stress on the powder during the first consolidation step.
- The shear head: the device measures the torque necessary to shear the sample by rotating at a constant speed on the sample surface while applying a normal stress.

At the end of the test, an Excel file is created with the shear stress as a function of the normal stress.

2.1.1.1. Shear test points

The powder is filled in an 85 mL split vessel, aerated with the propeller and preconsolidated with a piston. In this work, three preconsolidation normal stresses have been used: 2, 3 and 5 kPa. Then the vessel is split (the top layer of the powder is removed, the surface is flat) as shown in the figure:

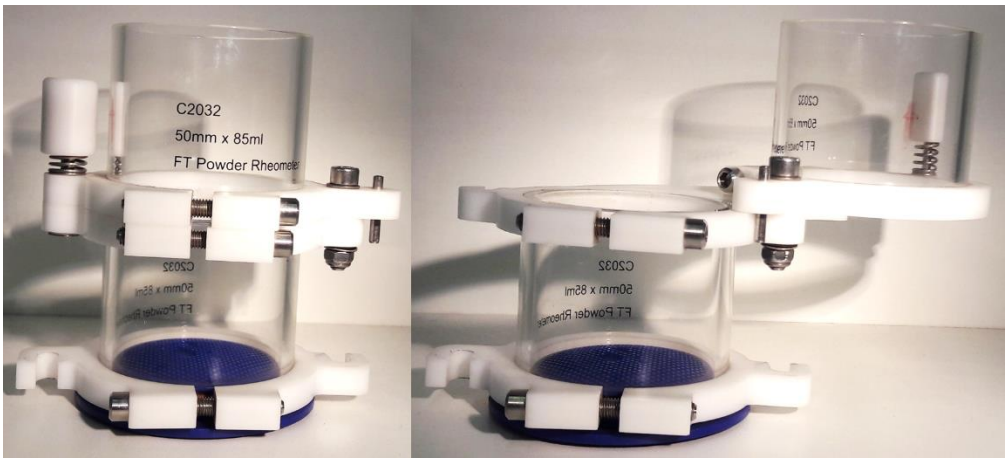

Figure 43: split vessel. Left, before splitting. Right, after splitting.

Finally, the shear cell is placed on the top of the powder sample, which is consolidated and then sheared at 18°/min until it yields for different normal stresses. The normal stresses applied for each preconsolidation are presented in the table below:

Table 5: Normal stresses applied to build the yield loci

	Preconsolidation normal stress (kPa)		
	2	3	5
Applied normal stresses (kPa)	1.75	2.5	4
	1.5	2	3
	1.25	1.75	2.5
	1	1.5	2
	0.8	1.25	1.5
	0.5	1	1
	0.3	0.8	0.5
	0.2	0.5	0.3
	0.15	0.3	0.2
	0.1	0.1	0.15
	0.05	0.05	0.1
	0.01	0.01	0.05

When sheared, the powder can dilate and compact. The FT4 measures the normal stress applied on the shear head during shear, and adjusts its height for it to be constant. However, it is possible that the applied normal stress is slightly different than the set value. Consequently, the FT4 displays the actual applied normal stress and the corresponding shear stress in the Excel file at the end of the test.

2.1.1.2. Angle of internal friction

The angle of internal friction represents the friction between particles in flowing conditions. It corresponds to the slope of the Mohr-Coulomb description of the yield locus. Thus, a straight line is fitted to the four points of the yield locus corresponding to the highest normal stresses (excluding the preconsolidation point) and the slope is considered as the coefficient of internal friction (Figure 44).

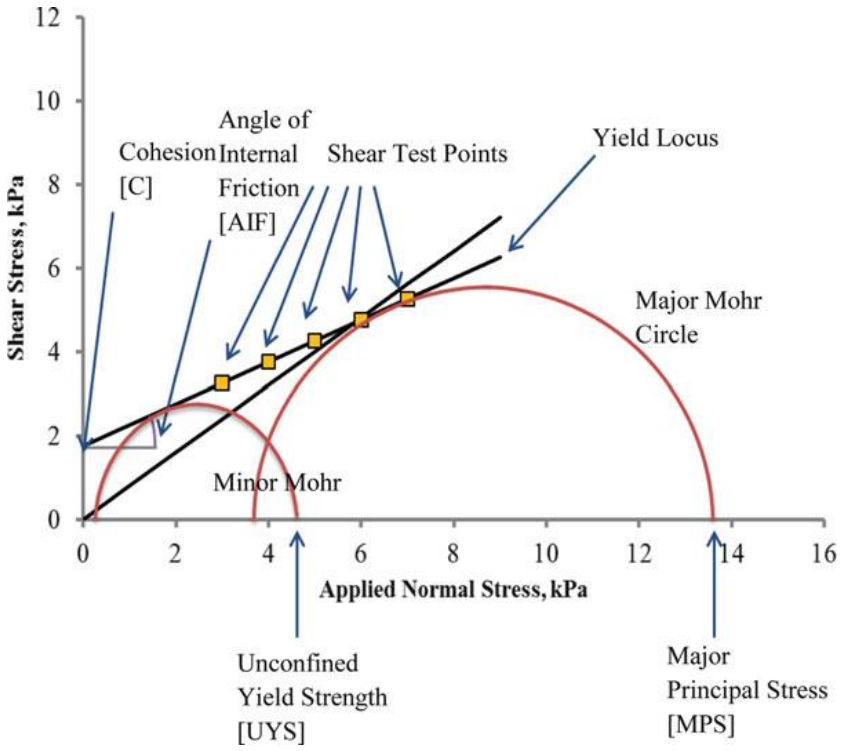

Figure 44: Example of description of a yield locus with angle of internal friction [28]

2.1.2. Revolution

The avalanche angle is measured with the Revolution Powder analyzer from Mercury Scientific Inc. It consists of a see-through cylindrical drum (10cm diameter, 3.3cm length). A volume of 79 mL of powder is introduced into the drum and then placed into the analyzer (Figure 45).

Figure 45: Left, drum containing the powder, to be placed in the analyzer. Right, Revolution powder analyzer [32]

The drum rotates at 0.6 rpm during a minute to prepare the powder and limit the operator effect. Then, a camera records the movements of the powder in the drum. The avalanche angle is calculated by a software. It is the angle of the surface of the powder before it collapses due to the rotation of the drum (an avalanche is considered as the rearrangement of at least 0.65 vol% of the sample in the drum). Several events can occur in the drum and are considered as an avalanche. For example, slumping, where a mass a material breaks and collapses downhill. A schematic of a slumping event is shown in Figure 46:

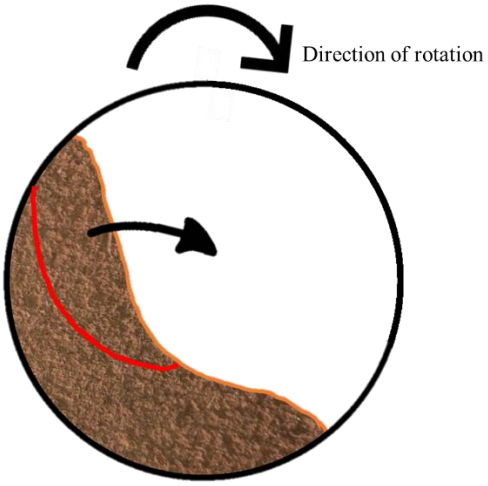

Figure 46: Schematic representation of a slumping event, considered as an avalanche.

In this configuration, a straight line is fitted to the powder surface and the avalanche angle can be measured with the horizontal. Other smaller events are considered as avalanches, as long as more than 0.65% of the powder volume starts moving. 150 avalanches are recorded. The chosen avalanche angle is the median of the angle distribution. In this way, aberrant values (close to 0° or 180°) do not have an influence on the result.

The time between two consecutive avalanches is also measured. The median of the distribution is considered as the avalanche time.

2.1.3. Aerated density

The aerated density is measured with the FT4. The powder sample is placed in the split vessel with a raised base, as presented in Figure 47:

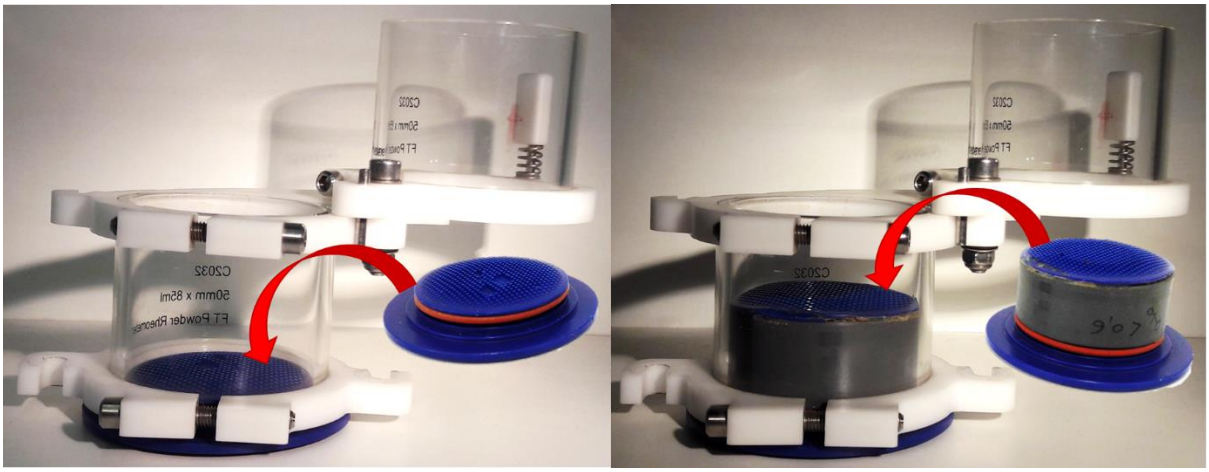

Figure 47: Left, base used for shear tests. Right, base used for aerated density measure.

The raised base decreases the height of powder in the vessel. Thus, the powder in the bottom of the sample is not compacted by the layers above it. Then, the sample is aerated three times with the propeller. The vessel is then split (the exact volume of the sample is known, 42.5 mL) and weighed. The aerated density is the ratio of the mass of the sample after is has been split over its volume.

2.1.4. Tapped density

The tapped density is used in the calculation of the Hausner ratio. 100 mL of aerated powder are weighed and placed in a 100 mL measuring cylinder. The cylinder is placed on the Autotap (Quantachrome instruments) and 4000 calibrated taps are performed. The tapped volume is read on the measuring cylinder and the tapped density can be calculated, knowing the sample mass.

2.2. Size distribution

The size distribution of the powders is measured with the Camsizer XT (Figure 48). It is a 2D image analyzer. Its measurement principle (Figure 48, right) is the dynamic image analysis. The particles are conveyed by a vibratory feeder to the measurement field: the particles drop between a light source and two cameras. The particles projected shadows are recorded and analyzed. The zoom camera has a resolution of 1µm per pixel. It analyses small particles (from 1 to 30µm). The basic camera analyses larger particles (up to 3mm) with a resolution of 15µm per pixel.

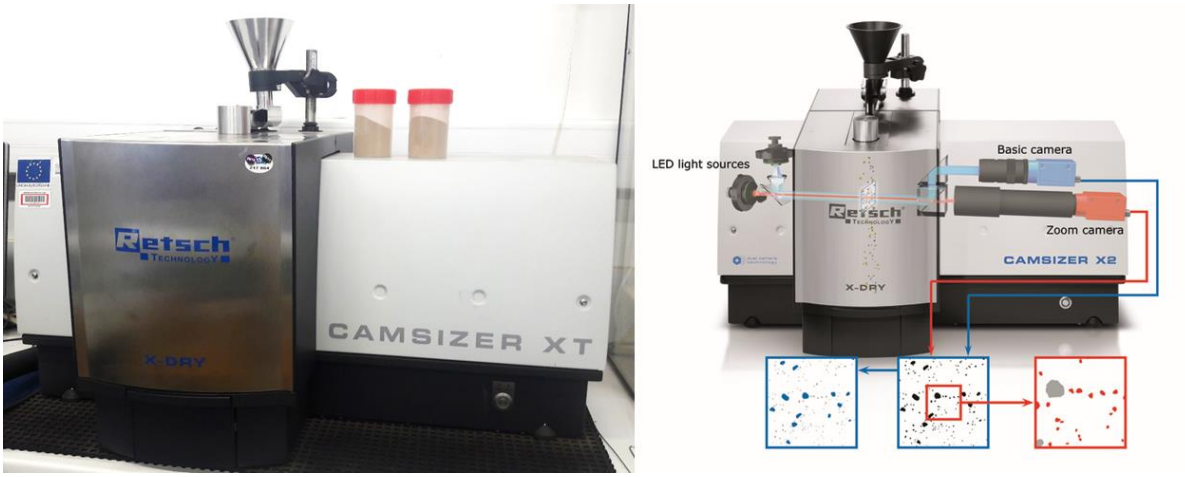

Figure 48: Left, particle size analyzer Camsizer XT from Retsch. Right, Camsizer operating principle [74]

Approximately 40 mL of powder is placed in the funnel on top of the analyzer. Depending on the powder nature, two plug-ins can be used. With the X-fall plug-in, a non-agglomerated powder is dispersed by gravity only. With the X-jet plug-in, pressurized air breaks the agglomerates formed due to Van der Waals forces and electrostatic forces.

2D images of the particles are recorded. From these 2D images, the software measures the maximum and the minimum Feret's diameter. The Feret's diameter (or caliper diameter) is the measure of a particle size along one specified direction. It is the distance between the two parallel lines restricting the object perpendicular to that direction (Figure 49):

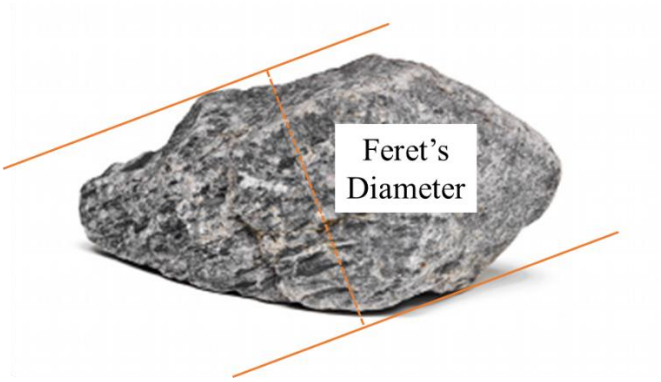

Figure 49: Feret's diameter of an object

Due to the fibrous nature of biomass, biomass powder particles can be considered as cylinders. Thus, for these powders, the minimum Feret's diameter corresponds to the cylinder diameter, and the maximum Feret's diameter corresponds to the cylinder length. The inorganic powder particles (talcum, sand, olivine…) are more spherical. The minimum Feret's diameter is considered as the sphere diameter. The relations between particles dimensions and Feret's diameters for both shapes are presented in Figure 50:

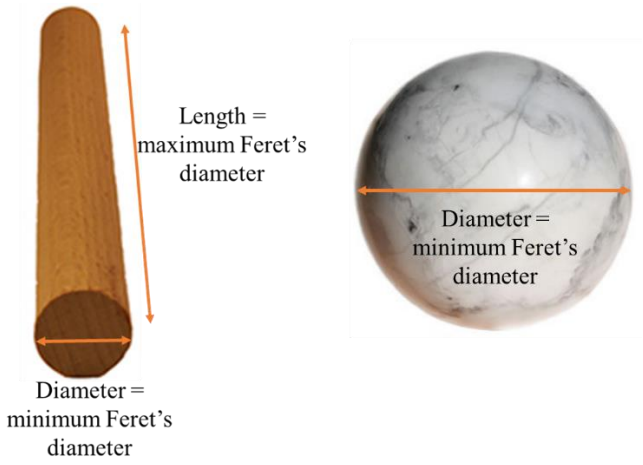

Figure 50: Relationship between a biomass particle dimensions and Feret's diameters for a cylinder (left) and a sphere (right).

The software calculates the volume of each particle knowing its shape and Feret's diameters. Therefore, the volumetric fraction of each grain size is known. For example, a powder grain size distribution can be presented as the volumetric fraction as a function of the minimum Feret's diameter.

The aspect ratio is the ratio of the minimum Feret's diameter over the Maximum Feret's diameter. It ranges from 0 for a very elongated particle to 1 for a particle as large as it is long.

2.3. Moisture content

The moisture content is the quantity of water contained by the powder sample. It is presented in mass percentage and in wet basis (wt%, wet basis)

Humid mass definition:

$$m_H = m_W + m_D$$

Moisture content definition:

$$H = \frac{m_W}{m_H}$$

m_H: Mass of the humid powder (kg)
m_D: Mass of the dry powder (kg)
m_w: Mass of water in the humid powder (kg)
H: Powder moisture content (wet basis) (-)

2.3.1. Moisture content measurement

The moisture content measurements are performed in the moisture balance Orma Thermored (Figure 51). It consists of a cup, placed on a balance and heated by a halogen lamp. The cup is preheated to 120 °C before the tare. Then, three to six grams of powders are placed in the cup. The balance is heated to 120°C until the powder mass is a constant (0% moisture content). The sample moisture content is displayed on the balance screen.

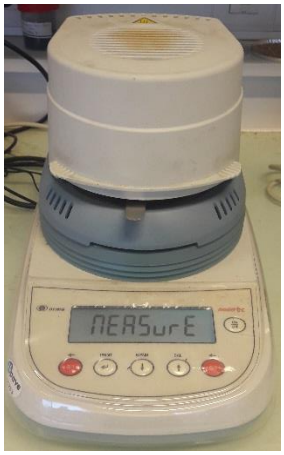

Figure 51: moisture balance Orma thermored

This method has several benefits:

- It is quick (less than an hour) compared with the oven drying method for example
- A small sample is required (4 to 6 grams)

2.3.2. Powder humidification

Flowability tests are performed for different moisture contents. The different moisture contents are obtained by spraying water on a powder until it reaches around 20 wt% , knowing that the initial moisture content of the powders is between 2 and 5 wt%. Then the powder is dried in a hoven, as presented in Figure 52:

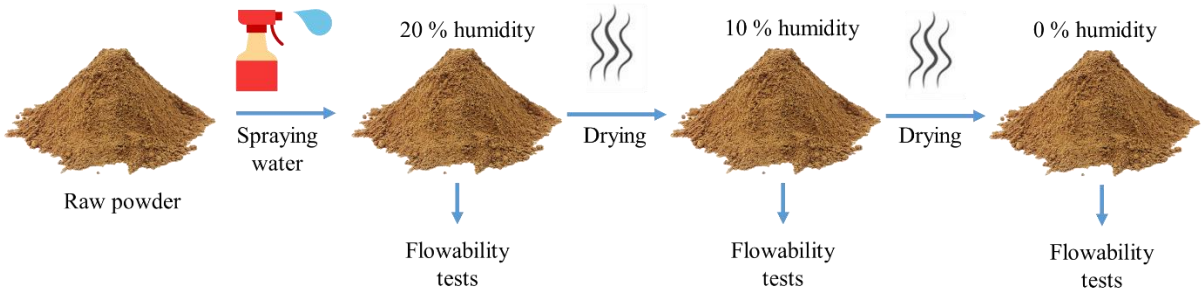

Figure 52: process to change the moisture content of powders

After it has been humidified or dried, the powder is placed in an airtight bucket for at least two hours. Then, flowability tests are performed: shear test, avalanche angle measurement and density measurement.

2.3.3. Volume increase calculations

To evaluate the volume increase of the powder with the addition of water, the swell factor is calculated, knowing the aerated densities and the moisture content of the powder:

Swell factor:

$$V_H = V_D(1 + Swell\ factor)$$

$$Swell\ factor = \frac{V_H}{V_D} - 1 = \frac{\rho_D}{\rho_H} * \frac{m_H}{m_D} - 1$$

Thus, by combining the equations:

$$Swell\ factor = \frac{\rho_D}{\rho_H} * \frac{1}{1 - H} - 1$$

With:
V_H: Volume of the humid powder (m^3)
V_D: Volume of the dry powder (m^3)
m_H: Mass of the humid powder (kg)
m_D: Mass of the dry powder (kg)
ρ_H: Density of the humid powder (kg/m^3)
ρ_D: Density of the dry powder (kg/m^3)
H: Powder moisture content (wet basis) (-)

2.4. Granulation process

The granulated powder preparation comes from the patent “Method for processing a biomass powder by wet granulation with a view to introducing same into a reactor, associated biomass powder, application to biomass gasification,” [73]. It consists of producing spherical granules with a diameter below 1mm, by adding a binder and water to a powder until liquid bridges appear between the particles. The selected method is the following: a mass of 70g of oak powder is mixed with 7g of ground binder (below 100 µm) and 140 g of water (starch is transformed in a gel by boiling it in 140g of water and then added to the wood powder). The mixture is placed in a tray and agitated with rotary motions until spheres appear (Figure 53):

Figure 53: Granulation method. On the left, mixture in the tray being agitated. On the right, wet granulated mixture.

The granules are then placed in an oven at 105°C for eight hours. By evaporation of the water, the liquid bridges become solid bridges. Solid bridges give enough strength to the spheres for them to be manipulated in the gasification process context. The granules are then sieved under 900µm (for the different batches to have approximately the same size distribution).

CHAPTER III: LABORATORY CHARACTERIZATION OF BIOMASS POWDER FLOW

Biomass powders present specific properties: low bulk density, elongated particles and polydispersed particle size. Due to these specific properties, they have poor flow properties. In the context of the process of gasification in entrained flow reactor, their flow is expected to be problematic. For example, they may form arches in hoppers, leading to interruptions in the process.

Therefore, the characterization of these powders is fundamental, to be able to anticipate the risks of interruption. The first steps of characterization take place in the laboratory. The avalanche measurements in a rotating drum and the shear tests are common tests to assess powder flow properties. Avalanche tests are easy to perform and give information on the flow of powders under their own weight. Shear tests were first established by Jenike [41]. They give information on confined flows of powders. Here, these tests are adapted to biomass powders and relations between the results they give are investigated.

Moisture content is known to have an influence on the flow of powders [75], [76]. However, few studies on the effect of moisture content on the flow of biomass powders have been done (For example, Sun [77] on cellulose powders and Crouter et al. [78] on starch and cellulose). The effect of moisture content on wood powders is assessed between 0 and 20 wt% (wet basis) on parameters derived from shear and avalanche tests.

Granulation consists of densifying the powder particles to form granules. Granulated biomass present better handling characteristics than raw biomass [43].

1. Preliminary experiments with the FT4

The biomass powders particles are elongated. Moreover, the shear cell used in this work, the FT4 from Freeman tech, is a rotational shear cell. Thus, a particle orientation on the shear plane when using the same sample for measuring the different shear points can be expected. This particle orientation could lead to a modification of the powder properties with the increasing number of measured points.

To assess the effect of particle orientation, a shear test at 3 kPa has been performed on a fine wood powder (powder D). At the end of the test, three points have been measured again, as presented in the table:

Table 6: Normal stress applied during the shear test. Repeated normal stresses are in bold.

Normal stress (kPa)
2.50
2.00
1.75
1.50
1.25
1
0.8
0.50
0.30
0.10
0.05
0.01
2.50
1.50
0.50

If there is a particle orientation, the measured shear stress of the repeated points will be different from the first measured point. The results are gathered in Figure 54:

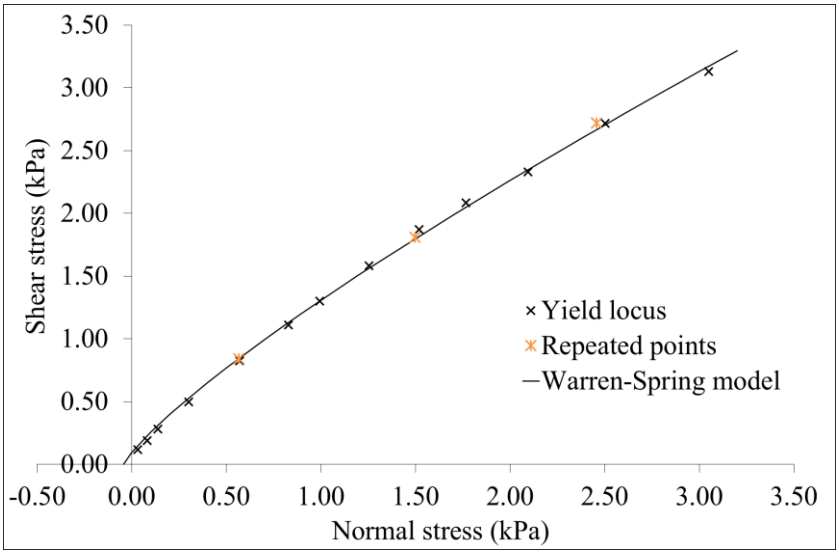

Figure 54: Yield locus of a wood powder and repeated points

The repeated points are close to the first measured points. Thus, if there is a particle orientation phenomenon, it does not affect the shear test results.

2. Effect of the number of avalanches with Revolution

The avalanche measurements are performed in a rotating drum. The drum rotates at 0.6 rpm and the powder behavior inside the drum is recorded thanks to a camera and a software. Several parameters can be derived from this experiment, such as the avalanche angle and the avalanche time. In this preliminary part, the influence of the number of recorded avalanches on those parameters is explored. Three experiments are performed by recording 150 avalanches, and 3 other experiments are performed recording 500 avalanches with the reference powder (fine oak powder). The results are gathered in the table:

Table 7: Influence of the number of avalanches recorded on avalanche parameters

	Av. angle (°)		**Av. angle span (-)**		**Av. time (s)**		**Av. time std dev. (s)**	
	Average	Std dev.	Average	Std dev.	Average	Std dev.	Average	Std dev.
500 avalanches	62.7	0.6	0.55	0.06	1.1	0.0	0.8	0.0
150 avalanches	65.3	1.2	0.43	0.06	1.1	0.1	0.8	0.1

There is an influence of the number of avalanches recorded on the avalanche angle distribution. With 500 avalanches, the avalanche angle (median of the distribution) is 2.6° lower. Moreover, the standard deviation of the avalanche is lower, meaning that experiments are more reproducible with more avalanches. However, this difference can be considered as low. The number of recorded avalanches has little influence on the span of the distribution.

Concerning the avalanche time distribution, the influence of the number of recorded avalanches is negligible. The experiments are highly reproducible even with only 150 avalanches.

In conclusion, the number of recorded avalanches only has a small influence on the avalanche angle, and a negligible influence on the other parameters. For the next experiments, 150 avalanches will be recorded.

3. Avalanche angle and shear test parameter correlation

Avalanche measurements and shear tests are common tests to assess the flowability of powders. The avalanche measurements are easy to perform. In the rotating drum Revolution, 150 avalanches are recorded and the avalanche angle is considered as the median of the angle distribution. This parameter is interesting because it is easy to get, however it is not yet well related to particle properties (other rotating drum measurements seem to be related to the inter-particular forces, such as the time between two avalanches [34], [79]).

The shear test in the FT4 requires more skills to be performed although it is automated. Numerous quantitative parameters can be derived from this test, such as the cohesion, which is representative of the inter-particular forces (van der Waals forces [80] and electrostatic forces [33] for instance). The flow of powders is influenced by the cohesion. Thus, this parameter can be used to compare the flowability of powders.

The objective of the study is to find a relationship between the avalanche angle and the parameters derived from a shear test. Thus, measuring a simple parameter, the avalanche angle, will give access to the whole yield locus of a powder, and the cohesion in particular.

First, the description method for the non-linear yield loci is described. Then, the model is built by finding relations between shear test parameters and the avalanche angle.

3.1. Description of non-linear yield loci

The Jenike procedure for shear tests consists of several steps (Chapter I, 2.4):

- First, the powder is preconsolidated by applying a normal stress. A shear stress is applied under this preconsolidation normal stress to reach the critical state.
- After this state is reached, decreasing normal stresses lower than the preconsolidation normal stress are applied, and a shear stress is applied until the sample yields.
- Between two measures of the shear stress at yield, the preconsolidation normal stress is applied to reach the critical state again.

The graph of the shear stress at yield as a function of the applied normal stress is the yield locus. With non-cohesive powders, the locus can be described with a straight line (with the preconsolidation point under the line). However, when plotting the data measurements performed at lower normal stresses (close to zero), the shear yield locus of the tested wood powders appears to be non-linear. An example of such a yield locus is presented in Figure 55 for the reference powder at 3 kPa preconsolidation.

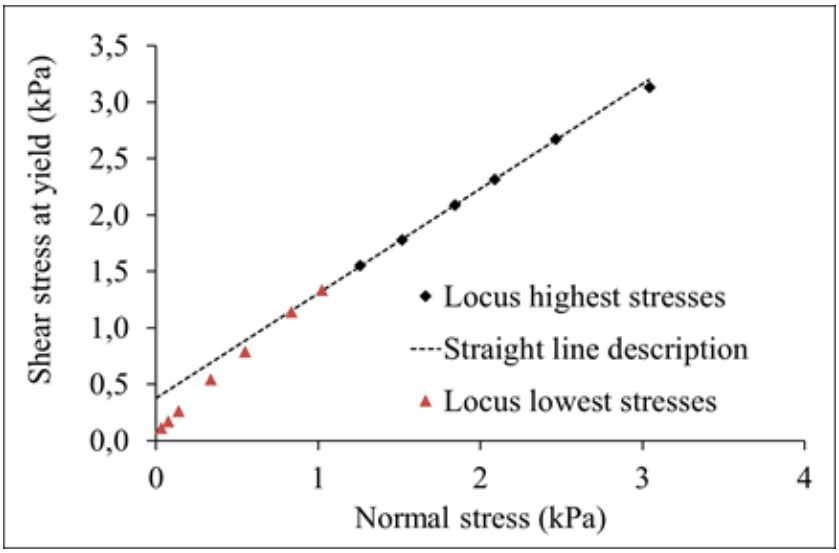

Figure 55: Shear yield locus of the reference powder at 3 kPa preconsolidation.

Thus, when fitting the data with the Mohr-Coulomb model (straight line), the cohesion, defined as the shear stress at 0 normal stress (Y-Intercept) is overestimated.

The Warren-Spring equation describes non-linear yield loci (see Chapter I, 2.4.3):

$$\left(\frac{\tau}{C}\right)^n = \frac{\sigma + T}{T}$$

Equation 1

τ: Shear stress (Pa)
C: Cohesion (Pa)
n: Warren-Spring index (-)
σ: Normal stress (Pa)
T: Tensile strength (Pa)

To fit the Warren-Spring equation to the experimental yield locus, one of the 3 parameters has to be measured first. Ashton et al. recommend [44] to measure separately the tensile stress T. To avoid this measurement which requires an additional device, it is proposed here to determine the cohesion by extrapolation of the yield locus. A second order polynomial fits correctly the data. The Y-Intercept of the polynomial is taken as the cohesion C. Then the parameter tensile stress T and the Warren-Spring index n are determined by fitting the Warren-Spring equation to the experimental data (with $1 < n < 2$). An example of a yield locus described with this method is presented in Figure 56.

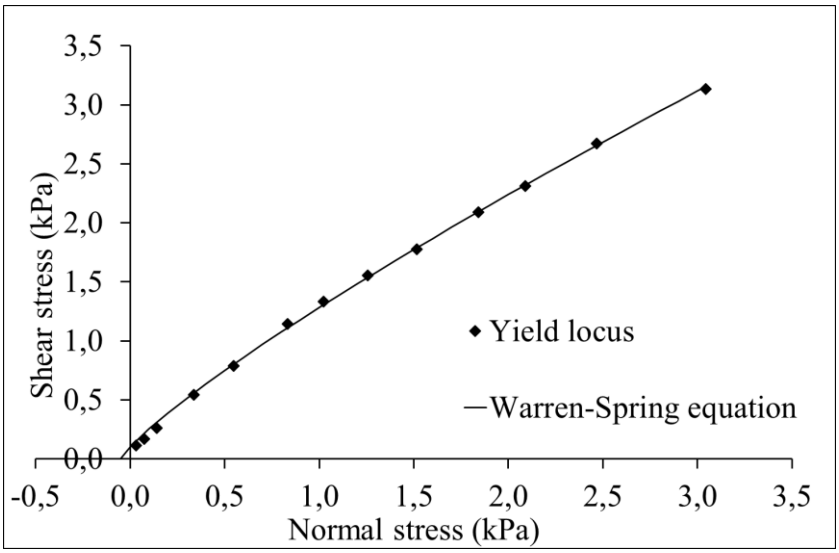

Figure 56: Shear yield locus of a wood powder at 3 kPa preconsolidation, described with the Warren-Spring equation (parameter C derived from a polynomial).

This method enables to describe the yield locus without measuring T. The Warren-Spring equations fits correctly the experimental data ($R^2 = 0.9997$).

3.2. Correlation between Warren-Spring parameters and other flowability measurements

The method presented above allows to obtain the Warren-Spring parameters for each powder. In this part, relationships are determined between each Warren-Spring parameter, and then between the Warren-Spring parameters and the avalanche angle.

3.2.1. Relation between C and T

First, a relation between C and T has to be found. The tensile strength as a function of the cohesion is presented in Figure 57:

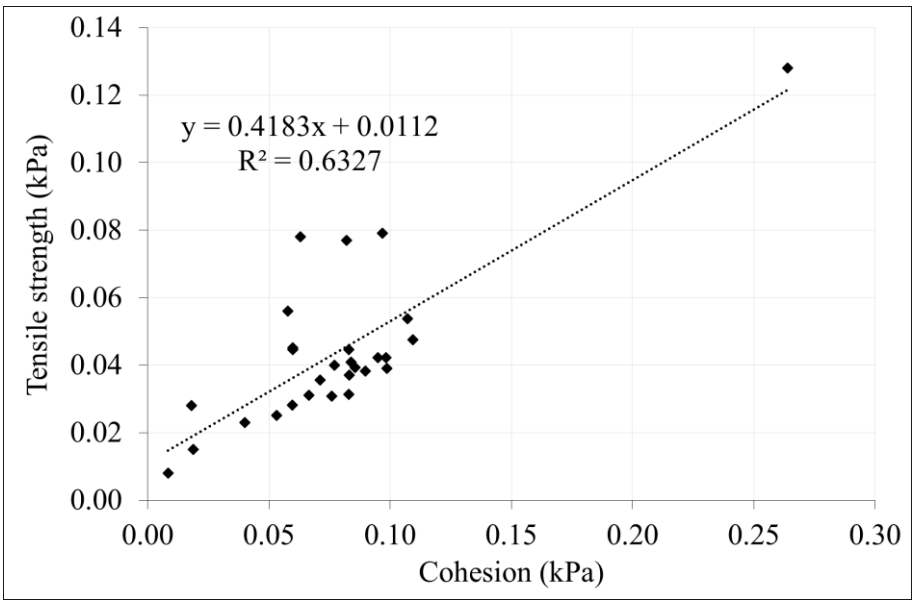

Figure 57: Relation between the tensile strength and the cohesion of the powders at 3 kPa preconsolidation.

There is no clear relation between these two parameters. Thus, the cohesion length is introduced. This parameter involves the aerated density. It is calculated as follows:

$$l = \frac{c}{\rho g}$$

Equation 2

With:
l: Cohesion length (m)
C: Cohesion (Pa)
ρ: Aerated density (kg/m3)
g: Acceleration of gravity (m/s²)

This length estimates the influence of the cohesive forces acting within the powder over the weight. The larger it is, the greater are the cohesive forces compared to the weight.

There is a relation between the parameters l and T/(ρg), as presented Figure 58 for the three preconsolidation stresses.

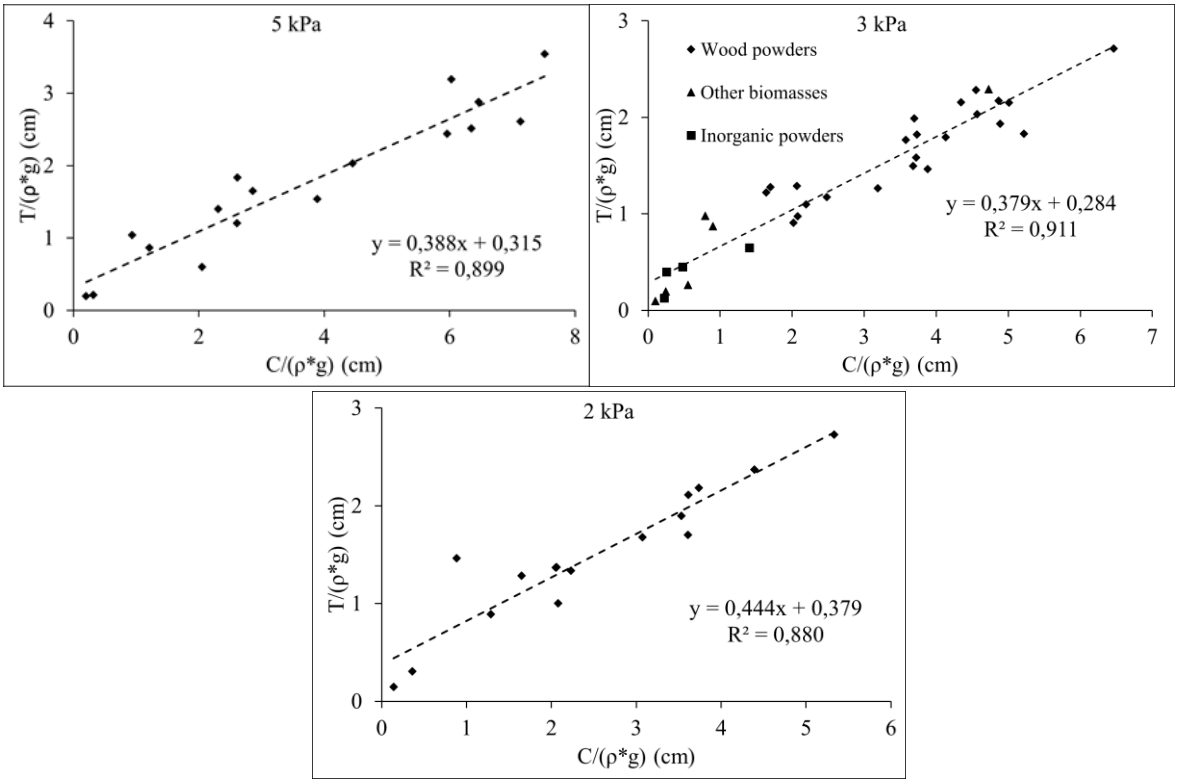

Figure 58: Relations between the parameters l and T for the three preconsolidations. In these graphs, each points corresponds to a single powder. Dotted lines are linear regressions.

The evolution of $\frac{T}{\rho g} = f\left(\frac{C}{\rho g}\right)$ is different than that of $T = f(C)$. There is a linear relation between $\frac{T}{\rho g}$ and $\frac{C}{\rho g}$ whereas there is no clear relation between C and T.

The relation is:

$$\frac{T}{\rho g} = a l + b$$

Equation 3

With:
T: Tensile stress (Pa)
ρ: Powder aerated density (kg/m3)
g: Acceleration of gravity (m/s²)
l: Cohesion length (m)
a: Constant (-)
b: Constant (m)

The parameters of this relation are gathered in the table below for the three consolidations stresses.

Table 8: Parameters of the relations between T and l

	Consolidation stress (kPa)		
	2	3	5
a (-)	0.444	0.379	0.388
b (mm)	3.79	2.84	3.15
R² (-)	0.880	0.911	0.899

This relation enables to get rid of the parameter T. But it is necessary to measure the aerated density. However, the aerated density is easier to measure than the tensile stress.

A relationship between these parameters is searched, derived from the Warren-Spring fit, and quantifying the powder flowability, and another flowability index obtained by the mean avalanche angle (the relation between the Warren-Spring index n and the other parameters is discussed later).

3.2.2. Relation between l and the avalanche angle

There is a relation between the cohesion and the aerated density, as presented Figure 59:

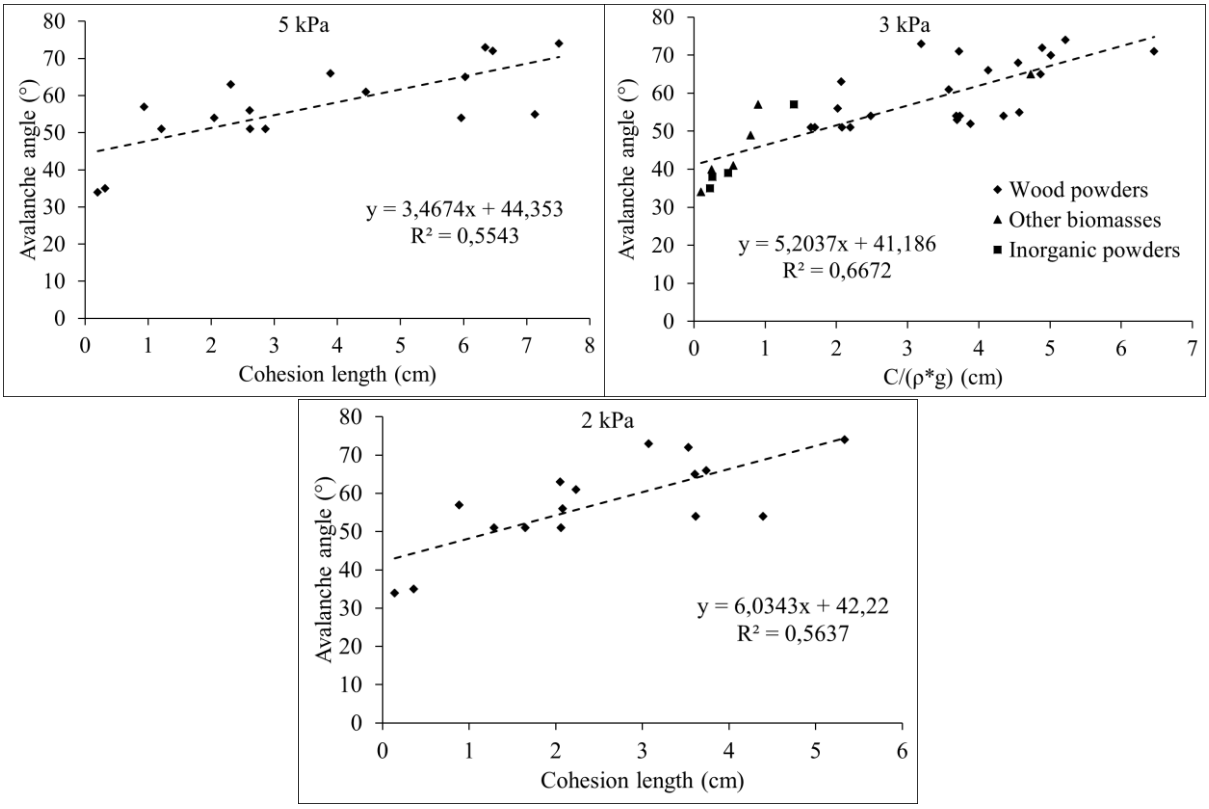

Figure 59: Relations between the parameters l and the avalanche angle for the three consolidations

The relation is:

$$\text{Angle} = \alpha l + \beta$$

Equation 4

With:
Angle: Avalanche angle (°)
α: Constant (°/m)
l : Cohesion length (m)
β: constant (°)

The parameters of the equation 4 for the three preconsolidation stresses considered in this work are gathered in the table below:

Table 9: Parameters of the relations between the avalanche angle and l

	Consolidation stress (kPa)		
	2	3	5
α (°/cm)	6.03	5.20	3.47
β (°)	42.22	41.19	44.35
R^2 (-)	0.564	0.667	0.554

Thus, it is possible to approximate the cohesion of a powder by only measuring its avalanche angle and aerated density. Measuring these 2 parameters requires much less time, effort (and skill) than the determination of the yield locus with a shear cell device.

However, the correlation is not perfect. In particular, the powder with the lowest cohesion length, have an avalanche angle of 30° whereas 40° are predicted. The relative gap between the cohesion obtained with the yield locus description method (part 3.1) and the cohesion calculated with Equation 4 is:

$$\text{Relative gap} = \frac{C_{method} - C_{equation6}}{C_{method}} * 100$$

Equation 5

With:
Relative gap: Relative gap (%)
C_{method}: Cohesion obtained with the yield locus description method (Pa)
$C_{equation4}$: Cohesion calculated with Equation 4 (Pa)

The relative gap as a function of the cohesion length is presented in Figure 60 for the three preconsolidations that have been considered in this work.

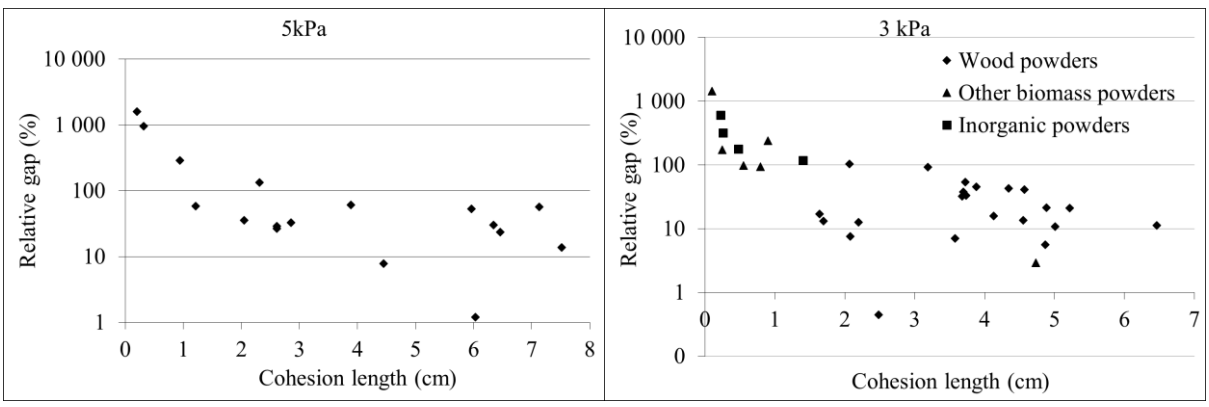

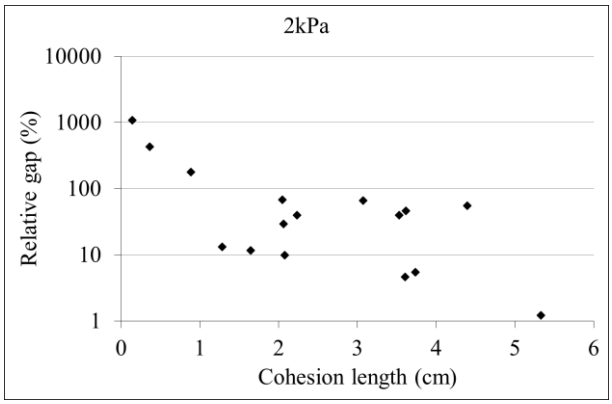

Figure 60: Relative gap as a function of the cohesion length for the three preconsolidation stresses

The relative gap is very high (> 100 %) for low cohesion lengths (< 1.5 cm). For cohesion lengths higher than 1.5 cm, the average relative gaps drop: 39 % at 5 kPa, 29 % at 3 kPa and 32% at 2 kPa. From the Equation 4, a cohesion length 1.5 cm corresponds to an avalanche angle of 50°. Thus, for the relative gaps to be as low as possible, the cohesive length has to be greater than 3 cm, which corresponds to an avalanche angle of 50° for this series of material.

3.2.3. Relation between n and the other Warren-Spring parameters

The preconsolidation point is not a constant for different powders at a given preconsolidation stress. However, for all the tested powders with l > 1.5 cm, at a given preconsolidation, the shear stress at the consolidation point can be considered as a constant, as presented in the table below. This may be due to the close nature of these powders (biomass, mainly wood).

Table 10: Average value of the shear stress at the preconsolidation point

σp (kPa)	Average τp (kPa)	Standard deviation (kPa)
5	4.96	0.33
3	3.03	0.17
2	2.06	0.14

Thus, it is possible to write the Warren-Spring equation at the preconsolidation point (σp; τp):

$$n = \frac{\ln\left(\frac{\sigma_p}{T}+1\right)}{\ln\left(\frac{\tau_p}{c}\right)}$$

Equation 6

With:
n: Warren-Spring index (-)
σp: Preconsolidation normal stress (Pa)
τp: Preconsolidation shear stress (Pa)
T: Tensile stress (Pa)
C: Cohesion (Pa)

By combining Equation 6 with Equation 3 and Equation 4, the Warren-Spring index n can be expressed as a function of the avalanche angle and the aerated density.

3.2.4. Model for the yield locus

The three parameters of the yield locus are related to the avalanche angle and the aerated density, with Equation 6, Equation 3 and Equation 4. Thus, it is possible to predict the yield locus of the powders (with an avalanche angle > 50°) at 2, 3 and 5 kPa preconsolidation stresses by measuring the avalanche angle and the aerated density. An example of predicted yield loci at 3 kPa preconsolidation with the model is presented below:

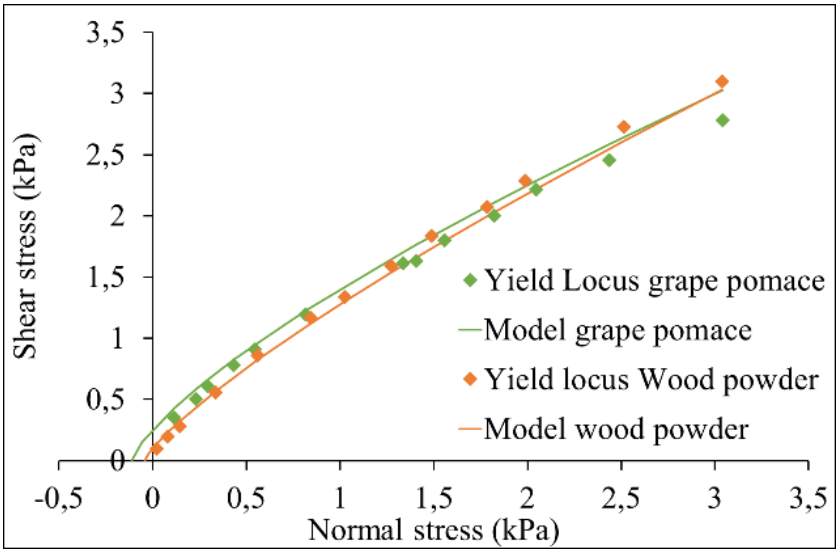

Figure 61: Yield locus at 3 kPa preconsolidation and corresponding model for two biomasses

As the model is forced to go through the average preconsolidation point (3; 3.03), it does not fit accurately to the data obtained with the highest normal stresses. This model is adapted for a powders with a close angle of internal friction. However, for low normal stresses, and the cohesion in particular (Y-intercept), the model describes correctly the data.

3.3. Conclusions on the correlation

A new method for non-linear yield locus description is proposed, based on the Warren-Spring equation. It does not require to measure the tensile stress. The model describes accurately the experimental data.

Based on experimental data obtained with thirty-three different powders (mainly wood) and at three preconsolidation stresses (2, 3 and 5 kPa), the Warren-Spring parameters cohesion, tensile stress and Warren-Spring index have been expressed as functions of easy to measure parameters: the avalanche angle and the aerated density. The cohesion, which is a key physical parameter of powder flowability, can be assessed with this method.

For cohesive biomass powders with an avalanche angle higher than 50°, the yield locus can be modelled. This model is particularly adapted to model the mechanical behavior in the lowest stress range.

This work has highlighted a method to estimate the cohesion and describe the yield locus of cohesive biomass powders from easy to measure parameters. It enables to compare their flowability in the context of a confined flow, for example the emptying of a hopper

4. Influence of moisture content on the flowability

The influence of moisture content on the flowability of wood powders is assessed by performing flowability tests at different moisture contents. The flowability tests consist of shear tests, measurements of the avalanche angle and measurements of the aerated density.

4.1. Swelling and density

The aerated density measures show that density is approximately a constant when the moisture content of powders is modified, as shown in the table:

Table 11: Aerated density measurements and corresponding swell factors for the eight powders at different moisture contents

Powder	H dry basis (wt%)	Aerated density (-)	Swell factor (%)
1. Resinous	0.0	0.159	0.0
	9.9	0.172	9.1
	24.1	0.178	21.5
2. Ground resinous	0.8	0.2	0.8
	5.4	0.208	5.1
	23.2	0.208	22.3
3. Beech 0-1000	0.0	0.315	0.0
	16.7	0.337	15.6
	31.2	0.333	29.5
4. Beech 0-200	0.0	0.213	0.0
	15.1	-	-
	30.2	0.211	30.5
5. Oak 1	0.0	0.27	0.0
	12.3	0.275	12.1
	28.5	0.26	29.6
6. Coarse oak 1	0.0	0.276	0.0
	11.0	0.293	10.4
	23.6	0.292	22.3
	41.4	0.276	41.4
7. Oak 2	0.0	0.248	0.0
	11.1	0.254	10.8
	25.0	0.249	24.9
8. Whillow	0.0	0.221	0.0
	12.9	0.243	11.7
	24.2	0.241	22.3

This is attributed to the swelling of wood powders with the addition of water. A constant density means that the increase in mass due to the addition of water is offset by the swelling.

4.2. Moisture adsorption isotherm

Moisture adsorption isotherms give information on the tendency of a powder to adsorb humidity when exposed to a humid atmosphere. The moisture adsorption isotherm of wood at 21°C is taken from the Wood Handbook [81] and is shown in Figure 62. It is fitted using last square regression to the GAB equation [78]:

$$Moisture\ content\ (dry\ basis) = \frac{C_G K W_M \left(\frac{P}{P_0}\right)}{(1 - K\left(\frac{P}{P_0}\right))(1 - K\left(\frac{P}{P_0}\right) + K C_G \left(\frac{P}{P_0}\right))}$$

C_G: Constant parameter (-)
K: Constant parameter (-)
W_M: Mass of water taken up per gram of solid equivalent to monomolecular coverage (-)
P/P_0: Relative vapor water pressure (-)

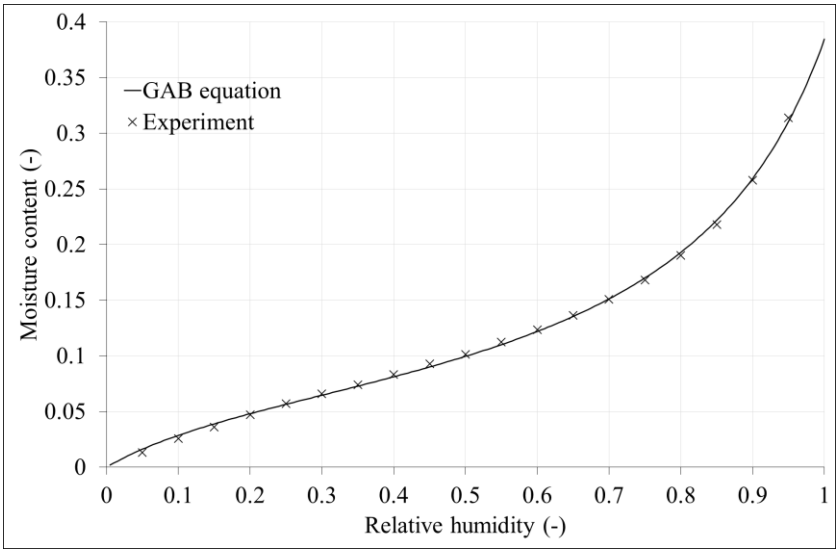

Figure 62: moisture adsorption isotherm of wood at 21 °C [81] and GAB equation description

From this isotherm and the GAB equation fitting, parameters can be derived. W_M (GAB equation parameter) corresponds to the fraction of water sorbed equivalent to monomolecular coverage of the particles. Another transition can be derived, W_G. It corresponds to the transition from glassy to rubbery state. It is identified as the point at which the isotherm curves rapidly upward. The obtained parameters for a wood powder are summarized in the table below:

Table 12: Summary of the parameters from the fitted GAB equation

Parameter [81]	
W_M (wet basis) (wt%)	6.7
W_G (wet basis) (wt%)	15
K (-)	0.82
C_G (-)	6.5

However, in this study, the powders have not be humidified by water vapor adsorption, but with liquid water and the dried (desorption). The involved phenomena are different, thus the transition parameters

W_M and W_G can be different. Moreover, these results are presented for one wood powder, whereas six different woo powders (including torrefied powders) are presented in this study. These parameters are provided for informational purpose.

4.3. Influence of moisture content on flow parameters

The influence of moisture content on the flowability is assessed using five parameters: avalanche angle, avalanche time (time between two avalanches), avalanche angle, avalanche angle distribution span, cohesion length and coefficient of internal friction.

4.3.1. Avalanche angle and avalanche angle distribution span

The behavior of the powder inside the drum while it rotates can give information on its flowability. The avalanche angle is a dynamic measurement: it is the angle of the surface of the powder before an avalanche, while the drum rotates. It assesses the ability of a powder to flow under its own weight: a low avalanche angle indicates that the powder has a high flowability. On the contrary, a high avalanche angle means the powders has a low flowability. Indeed, while the drum rotates, the powder rises in the drum. Thus, a non-cohesive powder will start to flow for a small increase of the angle since its angle of repose is low. A cohesive powder will be able to be moved from this position thanks to the cohesion between its particles, and will collapse at a higher angle.

For a powder with a high flowability, the avalanches occur at a similar angle, the avalanche angle distribution span is narrow. On the contrary, for a powder with a low flowability, avalanches of small amounts of powder can occur for different avalanche angles, resulting in a large span. Figure 63 shows the avalanche angle of the eight powders:

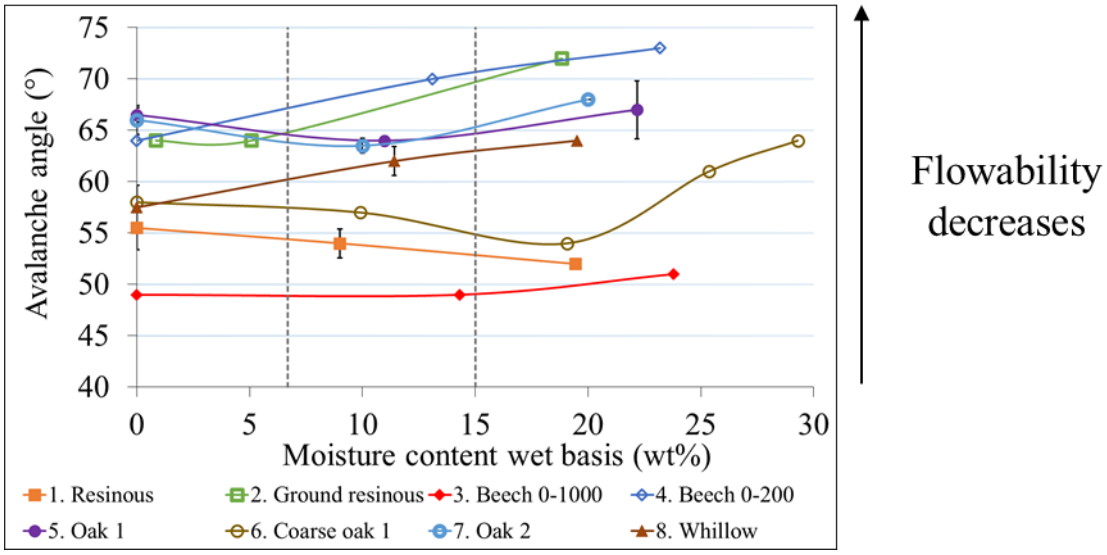

Figure 63: Evolution of the avalanche angle with moisture content.

As presented in the correlation between Warren-Spring parameters and avalanche angle (3.2), the avalanche angle varies with both the cohesion and the aerated density. Since the density is approximately a constant because of the offset between swelling and mass increase due to the addition of water, the only effect on flowability is the contribution of cohesion. The effect of addition of water on cohesion is the apparition of liquid bridges. The liquid bridges may appear after the monolayer coverage is reached (the fraction of water necessary has been assessed in the previous part: WM = 6.7 wt% wet basis). However, it seems that the changes in flowability due to the addition of water were not large enough to

be observable on the avalanche angle. Thus, the effect of moisture content on the avalanche angle distribution span is summarized in Figure 64:

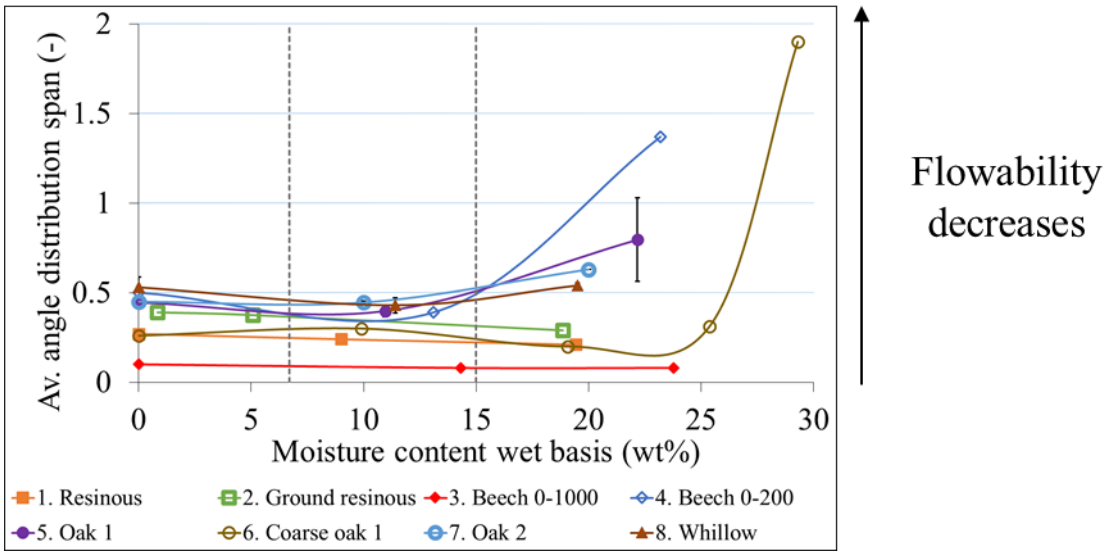

Figure 64: Evolution of the avalanche angle distribution span with moisture content.

There is a visible effect of the moisture content increase on the span for powders 4, 5, 6 and 7. Indeed, with increasing moisture content and the apparition of liquid bridges increasing the cohesion, the powder can reach higher avalanche angles, but the small avalanches keep occurring. This results in a higher span, observable on powders 4, 5, 6 and 7. For powder 1, 2, 3 and 8, this effect is not observed in the range of moisture content investigated.

4.3.2. Avalanche time and avalanche time standard deviation

The avalanche time is the time between two avalanches. When a powder is cohesive, the powder can rise over a long period of time while the drum rotates before collapsing. On the contrary, a non-cohesive powder while collapse as soon as it rises, like a liquid. Therefore, there is an inverse relationship between avalanche time and flowability. Moreover, a powder with a high flowability flows regularly and the avalanche time has a low standard deviation. The results of avalanche time measurements are gathered in Figure 65:

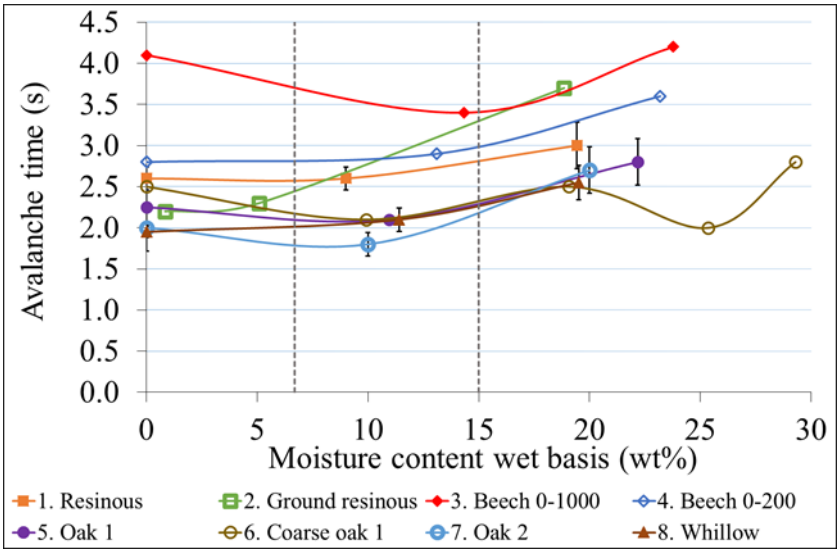

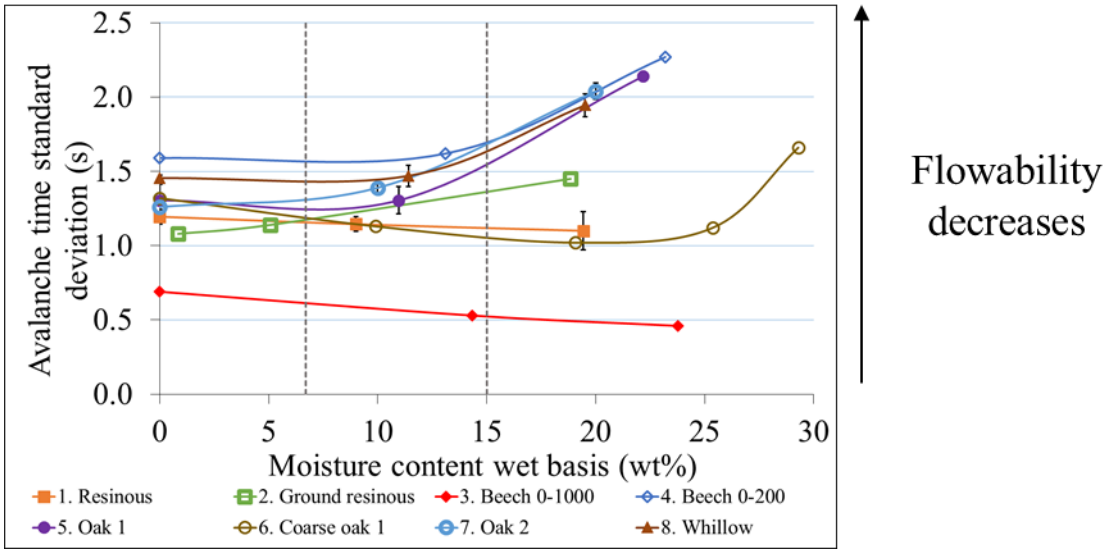

Figure 65: Top, Evolution of the Avalanche time with the moisture content. Bottom, evolution of the avalanche time standard deviation with moisture content for the eight powders

About the avalanche time, except for the powders 3 and 6, the avalanche time is initially constant and then increases after 15% moisture content is reached. This is due to the increase of particle cohesion because of the formation of liquid bridges, after the monomolecular coverage is reached. The increased cohesion results in a decreased flow uniformity. However, the increase is small. It would have been more easily observable with a slower rotation of the drum. Indeed, the time between two avalanches depends on the rotation speed. The lower the rotation speed, the longer the time between two avalanches.

This trend is also observable, and more obviously, with the increased standard deviation after 15% moisture content is reached.

Concerning the powders with no observable trend (3 and 6 on the avalanche time graph), the liquid bridges between particles may appear for a larger moisture content. This is why no evolution is observed for these powders in this moisture content range.

4.3.3. Cohesion length

The cohesion length assesses the intensity of cohesive forces over the weight. A high cohesion length indicates that the cohesive forces are stronger than the weight. Thus, the powder has a low flowability. On the contrary, a low cohesion length indicates that the weight is stronger than the cohesive forces, thus the powder has a good flowability. The results of cohesion length measurements are gathered in Figure 66:

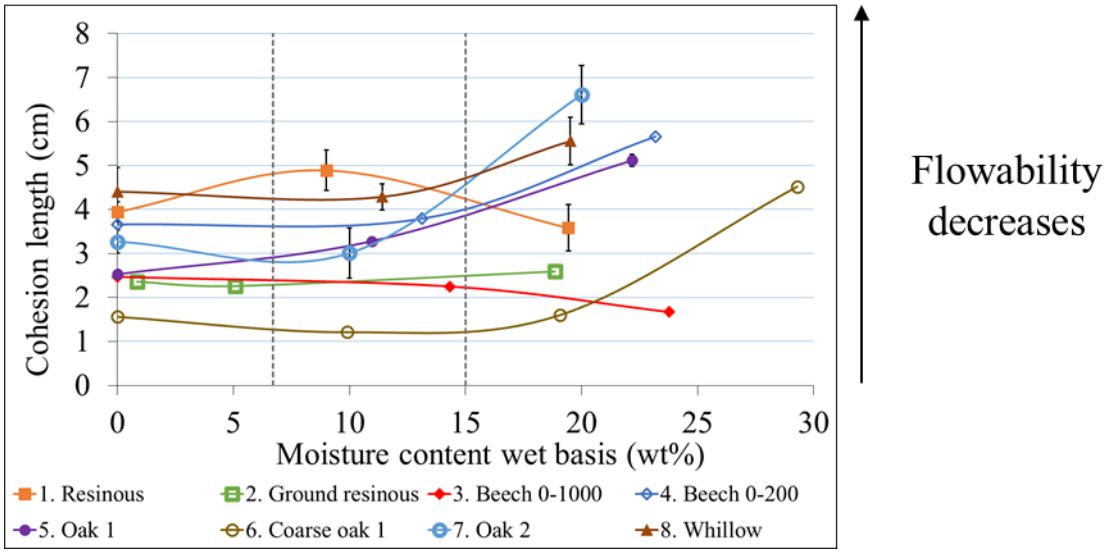

Figure 66: Evolution of cohesion length with moisture content for the eight powders

The same trend than for the avalanche time measurements are observed with this parameter. After 15% moisture content is reached, the cohesive forces start to take precedence over the weight, which has been shown to remain approximately a constant with the increasing moisture content. However, the cohesion length is more difficult to get because two experiments are necessary, and one of them is the shear test. Thus, to assess the changes in flowability of a powder with its moisture content, the avalanche time measurements seem to be more appropriate because they are easier and faster to perform.

4.3.4. Coefficient of internal friction

The coefficient of internal friction assesses the intensity of the friction between the grains within the powder. It depends on the surface properties and chemical nature of the grains. The results are gathered in Figure 67:

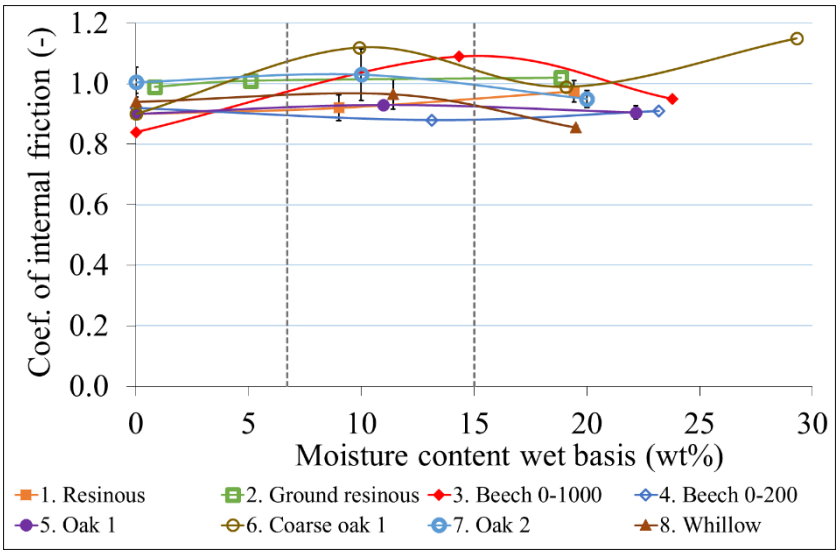

Figure 67: Evolution of the coefficient of internal friction with moisture content for the eight powders

It appears that the coefficient of internal friction is approximately constant and equal to 1 for all the powders. Here again, it seems that the changes in the surface properties due to the addition of water

were not large enough to change the coefficient. With this parameter, there is no observable or consistent trend.

4.3.5. Effect of grinding

Wood can be either softwood or hardwood. The structures of both these types of wood are different at a microscopic scale, as presented in the figure below:

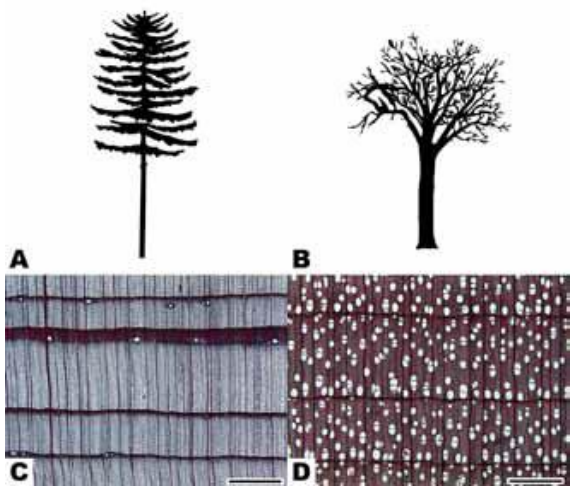

Figure 68: A, the general form of a generic softwood tree. B, the general form of a generic hardwood tree. C, transversesection of Pseudotsuga mensiezii, a typical softwood; the thirteen round white spaces are resin canals. D, transverse section of Betula allegheniensis, a typical hardwood; the many large, round white structures are vessels or pores, the characteristic feature of a hardwood. scale bars = 780 µm. [81]

One feature of hardwood is the presence of pores, which are vessels conducting water. Their diameter typically ranges from 50 to 200 µm. Thus, for coarse ground powders (around 1mm), the pores may be still present, while for fine ground powders (like the reference powder) they may disappear.

There is an effect of grinding on the flowability of the powders. Powders 5 and 6 come from the same wood chips. They have comparable behavior for moisture contents below 15%. When 15% is reached, the flowability of the fine powder 5 decreases strongly whereas the coarse powder 6 does not change before 25% moisture content is reached. Moreover, powder 7, which is an oak powder with the same grinding as powder 5, has a similar comportment to that of powder 5. Thus, an explanation is that for the fine powders, the pores have disappeared, whereas they are still present in the coarse powder. The water accumulates on the surface of the fine powder, resulting in the formation of liquid bridges and decreasing the flowability. However, the water first accumulates in the pores of the coarse powder, the liquid bridges in powder 6 appear once the pores are filled with water, for a higher moisture content.

The effect is less obvious with powders 1 and 2, which are softwood, without pores.

4.4. Conclusions on the influence of moisture content on the flowability

Moisture content is known to be a parameter influencing the cohesion of powders, and therefore their flowability [75], [76]. In the case of biomass powders, wood in particular, the effect of moisture content up to around 20 wt% (wet basis) has been assessed by performing avalanche and shear tests, and measures of the aerated density.

First the addition of water in biomass powders has a small influence on their density, due to a swelling phenomenon, offsetting the mass increase.

The effect of addition of water on the different parameters shows that the flowability of wood powders starts to change when the moisture content reaches 15 wt% (wet basis), which corresponds to the glass-rubber transition, as shown in part 4.2. This effect is more obvious on parameters such as avalanche time and avalanche time distribution standard deviation.

There is an effect of the particle size on the flowability with increasing moisture content for hardwoods (oak, beech). Indeed, hardwood present small pores, that disappear for fine grinding. For a fine powder, the liquid bridges can form directly on the surface of particles, whereas for a coarse grinding, the water has to fill the pores first. Therefore, the flowability of fine powders decreases more for smaller moisture contents than coarse powders.

5. Granulation

The granulation process investigated in this work is based on a patent [73] (see appendice). It consists of transforming a raw, cohesive biomass powder into spherical granules with a diameter around one millimeter by wet granulation using a binder (preferably a biomass waste, but also starch). The interests of this method are:

- A small maximum grain size, around 1 mm, which is the maximum grain size of a powder that can be injected in an entrained flow gasifier.
- The use of biomass waste binders. They do not change the thermal parameters of the raw powder. Moreover, this method is a way to valorize them.
- The improvement of the powder flowability.

In this part, the influence of granulation on the flowability of the reference powder is assessed.

5.1. Influence on the particle shape and size

Particle size and particle shape are parameters with a strong influence on the flowability. For a particle size below 100 µm approximately, cohesive forces become stronger than the weight. Moreover, spherical particles are not subjected to interlocking particles, contrary to elongated particles. The raw oak powder and a granulated oak powder (with orange peels) have been observed with a binocular magnifier, as presented in the figure below:

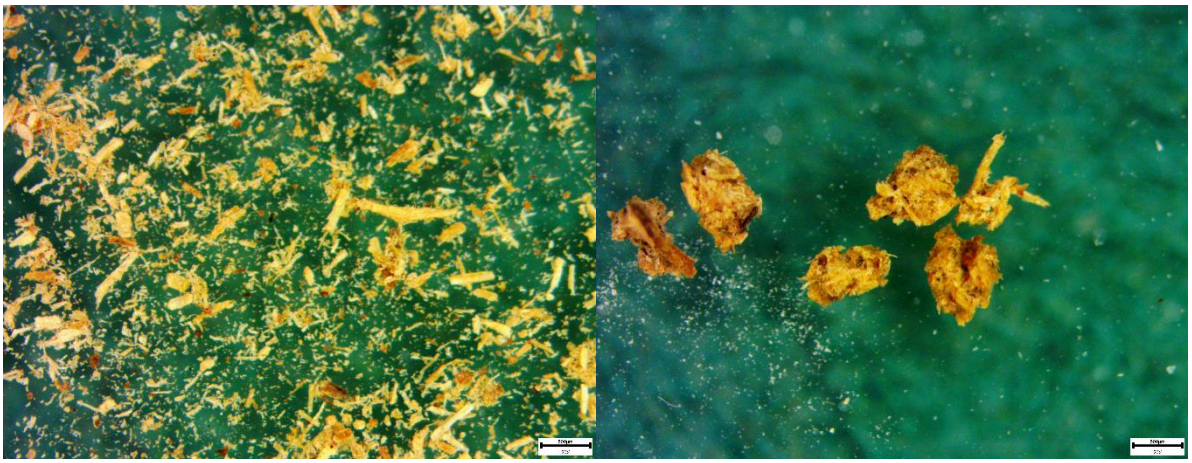

Figure 69: Left, raw oak powder (scale: 500µm). Right, granulated oak powder with orange peels (scale: 500 µm)

As a first observation, the raw powder seems to have a larger size distribution, more elongated particles and to be generally smaller than the granulated powder. The granulated powder particles look spherical, however some particles protrude out of the aggregate. They are not perfectly spherical and can therefore be subject to interlocking too.

The results obtained with the particle size analyzer Camsizer-XT are gathered in the table below and in Figure 70. The aspect ratio is the ratio of the minimum Feret's diameter of the maximum Feret's diameter. It ranges from 0 for a very elongated particle to 1 for a particle as large as it is long.

Table 13: Size measurement results obtained with the camsizer-XT for the raw oak powder and the granulated powder (with orange peels)

	Granulated oak (orange peels)	Raw oak
d10 (µm)	364	9.3
d50 (µm)	586	22
d90 (µm)	830	98.5
Span (-)	0.8	4.1
Mean aspect ratio (-)	0.70	0.62

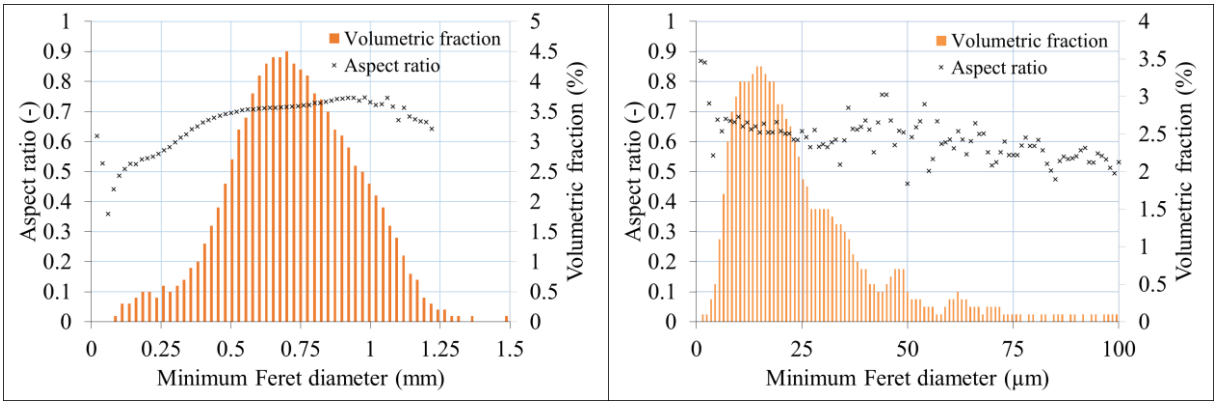

Figure 70: Particle size distribution and aspect ratio of the granulated oak powder (left) and the raw reference powder (right)

As observed with the binocular magnifier, the particle size of the granulated powder is larger than the raw powder (see table 13). Most of the particles of the raw powder have a diameter far below 500 µm, which is the magnifier scale. Thus, they are note observable on the picture. The d_{10} of the granulated powder is above 100 µm, meaning that the majority of the particles is above the threshold where the cohesive forces become greater than the weight. On the contrary, the d_{90} of the raw powder is below 100 µm, meaning that the majority of the particles are below the threshold. Thus, it is expected that the negative effect of a small particle size on the flowability is stronger with the raw powder than with the granulated powder.

The size distribution span measures the spread of the distributions. A large span means that small particles can be inserted between larger particles, thus increasing the number of contact points between the particles. A larger number of contact points means a higher friction and more interlocking, leading to a lower flowability. The span is 0 for a monodispersed particle size. For example, for a powder with a factor 10 between d_{10} and d_{90} it can be approximately 2. The raw powder span is very high, 4.1, meaning that the interlocking and friction forces are more intense than the granulated powder with a span of 0.8 (see table 13). Here again it is expected that the negative effect of a large span is stronger with the raw powder than with the granulated powder.

The aspect ratio is the ratio of the minimum Feret diameter over the maximum Feret diameter of a particle. In the case of biomass particles, which are identified as cylinders, it corresponds to the diameter and the length of the cylinder. An aspect ratio close to 1 means that the particle is not elongated, and therefore less prone to interlocking. An aspect ratio below one means that the particle is elongated and prone to interlocking. The mean aspect ratio of the raw powder is lower than the granulated powder (table). Indeed, the global aspect of the raw powder particle is cylinders, whereas the aggregates are more spherical. Thus the granulation lowers the aspect ratio of the powder and lowers its tendency to interlock.

However, the mean aspect ratio of the raw powder could have been expected to be lower, considering the needle-like particles observed in Figure 69 (picture on the left). However, as explained by Guo et al. [24], for high energy breakage of the particles (like grinding), cross-sectional breakage is possible, leading to a higher aspect ratio for smaller particle size. Thus, the smaller particles (not visible on the picture, but representing a bigger proportion of the volume) have a higher aspect ratio than the larger particles (visible on the picture) (see evolution of the aspect ratio with the minimum Feret diameter in Figure 70).

A decrease of the aspect ratio is observed at lower particle size for the granulated powder. This decrease can be due to the presence of non-granulated powder with a smaller aspect ratio.

Finally, the aspect ratio is more dispersed with the raw powder than with the granulated powder. This may be due to the size of the of the particle size ranges, which are very small for the raw powder (1µm) and larger for the granulated powder (20µm). Larger particle size ranges smooth the results.

5.2. Influence on flowability

To assess the effect of granulation of the flowability, avalanche angle and aerated density measurements have been performed. The granulated powders results are gathered in the table below.

Table 14: Avalanche angle and aerated density tests results for powders granulated with different binders and the raw powder

Binder	Avalanche angle (°)	Av. Angle span (-)	Density (-)	Av. time (s)	Av. time std dev. (s)
Sunflower seed shells	48	0.08	0.22	5.5	0.31
Sorghum	50	0.08	0.19	5.6	0.34
Grape seed cake	50	0.08	0.21	5.5	0.36
Empty fruit bunch (palm tree)	50	0.08	0.21	5.8	0.48
Sugar cane	52	0.08	0.18	6.2	0.32
Starch	48	0.06	0.25	5.2	0.27
Seaweed	51	0.07	0.2	5.9	0.4
Orange peel	50	0.07	0.24	5.2	0.26
No binder (raw powder)	61	0.41	0.29	2.4	1.51

A first observation is that the binder used to granulate the powder has a low influence on the behavior of a granulated powder. In the next parts, the granulated powder flowability will be compared with the raw oak powder.

5.2.1. Avalanche angle and span

The avalanche angle assesses the ability of a powder to flow under a low normal stress. A low avalanche angle means a high flowability (fluid-like behavior) and a high avalanche angle means a low flowability. It varies from about 35° for non-cohesive powders (sand, semolina) to about 70° for biomass powders with a low flowability (low density, high cohesion) (see part 3). The avalanche angle of the granulated powders is 49.9° in average (1.36° standard deviation). The avalanche angle of the raw powder is 61°. Thus, the granulation allows to improve the avalanche angle by 11.1° over a 35° range. There is a strong improvement of the flowability with the granulation method.

The avalanche angle distribution span measures the spread of the distribution. For a powder with a high flowability, the avalanches occur at a similar angle, the avalanche angle distribution span is narrow. On the contrary, for a powder with a low flowability, avalanches of small amounts of powder can occur for

different avalanche angles, resulting in a large span. It is thus an assessment of the powder flowability. The span of the granulated powders is 0.08 in average. The span of the raw powder is 0.41, that is, 5 times as large as the granulated powders. Thus, as well as the avalanche angle, the span indicates a strong improvement of the powder flowability with the granulation.

5.2.2. Avalanche time and avalanche time standard deviation

The avalanche time is the time between two avalanches while the drum rotates. A non-cohesive powder collapses regularly, whereas for a cohesive powder small amounts of powders fall irregularly between two large avalanches, resulting in a smaller avalanche time with a larger standard deviation on the distribution. Thus, there is a negative relation between avalanche time and flowability and a relation between avalanche time standard deviation and flowability. For the granulated powders, the avalanche time is 5.6s in average (0.34s standard deviation). It is approximately twice as small for the raw powder, indicating once more an improvement of the flowability with the granulation. This conclusion is even more obvious with the standard deviation of the avalanche time distribution: it varies from 1.51s for the raw powder to 0.34s in average (0.07s standard deviation) for the granulated powder, indicating a large improvement in the flow regularity.

5.2.3. Aerated density

The aerated density has been shown to be a parameter with a positive effect on the flowability (see chapter II, 3.2). In this case, the density decreases with the granulation. It was originally 0.29 and decreases to 0.21 in average with the granulation (0.02 standard deviation). However, the density of the granulated powder depends on the way it has been sieved. Indeed, in this case, the granulated powder is sieved under 900µm. However, a starch granulated powder sieved under 1.5mm shows a density of 0.31. Indeed, for a more polydispersed powder, the smaller grain can fill the empty spaces between the larger particles, increasing the density.

5.3. Comparison with a coarse raw powder

The improvement of flowability observed with the granulation could be attributed to the size increase. To assess the effect of size, a coarse raw powder has been produced using the same oak chips that have been used to produce the reference powder. Then it has been sieved to 900 µm (like the granulated powder).

5.3.1. Size and shape considerations

The results obtained with the Camsizer-XT are presented in Figure 71 and table below:

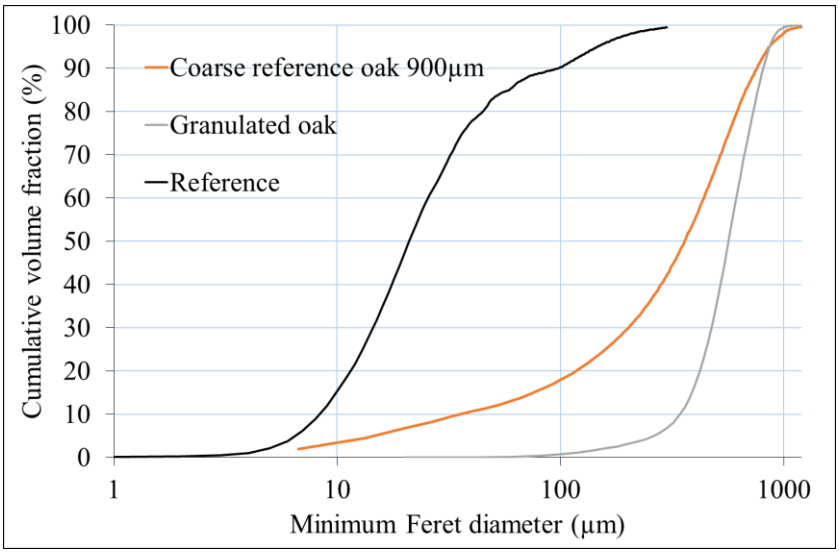

Figure 71: Volumetric size distribution of the granulated, coarse and raw powders

Table 15: Size measurements results obtained for the granulated, coarse and raw powders

	Granulated oak (orange peels)	**Reference (raw oak)**	**Coarse oak**
d_{10} (µm)	364	9.3	43
d_{50} (µm)	586	22	367
d_{90} (µm)	830	98.5	760
Span (-)	0.8	4.1	1.95
Mean aspect ratio (-)	0.70	0.62	0.47

Concerning the size distribution, the coarse powder mean diameter is higher than 100µm (367µm). Thus its size is closer to the granulated powder than the raw powder. Moreover, both the granulated and the coarse powders have been sieved under 900µm, resulting in close d90 (830 and 760 µm respectively). However, like often observed with biomass powders, it contains fine particles (d10 = 43µm), resulting in a high span (1.95). Concerning the shape, the mean aspect ratio of the coarse powder is 0.47, which is lower than the raw powder (0.62). This means it is more elongated. Indeed, as explained in 5.1, for high energy breakage of the particles (like grinding), cross-sectional breakage is possible, leading to a higher aspect ratio for smaller particle size.

The coarse powder has a higher mean particle size than the raw powder, which can be considered comparable to that of the granulated powder. Thus, only considering this parameter, it could be expected to have an improved flowability. However, it contains fine particles, has a large span and a low aspect ratio, decreasing the flowability. The coarse powder is expected to have a lower flowability than the granulated powder. The flowability will be assessed in the next part with the avalanche angle measurement.

5.3.2. Avalanche angle measurement

The avalanche angle measurements for the reference powder, the granulated powder and the coarse powder are gathered in the table below:

Table 16: Avalanche angle measurements for the coarse powder, compared with the granulated and the reference powders

	Avalanche angle (°)	Avalanche angle span (-)	Avalanche time (s)	Av. time std deviation (s)
Reference	61	0.41	2.4	1.51
Granulated oak (orange peels)	50	0.07	5.2	0.26
Coarse oak	59	0.28	2	1.03

As expected in the previous part, the flowability of the coarse powder is lower than the granulated powder. The avalanche angle is 59°, close to the reference with 61°. The elongated particles (interlocking) and fine particle content (cohesion forces) allow the powder to rise in the drum, whereas the granulated powder particles collapse for a lower angle (50°).

Moreover, the avalanche angle span is comparable for the reference powder and the coarse oak (0.41 and 0.28) and substantially smaller for the granulated powder with 0.07. A small span indicates that the avalanches occur at the same angle, and the powder has a good flowability. Once again, the coarse oak in comparable to the reference powder and has a low flowability compared with the granulated powder.

Conclusions are the same for the avalanche time and the avalanche time standard deviation. Thus, the improvement of the granulated powder flowability is not only due to the increase in grain size. Rounder particles, low fine particle content and small grain size span are the main parameters improving the flowability of powders granulated with this method.

5.4. Conclusions on the granulation method

One of the first observable effect of the granulation method on the powder is an increase of the aspect ratio, meaning that the particles are less elongated. Less elongated particles are less likely to interlock, which improves their flowability. Another effect of the granulation is the modification of the particle size. The fine particle content (which strongly influences the flowability) is lower in the granulated powder (almost zero) and the mean size is larger. Moreover, the span of the granulated powder size distribution is very low compared to the raw powder, meaning that its size distribution is narrow. Powders with a narrow size distribution have a better flowability because of the reduced number of contact points between particles. These features give the granulated powder an expected improved flowability compared with the raw powder.

The effect of granulation on flowability has been assessed with avalanche measurements. Avalanche angle, avalanche angle span, avalanche time and avalanche time standard deviation show a strong improvement of the flowability with the granulation compared with the raw powder.

One could argue that the improvement of the granulated powder flowability is due to the size increase. To assess the effect of size, a coarse raw powder has been tested. Results show that the coarse raw powder has a similar behavior to the fine raw powder. The improvement of flowability is due to several factors (narrowing of the distribution, low fine content, sphericity), not only the size.

This method shows an improvement of the flowability of biomass powders at small scale. In the next part, the flowability of a granulated powder will be evaluated at the pilot scale.

CHAPTER IV: MATERIAL AND METHODS FOR THE STUDIES AT PILOT SCALE

Two studies are performed at pilot scale to characterize the flowability of biomass powders in conditions close to industrial conditions. The first one is a study of the flow of powders in an injection pilot called IRIS. The second is the injection of granulated powder in an entrained flow gasifier called Giroflé. The materials and methods used to perform these studies are presented in this chapter.

1. General description of the experiments

1.1. Description of the injection pilot IRIS

The injection pilot IRIS (**I**njection g**R**avitaire de b**I**oma**S**se) allows to experimentally study the gravity-driven injection of powder in a vessel (which acts as an entrained flow reactor). It already existed before the tests were performed and has not been modified. The objective is to inject powder with no variations of the flow rate. IRIS is composed of three hoppers, a screw feeder, an injection system and a vacuum pump (to recycle the powder and operate as a closed circuit). The injector tubes are long enough to pass through the reactor layers of insulation, and must have the smallest diameter to prevent backflow from the reactor to the hopper. The circuit is in a neutral atmosphere (nitrogen) to avoid the ATEX risk (O2 level below 8%). A picture and a schematic of the pilot are presented in Figure 72:

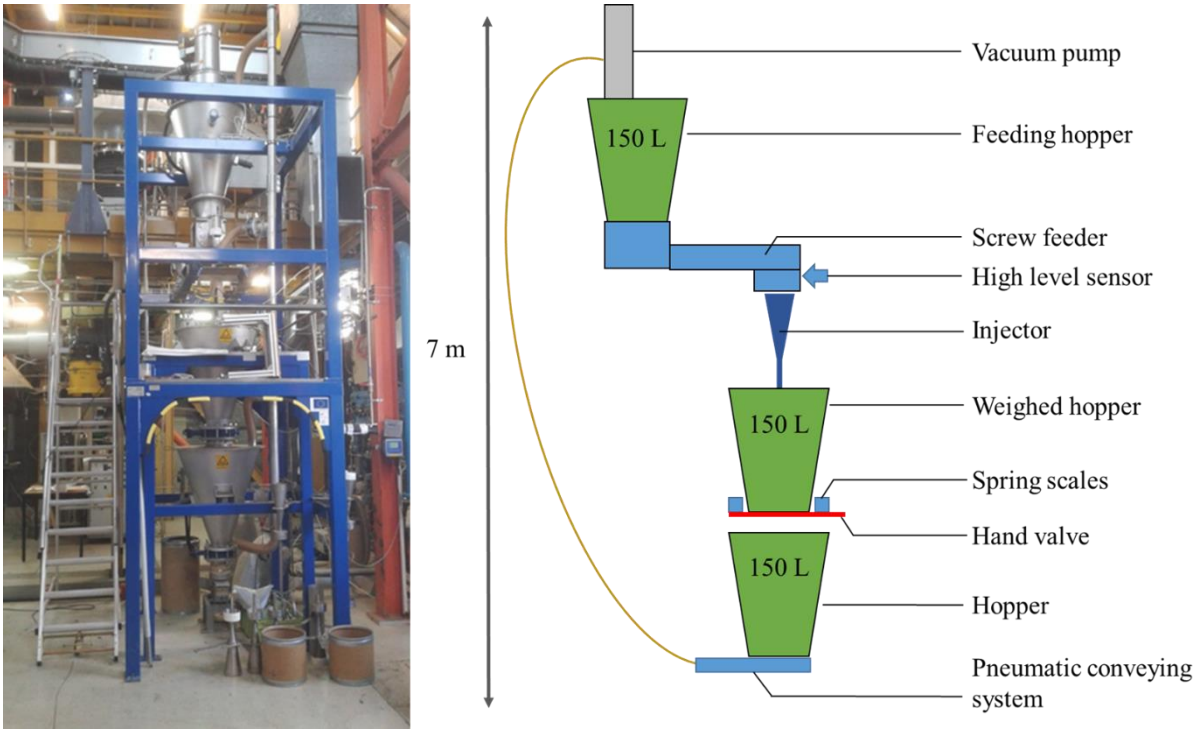

Figure 72: Picture and schematic of the injection pilot IRIS

An experiment is performed as follows: the powder from the feeding hopper is fed in the injector thanks to a Gericke screw feeder type GAC. The screw is equipped with an anti-bridging system (or bridge breaker), presented in Figure 73. This system rotates around the screw, ten times slower, and breaks the arches that could form above it.

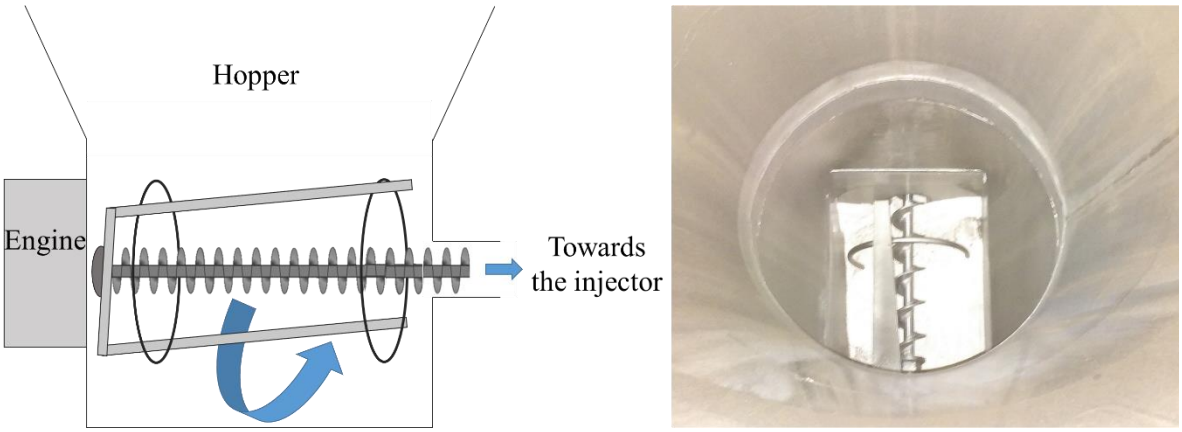

Figure 73: Schematic of the bridge breaker from the side and picture from above.

The injector consists of a conical part, followed by a discharge tube. The geometry of the injectors is presented in the next part. The powders flow through the injector and fall in the weighed hopper. If the level of powder in the injector increases (due to an arch for example), a high level sensor detects it and stops the experiment. The evolution of the injected powder mass is recorded with spring scales (maximum mass in the hopper: 30 kg). At the end of the test, the hand valve is opened to let the powder fall in the last hopper. Is sucked by the vacuum pump in the feeding hopper. Then, a new experiment can start.

1.2. Description of the gasification pilot Giroflé

Giroflé is a pilot of entrained flow gasification, located in the biomass research platform of CEA Grenoble (Génépi). A schematic and a picture of the gasifier are presented in Figure 74.

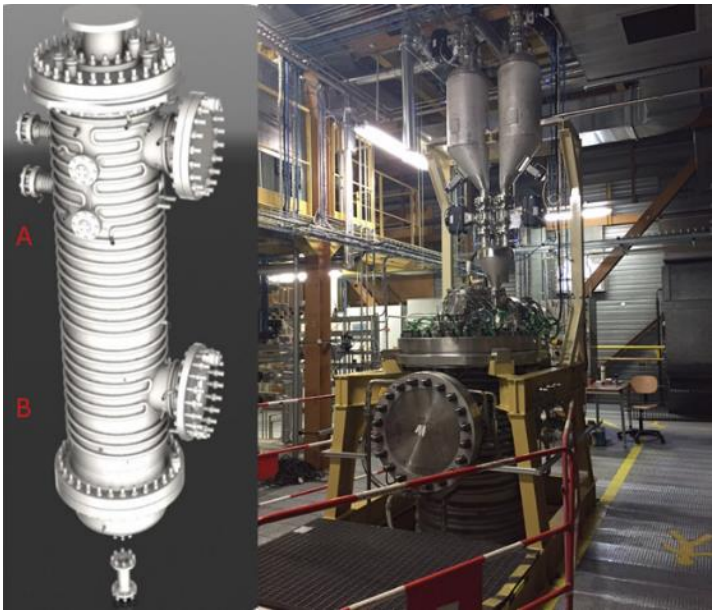

Figure 74: Left, schematic of the entrained flow gasifier. Right, picture of the upper part of the gasifier and the injection system

The biomass mass flow can reach a maximum of 50 kg/h, and the pressure will ultimately be able to reach 30 bars. It is heated either by oxycombustion of natural gas (allothermal mode) or by combustion of biomass (autothermal mode). The outside casing is cooled at 40°C using tubes coiled around the reactor.

The major gas productions are measured (CO, H_2, H_2O and CO_2), as well as minor gases, by gas chromatography. The flow rates are measured with a Coriolis flowmeter. The tar production is measured with a tar protocol. The rest of the production is burnt in a post-combustion system. Ashes and unburnt particles are collected in a quenching bath in the bottom of the reactor.

2. Materials

In this part, the materials used to perform the experiments at pilot scale are presented. First, the granulated powder, used in both facilities, is presented. Then, the powders used in the injection pilot are described. Finally, the powders injected powders in the gasifiers are presented.

2.1. Granulated powder

In both studies, a granulated powder is used to assess the benefit of this process on the flowability. The reference powder (see material and methods lab scale) is used as raw powder. The different steps for the manufacturing of the granulated powder are presented in Figure 75. The granulation process has been patented (see annex and reference [73]).

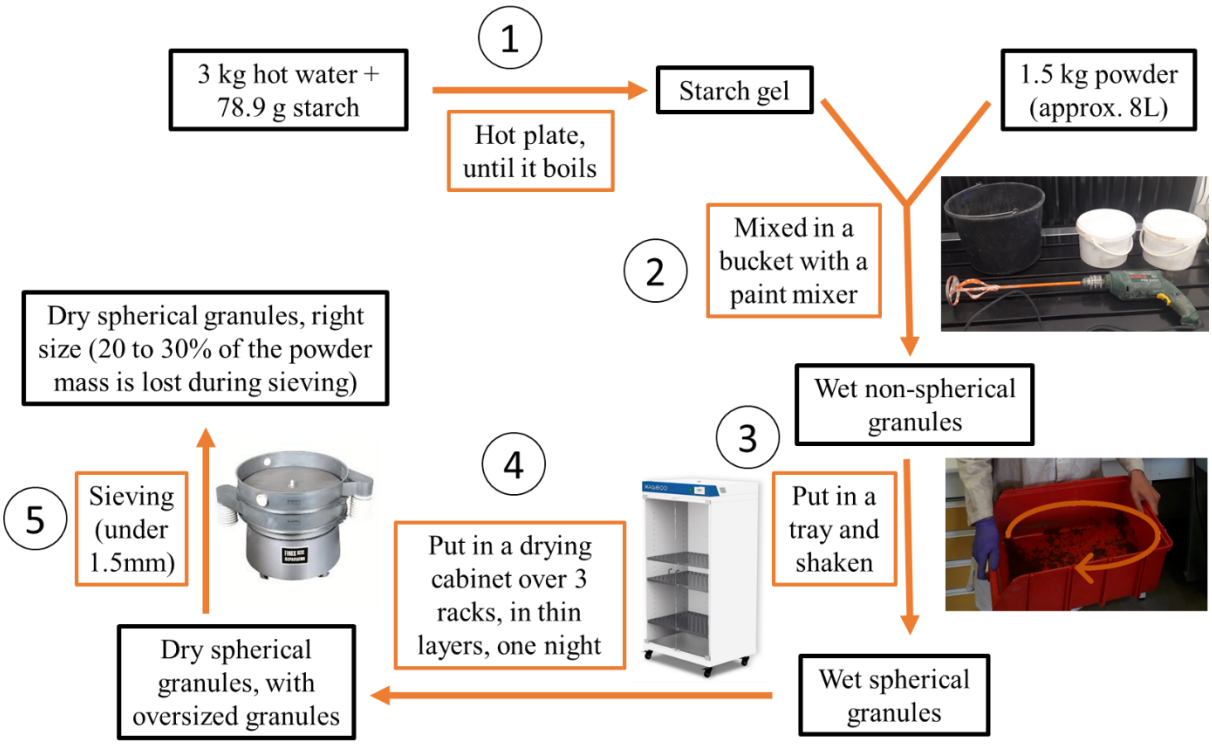

Figure 75: Procedure for the preparation of 1.5kg of granulated powder.

The different steps of the preparation are presented below:

Step 1: A starch gel is prepared by mixing 79 g of starch with 3kg of water and boiling the mixture.

Step 2: The starch gel is mixed with 1.5 kg of dry powder (5% by weight of starch in the dry matter). The mix is placed in a bucket and mixed with a paint mixer mounted on a drill. Small non-spherical granules appear.

Step 3: The handful of non-spherical granules is placed in a tray and shaken with circular motions until the granules are spherical.

Step 4: The wet spherical granules are placed in a drying cabinet in thin layers. They dry until their moisture content is approximately 7 wt%, wet basis (approximately 12h).

Step 5: The dry granules are sieved below 1.5 mm. 20 to 30% of the mass is lost during this step.

The dry sieved granules are places in a closed barrel to protect them from humidity. Wood stored with a moisture content below 17 wt% (wet basis) is prevented from decay [81].

A mass of 10 kg (33 L) is produced for the injection pilot tests, and 16 kg for the entrained flow gasifier test. The aerated density of the granulated powder measured with the FT4 is 307 kg/m^3.

2.2. Injection pilot IRIS

Six powders have been used to perform the tests in the injection pilot IRIS. They are presented in the table below:

Table 17: Powders used for the tests of injection with the pilot IRIS

No.	Supplier	Nature	Comment
1	cea	Reference oak.	Ground in a chain mill (see Chapter II, 1.1). Reference powder.
2a	cea	Reference oak torrefied (250°C, 1h15).	Ground in a universal knife grinder Forplex type FL2.
2b	cea	Powder 2a ground in a vibratory mill RITEC.	Sieved under 200µm. The fraction above 200µm is ground again in the vibratory mill.
3	cea	Reference oak granulated with 5% starch.	Dried and sieved under 1,5mm.
4	Lignex	Spruce or pine, 0-1000 µm.	Raw commercial product.
5	Oberflächentechnik Seelmann	Sandblasting glass microbeads, 70-110 µm.	Raw commercial product.

The size, shape and flow properties are presented in the results. The grinders are presented below.

2.2.1.1. Grinder Forplex type FL2

This grinder reduces the biomass size from chips (several cm) to a powder (< 2 mm). A picture of the grinder is presented in Figure 76:

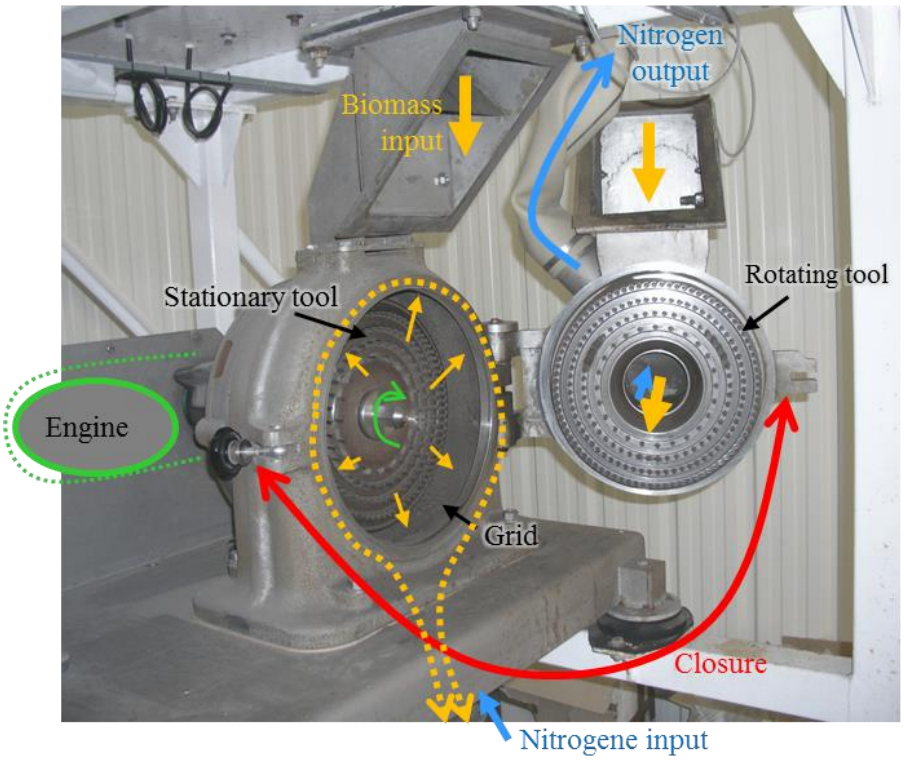

Figure 76: Picture of the grinder Forplex type FL2.

The biomass stored in a hopper passes on a vibrating conveyor and falls in the grinder. The rotating tool (knifes) reduces the biomass size. When the particles are small enough, they exit the grinder through the grid (1 mm). The ground biomass is stored in a barrel.

2.2.1.2. Vibratory mill RITEC

This mill reduces the biomass size and modifies the particle shape to improve their flowability. A picture of the mill is presented in Figure 77:

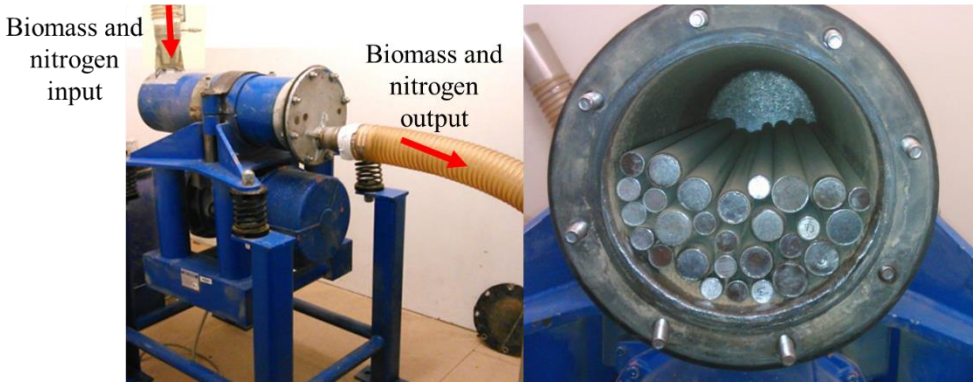

Figure 77: Picture of the vibratory mill RITEC. Left: closed. Right: open and filled with bars.

The grinding chamber is filled with steel bars. The mill, placed on springs, is shaken so that the bars bump into each other and against the walls. Biomass is introduced and the impacts reduce its size and modify its particle shape.

The mill is followed by a sieve (200 µm). The oversized fraction is ground again in the mill until it is small enough to pass through the sieve.

2.3. Gasification pilot Giroflé

For the entrained flow reactor test, the granulated powder has been used. To assess the effect of the granulation process both on the injection and the gasification, the same tests are performed with a raw wood powder. As the reference powder could not be injected because of its poor flowability, a raw commercial powder, Savour'hêtre SPPS (beech), has been selected for its improved flowability. First, as presented in Figure 78, it has a low content of fine particles, because it is sieved after grinding.

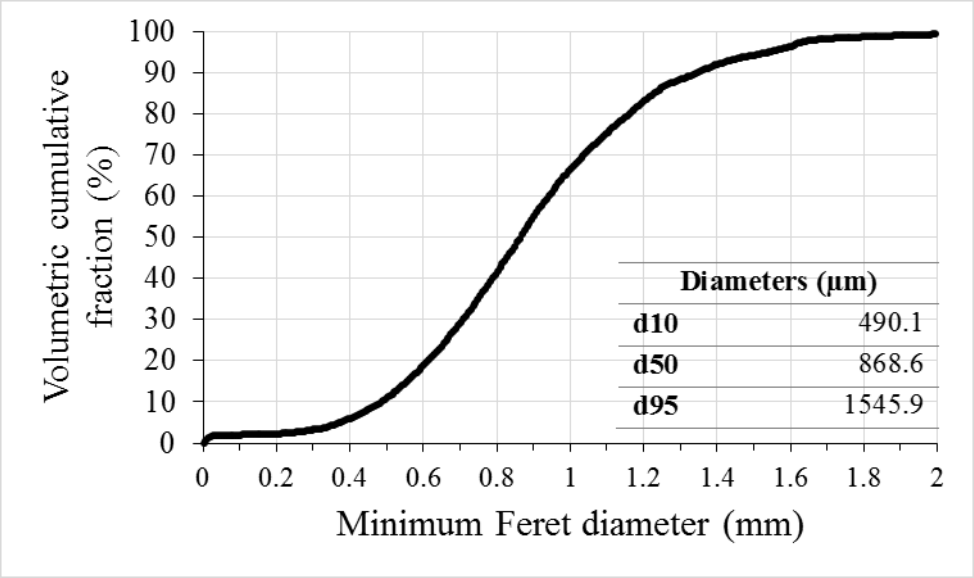

Figure 78: Cumulative particle size distribution of Savour'Hêtre SPPS (beech). Measure performed with the Camsize XT.

The d_{10} is 490.1 µm, meaning that 10% (in volume) of the particles have a diameter below 490.1 µm. This sieving is in favor of a good flowability. Moreover, the particles are not very elongated, as presented in Figure 79:

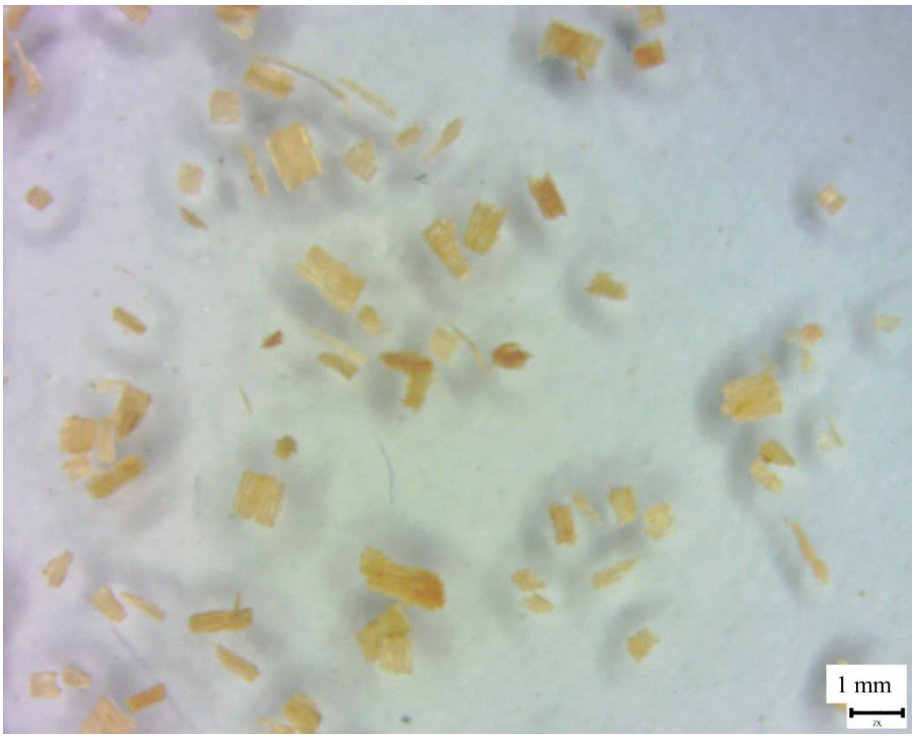

Figure 79: Picture of the particles of Savour'Hêtre SPPS.

They look like slightly parallelepipedal chips. Thus, the interlocking phenomena are less pronounced than with other biomass powders. The aerated density is 180 kg/m^3.

3. Methods

In this part, the methods used in the experiments are presented, first in the injection pilot and then in the gasifier.

3.1. Injection Pilot IRIS

3.1.1. Injector geometry

Injectors consist of a conical part followed by a discharge tube, made of standard stainless steel. The conical part has been sized according to Jenike's procedure, based on wood powder mechanical properties [41]. The optimal half vertical angle does not change for the different wood powders and it has been set to 10°. The length of the discharge tube is 200 mm. However, the diameter of the each injector is different, ranging from 6 mm to 20 mm.

A schematic and a picture of the injectors are presented below:

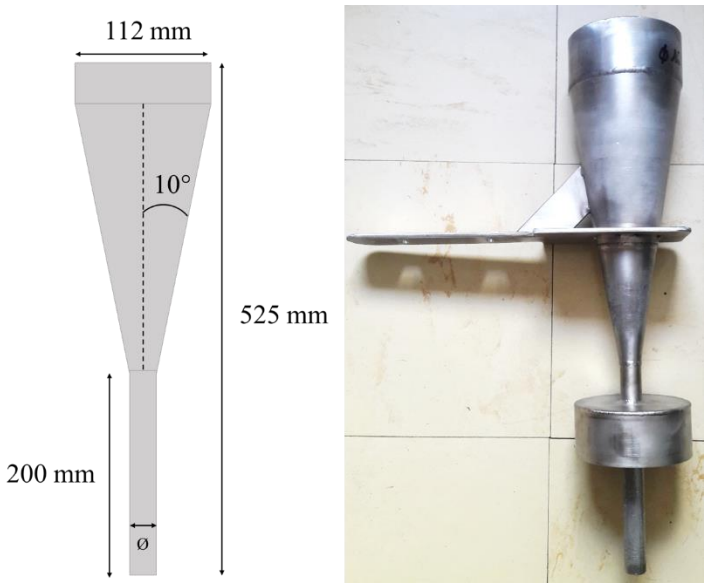

Figure 80: Schematic (not to scale) and picture of an injector

The parts appearing on the picture and not on the schematic are the fixation system.

3.1.2. Screw feeder geometry

The screw feeder is placed in the bottom part of the feeding hopper. It conveys the powder from the feeding hopper to the injector, as presented in the figure below:

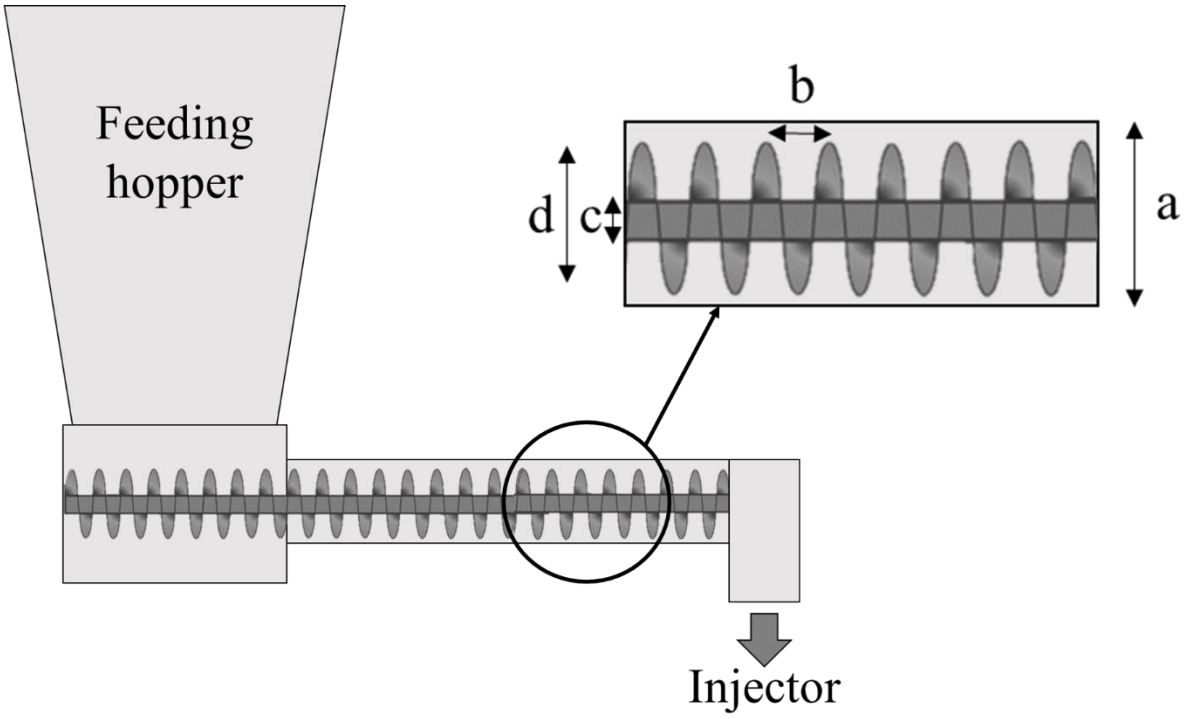

Figure 81: Location of the screw driver in the pilot and zoom on the screw to show the dimensions (not to scale). a, casing diameter; b, pitch; c, core shaft; d, screw flight

The geometric parameters of the screw feeder are gathered in the table below:

Table 18: Geometric parameters of the screw feeder.

	Diameter (mm)
a) Casing	57
b) Pitch	45
c) Core shaft	15
d) Screw flight	45

3.1.3. Conduct of the experiments

For each powder, the maximum injector diameter in which the level of powder increases in the injector (until it activates the level sensor) is searched, for each screw speed. Indeed, this diameter is expected to be an indicator of the powder flowability.

Before an experiment, the hoppers are filled with nitrogen to avoid explosive atmospheres. Once the O_2 level is below 8%, the feeding hopper is filled with the powder thanks to the vacuum pump. The powder is sucked from its container to the hopper with the tube (in yellow in Figure 72). The hand valve below the weighed hopper is closed. Thus, the powder mass will be recorded. An injector is attached between the screw end and the weighed hopper. Airtightness between the screw, the injector and the weighed hopper is maintained thanks to rubber sleeves.

At this point, the experiment can be started. It is controlled thanks to a software. The screw speed is set and the recording of the weight in the hopper is started. If the O_2 level is below 8% the injection starts. After powder started to be injected, the experiment can end for several reasons:

- **There is no more powder in the feeding hopper**: the mass displayed in the software is constant. The screw rotation is stopped manually in the software. In this case, after stopping the mass recording, the hand valve is opened. The powder falls in the bottom hopper and can be sucked again in the feeding hopper.
- **The high level sensor is activated**. In this case, the screw rotation stops automatically. There are two possibilities. The first case is the screw flow rate was too high compared with the outflow of the injector: the powder level rises in the injector. When the screw stops, the powder can exit the injector on its own. The experiment can be started again with a lower screw speed. The other case is an arch formed in the injector. In this case, the powder cannot exit the injector. The injector has to be detached and cleaned manually.
- **The maximum mass in the weighed hopper is reached**. The screw stops automatically to protect the spring scales. The hand valve is opened and the powder falls in the bottom hopper. The experiment can start again.

After an experiment, the hand valve is opened and the powder falls in the bottom hopper. The hand valve is closed again and the powder is sucked in the feeding hopper. Another experiment can start.

When the pilot is unused for a period of time (night, week-end), the powder may compact in the hopper. Thus, in this case, the powder is injected a first time without recording the mass to aerate it. Once aerated, the recorded experiments can start. With this procedure, the experiments are always performed with an aerated powder.

Several parameters can be set for an experiment:

- Nature of the powder. Six powders are tested.

- Volume of powder in the feeding hopper. The hopper is filled with 33.4 L (between 40 and 50 cm of powder in the hopper) for all the powders. The reference powder is also tested with 95 L (80 cm) and the microbead powder with 64.4 L (70 cm).
- Screw speed. Four speeds are tested: 47, 78, 125 and 155 rpm.
- Injector diameter. Six diameters are available, ranging from 6 to 20 mm.

3.1.4. Changing powders

To change the powder, the powder present in the pilot has to be gathered in the feeding hopper. The injector is replaced with a tube, connecting the end of the screw and the powder container placed on the ground. The screw is activated and the powder injected in the container. Some powder remains in the feeding hopper below the screw. The casing of the screw is removed and the powder sucked with a vacuum cleaner. Then, the casing is replaced and a new powder can be placed in the feeding hopper.

3.1.5. Interpretation of the results

The results of the experiments consist of the mass of powder injected in the weighed hopper. An example of graph obtained with the microbead powder is presented in Figure 82:

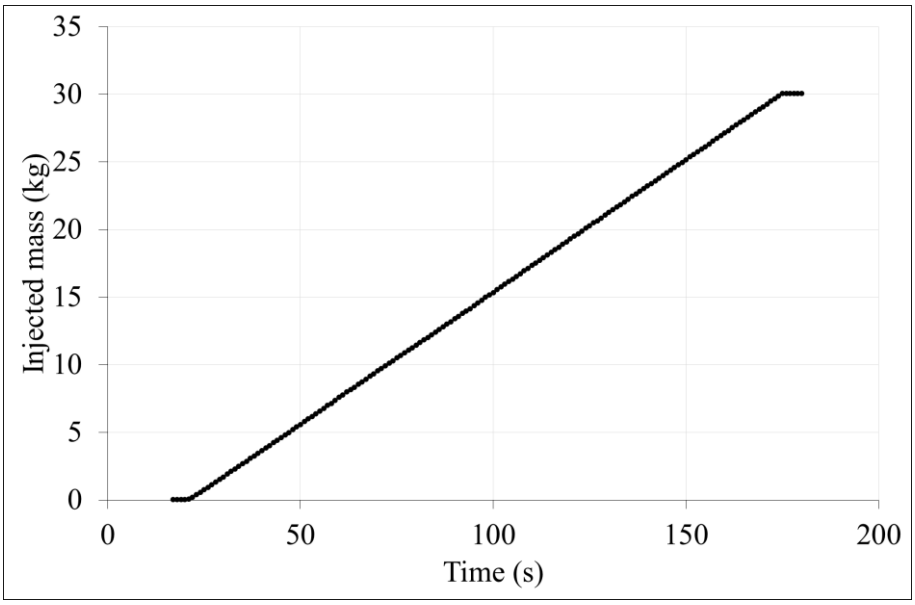

Figure 82: Evolution of the injected mass in the weighed hopper with the glass microbeads, 125 rpm and 14mm injector diameter.

In this case, the level of powder does not increase in the injector. However, the maximum mass of 30 kg is reached and the injection stops. The mass flow rate can be calculated in two ways:

- Calculation of the slope.
- Calculation of the average instantaneous flow rate.

Both methods give similar results.

3.2. Entrained flow gasifier Giroflé

3.2.1. Description of the system of injection

In this study, the injection of biomass in the gasifier is explored. The system of injection is presented in Figure 83:

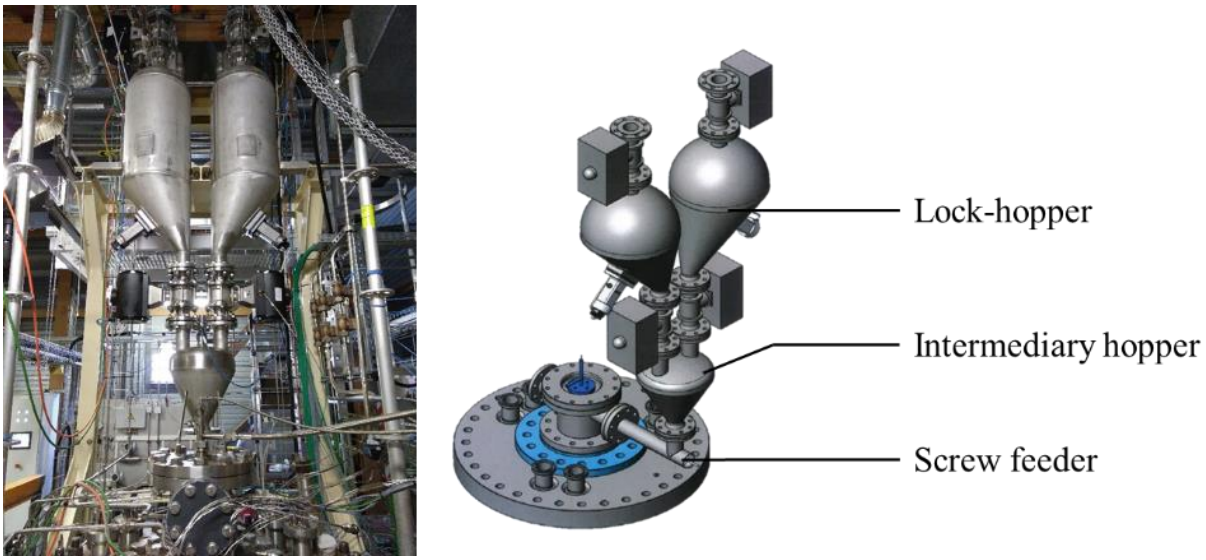

Figure 83: Injection system of the gasifier. Left, schematic of the whole injection system (lock-hoppers and screw feeder). Right, screw feeder, injection cone and injection tube.

The injection system stays at room temperature. First, the powder is placed in the lock hoppers, where it is pressurized. The dimensions of the lock-hoppers are given in Figure 84:

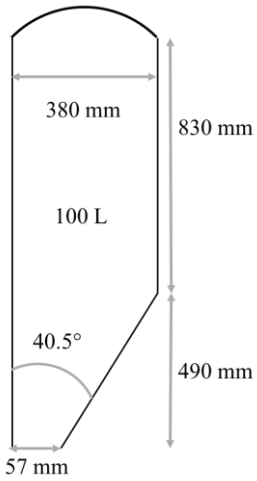

Figure 84: Dimensions of the lock-hoppers (side view).

Then, it is collected in an intermediary hopper (15 L, angle at the base of 60° and 7.6 cm opening), presented below:

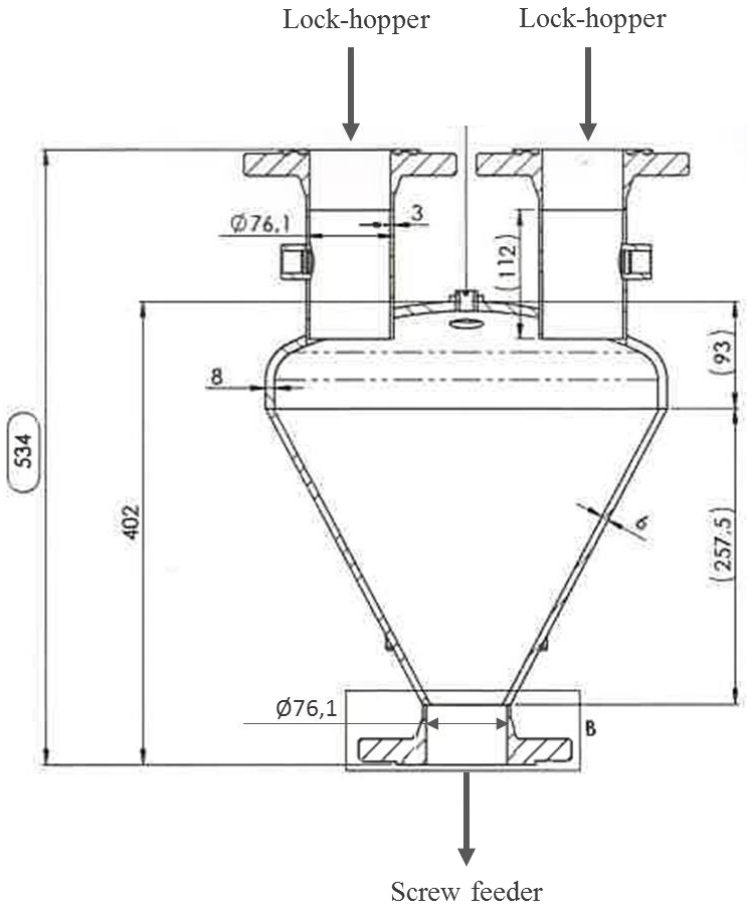

Figure 85: Dimensions of the intermediary hopper.

The powder flow from the intermediary hopper to the screw. The powder is conveyed by the shaftless screw in the injection cone, then in the injection tube (17.8 mm inner diameter). A picture of the screw driver and a schematic of the bottom part of the injection system are presented in Figure 86:

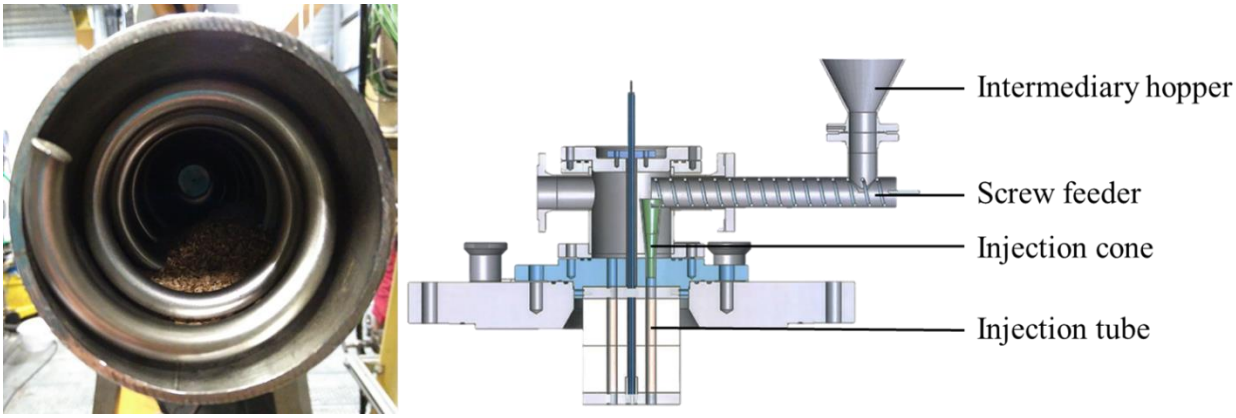

Figure 86: Left, picture of the shaftless screw feeder (axial view). Right, section of the reactor showing the bottom part of the injection system (side view).

The dimensions of the screw are gathered in Figure 87:

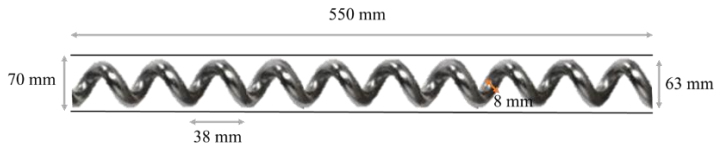

	Diameter (mm)
Cylinder	70
Pitch	38
Screw flight	63
Wire	8
Screw length	550

Figure 87: screw feeder dimensions

The reactor zone starts at the end of the injection tube. The injection tube is cooled with nitrogen (1 Nm^3/h) thanks to a pipe-in-pipe technology.

3.2.2. Operating conditions

The objective of the study is to observe the regularity of the flow of the two powders (granulated powder and beech powder) in the injection system. For the experiments, the set parameters are:

- A pressure of 7 bars. The entrained flow gasifier Giroflé is still in a development phase and cannot reach 30 bars at the moment. Thus, the experiment is performed at the maximum pressure available which is 7 bars.
- A screw feeder speed of 5 rpm. At low pressure, the pressure gradient is low. This limits the burner power and gas evacuation. Thus the biomass flow rate must be low (around 5 kg/h). Moreover, we wanted the injection time to be long enough to analyze the injection in steady state. This screw speed allows injection times longer than 2 hours.
- A temperature of 1360 °C. This temperature provides the best biomass conversion in syngas.

The temperature corresponds to the average temperature in the reactor, measured thanks to thermocouples distributed on the inner walls of the reactor.

The productions of CO and H_2 are recorded online.

3.2.3. Conduct of the experiments

The experiments with Giroflé are conducted as follows:

- Gas leak tests are performed in the lock-hoppers and the reactor.
- The lock-hoppers are filled with powder (100 L each). In our case, one lock-hopper is filled with granulated powder and the other with the beech powder.
- The reactor is heated and pressurized, as presented in Figure 88. First, in the afternoon, the reactor is heated at 20 kW at atmospheric pressure. The pressure is set to 2 bars before the night, and the reactor is heated during the night. In the morning, the temperature has reached 900 °C. From this moment, nitrogen is injected in the double-envelop of the injector tube to cool it (it would melt at higher temperature). The pressure is set to 7 bars and the heating power to 30 kW to reach 1360°C. The lock-hopper pressure is always slightly higher than the reactor pressure (approximately 0.5 bar).

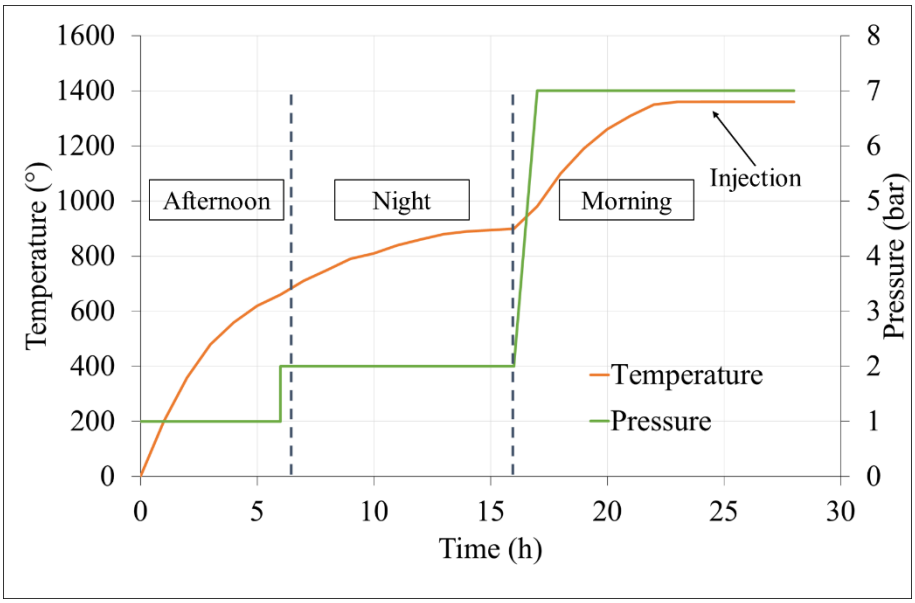

Figure 88: Heating and pressurization of the reactor

- When the temperature is stable, the powder can be injected. The biomass flow rate is set to 7 kg/h, which corresponds to a screw speed of 3-5 rpm. A flow rate of 2 Nm3/h of nitrogen is injected in the injector tube to help the injection.
- The produced gases are sampled at the reactor outlet and analyzed, while the rest of the production is burnt in the post-combustion system.
- At the end of an experiment, the ashes and unburnt particles are collected in the quenching bath to be analyzed. The Coriolis flowmeter filter is cleaned.

CHAPTER V: RESULTS OF THE STUDIES AT PILOT SCALE

The lab scale study has led to several conclusions. Firstly, it is possible to link flow parameters derived from a shear test with parameters much easier to measure: the avalanche angle and the aerated density. Then, it has been shown that moisture content has an influence on the flowability of biomass powders, above 15 wt% (wet basis). Finally, a granulation method has been proposed, which significantly improves the flow properties of cohesive biomass powders.

These studies have been performed on small amounts of powders (mL). In the context of the gasification process in entrained flow reactor, the volumes of powder involved are larger: liter, cubic meter. Thus, some of the results obtained at lab scale are going to be tested at pilot scale in the injection pilot IRIS.

The objective of the injection pilot IRIS is to mimic the conditions of the injection of powder into an entrained flow reactor, at atmospheric pressure. A detailed presentation of the pilot is made in chapter IV part **Erreur ! Source du renvoi introuvable.**. The feeding hopper is followed by a screw feeder, an injector and a second hopper. The second hopper, which is weighed, corresponds to the gasifier. Several parameters can be set: feeding hopper level, powder nature, screw speed and injector tube diameter.

In this part, the flowability of powders at large scale (more than 30L) is assessed. The criterion to assess a powder flowability in this experiment is the minimum orifice diameter (which corresponds to the injector tube diameter) a powder can pass through. The smaller the orifice diameter, the better the flowability.

Six different powders are used in this study. One is a glass microbead powder, an inorganic powder expected to have a good flowability. The spherical particles and low polydispersity (70-110 µm) were chosen to get closer to ideal powders often studied in the literature. Two are powders made of raw biomass: a resinous wood powder and the reference oak powder. Finally, from the oak used to produce the reference powder, three powders were produced by flowability improvement processes [72], [82]. A granulated powder (with the granulation process presented in the lab scale study) and two powders made of torrefied wood (a fine one, comparable with the reference powder and a coarse one). Thus, the effects of torrefaction and granulation will be assessed at pilot scale.

A relationship between flow parameters at lab scale and pilot scale will be investigated. Moreover, the granulation process, showing promising results at lab scale, will be up-scaled and an energetic study will be proposed.

1. Lab scale characterization of the powders

The powders used in this work have been tested at lab scale. Thus, the pilot scale results will be compared to the lab scale results.

1.1. Flowability measurements

Flowability measurements have been performed: aerated density, moisture content, avalanche and shear tests. The results are shown in the tables below:

Table 19: Aerated density and moisture content measurements for the powders used in the IRIS pilot study.

Powder	Aerated density (kg/m3)	Moisture content (wt%)
Glass microbeads	1580	0
Reference powder	294	7.5
Resinous	164	9.5
Granulated reference powder	293	7.0
Fine torrefied powder	326	3.5

Coarse torrefied powder	325	5.4

Firstly, the density of the glass microbeads is higher than that of the biomass powders (approximately five times). The wood powders have an aerated density around 300 kg/m^3, except the resinous powder with a density twice as small, 164 kg/m^3. The model (established in Chapter III, 3) shows that there is an inverse relationship between the flowability of a powder and its density. Thus, the glass microbeads are expected to have a better flowability than the biomass powders. Moreover, the resinous powder is expected to have the lowest flowability.

The flow of biomass powders started to change for moisture contents above 15% (see Chapter III, 4). The moisture content of all the biomass powders is below 10 wt% (wet basis). When they are in the pilot, the powders are protected from the atmosphere (airtight hoppers, nitrogen atmosphere). When not in use in the pilot, the powders are stored in closed barrels, protected from moisture. Thus, even if the moisture content varies during an experiment, it is assumed that the moisture content remains below 15% and the flow properties remain constant.

The avalanche measurements results are presented in the table below:

Table 20: Avalanche angle measurements for the powders used in the IRIS pilot study.

Powder	**Av. angle (°)**	**Av. angle span (-)**	**Av. time (s)**	**Av. time std dev. (s)**
Glass microbeads	36	0.1	3	0.49
Reference powder	59	0.4	2.1	1.38
Resinous powder	62	0.2	2.4	1.3
Granulated reference powder	45	0.1	3.9	0.35
Fine torrefied powder	50	0.4	2	1.04
Coarse torrefied powder	54	0.3	1.9	0.85

The avalanche angle of the glass microbead powder is lower than that of the other powders. It are expected to flow better under its own weight. Moreover the avalanche angles of the resinous powder and the reference powder are high compared with the torrefied powders and the granulated powder. This shows the interest, at lab scale, to apply flowability improvement processes to the biomass powders. Concerning the avalanche angle span, the glass microbeads and the granulated powder stand out with low span compared to the other powders, which is confirmed by the avalanche time standard deviation. They are expected to have a better flow regularity than the other powders. The torrefied powders seem to have a flow regularity comparable to that of the raw powders.

The avalanche time is higher for the powders with the lowest avalanche angle and avalanche time standard deviation: the glass microbeads (3 s) and the granulated powder (4 s), and is low for powders with a higher avalanche angle and avalanche time standard deviation (around 2 s). This is due to the presence of small avalanches between to bigger events in the flow of the cohesive powders. The small avalanches lower the time between two avalanches for the cohesive powders. This small events do not occur with the non-cohesive powders, which explains their high avalanche time.

The avalanche measurements show again that the lab scale flowability of the glass microbeads is better than that of the biomass powders. However, a positive effect of the flowability improvement methods (torrefaction and granulation) on the flowability is observed, compared with raw powders. The granulation method shows a stronger improvement than the torrefaction at lab scale, particularly on the flow regularity.

The shear test results are gathered in the table below:

Table 21: Shear test results (3kPa preconsolidation stress) for the powders used in the IRIS pilot study.

Powder	Cohesion (Pa)	Cohesion length (cm)
Glass microbeads	67	0.4
Reference powder	77	2.7
Resinous powder	75	4.7
Granulated reference powder	40	1.4
Fine torrefied powder	36	1.1
Coarse torrefied powder	43	1.4

The cohesion is an indicator of flow resistance of a powder after it has been preconsolidated under a vertical load. The cohesion length can be interpreted as the length a powder can hold itself as a unit without collapsing. The cohesion length has been shown to be related to the avalanche angle (Chapter III, 3).

The glass microbeads exhibit a cohesion comparable to that of the raw biomass powder. It is attributable to the size of this powder particles (see next part): the microbead powder contains mainly fine particles (below 100 µm), and is subject to interparticle forces, such as van der Waals forces. But since the glass microbead powder has a high density, it stands out with a low cohesion length. Thus, the cohesion parameter alone is not a relevant parameter to characterize the flowability of powders: the balance between cohesive forces and weight is more relevant, and thus the use of the cohesion length.

The effect of the flowability improvement processes is visible, with a lower cohesion length for the torrefied and granulated powders than for the raw powders. In both cases, the cohesion has been decreased with a small change in the density. In the case of granulation, the cohesion decrease is attributable to the decrease of the number of contact points and the decrease of the interlocking phenomenon (rounder particles). In the case of torrefaction, surface roughness has been decreased, decreasing the interlocking phenomenon. The resinous powder, with low density, exhibits the highest cohesion length. The cohesion length results are consistent with the avalanche angle results. However, cohesion and density alone are not relevant parameters to characterize the powder behaviors.

1.2. Size and shape measurements

The particle size distribution of the powders has been measured with the Camsizer. The results are presented in the table below. The particle size distributions are plotted in Figure 89. A picture of the powders is shown in Figure 90.

Table 22: Particle size measurements of the powders used in the IRIS pilot study.

Powder	d10	d50	d90	Size span (-)	Aspect ratio (-)
Glass microbeads	52	82	112	0.65	0.92
Reference powder	9	22	99	4.1	0.62
Resinous powder	12	220	440	1.95	0.57
Granulated reference powder	289	792	1260	1.2	0.70
Fine torrefied powder	10	21	129	5.6	0.70
Coarse torrefied powder	16	192	593	3	0.53

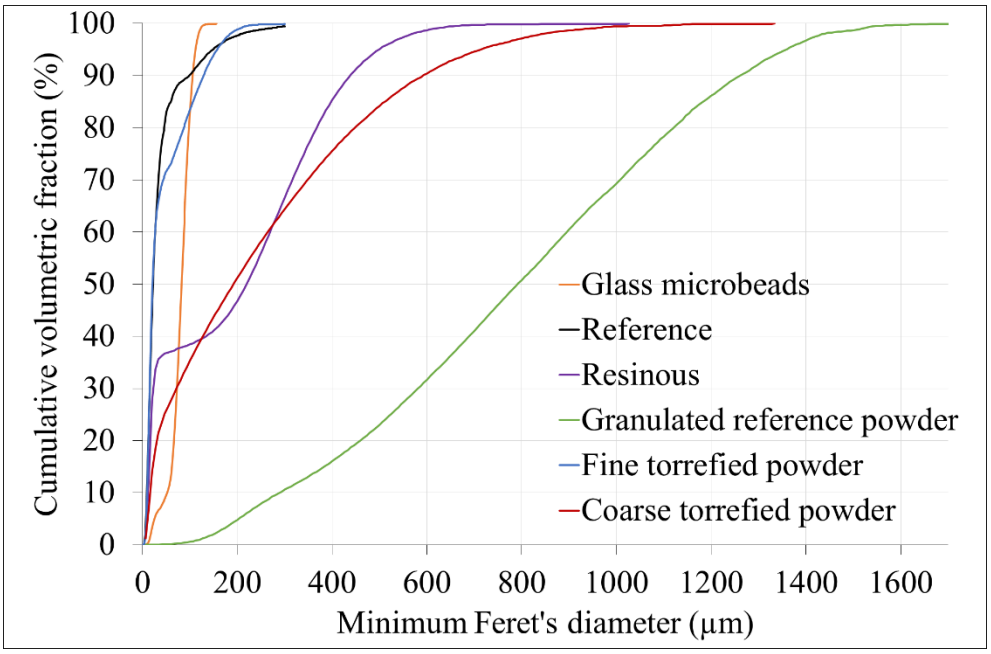

Figure 89: Particle size distributions of the powders used in the IRIS pilot study.

The microbeads, the reference powder and the fine torrefied contain mainly fine particles (d_{50} < 100 µm). Moreover, the reference and the fine torrefied powder have similar particle size distributions.

The reference powder and the fine torrefied powder have a similar aspect (size and shape of the particles), except for the color (see Figure 90). Moreover, their d_{90} is far below the smallest injector tube diameter available (6 mm). Yet, for particles with a diameter far below the orifice size, jamming in the injector is expected to be caused by the cohesion forces within the powder. Moreover, the particles have a high mean aspect ratio (they are almost spherical), limiting the particle interlocking. Thus, jamming in the injector is expected to be caused by the cohesion forces.

The resinous powder and the coarse torrefied powder contain simultaneously fine particles (d_{10} < 20 µm) and coarse particles with a diameter close from the injector diameter (d_{90} > 0.4 mm and injector tube diameter between 6 and 20 mm). Moreover, the particles are very elongated (around 0.5 aspect ratio). Their aspect is comparable, except the color, Figure 90. Thus, if jamming occurs in the injector tube, it could be caused by both the cohesion forces and particle interlocking.

The granulated powder has a particle size with the same order of magnitude than the injector tube diameter (d_{50} = 0.8 mm) and a low fine content, (d_{10} = 289 µm). Thus, if jamming occurs in the injector, it is expected to be caused by interlocking of the particles, even if the aspect ratio is high (0.7).

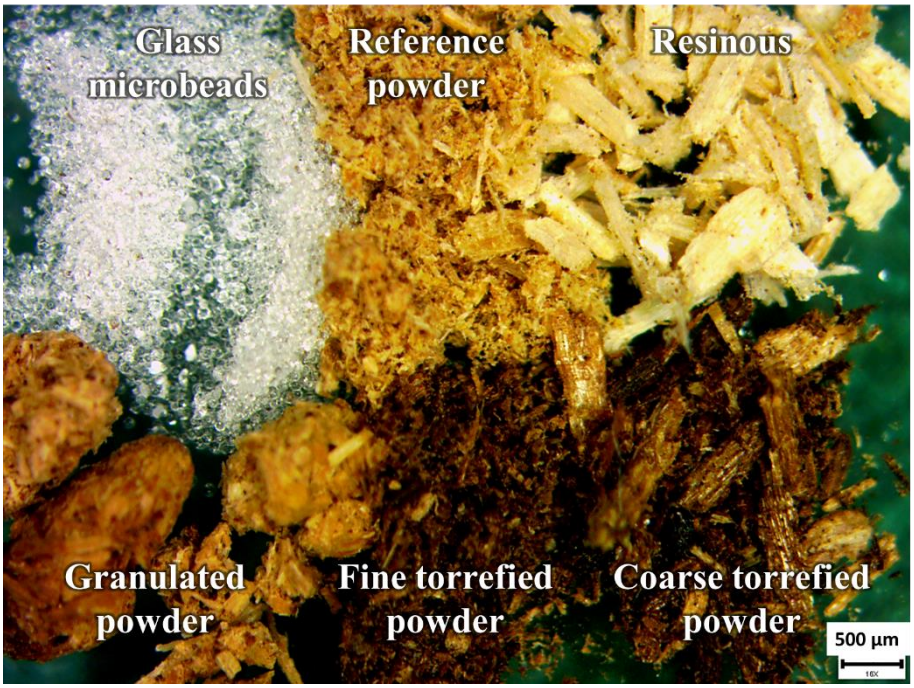

Figure 90: Picture of the six powders, observed with a 16x binocular magnifier.

1.3. Conclusions of the lab scale characterization

The lab scale study gives information on the powder flowability. The microbead powder presents a high density (1580 kg/m^3), low size distribution span and high aspect ratio. Thanks to these features, its flowability parameters (avalanche angle, cohesion length, avalanche time standard deviation for example) are better than that of the biomass powders. It flows regularly under its own weight. The raw biomass powders show a low density, high size distribution span and low aspect ratio. These poor features give the raw biomass powders a low ability to flow under their own weight and compacted under 3kPa, and a low flow regularity (small avalanching events occur in the rotating drum between two avalanches). The flowability improvement methods, granulation and torrefaction, have a positive effect on the different aspects of the flowability, compared with the raw powders. Thus, the powders can be ranked based on these flow parameters.

- The microbeads powder is expected to have the best flow properties in the pilot (storage in silo, screw feeding and flow through an orifice).
- The granulated and torrefied powders are expected to have a better flowability than the raw wood powders.
- The raw wood powders are expected to be the most problematic powders.

Considerations on the size and shape of the particles have led to proposition about the jamming mechanism occurring in the injector tube. The microbeads, reference powder and fine torrefied powder may block in the injector due to cohesion forces. The granulated powder, whose size is the same order of magnitude as the injector diameter, may block in the injector due to particle interlocking, forming an arch. The coarse torrefied powder and resinous powder, with their broad size span, could block in the injector due to both phenomena.

The objective is now to link these results at small scale with the observations in the injection pilot. For example, by finding a small scale parameter able to predict the jamming injector diameter.

2. Study of the screw feeder flow rate and effect of the filling height in the hopper

The screw feeder is placed at the bottom of the feeding hopper. It feeds the injector. It is a volumetric device: it delivers a given volumetric flow rate at a given screw rotation speed. Knowing accurately its speed as a function of the engine frequency (set by the user) is essential to assess the volumetric feed rate it delivers. The screw speed and the ideal volumetric flow rate are studied. The ideal flow rate is then compared with the actual volumetric flow rate, calculated knowing the mass flow rate (measured in the weighed hopper) and the density of the powder.

The effect of the height of powder in the feeding hopper on the mass flow rate delivered by the screw is also investigated. J. Dai and J. R. Grace concluded that the effect of hopper filling height (on the torque requirement) depends on powder properties (moisture content, size, shape, moisture content and compressibility), packing density and geometries of both the hopper and the screw [27]. This investigation will be carried out with two powders, chosen because of their different properties: the glass microbead powder, which is the densest powder and incompressible and monodisperse, and the reference powder, which is compressible and highly polydispersed.

This study is divided in six parts. Firstly, the screw frequency is measured as a function of the engine frequency. Then the repeatability of the experiments is assessed. In the next part, the stresses on the powder near the screw are calculated thanks to the software silo stress tool, for different filling heights. From this calculations, the evolution of the powder properties between the surface of the powder in the hopper to the bottom, near the screw, are investigated. Then, the effect of the filling heights is evaluated on the flow rate delivered by the screw. Finally, the ideal volumetric feed rate of the screw is compared with the actual volumetric feed rate for the six powder.

2.1. Screw frequency

When performing an experiment with IRIS, the screw speed is monitored by setting the engine frequency. The objective of this part is to determine the screw rotation speed as a function of the engine frequency. The screw is enclosed in a casing, thus it is not possible to observe it from outside. However, a part of it is observable from the event on top of the feeding hopper when it is empty (see Figure 91).

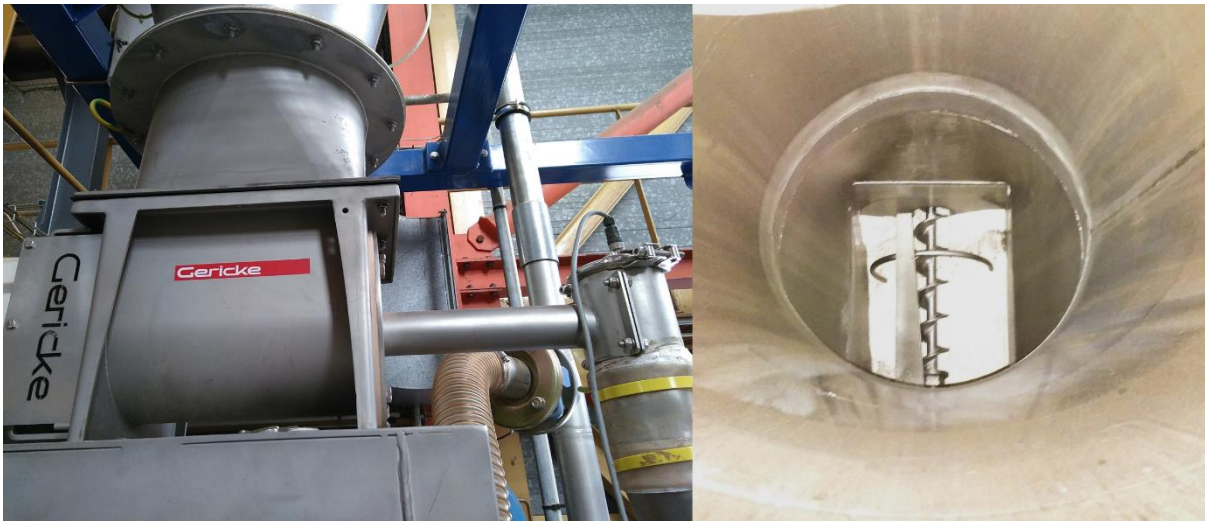

Figure 91: Left, picture of the screw in its opaque casing. Right, picture of the screw and the anti-bridging system from the top of the empty feeding hopper.

A red tape is stuck on the screw so that it is observable once per rotation of the screw when observed from above. The engine is started and the number of rotations of the screw are counted over a given period of time (approximately one minute).

The screw frequency corresponds to the number of rotations divided by the time and the rotation speed is the number of rotations per minute. As expected, the relationship between the engine frequency and the screw frequency is linear, as presented in Figure 92:

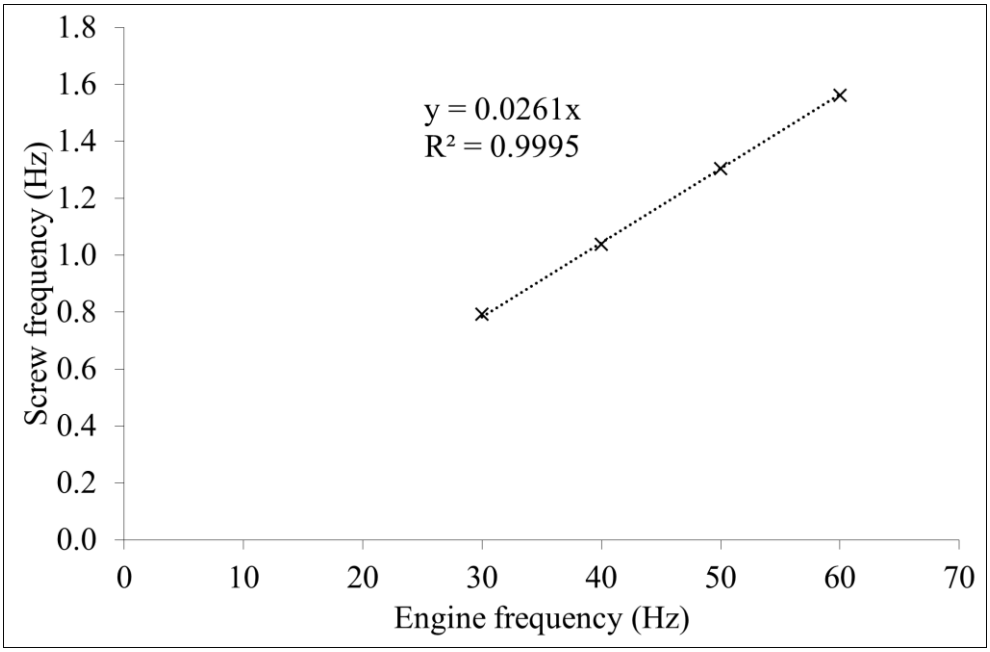

Figure 92: Linear relationship between the engine frequency and the screw frequency between 30 and 60 Hz.

The experiments with IRIS are performed at four engine frequencies: 30, 50, 80 and 99 Hz. In the next parts, the screw rotation speed will be used to present the results.

2.2. Repeatability of the microbead powder injection

In this part, the ability of the screw feeder to deliver a repeatable flow rate at a given screw speed is assessed. Therefore, the injector is removed and the powder exiting the screw falls directly in the weighed hopper. This way, the screw output rate can be directly measured. The glass microbead powder has the highest density. It has been chosen to be able to spot the smallest flow variations. The flow rate has been measured twice for each screw speed. The results are presented in the table below:

Table 23: Repeatability of the flow rate of microbead powder delivered by the screw at different screw speeds. The flow rate has been measured twice at each screw speed and averaged values are given.

Screw speed (rpm)	Average (kg/h)	Relative std deviation (%)
47	262	0.01
78	438	0.12
125	702	0.28
155	864	0.23

The relative standard deviation is very low (below 0.3%), meaning that the screw delivers the same mass flow rate at a given screw speed. The experiments are considered as repeatable.

2.3. Calculation of the vertical stresses in the feeding hopper

In this part, the stresses on the bottom of the hopper, near the screw are calculated. This calculation gives information on the evolution of the powders properties between the surface where it is not compacted and near the screw where it is compacted.

As the feeding hopper is not equipped with stress sensors, the stresses are calculated thanks to a software, Silo stress tool, developed by Schulze [83]. The software calculates stresses in silo with simple geometries (hopper + vertical sections). The stresses in vertical sections are calculated with Janssen's theory [28], [40]. In these sections, the stresses in the filling state (when the silo has been filled and not discharged yet) and in the discharge state (just after the silo discharge has started) are the same. However, they are different in the hopper section (with sloped walls). In the filling state, the Motzkus approach is used [84]. The stresses are calculated with slice element methods. The slices have different geometries, considering the deformations of the powder bed. In the discharge state, the stresses are calculated following a proposal of Arnold and McLean [85]. Arnold and McLean propose an analytical solution to the stress function at the walls of a mass flow hopper. From the stress function, parameters such as the flow function can be obtained. If the powder flow is not a mass flow, this method cannot be used.

The stresses are calculated based on bulk solid properties of the powder and geometry of the silo (the screw is placed in a casing, 35 cm below the hopper/vertical section transition). The stresses can be calculated in a mass flow situation. In case of a funnel flow, the discharging state stress cannot be calculated and an error message is displayed.

2.3.1. Stress in the hopper with the reference powder

The powder bulk properties of the reference powder are:

- Density of the powder. The bulk density of the reference powder varies with the applied stress, it is compressible. Thus, a compressibility test has been performed, from 0.5 to 15 kPa with the FT4. The results are presented in the table below. The results are input in the software. Thus the density is recalculated when the normal stress increases.

Table 24: Measurement of the reference powder compressibility from 0.5 to 15 kPa, with the FT4 rheometer

Vertical stress (kPa)	0.5	1	2	4	6	8	10	12	15
Bulk density (kg/m3)	333	351	373	398	441	425	435	444	455

- Wall friction angle (measured with the FT4, 3 kPa preconsolidation and arithmetic average roughness of the wall Ra = 0.28): 19°.
- Internal friction (derived from a shear test at 3kPa): 40°.

The results of the calculations are shown in Figure 93:

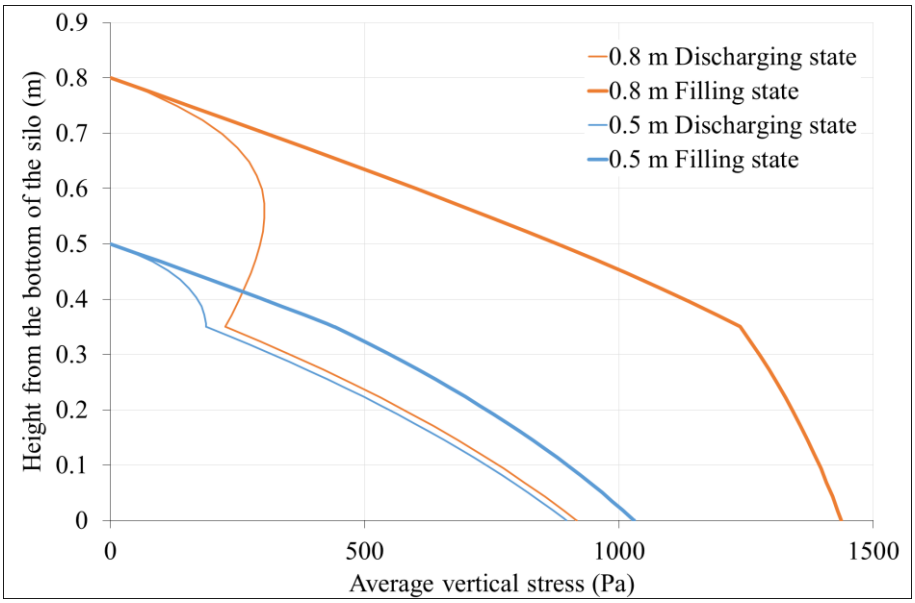

Figure 93: Stress profiles calculated in the powder bed feeding hopper for two different filling heights (0.5 and 0.8m) with the reference powder. 0 m corresponds to the screw level.

On the powder surface, the powder is unconsolidated, regardless of the filling height. The maximum stress on the powder is applied near the screw in the filling state and depends on the filling height. It corresponds approximately to a 1 kPa preconsolidation for 0.5 m filling height and 1.4 kPa preconsolidation for 0.8 m filling height.

2.3.2. Stress in the hopper with the glass Microbeads

The bulk properties of the glass microbead powder are:

- Density of the powder: 1580 kg/m3.
- Internal friction angle (derived from a shear test at 3kPa): 23°.
- Wall friction angle (measured with the FT4, 6 kPa preconsolidation and arithmetic average roughness of the wall Ra = 0.28): 8°.

The results of the calculations are shown in Figure 94:

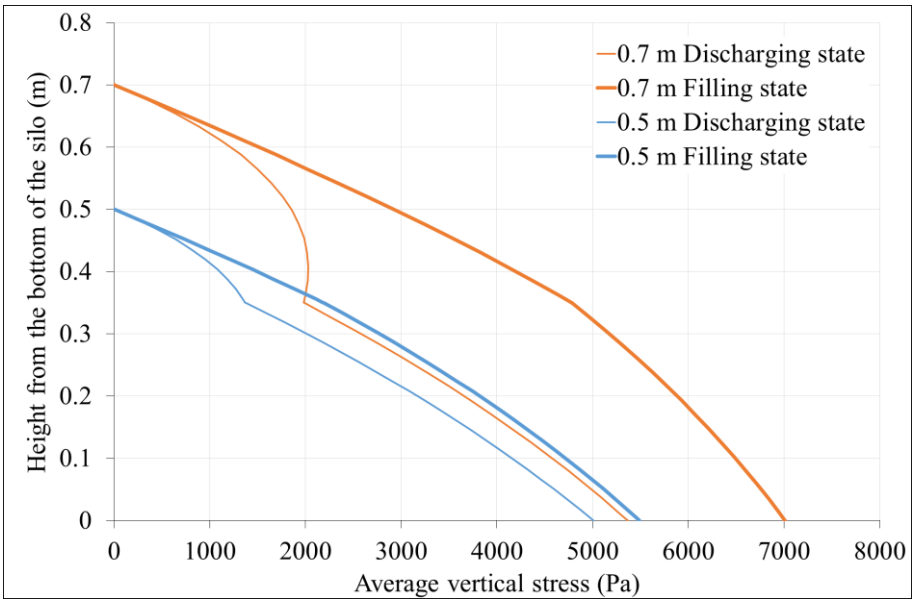

Figure 94: Stress profiles in the feeding hopper for two different filling heights with the microbead powder. 0 m corresponds to the screw level.

As well as with the reference powder, the powder is unconsolidated on its surface, regardless of the filling height. The maximum stress on the powder is applied near the screw in the filling state and depends on the filling height. It corresponds approximately to a 5.5 kPa preconsolidation for 0.5 m filling height and 7 kPa preconsolidation for 0.7 m filling height.

The consolidations in the feeding hopper are known for both powders for different heights. The evolution of the flow properties with the filling height can now be assessed.

2.4. Evolution of the powder properties with the filling height

The consolidations of the powders in the hoppers are known thanks to calculations with the software Silo Stress Tool. In Figure 95, the evolution of the powder properties are summarized:

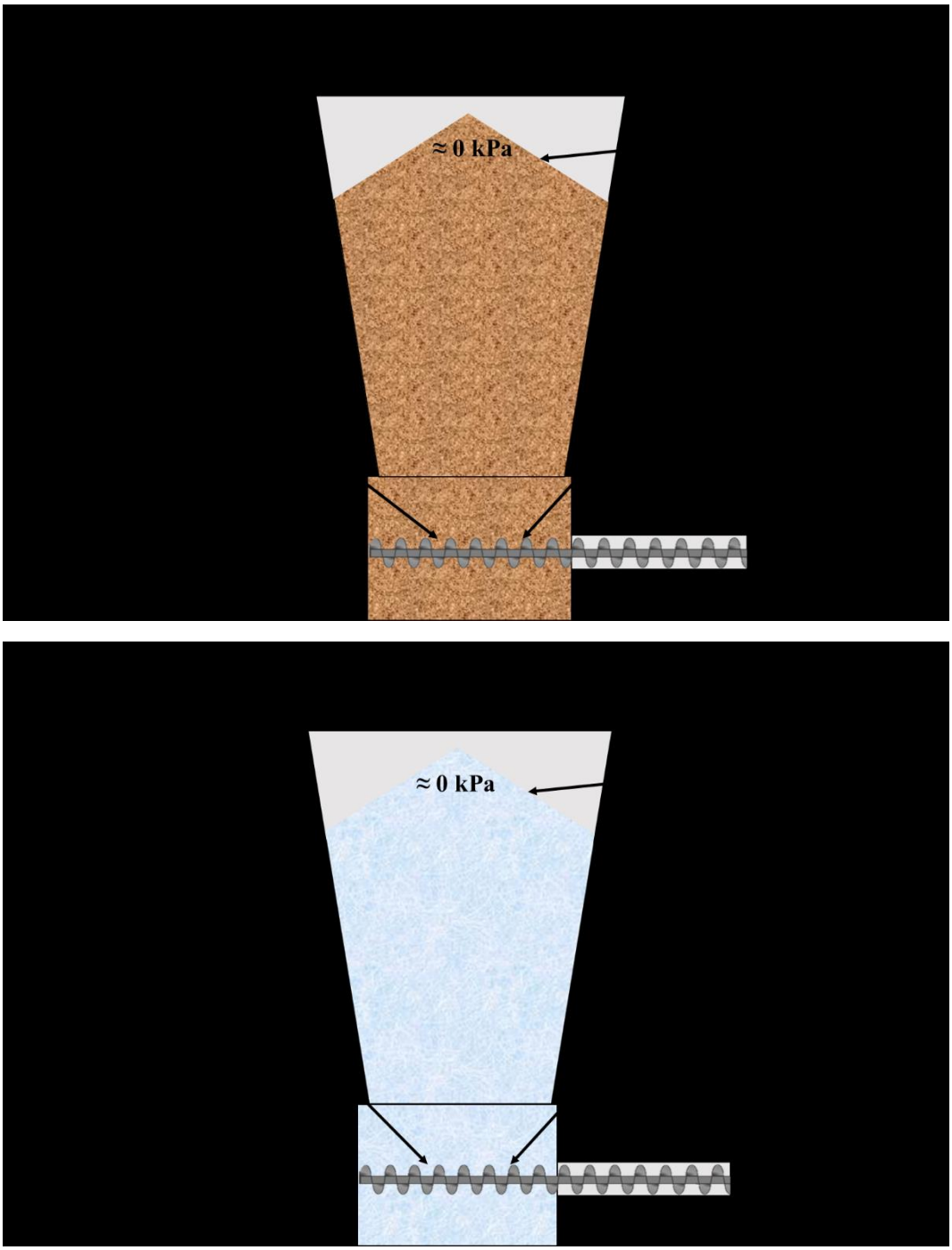

Figure 95: Evolution of the powder properties with the filling height

At the beginning of the injection (hopper is full):

The powders conveyed by the screw are consolidated, depending on their density and filling height: between 1 and 1.4 kPa for the reference powder and between 5.5 and 7 kPa for the microbead powder.

- Cohesion length. It has been measured for 3 different preconsolidations (2, 3 and 5 kPa) for the reference powder and two preconsolidations (3 and 5 kPa) for the microbead powder. The values of cohesion length are shown in the table below. The cohesion lengths corresponding to the compactions close to the screw will be extrapolated.

Table 25: Cohesion length of the microbead powder and the reference powder for 2, 3 and 5 kPa preconsolidation.

		Preconsolidation stress (kPa)		
		2	3	5
Cohesion length (cm)	Reference powder	2.2	3.6	4.5
	Microbead powder	-	0.43	0.47

- Wall friction with the screw (supposed to be constant for the different filling heights).
- Compacted density (equal to the aerated density for the microbead powder and assessed with the compressibility test for the reference powder with a linear interpolation).

At the end of the injection (hopper is almost empty):

The powders conveyed by the screw are unconsolidated, and the shear test cannot be performed. Their flowability is assessed with the following parameters:

- Avalanche angle.
- Aerated density.

The properties of the powders are summarized in the table:

Table 26: Evolution of the powder properties with the filling height.

	Wall friction (°)	**Compacted density (kg/m^3)**			**Cohesion length (cm)**			**Av. angle (°)**	**Aerated density (kg/m^3)**
		0.5 m	0.7 m	0.8 m	0.5 m	0.7 m	0.8 m		
Reference	19	351	-	382	1.8	-	2	59	294
Microbeads	8	1580	1580	-	0.5	0.5	-	36	1580

Close to the screw, the powder property evolution is low with the variation of filling height. Regarding the reference powder, the density varies from 382 (close to the screw) to 351 kg/m^3 (at the surface), which is a decrease of 8%. Its cohesion length shows a small variation as well, from 1.8 to 2 cm. The flow properties (cohesion length, wall friction) can be expected to remain the same as in the beginning of the injection and the effect on the flow rate should be low.

Regarding the microbead powder, the density is a constant because it is incompressible, and its cohesion length is constant as well. Thus, at the beginning of the injection, the filling height is expected to have a minor effect on the screw flow rate for both powders. At the end of the injection, the density of the microbead powder is still 1580 kg/m^3. The flow properties (cohesion length, wall friction) can be expected to remain the same as in the beginning of the injection and the effect on the flow rate should be low as well.

2.5. Measure of the flow rate for different filling heights

The evolution of the powder properties with the filling height has been assessed. In this part, the mass flow rate delivered by the screw is measured for different filling heights with both the reference powder and the microbead powder.

2.5.1 Reference powder

The feeding hopper has been filled with 0.8 m and 0.5 m of powder. The injector diameter is 24 mm and the screw speed is 78 rpm. In this configuration, there is no accumulation of powder in the injector (see 3.2). The screw flow rate is recorded. The results are presented in the Figure 96:

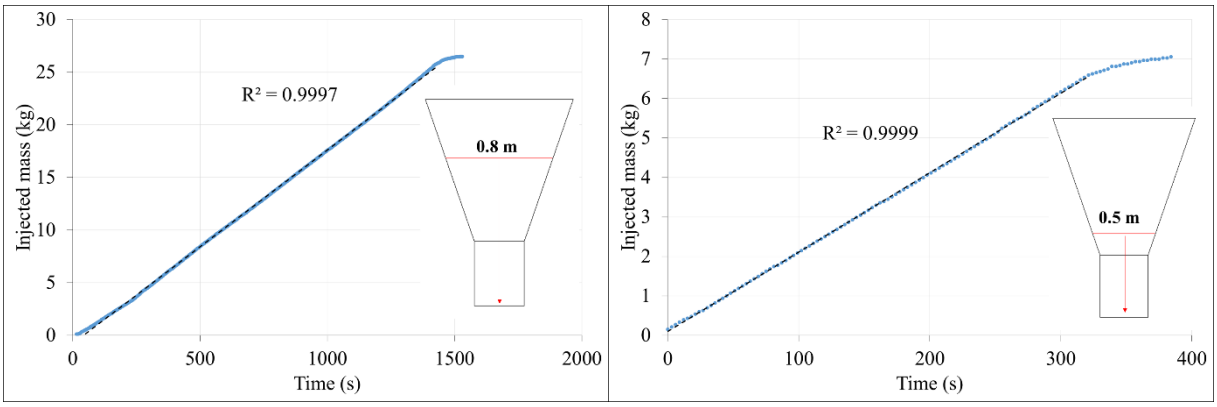

Figure 96: Mass injected in the weighed hopper as a function of time for different initial filling heights with the reference powder.

The experiment with 0.5 m filling height is repeated four times. The average flow rate is 67 kg/h with 0.8 m filling height and 70 kg/h (3.05 kg/h standard deviation) with 0.5 m filling height. There is no difference when the height in the hopper is 0.8 m and when it is close to 0 m. There is no significant effect of the filling height with the reference powder on the screw flow rate, except a small decrease at the very end of the injection. These results are consistent with the small variations of the properties of the powder calculated in the previous part.

2.5.2. Glass microbeads

The maximum mass the weighed hopper can contain is 30 kg (to protect the spring scales). Two initial filling heights are tested and in both cases, injection is stopped as soon as the mass accumulated in the weighed hopper has reached 30 kg.

- Initial height of 0.7 m, corresponding to 100 kg and 64 L. After 30 kg are injected, the remaining height is 0.6 m.
- Initial height of 0.5 m, corresponding to 53 kg and 34 L. After 30 kg are injected, the remaining height is 0.3 m.

The experiments are performed with microbeads. The screw speed is 155 rpm and the injector diameter is 14 mm. In this configuration, there is no accumulation of powder in the injector (see 3.2). The results are presented in Figure 97:

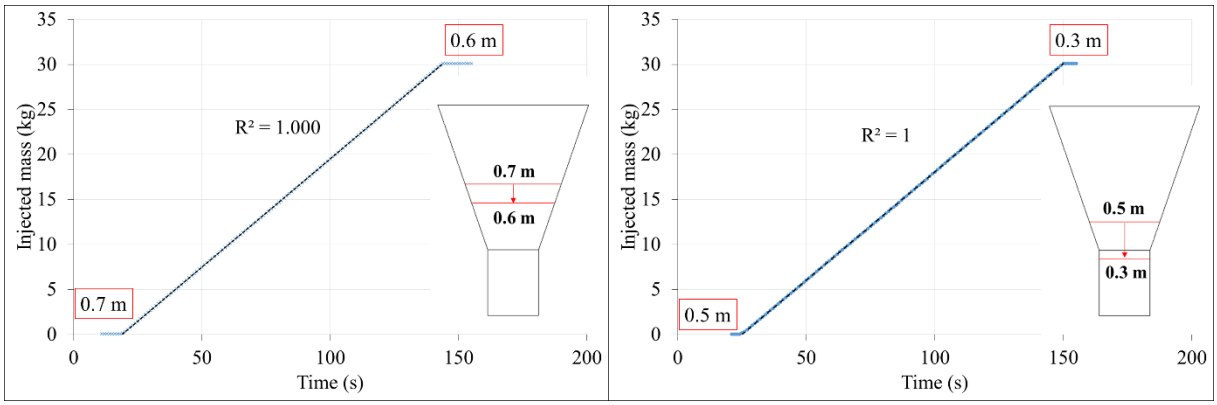

Figure 97: Mass injected as a function of time with initial feeding heights of 0.7 m (right) and 0.5 m (left). In the red boxes, height of powder in the feeding hopper.

The flow rates are equal with both initial fillings, with 867 kg/h. Thus, there is no effect of the initial filling height on the flow rate of the microbead powder. The end of the injection is not observable in this configuration because of the maximum mass that can be injected in the weighed hopper. Once again, the results are consistent with the small variations of the flow properties of the powder calculated in the previous part.

In conclusion, the filling height of the feeding hopper has no influence on the screw mass flow rate.

2.6. Ideal and effective volumetric flow rate

In this part, the volumetric flow rate is investigated and compared with the ideal volumetric flow rate the screw could deliver.

The ideal volumetric flow rate delivered by the screw is the flow rate it would deliver in ideal conditions (for example if the space between the screw flights were fully filled with powder). However, in practice, the volumetric flow rate is lower than the ideal. In this part, the actual volumetric flow rates of the six powders are compared with the ideal flow rate.

2.6.1. Ideal volumetric flow rate

The ideal volumetric flow rate of the screw feeder depends on the screw and casing geometry: pitch (distance between adjacent flights), screw flight diameter, core shaft diameter and fill rate [27]. For compressible powders such as biomass powders, the density can change, thus the mass flow rate can vary.

The ideal volumetric flow rate of a screw can be calculated based on its geometry and its frequency (the thickness of the screw flights is neglected) [27]:

$$V_{th} = A\,v$$

Equation 1

V_{th}: Theoretical volumetric flow rate (m^3/s)
A: Cross-sectional area of the screw feeder (m^2)
v: Ideal axial feeding velocity (m/s)

The cross-sectional area is given by:

$$A = \pi \left(\frac{D_S^2 - D_C^2}{4} \right)$$

Equation 2

A: Cross-sectional area of the screw feeder (m²)
D_S: Screw flight diameter (m)
D_C: Core-shaft diameter (m)

With this formula, the area occupied by the screw flights is neglected. However, geometrical calculations show that only 3% of the cross sectional area is occupied by the screw flights.

And the ideal axial feeding velocity is given by:

$$v = \frac{\omega \, P}{2 \, \pi}$$

Equation 3

v: Ideal axial feeding velocity
ω: Screw frequency (s^{-1})
P: Pitch (m)

The ideal axial feeding velocity is the speed the particles would have if their speed were exclusively axial. In reality, their speed also has a radial component due to their helical path in the screw. This radial component is neglected.

The IRIS screw geometry is presented in the table below:

Table 27: IRIS screw geometry.

Screw flight diameter (m)	4.5E-02
Core shaft diameter (m)	1.3E-02
Pitch (m)	4.7E-02
A (m²)	1.47E-03

Thus, the ideal flow rate for the four screw speed used in this work can be calculated. The results are presented in the table below:

Table 28: Theoretical volumetric flow rate

Screw speed (rpm)	Theoritical volumetric flow rate (m3/h)
155	0.64
125	0.52
78	0.32
47	0.19

The efficiency of a screw feeder for a given powder is:

$$Efficiency = \frac{V}{V_{th}}$$

Equation 4

Efficiency: Efficiency of the screw, between 0 and 1 (-)

V: Measured volumetric flow rate (m^3/s)
Vth: Ideal volumetric flow rate (m^3/s)

The efficiency of the feeder can be lower than one for several reasons [27]:

- The efficiency decreases as the space between the screw flights and the casing increases. Indeed, slip may occur in this space, decreasing the flow rate.
- The particle motion is not only axial. The screw also applies a rotary motion to the particles. Thus, the axial velocity is below the ideal axial velocity.
- The spaces between the screw flights (screw pockets) may be partially filled with particles. As the screw speed increases, the filling fraction of the pockets may decrease.

2.6.2 Measured volumetric flow rate

In an experiment with the injection pilot IRIS, the volumetric flow rate is determined by measuring the mass flow rate of a powder at a given screw speed (47, 78, 125, 155 rpm). Then, the mass flow rate is divided by the aerated density, giving the volumetric flow rate:

$$Flow\ rate\ \left(\frac{m^3}{s}\right) = \frac{Flow\ rate\ \left(\frac{kg}{s}\right)}{Aerated\ density\ \left(\frac{kg}{m^3}\right)}$$

Equation 5

The results are gathered in Figure 98 and Figure 99:

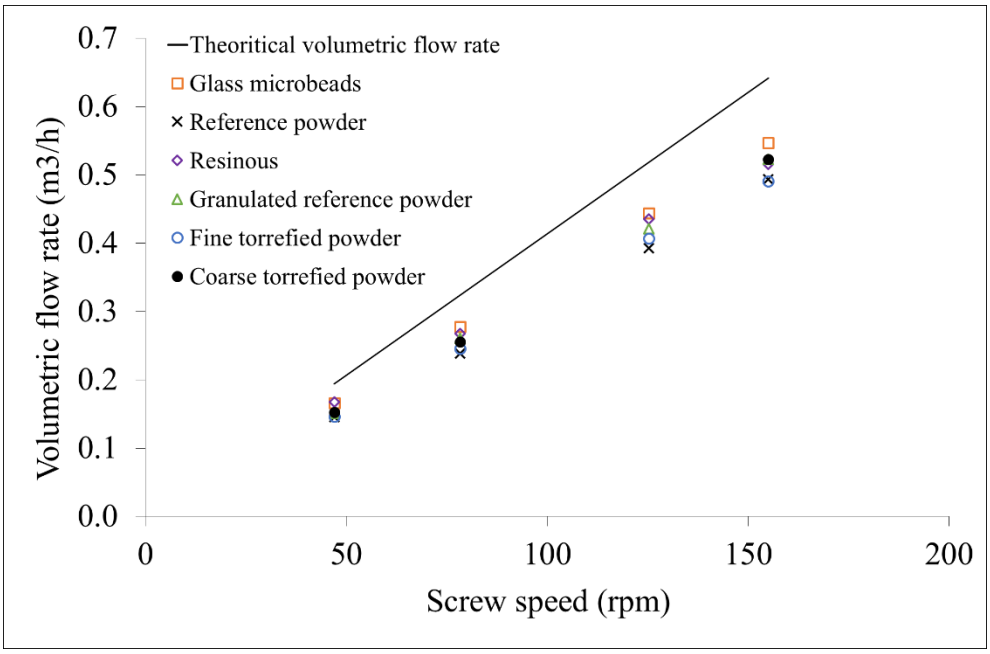

Figure 98: Relationship between volumetric flow rate and screw speed with the different powders and initial volume of 34L.

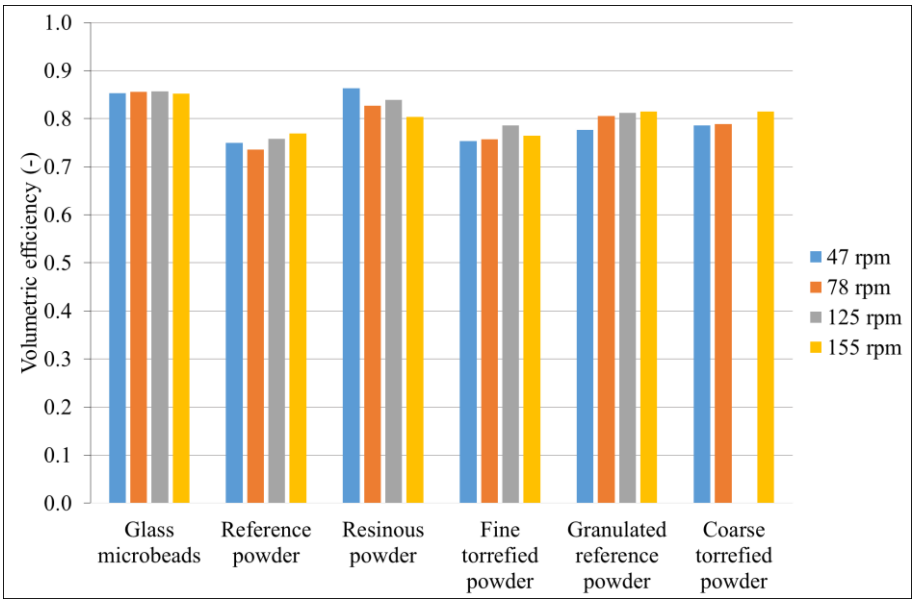

Figure 99: Evolution of the volumetric efficiency with the screw speed.

As expected, the effective volumetric flow rate is below the theoretical volumetric flow rate for all the powders, but there is no decrease of the efficiency with increased screw speed. The casing around the screw is opaque, thus the origin of the volumetric flow rate decrease compared with the ideal is not directly observable (slippage, spaces between the flights not fully filled with powder…). However, the flowability measurements can give ideas on the involved phenomena. The Hausner ratios of the six powders are given in the table below:

Table 29: Hausner ratio of the different powders.

Powder	Reference	Granulated reference	Fine torrefied	Coarse torrefied	Resinous	Glass microbeads
ρ tapped (g/mL)	0.38	0.35	0.40	0.39	0.21	1.6
ρ aerated (g/mL)	0.29	0.29	0.33	0.33	0.16	1.6
Hausner ratio	1.3	1.2	1.2	1.2	1.3	1.0

Regarding the glass microbeads, Hausner ratio is 1, meaning the powder is incompressible. Thus, the spaces between the screw flights can be expected to be full. However, the wall friction angle is 8°, whereas it is 19° for the reference powder. Thus, the main phenomenon decreasing the volumetric flow rate is expected to be slippage.

Regarding the biomass powders, they are compressible (Hausner ratio ≥ 1.2). Thus, the space between the screw flights may be incompletely filled with powder. However, the wall friction coefficient is higher than that of the microbead powder (19° for the reference powder), thus the slippage phenomenon is assumed to have a lower impact on the volumetric flow rate decrease.

2.7. Conclusion on the study of the screw

In this part, the screw speed has been shown to vary linearly with the engine speed, which is the parameter set to perform an experiment with IRIS. Thus, the results of the experiments are presented as function of the four screw speed chosen: 47, 78, 125 and 155 rpm. The mass flow rate has been shown

to be highly repeatable at different screw speeds with the microbead powder. A similar repeatability for the biomass powders is assumed.

The variation of vertical stress on the screw with the filling height has been calculated with the software SiloStressTool, for the reference powder and the microbead powder. The influence on cohesion length and density are negligible for the microbead powder and small for the reference powder. These small variations have been shown to have no influence on the screw flow rate. However, the influence of the height of powder on the engine torque is worth investigating.

The theoretical volumetric flow rate has been calculated thanks to the screw geometry. The volumetric flow rate of the different powder is below the theoretical volumetric flow rate, as expected. Indeed, the volumetric efficiency is decreased by several phenomena (incomplete filling of the screw pockets, non-ideal axial velocity and space between casing and screw flights leading to slippage of the particles). The powders in the screw are not directly observable because of the opaque casing. However, the decrease in volumetric efficiency is supposed to be due to the slippage between the powder and the screw for the microbead powder (low wall friction angle) and to uncomplete filling of the screw pockets for the biomass powders (compressible powders).

3. Accumulation in the injector

The injector is placed between the feeding hopper and the weighed hopper. It is equipped with a level sensor. When the powder accumulates in the injector, the level rises and reaches the level sensor. Once activated, the level sensor stops the screw rotation. The level rising in a given injector diameter depends on the powder properties and the flowrate. In this part, the objective is to determine the injector diameter for which the powder level rises, at different screw speeds.

3.1. Phenomena causing powder level rising

The powder level increase in the injector can originate from two mechanisms, which are:

- The inflow rate in the injector is larger than the outflow rate (see Figure 100). The outflow rate of the injector depends mainly on the powder nature (bulk density, particle size and shape, friction, permeability) and the tube diameter [86]. When the tube diameter is too small at a given screw speed, the level of powder in the injector starts increasing until it reaches the level sensor. With this mechanism, when the screw rotation stops, the powder exits the injector on its own.

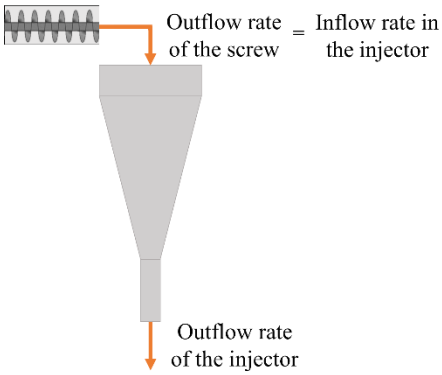

Figure 100: Flow rates in an injector

- Arching due to cohesion or particle interlocking (called jamming) (see Figure 101). As explain in part 1 the powder is expected to form arches due to its cohesion (when it contains fine particles) or by particle interlocking (when its particles are elongated). When an arch is formed, it is stable and stopping the screw rotation does not solve the jamming issue. The injector needs to be removed and cleaned.

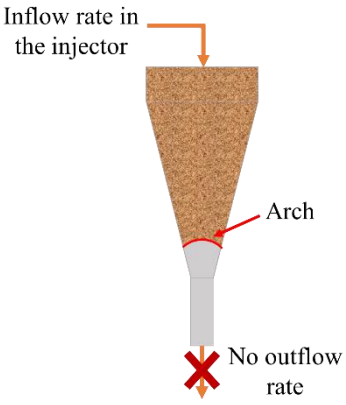

Figure 101: Formation of an arch in an injector.

The first mechanism is less problematic than the second. Indeed, in an injection situation, the first situation only requires to decrease the screw speed to empty the injector whereas the second situation requires to stop the system. In the next part, the second type of jamming will be indicated.

3.2. Jamming during the discharge of powder from a silo

Zuriguel et al. [87] studied the jamming during the discharge of a silo using the parameter R:

$$R = D_0/D_P$$

Equation 6

With:

D_0: Diameter of the opening (m)
D_P: Particle diameter (m)

R is to be the only relevant parameter concerning size: the absolute measure of the particle is irrelevant if R is the same [86], [87]. If R is the same for powders with different grain size, the probability that jamming occurs is the same. Jamming is not directly related to density or elasticity of the material, nor to the surface properties or moderate size dispersion of the particles. However, it is strongly related to the particle shape [87].

There is a critical value of R above which the jamming probability is zero, R_C. R_C is strongly related to the particle shape. In a flat bottomed silo (90° half-angle with the vertical), R_C = 4.94 for spherical particles, 5.03 for cylindrical, slightly elongated particles and 6.15 for rice grains [87]. The geometry of the container affects the jamming. To [88] showed that Rc increases with increasing half angle with the vertical (with a 2D silo, and half-angles 15 and 38°).

3.3. Powder level rising diameter

During an experiment, the level of powder can increase until it reaches the level sensor. Then, the screw rotation stops automatically. For each powder, the critical powder rising diameter as a function of the screw speed is investigated. The critical diameter is the largest injector diameter in which the powder activates the level sensor at a given screw speed. In a larger injector diameter, the powder does not activate the sensor. The results are presented in Figure 102:

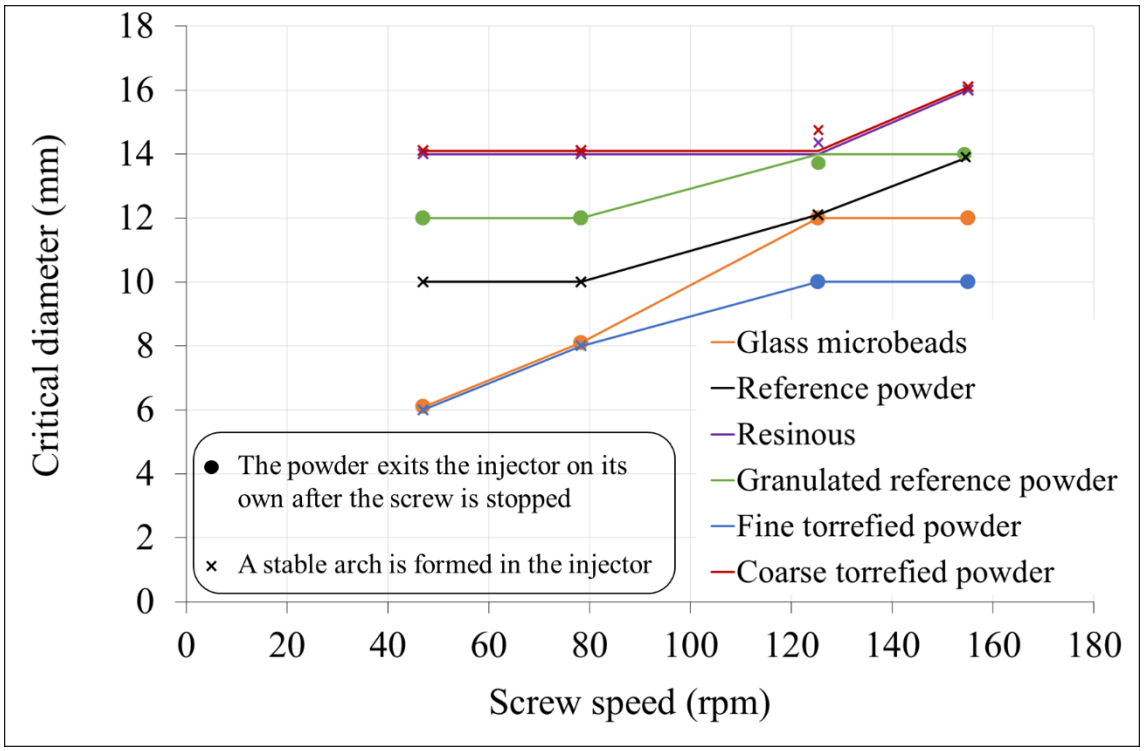

Figure 102: Accumulation critical diameter as a function of the screw speed.

3.3.1 Evolution of the critical diameter

The available injector diameters are 6, 8, 10, 12, 14, 16 and 20 mm. There are 2 or 4 mm between two successive diameters. However, the critical diameter can be between two injector diameters. Thus, when a powder activates the level sensor, it may have activated it for a larger diameter:

$$\text{Injector diameter } n \leq \text{Critical diameter} < \text{Injector diameter } n+1$$

For example, the granulated powders activates the level sensor with the 12 mm injector at 47 rpm. However in reality, the critical diameter could be between 12 and 14 mm. As the critical diameter is the biggest injector diameter in which the powder level rises, the powder can flow in the 14 mm injector, but the level rises in the 12 mm injector.

The critical diameter is not a constant with increasing screw speed. The larger the screw speed, the larger the critical diameter for a given powder. Indeed, the outflow of an injector is approximately constant for a given couple powder/injector diameter. Thus, the injector diameter has to be increased to compensate the increased screw flow rate, caused by the increased screw speed.

3.3.2 Arch formation

Zuriguel et al. [87] stated the existence of a value of R above which the formation of an arch in a silo is not possible in a flat-bottom silo for spherical monodispersed particles: R = 4.94. To [88] showed that this value decreases with decreasing half-angle with the vertical. The injectors used in IRIS have 10° half-angles, thus the value of R in this configuration is below 4.94. In this study, two powders are approximately spherical and monodispersed: the microbead powder and the granulated powder. For the four screw speeds, the values of R_X = Critical diameter / d_X (with X = 10, 50 or 90) are given in the table below:

Table 30: Critical diameter/d_X for the granulated powder and microbead powder.

Glass microbeads				
Injector diameter (mm)	**Screw speed (rpm)**	**R_{10} (-)**	**R_{50} (-)**	**R_{90} (-)**
12	155	231	146	107
12	125	231	146	107
8	78	154	98	71
6	47	115	73	54

Granulated powder				
Injector diameter (mm)	**Screw speed (rpm)**	**R_{10} (-)**	**R_{50} (-)**	**R_{90} (-)**
14	155	48	18	11
14	125	48	18	11
12	78	42	15	10
12	47	42	15	10

In each configuration, R_X = Critical diameter / d_X > 4.94. The probability of an arch formation is zero and the powders exit the injector freely.

Zuriguel et al. also stated that the particle shape has an influence on the jamming phenomenon. For example, the value of R above which arch formation is impossible in a flat bottom silo for rice grains is 6.15 [87]. Indeed, elongated particles can interlock, increasing the jamming diameter. Biomass particle shape could be assimilated to rice grains. However, biomass powders present a large particle size dispersion. Considerations about the factor R are not possible.

3.3.3. Relative positions of the curves

Granulated powder and microbead powder: In the previous part, the microbead powder and the granulated powder have been shown to be able to exit the injector after the level of powder rose and the level sensor activated. The powder rising in the injector intervenes for larger injector diameters with the granulated powder than with the microbead powder.

Beverloo's law [40] is a relation between the mass flow rate through an orifice and powder parameters:

$$\dot{m} = C.\rho_b.\sqrt{g}.(D_0 - k.d_P)^{2.5}$$

Equation 7

With:

$\dot{m}$: Mass flow rate (kg/s)
C: fitting parameter (0.55-0.65)
ρb: Bulk density (kg/m^3)
g: Acceleration of gravity (m/s²)
D_0: Diamater of the orifice (m)
k: Fitting parameter (1.5-3)
d_P: Particle diameter (m)

This law is not applicable for fine particles such as the microbead powder (particle diameter is below 200 µm) [28]. However, as a first approximation, the flow rate depends on the powder bulk density and

particle size. The microbead powder presents a high bulk density (1580 kg/m^3) and a small particle size (82 µm), whereas the granulated powder has a low bulk density (293 kg/m^3) and a large particle size (792 µm). Thus, the microbead powder outflow rate of the injector is higher than that of the granulated powder for the same injector diameter. That is why for the same screw speed, the granulated powder critical diameter is higher than that of the microbead powder.

Torrefied and raw powders: Zuriguel et al. [87] stated that size and shape of the particles are the main parameters influencing jamming. In our case, two groups of powders have similar shape and size distributions:

- The resinous powder and the coarse torrefied powder
- The reference powder and the fine torrefied powder

The coarse torrefied powder and the resinous powder have comparable size distributions and aspect ratios (elongated particles), but different densities (the resinous is twice as light as the coarse torrefied powder, but density does not influence jamming. However density influences the flow rate through an orifice). These two powders behave exactly the same in the injectors. They have the same critical diameter as a function of the screw speed (the injector diameter is discrete whereas the critic diameter is continuous. Thus their critical diameters can slightly differ. (See 3.3.1). This result confirms that long as the particles have the same shape and size distribution, the powder nature (essence, torrefaction, density…) does not have an impact on the critical diameter.

The fine torrefied powder and the reference powder have similar size distributions, aspect ratios (0.7 and 0.6 respectively), densities (326 and 294 kg/m3 respectively) and general aspect (see Figure 90), except the color. They come from the same oak chips. However, their behavior is very different in the injector. The reference powder has a higher critical diameter at a given screw speed. This contradicts the statement that powder nature does not affect the jamming. However, the studied powders have a very low particle size, and interparticular forces have a strong impact on their flow. The cohesion parameter derived from a shear test is supposed to reflect the intensity of interparticular forces within a powder. The lab scale study (see part) show that the reference powder cohesion is twice as high as that of the fine torrefied powder (77 and 36 Pa respectively). This result show that for fine particles, the nature of the powders influences jamming (and the cohesion in particular), and that torrefaction has a positive influence on the critical diameter.

Another difference between the fine torrefied powder and the reference powder is that the reference powder forms stable arches in the injector at every screw speed, whereas the torrefied powder does it only for lower screw speeds. One explanation is that the fine torrefied powder is less submitted to interparticular forces than the reference powder (the cohesion of the reference powder is 77 Pa and 36 Pa for the fine torrefied powder). Below 10 mm, the ratio R becomes smaller than the value for which jamming is impossible for the torrefied powder. This value is hard to get because the powder has a polydispersed grain size. The reference powder is strongly submitted to interparticular forces and the value of R is higher than for the torrefied powder.

3.4 Link with lab scale parameters

3.4.1 Selection of the pilot scale parameter

One of the objective of the study in the injection pilot IRIS it to find a relationship between laboratory scale parameters and pilot scale parameters. The critical diameter as a function of the screw speed has been found for the six powder. However, this is not a single parameter, but a parameter varying with the screw speed. It is not possible to compare it directly with small scale parameters. Indeed, a screw speed should be chosen to obtain a single parameter.

When observing the graph (Figure 102), a ranking appears: the fine torrefied powder has the lowest critical diameter, followed by the microbead powder, the reference powder, the granulated powder and finally the resinous powder and the coarse torrefied powder. However, when observing a particular screw speed, this ranking may disappear. For example, at 125 rpm, the reference and the microbead powders seem to have the same critical diameter, as well as the granulated, the resinous and the coarse torrefied powder. This is due to the phenomenon described in the part 3.3.1: the critical diameter is continuous whereas the injector diameters are discrete.

To maintain this ranking but getting only one parameter, the average critical diameter is proposed, for the four measured screw speeds. They are presented in the table below:

Table 31: Average critical diameter of the six powders.

Powder	Average critical jamming diameter (mm)
Glass microbeads	9.6
Reference powder	11.5
Resinous	14.5
Granulated reference powder	13
Fine torrefied powder	8.5
Coarse torrefied powder	14.5

This way, the ranking is maintained and a single parameter can be compared with the small scale parameters (see part 1).

3.4.2 Comparison with the laboratory scale parameters

No direct relation was found between the average criticical jamming diameter and the following parameters:

- Avalanche angle
- Avalanche angle span
- Avalanche time
- Avalanche time standard deviation
- Cohesion
- Cohesion length
- d_{10}, d_{50}, d_{90}
- Size span
- Aspect ratio

However, Mankoc et al. [86] and Zuriguel et al. [87] suggested that the parameter R is the most relevant to study jamming (3.3.2). However, this parameter is specific for monodispersed particles. Below, R_{10} is defined:

$$R_{10} = Average\ critical\ diameter / d_{10}$$

Equation 7

With:
R_{10} (-)
Average critical diameter (m)
d_{10}: 10 % of the cumulative volume has a diameter below this value (m)

The parameter R_{10} corresponds to the ratio between the average critical diameter and the d_{10} of the powders. The d_{10} is the diameter for which 10% of the volume of the sample has a diameter below it. Thus, the higher the d_{10}, the lower the fine content. The critical diameter is the injector diameter below which the powder level rises in the injector. Consequently, the R_{10} can be interpreted as how many time larger the critical diameter is compared to the smallest particles of the powder.

If R_{10} is large:

- The d_{10} is low (the fine content is high), the powder may be cohesive.
- The critical diameter is high, meaning that the powder is polydispersed and/or has elongated particle (the critical diameter is mainly influence by these parameters).

If R_{10} is low:

- The d_{10} is high (the fine content is low), the powder may be sparsely cohesive.
- The critical diameter is low, meaning that the powder has a low polydispersity and/or has spherical particles.

Thus, R_{10} grows when flowability decreases (increase of the fine particle content, increase of the critical diameter). It seems to be a good indicator of the powder flowability at pilot scale, taking in account the size and shape of the particles.

No direct relation was found between R10 and the following parameters:

- Avalanche angle
- Avalanche angle span
- Avalanche time standard deviation
- Cohesion
- Cohesion length
- Size span
- Aspect ratio

However, a relation is found with the avalanche time standard deviation. The avalanche time is the time between two avalanches in the rotating drum. A powder with a good flowability such as the microbead powder collapses very regularly in the rotating drum. On the contrary, a cohesive powder, besides the main avalanches, presents erratic avalanches of small amounts of matter. Thus there is an inverse relation between the ability of a powder to flow regularly and the avalanche time standard deviation. The avalanche time distribution of the powders are presented in Figure 103:

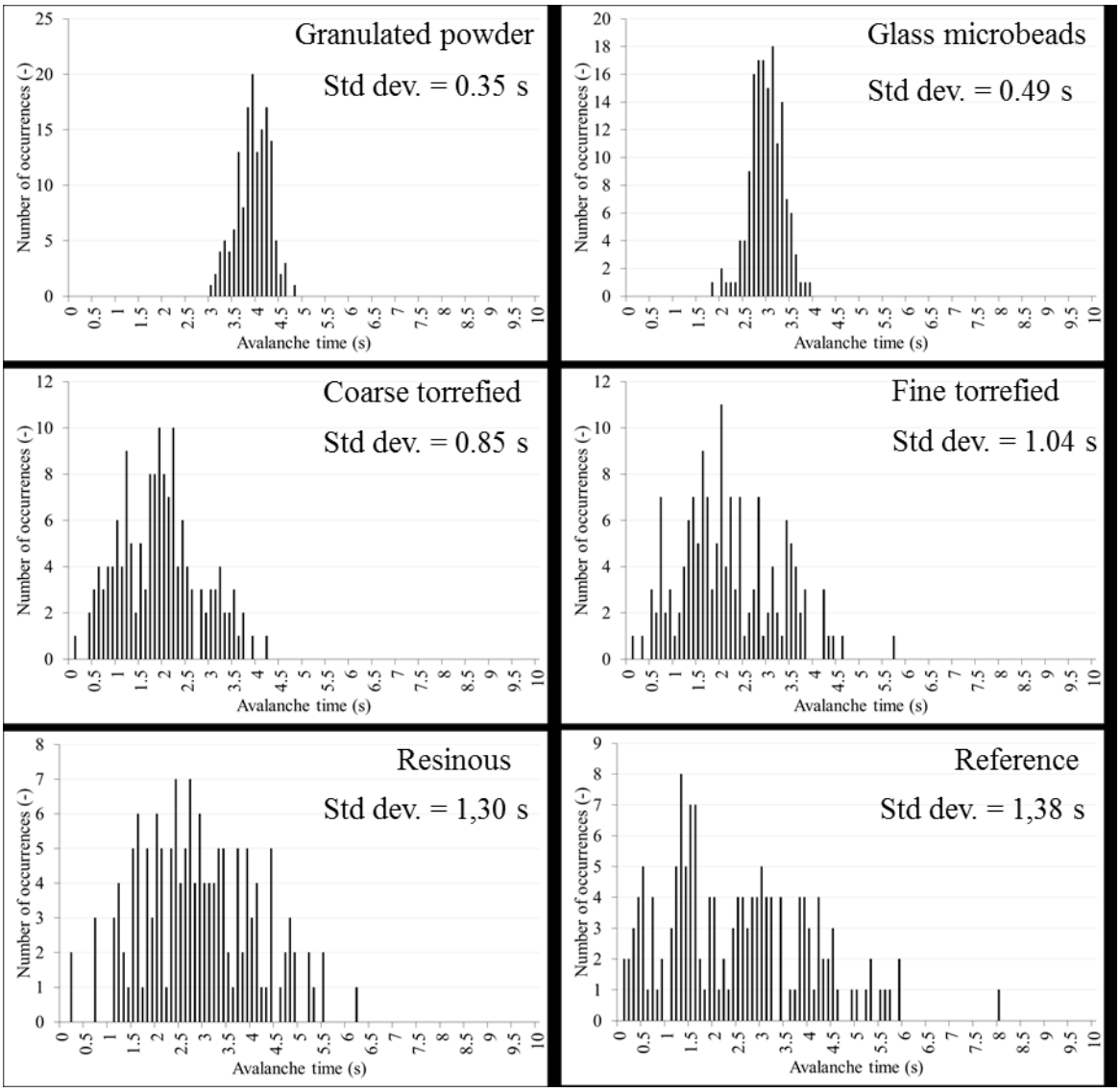

Figure 103: Avalanche time distributions of the six powders

The spherical particle powder present a low spreading of their avalanche time distribution. In the rotating drum, their flow is regular: the powder first rises and then, from a given angle, the particle start to flow. Between two avalanches, the powder bed acts like a solid.

The torrefied powders present a larger avalanche time distribution, but less large than the raw powders. Here the positive effect of the torrefaction process on a laboratory scale flow parameter is observed. Indeed, the coarse torrefied powder and the resinous powder on one hand, and the reference and fine torrefied powder on the other hand have similar particle shape and particle size distributions. They only differ by the treatment they have been submitted to.

The raw wood powders show very large distributions, due to their intermittent flow in the rotating drum. Small avalanches occur irregularly between to large avalanches.

The correlation between R_{10} and the avalanche time standard deviation is shown in Figure 104:

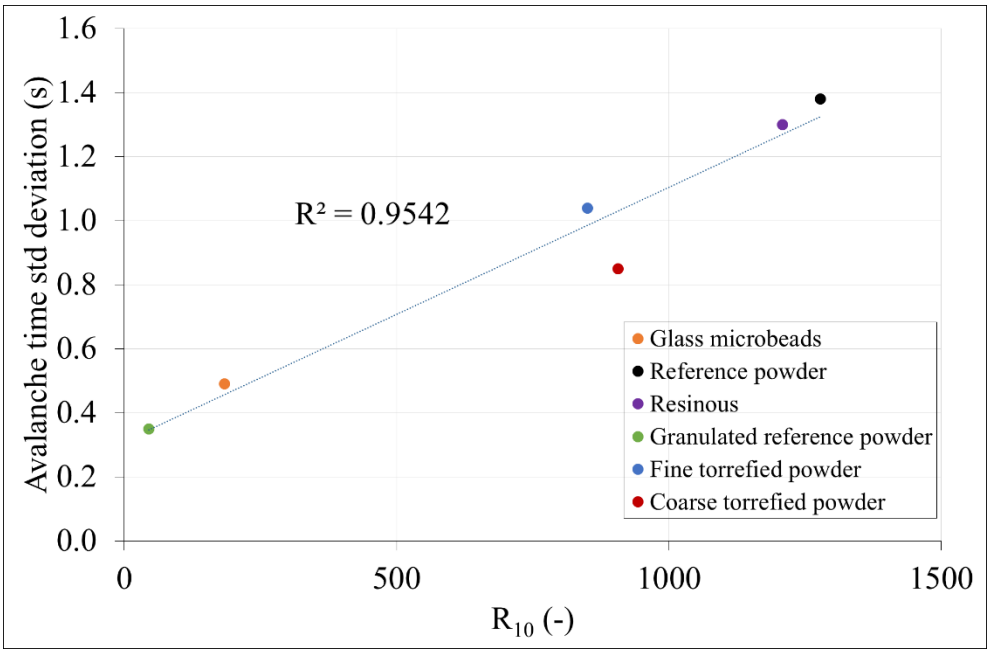

Figure 104: Correlation between the avalanche time std deviation and R_{10} for the six powders.

This relation is interesting: the critical diameter is related to the fine content of the powders and the ability of the powder to flow regularly. A particle size measurement and an avalanche measurement could give access to this critical diameter. Moreover, the relation gives new information on what happens in the rotating drum: the regularity of the avalanches is strongly related to the R_{10}, which is related to the particle shape and size.

3.5. Conclusion on accumulation in the injector

In this part, the accumulation of powder in the injector placed after the screw feeder has been investigated. Two types of accumulation phenomena have been highlighted: the inflow rate of the injector can be larger than the outflow rate, or an arch can form near the outlet of the injector, stopping the outflow rate, which is called jamming.

The parameter R has been chosen to assess the likelihood of jamming. The microbead and the granulated powder have spherical particles, almost monodispersed. They present values of R above the critical value for which jamming is impossible for spherical and monodispersed particles. For them, powder accumulation is due to a too large inflow rate. If powder accumulation in the injector occurs with these powders, decreasing the inflow rate in the injector (which is the screw feed rate) solves the problem. It is verified experimentally: when the level sensor is activated due to powder accumulation and the inflow rate stops, the powder exits the injector because no arch is formed.

However, biomass powders present elongated and polydispersed particles. For elongated particles, the critical value of R above which jamming is impossible increases compared with spherical particles. High particle size polydispersty is also expected to increase the critical value of R compared with monodispersed particles, due to the increased number of contact points between particles. But the calculation of the critical value of R is difficult due to the choice of a suitable particle diameter for polydispersed powder. The determination of the effect of polydispersed particles size on the critical value of R is an interesting prospect. Experimentally, jamming occurs in the injector with all the biomass powders. Thus, elongation and polydispersity have a significant effect on the jamming phenomenon. For these powders, if accumulation occurs in the injector, the process has to be stopped to clean the injector. This argument supports the interest of the granulation method.

In the literature, the nature of powders is assumed not to have an influence on jamming. This is verified for the resinous powder and the coarse torrefied powder. They both have comparable particle size and shape, and they present the same behavior in the injector. The effect of torrefaction of the flowability is not observable. However, the fine torrefied powder and the reference powder have comparable particle size and shape, but they behavior is very different in the injector. The torrefied powder can pass through smaller orifices than the reference powder. Moreover, for the larger injector diameters, the torrefied powder does not form arches, contrary to the reference powder. Thus, for this particle size, there is an observable effect powder nature on the flowability. Torrefaction has a positive effect on flowability for small particles sizes. This may be due to the effect of torrefaction on surface qualities, which has a smaller effect for larger particle size (with the coarse powder for example).

The parameter R has been adapted to polydispersed particles with the d_{10}, and linked with a lab scale parameter: the avalanche time standard deviation. This relation has to be used with caution: the small number of points may have led to a false positive. However, if the relation is correct, the avalanche time std deviation is linked to R_{10}. This relation gives information on the flow in the rotating drum: fine content, shape and polydispersity of the powder have an important role in the flow regularity.

4. Injection in the gasifier

The granulation process has shown an improvement of the flowability of biomass powders, while respecting the size criterion of the gasification in entrained flow reactor. At lab scale, the particles are more spherical and their size is less polydispersed than the raw powder. Moreover, the flowability parameters (derived from a shear test and avalanche measurements) are improved. At pilot scale, the granulated powder did not form arches in the injector, contrary to the raw powder. Thus, when jamming occurs in the injector, it is not necessary to stop the process to clean the injector. Decreasing the screw speed solves the problem.

These encouraging results showed the interest to conduct experiments with this process to the next level: The injection in the pilot scale gasifier Giroflé. The main difference with the IRIS experiments are:

- The pressure: IRIS experiments are performed at atmospheric pressure. However, the gasification process is performed at high pressure, around 30 bars. As a first step, the pressure is set to 7 bars.
- The injection system: in IRIS, the powders flows directly from the feeding hopper to the screw. In the gasifier injection system, the powders is pressurized in lock hopper before to reach the screw. Moreover, the screw has a different geometry (it is shaft-less).

The ideal case would have been to compare the granulated powder and the raw powder. However, the reference powder flowability is low. A powder with such a low flowability has never been injected in the gasifier; it was expected to form arches in the lock hoppers, which are difficult to clean. Thus, the results of the gasification of the granulated powder are compared with a sieved beech powder, with a high flowability and which has already been injected in the gasifier for other experiments.

There is no sensor in the injection system which records information on the flow (regularity, flow rate…). Thus, to assess flow parameters, we observe the production of gases after the gasification. The gas production is assumed to be directly linked with the biomass input flow. However, the balances of the experiments have been found to be inoperable. Thus, no conclusion can be drawn about the gas productions or the flow regularity.

One results is usable: during the injection of the beech powder, jamming in the injector is observed, which is visible in the hydrogen production (see Figure 105). The hydrogen production drops suddenly 15 minutes after the beginning of the injection due to the absence of outflow rate from the injector. The nitrogen pressure has been increased to break the arch. This phenomenon did not happen with the granulated powder.

The beech powder is a powder with a high flowability due to a special grinding (slightly elongated particles) and sieving (low fine content). These operations are not applicable at pilot scale, and a raw wood powder may have blocked in the injector, leading to a stop in the process. This highlights the interest of granulation, which prevents jamming in the injector.

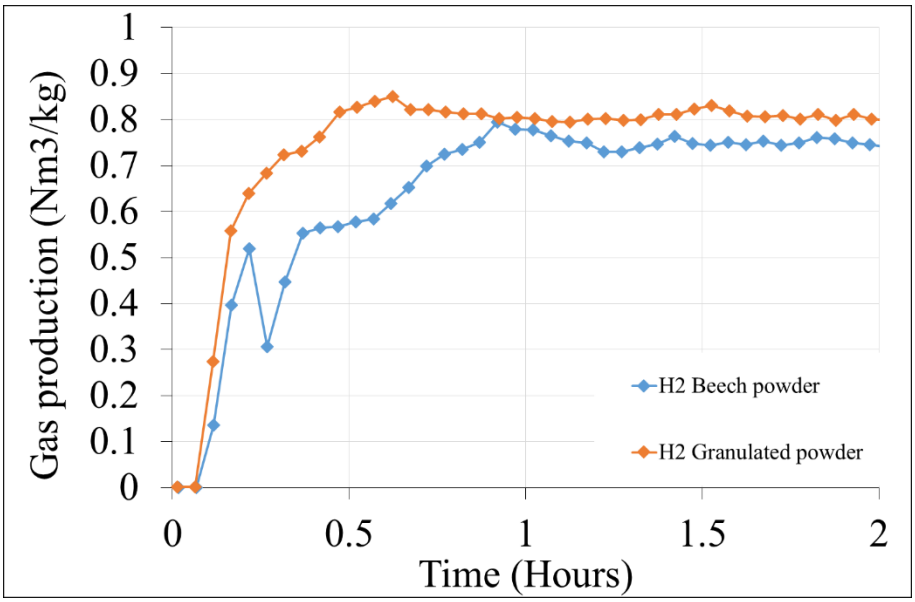

Figure 105: Hydrogen productions during the gasification of the granulated powder and the beech powder.

.

5. Energetic evaluation of the granulation process

An energetic evaluation gives information on the process and possible solutions to improve it. It is a first step before the economic study. The process can be modified and become more attractive than it first appeared. Concerning this granulation process, emphasis has been placed on the flowability improvement and not on the energetic optimization.

The granulation process has been studied both at laboratory scale and in pilot scale. It has been technically validated: an improvement of the flowability is observed compared with the raw powder. Small scale parameters (shear test parameters, avalanche parameters, shape) are improved. At pilot scale, the jamming phenomenon in the injector is modified: the raw powder forms arches whereas the granulated powder does not. If jamming occurs, decreasing the feeding speed solves the problem with the granulated powder whereas the raw powder requires an interruption of the process to clean the injector.

5.1. Objectives and hypothesis

Power is consumed at each step, from harvesting to syngas production. The total power consumed (taking in account the preparation steps and the syngas production and cleaning) must not be greater than the heat obtained by burning the syngas. The maximum power for the preparation steps for energetic profitability (from wood chips to the fuel ready to be injected in the reactor) has been assessed by Van der Drift et al. [12] and will be discussed in part 5.2.

The objectives of the energetic study are:

- To evaluate the power consumed in the different steps of the granulation process.
- To propose solutions to decrease the power consumption.

Schematics of the processes (with free heat and with chip combustion steps) are given in Figure 106:

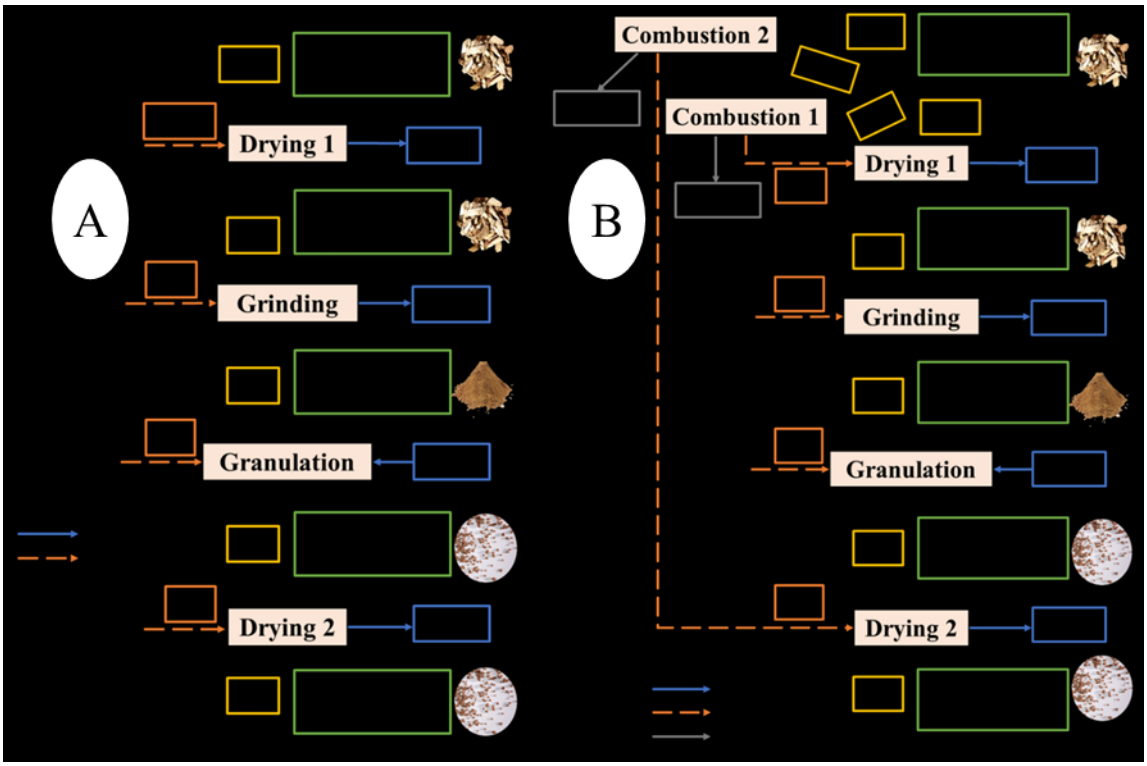

Figure 106: Schematics of the granulation processes. A: free heat. B: with chip combustion.

The assumptions used in the evaluation of the process are:

- The input flow rate is 10 t/h, because the power consumption of the granulator has been found for a flow rate at least 10 t/h.
- The species of wood is oak, because data have been obtained on its grinding for the reference powder.
- The study starts with wood chips. The power consumed during the cultivation of the wood, its shredding and transport to the plant are not taken in account.
- The initial moisture content of the oak chips is taken from the average moisture content of green heartwood of oak (different species), which is 44 wt% (wet basis) [81].
- In the entrained flow gasification process, the produced syngas is hot and has to be cooled. The exchanged heat can be used for the drying steps, and thus can be considered free. However, the situation where this free heat is unavailable will also be examined (heat is provided by burning the chips). In this case, the power consumed by the dryer will be considered to be the drying at 100°C (which could correspond to a belt dryer. Other technologies exist, working at higher temperatures [90]).
- The granulation process has been proved to improve the flowability of the reference powder, which has a very small grain size (below 100 µm). A lower grinding intensity is also considered, less power-consuming (below 500 µm).
- The grinder dries the biomass to approximately 3 wt% (wet basis).
- The granulation is performed in a high-shear mixer. The capacity of these granulators ranges between 10 and 200 t/h and the maximum energy consumption is 200 kW [71].
- There is no oversized particles after granulation.
- The water amount added in the granulation step corresponds to what has been proposed in the method (see material and methods). The granules moisture content is 53 wt% (wet basis).
- The binder is no taken in account. However, as a biomass waste, it can be considered as free.
- The output moisture content is 20 wt% (wet basis), which is the maximum allowed in an entrained flow reactor [60].

In a first part, another energetic study of a biomass preparation step for the injection in a gasifier is presented: torrefaction. The same methodology will be applied for this study. Then the balances of both granulation processes (with and without chip combustions) are established. The powers consumed in the drying steps are then calculated thanks to the balances, whereas the grinding step powers are assessed thanks to the data obtained with the reference powder grinding (100 µm) and the Van der Drift study (500 µm). Finally, solution are proposed to improve the process.

5.2. Energetic study of another preparation step: torrefaction

The biomass entering the plant (where it is going to be prepared and then transformed in syngas in an entrained flow reactor) contains a certain amount of energy that is released when burnt. The heat released during the combustion of a given amount of biomass is the Lower Heating Value (LHV) (for wood, the LHV has a low dependence on the species. However, it strongly depends on the moisture content [91]). Each preparation step consumes energy.

5.2.1. Torrefaction energetic study

Van der Drift et al. assessed the electric energy consumption for dry wood grinding before it is gasified in percentage of the LHV (LHV = 17 MJ/kg [89]). The results are gathered Figure 107:

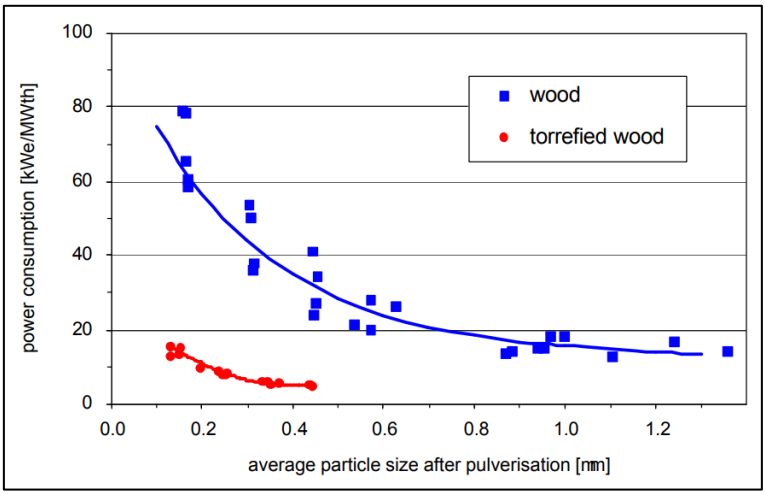

Figure 107: Power consumption of the wood chip grinding [89].

For an objective of 200 µm, the electric energy consumption is 5 % of the LHV, which they consider too high (considering the other preparation steps consume energy as well). They propose to torrefy wood chips before grinding to lower the energy consumption. Torrefaction is a mild form of pyrolysis performed between 200 and 300 °C, decreasing the grinding energy [18] The grinding energy consumption is reduced to 1-2 % of the combustion heat. However, some mass is lost. Typically during torrefaction, 30 % of the mass is lost as gaseous products. The solid contains 90 % of the initial energy content [18]. In this study, it is assumed that the combustion of gaseous products can produce enough heat to perform the torrefaction [18]. Thus, energetic cost of biomass preparation by torrefaction is the power consumed during the grinding, and a 10 % loss of the initial energy has to be taken in account.

5.2.2. Methodology of the granulation study

There is a significant increase of the power consumed with the decrease of the particle size. A powder ground below 500 µm can also be granulated with the process: the powder C1, a beech powder (see

chapter II, 1.2) is sieved below 500 µm and granulated. A picture of the obtained granules compared with the granulated reference powder is presented in Figure 108:

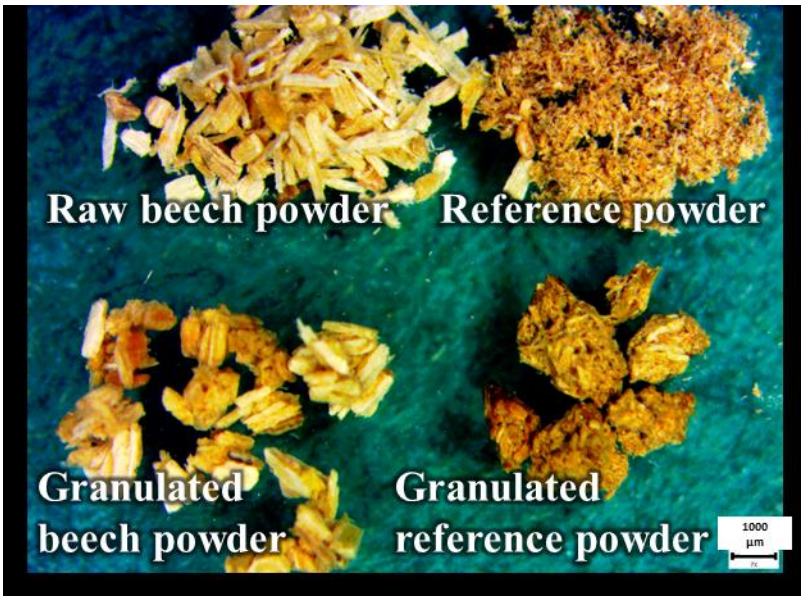

Figure 108: Picture of raw and granulated powders, observed with a 7x binocular magnifier.

The granules produced with a powder with a larger grain size present acute edges, contrary to the granulated powder made with the fine powder. The powder may have a lower flowability. Nevertheless, two particle sizes are investigated in the granulation process: 100 µm and 500 µm.

In the granulation study, the electric energy consumption is also compared with the LHV:

$$Electric\ consumption\ (\%) = \frac{Electric\ power\ (W)}{LHV\ \left(\frac{J}{kg}\right) * Input\ flow\ rate\ (\frac{kg}{s})}$$

Equation 8

The different steps of the process are described in the next parts. For each step, the electric consumption is evaluated. The following configurations are considered:

Table 32: Configurations for the energetic evaluation of the granulation process.

	Drying step	**Grinding intensity**
Configuration 1	Free heat	100 µm
Configuration 2	Free heat	500 µm
Configuration 3	Burning chips	100 µm
Configuration 4	Burning chips	500 µm

Configurations 1 and 2 correspond to the process A (free heat) and configuration 3 and 4 correspond to the process B (chip combustion) in Figure 106. The energy consumption measured during the grinding of the reference powder was **498 kWh/t**. For a grain size of 100 µm, van der Drift and al. found 0.08 kW per kWth (combustion enthalpy of the fuel, or LHV)[89]. This corresponds to 374 kWh/t. This is consistent with the energy consumption measured during the production of the reference powder, which is not dry. With the larger particle size (500 µm), the energy consumption falls to approximately **100 kWh/t** [89].

5.2.3. Balances

The balances are necessary to calculate the flow rates, and thus the power consumptions in the different configurations. In this part, the balances are established for both processes, A (with free heat) and B (chip combustion).

5.2.3.1. Process A

Mass balances

Balance on "Drying 1"

$$D_{in} = D_{D1} + D_{WD1}$$

Balance on "Grinding"

$$D_{D1} = D_G + D_{WG}$$

Balance on "Granulation"

$$D_G + D_{WGr} = D_{Gr}$$

Balance on "Drying 2"

$$D_{Gr} = D_{D2} + D_{WD2}$$

Flow rates

The obtained flow rates are gathered in the table:

Table 33: Flow rates of process A.

	D_{in}	D_{WD1}	D_{D1}	D_{WG2}	D_{G2}	D_{WGr}	D_{Gr}	D_{WD2}	D_{D2}
Flow rate (t/h)	10.00	2.63	7.37	1.60	5.77	6.14	11.91	4.91	7.00

With an initial flow rate of 10 t/h, with a moisture content of 44 wt% (wet basis), the obtained granule flow rate is 7 t/h, with a moisture content of 20 wt% (wet basis). The flow rate in the grinder is 7.37 t/h, thus the power consumed by the grinding step is:

Configuration 1

$$498 \left(\frac{kWh}{t}\right) * 7.37 \left(\frac{t}{h}\right) = 3669\ (kW)$$

Configuration 2

$$100 \left(\frac{kWh}{t}\right) * 7.37 \left(\frac{t}{h}\right) = 737\ (kW)$$

5.2.3.2. Process B

In this case, the mass balances and the calculation of the heat necessary for the drying steps have to be performed to calculate the flow rates. In a first part, the mass balances are presented. Then, the heat parameters are determined and the heat can be calculated. Finally, the flow rates are calculated.

Mass balances

Balance on the node between before "drying 1"

$$D_{in} = D_{C1} + D_{C2} + D_{in'}$$

Balance on "Drying 1"

$$D_{in'} = D_{D1} + D_{WD1}$$

Balance on "Grinding"

$$D_{D1} = D_G + D_{WG}$$

Balance on "Granulation"

$$D_G + D_{WGr} = D_{Gr}$$

Balance on "Drying 2"

$$D_{Gr} = D_{D2} + D_{WD2}$$

Calculation of the heat necessary for the drying steps

A part of the wood chips is burnt after the step "grinding 1" to bring the heat necessary for the drying steps. The heat released when biomass is burnt is the LHV (Lower Heating Value). The LHV at 45 wt% (wet basis) moisture content is [91]:

LHV (45 wt%) = 2474 kWh/t

Thus, there is a relation between the power produced by the combustions and the flow rates D_{C1} and D_{C2}:

$$P_{D1} = D_{C1} * LHV\ (45wt\%)$$

$$P_{D2} = D_{C2} * LHV\ (45wt\%)$$

The power necessary to dry the wood corresponds to two steps:

- Increase of the wood (containing water and dry wood) temperature.
- Water evaporation.

The heat capacity of wood depends on its water content. Above fiber saturation (approximately 23 wt% wet basis), water and dry wood can be considered two separate bodies. Below fiber saturation, water is bonded to the wood fibers and the heat capacity of wet wood has to be considered [81]. In this granulation process, the moisture content stays approximately above the fiber saturation. Thus, water and wood are considered as two separate bodies. The next equations allow to calculate P_{D1} and P_{D2}:

The next equations allow to calculate P_{D1} and P_{D2}:

$$P_{D1} = \left[C_{pwater} * \Delta T * H_{in} * D_{in'} + C_{pwood} * \Delta T * (1 - H_{in}) * D_{in'} + \Lambda * D_{WD1}\right]$$

$$P_{D2} = \left[C_{pwater} * \Delta T * H_{Gr} * D_{Gr} + C_{pwood} * \Delta T * (1 - H_{Gr}) * D_{Gr} + \Lambda * D_{WD2}\right]$$

With:

C_{pwater}: Heat capacity of water (J/kg/K)
ΔT: Temperature variation between 20 and 100°C (K)
C_{pwood}: Heat capacity of dry wood (J/kg/K)
Λ: Latent heat of water (J/kg)

Heat capacity of wood is [81]:

$$C_{pwood} = 0.1031 + 0.003867T$$

With:

C_{pwood}: Heat capacity of dry wood (kJ/kg/K)
T: Temperature (K)

The variation of heat capacities is considered negligible between 20 and 100°C. Thus the heat capacities at 20 °C are taken in account. The heat parameters are presented in the table:

Table 34: Heat parameters used to calculate the energy consumption of the drying steps.

Cpwood (20°C) [81]	1237	J/kg/K
Cpwater [93]	4182	J/kg/K
Latent heat of water [93]	2260	kJ/kg

The flow rates and heats can now be calculated for the process B.

Flow rates

The obtained flow rates are gathered in the table:

Table 35: Flow rates and drying heats of process B

	Din	**Din'**	**DC1**	**DC2**	**DWD1**	**DD1**
Flow rate (t/h)	10.00	8.04	0.72	1.24	2.12	5.92

	DWG	**DG**	**DWGr**	**DGr**	**DWD2**	**DD2**
Flow rate (t/h)	1.28	4.64	4.94	9.58	3.95	5.63

With an initial flow rate of 10 t/h, with a moisture content of 44 wt% (wet basis), the obtained granule flow rate is 5.6 t/h, with a moisture content of 20 wt% (wet basis). 20 wt% of the dry matter is lost in the combustion steps. The flow rate in the grinder is 6.21 t/h, thus the power consumed by this step is:

Configuration 3

$$498\left(\frac{kWh}{t}\right) * 5.92\left(\frac{t}{h}\right) = 2949\ (kW)$$

Configuration 4

$$100\ \left(\frac{kWh}{t}\right) * 5.92\ \left(\frac{t}{h}\right) = 592\ (kW)$$

The heats necessary for the drying steps are:

$$P_{D1} = 1780\ kW$$

$$P_{D2} = 3075\ kW$$

5.3. Discussions

In the table, the electric consumptions of the different configurations are summarized:

Table 36: Electric consumptions in the different configurations.

	Grinding power (kW)	Granulation power (kW)	Final energy content/ initial energy content (%)	Electric consumption (% of the LHV)
Configuration 1	3669	200	100	16
Configuration 2	737	200	100	4
Configuration 3	2949	200	80	13
Configuration 4	592	200	80	3
Torrefaction	-	-	90	1-2

Configurations 1 and 2 correspond to the process A, with free heat for the drying steps. This situation is a possible industrial option. Indeed, the gasification process produces heat that it is possible to recover. Configuration 3 and 4 correspond to the process B, where chips combustions steps provide the heat necessary for the drying steps. The advantage of configurations 1 and 2 compared with configurations 3 and 4 and the torrefaction process is that no matter is lost during the process.

Configurations 1 and 3 (grinding to 100 µm) and configurations 3 and 4 (grinding to 500 µm) present similar results regarding electric consumption. However, grinding to 500 µm is by far less power consuming (by a factor 4). Grinding to 100 µm leads to an electric consumption greater than 5 % of the LHV (13 to 16 %). If all the preparation steps of the syngas are taken in account (harvesting the biomass, transport to the plant, preparation for the injection…), the process is too much power consuming. Thus, grinding to 100 µm must be rejected.

Configuration 2 is the best alternative solution to torrefaction. The electric consumption is 4 % of the LHV, compared with 1-2 % for the torrefaction. However, no energy is lost during the process (10 % is lost in the torrefaction process). Configuration 4 is interesting too but 20 % of the energy is lost in the drying steps.

5.4. Conclusions on the energetic study of the granulation

The energy consumption of the granulation process has been investigated. Four process configurations have been studied: with free heat or with chip combustion steps for the drying steps and two grain size, 100 and 500 µm. The results have been compared with the torrefaction process, another biomass preparation method for gasification. The combustion of torrefaction gases has been assumed to produce enough heat to dry and torrefy the biomass. However, it is a strong hypothesis, and torrefaction could have a lower ratio of final over initial energy content.

Grinding to 100 µm leads to an excessive power consumption in the grinding step. This option has to be rejected. However, grinding to 500 µm leads to low energy consumptions, comparable with the torrefaction process. Further research has to be done to assess the impact of acute granule edges on the flowability of the granules. With free heat for the drying step, the granulation process consumes 4 % of the wood combustion heat, and no product is lost (contrary to the torrefaction process). With chip combustion steps for the drying steps, 20 % of the mass is lost. Using a wood species with a lower initial moisture content is a solution to decrease the drying power consumption. The initial moisture content of green wood depends on the species. For example, green oak (which was used in this study) has a moisture content of 44 wt% (wet basis), whereas green beech has a moisture content of 33 wt% (wet basis) [13]. Moreover, the quantity of water added for the granulation has not been optimized. Using less water for the granulation would lead to a lower heat requirement for the drying step, and thus a lower energy loss.

This energetic study has shown the interest of the granulation method. Moreover, the effect of granulation on the flowability has been shown in the previous parts. The granulation method is an interesting alternative to torrefaction from an energetic point of view. An economic study is the next step towards the up-scaling of this process.

GENERAL CONCLUSION

The objective of this thesis was to better understand the flow of biomass powders, and to propose solutions to improve the biomass powder handling in the context of gasification in EFR. In order to achieve this objective, the work was organized in two parts, at lab scale and at pilot scale.

The lab scale part was organized in five main studies. Firstly, preliminary experiments have been carried out with the FT4 to make sure particles did not orient during shear tests. Then the effect of the number of avalanches in the rotating drum on flowability parameters was studied. A correlation between shear test parameters and the avalanche angle derived from rotating drum tests was investigated. The next study focused on the influence of moisture content on flowability parameters. Finally, a new granulation method (adapted for EFR gasification) was tested.

The pilot scale part was organized in four main studies. Firstly, a study of feeding hopper and the screw feeder in the injection pilot IRIS was carried out. Then the accumulation in the IRIS injector was investigated. The granulated powder has been injected in the EFR Giroflé. Finally, an energetic study of the granulation process has been performed.

First of all, from experimental results at lab scale, the main conclusions are:

- A modified shear test program with repeated points at the end of the experiment has been used. The repeated points are close to the first measured points. Thus, if there is a particle orientation phenomenon, it does not affect the shear test results.

- In the rotating drum Revolution, the number of recorded avalanches only has a small influence on the avalanche angle, and a negligible influence on the other parameters. 150 avalanches are enough to get accurate flowability parameters (avalanche angle, avalanche time).

- A new method for non-linear yield locus description is proposed, based on the Warren-Spring equation. It does not require to measure the tensile stress. The model describes accurately the experimental data.

- Based on experimental data obtained with thirty-four different powders (mainly wood) and at three preconsolidation stresses (2, 3 and 5 kPa), the Warren-Spring parameters cohesion, tensile stress and Warren-Spring index have been expressed as functions of easy to measure parameters: the avalanche angle and the aerated density. The cohesion, which is a key physical parameter of powder flowability, can be assessed with this method. For cohesive biomass powders with an avalanche angle higher than 50°, the yield locus can be modelled. This model is particularly adapted to model the mechanical behaviour in the lowest stress range. This work has highlighted a method to estimate the cohesion and describe the yield locus of cohesive biomass powders from easy to measure parameters.

- The addition of water in biomass powders has a small influence on their density, due to a swelling phenomenon, offsetting the mass increase. The flowability of wood powders starts to change when the moisture content reaches 15 wt% (wet basis), which corresponds to the glass-rubber transition. This effect is more obvious on parameters such as avalanche time and avalanche time distribution standard deviation. There is an effect of grinding intensity on the flowability with increasing moisture content for hardwoods (oak, beech): hardwoods present small pores that disappear for fine grinding. For a fine powder, the liquid bridges can form directly on the surface of particles, whereas for a coarse grinding, the water has to fill the pores first. Therefore, the flowability of fine powders decreases more for smaller moisture contents than coarse powders.

- The granulation method allows to form granules with a diameter below 1 mm from a raw biomass powder (with elongated particles and a polydispersed particle size) by adding a biomass waste binder. The main results are:
  - Particles are less elongated than that of the raw powder. Less elongated particles are less likely to interlock.
  - The particle size is increased. The fine particle content (which strongly influences the flowability) is lower in the granulated powder (almost zero) and the mean size is larger.
  - The span of the granulated powder size distribution is very low compared to that of the raw powder, its size distribution is narrow. Powders with a narrow size distribution have a better flowability because of the reduced number of contact points between particles.
  - The effect of granulation on flowability has been assessed with avalanche measurements. Avalanche angle, avalanche angle span, avalanche time and avalanche time standard deviation show a strong improvement of the flowability with the granulation compared with the raw powder.
  - The effect of granulation on the flowability is not only due to the increased granule size compared with the raw powder, but also the decreased particle size of the distribution, the low fine content and increased sphericity.

The main conclusions of the pilot scale study are:

- IRIS feeding hopper and screw feeder:
  - The screw speed has been shown to vary linearly with the engine speed, which is the parameter set to perform an experiment with IRIS.
  - The mass flow rate has been shown to be highly repeatable at different screw speeds with the microbead powder. A similar repeatability for the biomass powders is assumed.
  - The variation of vertical stress on the screw with the filling height has been calculated with the software SiloStressTool, for the reference powder and the microbead powder. The influence on cohesion length and density are negligible for the microbead powder and small for the reference powder. These small variations have been shown to have no influence on the screw flow rate. However, the influence of the height of powder on the engine torque is worth investigating.
  - The theoretical volumetric flow rate has been calculated thanks to the screw geometry. The volumetric flow rate of the different powder is below the theoretical volumetric flow rate. Indeed, the volumetric efficiency is decreased by several phenomena (incomplete filling of the screw pockets, non-ideal axial velocity and space between casing and screw flights leading to slippage of the particles). The decrease in volumetric efficiency is supposed to be due to the slippage between the powder and the screw for the microbead powder (low wall friction angle) and to uncomplete filling of the screw pockets for the biomass powders (compressible powders).

- Accumulation in the injector:
  - The microbead and the granulated powder have spherical particles, almost monodispersed. They present values of R above the critical value for which jamming is impossible for spherical and monodispersed particles. For them, powder accumulation is due to a too large inflow rate. If powder accumulation in the injector occurs with these powders, decreasing the inflow rate in the injector (which is the screw feed rate) solves the problem.
  - Biomass powders present elongated and polydispersed particles. For elongated particles, the critical value of R above which jamming is impossible increases compared with spherical particles. High particle size polydispersty is also expected to increase the critical value of R compared with monodispersed particles, due to the increased number of contact points between particles. But the calculation of the critical value of R is difficult due to the choice of a suitable particle diameter for polydispersed powder. The determination of the effect of polydispersed

particles size on the critical value of R is an interesting prospect. Experimentally, jamming occurs in the injector with all the biomass powders. Thus, elongation and polydispersity have a significant effect on the jamming phenomenon. For these powders, if accumulation occurs in the injector, the process has to be stopped to clean the injector.

- In the literature, the nature of powders is assumed not to have an influence on jamming. This is verified for the resinous powder and the coarse torrefied powder. They both have comparable particle size and shape, and they present the same behavior in the injector. The effect of torrefaction of the flowability is not observable. However, the fine torrefied powder and the reference powder have comparable particle size and shape, but they behavior is very different in the injector. The torrefied powder can pass through smaller orifices than the reference powder. Moreover, for the larger injector diameters, the torrefied powder does not form arches, contrary to the reference powder. Thus, for this particle size, there is an observable effect powder nature on the flowability. Torrefaction has a positive effect on flowability for small particles sizes. This may be due to the effect of torrefaction on surface qualities, which has a smaller effect for larger particle size (with the coarse powder for example).
- The parameter R has been adapted to polydispersed particles with the d_{10}, and linked with a lab scale parameter: the avalanche time standard deviation. This relation has to be used with caution: the small number of points may have led to a false positive. However, if the relation is correct, the avalanche time std deviation is linked to R_{10}. This relation gives information on the flow in the rotating drum: fine content, shape and polydispersity of the powder have an important role in the flow regularity.

- Injection in the gasifier Giroflé: the balances in the pilot scale EFR were not operable. The only possible observation is that jamming did not occur with the granulated powder, whereas the beech powder formed an arch in the injector.

- Energetic evaluation of the granulation process: Four process configurations have been studied, with free heat or with chip combustion steps for the drying steps and two grain size, 100 and 500 µm. The results have been compared with the torrefaction process, another biomass preparation method for gasification.
  - Grinding to 100 µm leads to an excessive power consumption in the grinding step. This option has to be rejected.
  - Grinding to 500 µm leads to low energy consumptions, comparable with the torrefaction process. Further research has to be done to assess the impact of acute granule edges on the flowability of the granules.
  - With free heat for the drying step, the granulation process consumes 4 % of the LHV, and no product is lost (contrary to the torrefaction process). With chip combustion steps for the drying steps, 20 % of the mass is lost.
  - The quantity of water added for the granulation has not been optimized. Using less water for the granulation would lead to a lower heat requirement for the drying step, and thus a lower energy loss. The granulation method is an interesting alternative to torrefaction from an energetic point of view. An economic study is the next step towards the up-scaling of this process.

The main prospects on experimentations to arise from this work for future studies are:

- The correlation between parameters derived from a shear test and avalanche angle has been determined with the FT4. The validity of the correlation with another shear cell (Jenike or Schulze for example) could be investigated. Moreover, the aerated density has been chosen because of the low consolidations biomass powders are subjected to. However, other densities are worth trying (poured density or tapped density for example)

- The effect of moisture content has been investigated for six wood powders. The effect of this parameter could be studied for other wood species and other biomasses (agricultural residues for example).
- The granulation process has been shown to be interesting from an energetic point of view for biomasses with a large initial particle size (500 µm). However, the granules formed with large initial particles present acute edges. Therefore, the flowability of the granules with acute edges has to be assessed both at lab scale and pilot scale. Other biomasses and binders could be tried as well. Moreover, the economic interest of the process has to be investigated. Finally, the granulated powder could be injected again in the EFR Giroflé with correct balances to observe its behaviour in gasification.
- The parameter R could be expanded to polydispersed particle sizes, giving interesting clues on the ability of biomass powders to flow through orifices. Moreover, an effect of powder nature (torrefaction and raw powders) have been highlighted for small particle size. This could be an effect of gas permeability, friction between particles or the cohesion. Further research have to be made on this subject and these parameters could be taken in account in the expanded parameter R.
- In this work the minimum Feret's diameter has been taken in account regarding particle size. However, the maximum Feret's diameter could be worth using, for the jamming phenomenon study in particular.

BIBLIOGRAPHIC REFERENCES

[1] R. Warren, J. Price, A. Fischlin, S. de la Nava Santos, and G. Midgley, "Increasing impacts of climate change upon ecosystems with increasing global mean temperature rise," *Clim. Change*, vol. 106, no. 2, pp. 141–177, May 2011.
[2] B. K. Bose, "Global Warming: Energy, Environmental Pollution, and the Impact of Power Electronics," *IEEE Ind. Electron. Mag.*, vol. 4, no. 1, pp. 6–17, Mar. 2010.
[3] W. P. M. van Swaaij, S. R. A. Kersten, and W. Palz, Eds., *Biomass power for the world: transformations to effective use*. Singapore: Pan Stanford Publishing, 2015.
[4] J. Bridgwater, "The dynamics of granular materials – towards grasping the fundamentals," *Granul. Matter*, vol. 4, no. 4, pp. 175–181, Feb. 2003.
[5] S. Koynov, B. Glasser, and F. Muzzio, "Comparison of three rotational shear cell testers: Powder flowability and bulk density," *Powder Technol.*, vol. 283, pp. 103–112, Oct. 2015.
[6] P. McKendry, "Energy production from biomass (part 1): overview of biomass," *Bioresour. Technol.*, no. 83, pp. 37–46, 2002.
[7] W.-H. Chen, J. Peng, and X. T. Bi, "A state-of-the-art review of biomass torrefaction, densification and applications," *Renew. Sustain. Energy Rev.*, vol. 44, pp. 847–866, Apr. 2015.
[8] J. J. Harrington, R. Booker, and Astley R.J., "Modelling the elastic properties of softwood. Part I: The cell-wall lamellae," *Holz Als Roh- Werkst.*, no. 56, pp. 37–41, 1998.
[9] E. Sjöström, *Wood chemistry: Fundamentals and Applications*, 2nd ed. Academic Press, 1993.
[10] G. Henriksson, J. Li, L. Zhang, and M. E. Lindström, "Chapter 9: Lignin Utilization," in *Thermochemical Conversion of Biomass to Liquid Fuels and Chemicals*, 2010.
[11] P. F. H. Harmsen, W. J. J. Huijgen, L. M. Bermúdez López, and R. R. C. Bakker, "Literature Review of Physical and Chemical Pretreatment Processes for Lignocellulosic Biomass," Energy Research Centre of the Netherlands, Sep. 2010.
[12] B. Andreotti, Y. Forterre, and O. Pouliquen, *Les Milieux Granulaires Entre Fluide Et Solide*. EDP Sciences, 2011.
[13] P. Evesque, "Eléments de mécanique quasi-statique des milieux granulaires mouillés ou secs," *ResearchGate*, Jan. 2000.
[14] R. Condotta, "Coulabilité des poudres cohésives : mesures aux faibles contraintes, granulaires humides et application à une poudre industrielle.," 30-Sep-2005. [Online]. Available: http://ethesis.inp-toulouse.fr/archive/00000181/. [Accessed: 02-Jun-2016].
[15] A. W. Alexander, B. Chaudhuri, A. Faqih, F. J. Muzzio, C. Davies, and M. S. Tomassone, "Avalanching flow of cohesive powders," *Powder Technol.*, vol. 164, no. 1, pp. 13–21, May 2006.
[16] G. Lumay *et al.*, "Measuring the flowing properties of powders and grains," *Powder Technol.*, vol. 224, pp. 19–27, Jul. 2012.
[17] O. Reynolds, "LVII. On the dilatancy of media composed of rigid particles in contact. With experimental illustrations," *Lond. Edinb. Dublin Philos. Mag. J. Sci.*, vol. 20, no. 127, pp. 469–481, Dec. 1885.
[18] J. M. Rodriguez, T. Edeskär, and S. Knutsson, "Particle shape quantities and measurement techniques-A review," *Electron. J. Geotech. Eng.*, vol. 18 A, pp. 169–198, 2013.
[19] K. Johanson, "Effect of particle shape on unconfined yield strength," *Powder Technol.*, vol. 194, no. 3, pp. 246–251, Sep. 2009.
[20] A. G. Athanassiadis *et al.*, "Particle shape effects on the stress response of granular packings," *Soft Matter*, vol. 10, no. 1, pp. 48–59, Nov. 2013.
[21] D. Hann, "The influence of some parameters on the flow properties of bulk solids," *Strojniski VestnikJournal Mech. Eng.*, vol. 55, no. 5, 2009.
[22] D. Höhner, S. Wirtz, and V. Scherer, "A study on the influence of particle shape on the mechanical interactions of granular media in a hopper using the Discrete Element Method," *Powder Technol.*, vol. 278, pp. 286–305, Jul. 2015.
[23] D. Höhner, S. Wirtz, and V. Scherer, "Experimental and numerical investigation on the influence of particle shape and shape approximation on hopper discharge using the discrete element method," *Powder Technol.*, vol. 235, pp. 614–627, Feb. 2013.
[24] Q. Guo, X. Chen, and H. Liu, "Experimental research on shape and size distribution of biomass particle," *Fuel*, vol. 94, pp. 551–555, Apr. 2012.
[25] D. Barletta, R. J. Berry, S. H. Larsson, T. A. Lestander, M. Poletto, and Á. Ramírez-Gómez, "Assessment on bulk solids best practice techniques for flow characterization and storage/handling

equipment design for biomass materials of different classes," *Fuel Process. Technol.*, vol. 138, pp. 540–554, Oct. 2015.
[26] M. Stasiak, M. Molenda, M. Bańda, and E. Gondek, "Mechanical properties of sawdust and woodchips," *Fuel*, vol. 159, pp. 900–908, Nov. 2015.
[27] J. Dai and J. R. Grace, "Biomass granular screw feeding: An experimental investigation," *Biomass Bioenergy*, vol. 35, no. 2, pp. 942–955, Feb. 2011.
[28] H. G. Merkus and G. M. H. Meesters, *Production, Handling and Characterization of Particulate Materials*. Springer, 2015.
[29] I. Tomasetta, D. Barletta, and M. Poletto, "The effect of temperature on flow properties of fine powders," *Chem. Eng. Trans.*, vol. 24, pp. 655–660, 2011.
[30] S. Paulrud, J. E. Mattsson, and C. Nilsson, "Particle and handling characteristics of wood fuel powder: effects of different mills," *Fuel Process. Technol.*, vol. 76, no. 1, pp. 23–39, Apr. 2002.
[31] X. Jia and E. J. Garboczi, "Advances in shape measurement in the digital world," *Particuology*, vol. 26, pp. 19–31, Jun. 2016.
[32] "REVOLUTION Powder Analyzer | Mercury Scientific Inc." [Online]. Available: http://www.mercuryscientific.com/instruments/revolution-powder-analyzer. [Accessed: 28-Jun-2018].
[33] G. Lumay, J. Fiscina, F. Ludewig, and N. Vandewalle, "Influence of cohesive forces on the macroscopic properties of granular assemblies," in *AIP Conference Proceedings*, 2013, vol. 1542, pp. 995–998.
[34] S. C. Thakur *et al.*, "Characterization of cohesive powders for bulk handling and DEM modelling," in *PARTICLES 2013: Fundamentals and Applications*, Barcelona, Spain, 2013, pp. 310–321.
[35] M. Wojtkowski, O. I. Imole, M. Ramaioli, E. C. Montes, and S. Luding, "Behavior of cohesive powder in rotating drums," in *AIP Conference Proceedings*, 2013, vol. 1542, pp. 983–986.
[36] D. Geldart, E. C. Abdullah, and A. Verlinden, "Characterisation of dry powders," *Powder Technol.*, vol. 190, no. 1–2, pp. 70–74, Mar. 2009.
[37] H. Y. Saw, C. E. Davies, A. H. J. Paterson, and J. R. Jones, "Correlation between Powder Flow Properties Measured by Shear Testing and Hausner Ratio," *Procedia Eng.*, vol. 102, pp. 218–225, 2015.
[38] D. Geldart, N. Harnby, and A. C. Wong, "Fluidization of cohesive powders," *Powder Technol.*, vol. 37, no. 1, pp. 25–37, Jan. 1984.
[39] G. Ovarlez, *Statique et rhéologie d'un milieu granulaire confiné*. Paris 11, Orsay, 2002.
[40] D. Schulze, *Powders and Bulk Solids: Behavior, Characterization, Storage and Flow*. Springer Science & Business Media, 2007.
[41] A. W. Jenike, *Storage and Flow of Solids*. University of Utah, 1964.
[42] D. Schulze and A. Wittmaier, "Flow Properties of Highly Dispersed Powders at Very Small Consolidation Stresses," *Chem. Eng. Technol.*, vol. 26, no. 2, pp. 133–137, Feb. 2003.
[43] J. W. Carson and H. Wilms, "Development of an international standard for shear testing," *Powder Technol.*, vol. 167, no. 1, pp. 1–9, Sep. 2006.
[44] M. D. Ashton, D. C.-H. Cheng, R. Farley, and F. H. H. Valentin, "Some investigations into the strength and flow properties of powders," *Rheol. Acta*, vol. 4, no. 3, pp. 206–218, Oct. 1965.
[45] M. Hirota, K. Takenaka, K. Iimura, and M. Suzuki, "Proposal of an approximation equation for the yield locus to evaluate powder properties," *Adv. Powder Technol.*, vol. 18, no. 3, pp. 287–302, Jan. 2007.
[46] J. L. Amorós, G. Mallol, C. Feliu, and M. J. Orts, "Study of the rheological behaviour of monomodal quartz particle beds under stress. A model for the shear yield functions of powders," *Chem. Eng. Sci.*, vol. 66, no. 18, pp. 4070–4077, Sep. 2011.
[47] J.-M. Geoffroy and J. T. Carstensen, "Modified Warren-Springs equation," *Powder Technol.*, vol. 76, no. 2, pp. 135–140, Aug. 1993.
[48] M. Peleg, M. D. Normand, and M. G. Corradini, "Interactive software for calculating the principal stresses of compacted cohesive powders with the Warren-Spring equation," *Powder Technol.*, vol. 197, no. 3, pp. 268–273, Jan. 2010.
[49] F. da C. François Chevoir, "DENSE GRANULAR FLOWS : FRICTION AND JAMMING."
[50] P. G. Rognon, J.-N. Roux, D. Wolf, M. Naaïm, and F. Chevoir, "Rheophysics of cohesive granular materials," *Europhys. Lett. EPL*, vol. 74, no. 4, pp. 644–650, May 2006.

[51] H.-G. Matuttis and A. Schinner, “Particle simulation of cohesive granular materials,” *Int. J. Mod. Phys. C*, vol. 12, no. 07, pp. 1011–1021, Sep. 2001.
[52] F. Radjai and F. Dubois, *Discrete-element modeling of granular materials*. Wiley-Iste, 2011.
[53] A. Castellanos, “The relationship between attractive interparticle forces and bulk behaviour in dry and uncharged fine powder,” *Adv. Phys.*, vol. 54, no. 4, pp. 263–376, 2005.
[54] A. Singh, V. Magnanimo, K. Saitoh, and S. Luding, “Effect of cohesion on shear banding in quasistatic granular materials,” *Phys. Rev. E*, vol. 90, no. 2, p. 022202, Aug. 2014.
[55] M. Capece, R. Ho, J. Strong, and P. Gao, “Prediction of powder flow performance using a multi-component granular Bond number,” *Powder Technol.*, vol. 286, pp. 561–571, Dec. 2015.
[56] P. Lamarche, *Contribution à l’étude expérimentale et à la modélisation de la gazéification étagée de biomasse en lit fixe*. Nantes, 2011.
[57] R. Warnecke, “Gasification of biomass: comparison of fixed bed and fluidized bed gasifier,” *Biomass Bioenergy*, vol. 18, no. 6, pp. 489–497, Jun. 2000.
[58] D. Ballerini, *Biocarburants (Les)*. Editions OPHRYS.
[59] P. McKendry, “Energy production from biomass (part 3): gasification technologies,” *Bioresour. Technol.*, vol. 83, no. 1, pp. 55–63, May 2002.
[60] A. Molino, V. Larocca, S. Chianese, and D. Musmarra, “Biofuels Production by Biomass Gasification: A Review,” *Energies*, vol. 11, no. 4, p. 811, Mar. 2018.
[61] K. Svoboda, M. Pohořelý, M. Hartman, and J. Martinec, “Pretreatment and feeding of biomass for pressurized entrained flow gasification,” *Fuel Process. Technol.*, vol. 90, no. 5, pp. 629–635, May 2009.
[62] P. W. Wypych and J. Yi, “Minimum transport boundary for horizontal dense-phase pneumatic conveying of granular materials,” *Powder Technol.*, vol. 129, no. 1–3, pp. 111–121, Jan. 2003.
[63] M. Hopkins, “LOSS in weight feeder systems,” *Meas. Control*, vol. 39, no. 8, pp. 237–240, 2006.
[64] C. Wilén and A. Rautalin, “Handling and feeding of biomass to pressurized reactors: Safety engineering,” *Bioresour. Technol.*, vol. 46, no. 1–2, pp. 77–85, 1993.
[65] K. R. Cummer and R. C. Brown, “Ancillary equipment for biomass gasification,” *Biomass Bioenergy*, vol. 23, no. 2, pp. 113–128, Aug. 2002.
[66] J. M. Craven, J. Swithenbank, V. N. Sharifi, D. Peralta-Solorio, G. Kelsall, and P. Sage, “Development of a novel solids feed system for high pressure gasification,” *Fuel Process. Technol.*, vol. 119, pp. 32–40, Mar. 2014.
[67] S. Hinterreiter, H. Hartmann, and P. Turowski, “Method for determining bridging properties of biomass fuels—experimental and model approach,” *Biomass Convers. Biorefinery*, vol. 2, no. 2, pp. 109–121, Jun. 2012.
[68] F. Miccio, N. Silvestri, D. Barletta, and M. Poletto, “Characterization of woody biomass flowability,” *Chem. Eng. Trans.*, vol. 24, pp. 643–648, 2011.
[69] R. M. Nedderman, U. Tüzün, S. B. Savage, and G. T. Houlsby, “The flow of granular materials—I: Discharge rates from hoppers,” *Chem. Eng. Sci.*, vol. 37, no. 11, pp. 1597–1609, Jan. 1982.
[70] Khashayar Saleh and P. guigon, “Mise en œuvre des poudres - Granulation humide : bases et théorie,” *Tech. Ing.*, Sep. 2009.
[71] B. J. Ennis, “Agglomeration technology: Equipment selection,” *Chem. Eng.*, vol. 117, no. 5, pp. 50–54, 2010.
[72] V. Yandapalli, “Granulation of lignocellulosic powders,” University of Georgia, 2013.
[73] C. Vanneste-Ibarcq and M. González-Martínez, “Method for processing a biomass powder by wet granulation with a view to introducing same into a reactor, associated biomass powder, application to biomass gasification,” WO2018096056, 31-May-2018.
[74] “CAMSIZER X2 - particle size & shape analyzer - Retsch Technology.” [Online]. Available: https://www.retsch-technology.com/products/dynamic-image-analysis/camsizer-x2/function-features/. [Accessed: 04-Jul-2018].
[75] P. Tegzes, R. Albert, M. Paskvan, A.-L. Barabási, T. Vicsek, and P. Schiffer, “Liquid-induced transitions in granular media,” *Phys. Rev. E*, vol. 60, no. 5, pp. 5823–5826, Nov. 1999.
[76] T. C. Halsey and A. J. Levine, “How Sandcastles Fall,” *Phys. Rev. Lett.*, vol. 80, no. 14, pp. 3141–3144, Apr. 1998.
[77] C. C. Sun, “Quantifying effects of moisture content on flow properties of microcrystalline cellulose using a ring shear tester,” *Powder Technol.*, vol. 289, pp. 104–108, Feb. 2016.

[78] A. Crouter and L. Briens, "The Effect of Moisture on the Flowability of Pharmaceutical Excipients," *AAPS PharmSciTech*, vol. 15, no. 1, pp. 65–74, Oct. 2013.
[79] M. A. S. Quintanilla, J. M. Valverde, A. Castellanos, and R. E. Viturro, "Looking for Self-Organized Critical Behavior in Avalanches of Slightly Cohesive Powders," *Phys. Rev. Lett.*, vol. 87, no. 19, p. 194301, Oct. 2001.
[80] J. M. Valverde and A. Castellanos, "Random loose packing of cohesive granular materials," *EPL Europhys. Lett.*, vol. 75, no. 6, p. 985, Aug. 2006.
[81] R. J. Ross and F. P. L. U. F. Service, "Wood handbook : wood as an engineering material," *USDA For. Serv. For. Prod. Lab. Gen. Tech. Rep. FPL- GTR-190 2010 509 P 1 V*, vol. 190, 2010.
[82] J. Pachón-Morales, J. Colin, F. Pierre, T. Champavert, F. Puel, and P. Perré, "Flowability of lignocellusic biomass powders: influence of torrefaction intensity," *EPJ Web Conf.*, vol. 140, p. 13017, 2017.
[83] "Dr. Dietmar Schulze Schüttgutmesstechnik." [Online]. Available: http://www.dietmar-schulze.de/fre.html. [Accessed: 22-Aug-2018].
[84] D. Schulze and J. Schwedes, "An examination of initial stresses in hoppers," *Chem. Eng. Sci.*, vol. 49, no. 13, pp. 2047–2058, Jul. 1994.
[85] P. C. Arnold and A. G. McLean, "An analytical solution for the stress function at the wall of a converging channel," *Powder Technol.*, vol. 13, no. 2, pp. 255–260, Mar. 1976.
[86] C. Mankoc *et al.*, "The flow rate of granular materials through an orifice," *Granul. Matter*, vol. 9, no. 6, pp. 407–414, Nov. 2007.
[87] I. Zuriguel, A. Garcimartín, D. Maza, L. A. Pugnaloni, and J. M. Pastor, "Jamming during the discharge of granular matter from a silo," *Phys. Rev. E Stat. Nonlin. Soft Matter Phys.*, vol. 71, no. 5 Pt 1, p. 051303, May 2005.
[88] K. To, "Effect of Hopper Angles on Jamming Probability in 2-Dimensional Hoppers," *Chin. J. Phys.*, vol. 40, no. 4, pp. 379–386, Aug. 2002.
[89] A. van der Drift, H. Boerrigter, B. Coda, M. K. Cieplik, and K. Hemmes, "ECN Publication ECN-C--04-039." [Online]. Available: http://www.ecn.nl/publications/ECN-C--04-039. [Accessed: 31-Aug-2018].
[90] N. Haque and M. Somerville, "Techno-Economic and Environmental Evaluation of Biomass Dryer," *Procedia Eng.*, vol. 56, pp. 650–655, Jan. 2013.
[91] "Mesure des caractéristiques des combustibles bois : évaluation et proposition de méthodes d'analyse de combustible," *ADEME*. [Online]. Available: https://www.ademe.fr/en/content/mesure-caracteristiques-combustibles-bois-evaluation-proposition-methodes-danalyse-combustible. [Accessed: 29-Aug-2018].
[92] J. S. Tumuluru, S. Sokhansanj, J. R. Hess, C. T. Wright, and R. D. Boardman, "A review on biomass torrefaction process and product properties for energy applications," *Ind. Biotechnol.*, vol. 7, no. 5, pp. 384–401, 2011.
[93] D. R. Lide and Chemical Rubber Company, Eds., *CRC handbook of chemistry and physics: a ready-reference book of chemical and physical data*, 77. ed., 1996 - 1997. Boca Raton: CRC Press, 1996.

APPENDIX

(19) RÉPUBLIQUE FRANÇAISE

INSTITUT NATIONAL
DE LA PROPRIÉTÉ INDUSTRIELLE

COURBEVOIE

(11) N° de publication : **3 059 008**
(à n'utiliser que pour les commandes de reproduction)

(21) N° d'enregistrement national : **16 61477**

(51) Int Cl[8] : ***C 10 J 3/54*** *(2017.01), C 10 J 3/48, C 10 L 5/44*

(12) DEMANDE DE BREVET D'INVENTION A1

(22) **Date de dépôt :** 24.11.16.

(30) **Priorité :**

(43) **Date de mise à la disposition du public de la demande :** 25.05.18 Bulletin 18/21.

(56) **Liste des documents cités dans le rapport de recherche préliminaire :** *Se reporter à la fin du présent fascicule*

(60) **Références à d'autres documents nationaux apparentés :**

( ) **Demande(s) d'extension :**

(71) **Demandeur(s) :** *COMMISSARIAT A L'ENERGIE ATOMIQUE ET AUX ENERGIES ALTERNATIVES Etablissement public* — FR.

(72) **Inventeur(s) :** VANNESTE-IBARCQ CLEMENT et GONZALEZ-MARTINEZ MARIA.

(73) **Titulaire(s) :** COMMISSARIAT A L'ENERGIE ATOMIQUE ET AUX ENERGIES ALTERNATIVES Etablissement public.

(74) **Mandataire(s) :** CABINET NONY.

(54) PROCEDE DE TRAITEMENT D'UNE POUDRE DE BIOMASSE PAR GRANULATION HUMIDE EN VUE DE SON INTRODUCTION DANS UN REACTEUR, POUDRE DE BIOMASSE ASSOCIEE, APPLICATION A LA GAZEIFICATION DE BIOMASSE.

(57) La présente invention concerne un procédé de gazéification de biomasse, comprenant les étapes successives suivantes :

a/ séchage d'une biomasse ;

b/ broyage de la biomasse afin d'obtenir une poudre sèche,

c/ granulation humide de la poudre de biomasse pour obtenir des granulés de biomasse sous la forme d'une semoule ;

d/ séchage des granulés de semoule ;

e/ injection de la semoule sèche dans un réacteur de gazéification.

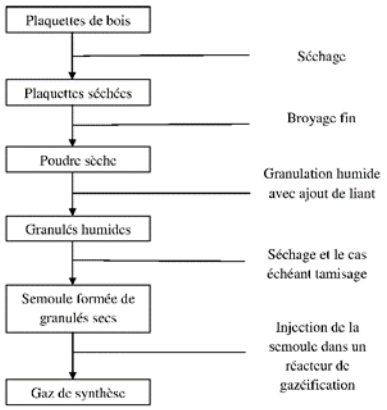

FR 3 059 008 - A1

3059008

PROCEDE DE TRAITEMENT D'UNE POUDRE DE BIOMASSE PAR GRANULATION HUMIDE EN VUE DE SON INTRODUCTION DANS UN REACTEUR, POUDRE DE BIOMASSE ASSOCIEE, APPLICATION A LA GAZEIFICATION DE BIOMASSE

Domaine technique

La présente invention concerne le domaine général de la gazéification de la biomasse, plus particulièrement de la biomasse ligno-cellulosique.

Par « biomasse », on entend ici et dans le cadre de l'invention, c'est-à-dire tout matériau inhomogène d'origine végétale contenant du carbone, tel que de la biomasse ligno-cellulosique, des résidus forestiers ou agricoles (paille), ou des déchets ménagers. Toutes ces charges peuvent être sèches ou humides.

L'invention a plus particulièrement trait au traitement de biomasse préalablement broyée sous forme de poudre, en vue de son injection sous forme pulvérisée dans un réacteur de gazéification en aval.

L'invention s'applique avantageusement à la gazéification de biomasse en vue de la réalisation de biocarburants à partir du gaz de synthèse largement connu sous l'appellation Syngaz.

Etat de la technique

Le traitement mécanique de la biomasse (tronc d'arbre, balles de paille) comprend classiquement une première étape de broyage grossier, en général sur le lieu même de la récolte, qui permet notamment de faciliter le transport et d'en réduire son coût. Cette première étape de broyage est réalisée au moyen de déchiqueteuse (en anglais « *shredder* ») et conduit à des particules de dimensions centimétriques ou millimétriques, typiquement des plaquettes forestières dans les filières bois. Elle est réalisée au moyen de broyeurs à la technologie éprouvée (broyeur à marteaux, à couteaux ou à ciseaux). Les particules ainsi broyées grossièrement constituent ainsi ce que l'on appelle les intrants dans les voies de gazéification ou de combustion de biomasse (cogénération de chaleur et d'électricité, production de chaleur, production de biocarburants).

Les procédés actuels en cours d'étude ou à l'échelle de pilote industriel, permettant de convertir par voie thermochimique la biomasse comprennent nécessairement une étape de gazéification de la biomasse pour obtenir un gaz de synthèse contenant du monoxyde de carbone (CO) et de l'hydrogène (H_2).

L'étape de gazéification proprement dite est réalisée en continu à partir de la biomasse de nature et de granulométrie différentes stockée habituellement à la pression atmosphérique.

Ainsi, les procédés de gazéification de la biomasse ligno-cellulosique permettent de générer un gaz de synthèse qui permet de produire en aval soit des carburants liquides soit d'autres produits organiques. Cette gazéification se déroule en présence typiquement de vapeur d'eau vers 1400-1600°C pour des réacteurs à flux entrainé. Classiquement, ces procédés convertissent le carbone de la biomasse avec un gaz en sortie du gazéifieur avec une composition moyenne de 20-25 % en CO, 8-12 % en CH_4, 18-22 % en CO_2 et environ 38-42 % en H_2 et, des composés organiques C_2 à C_{16} plus des composés inorganiques.

A ce jour, pour une application de gazéification de la biomasse dans un réacteur de type réacteur à flux entrainé, les particules de biomasse nécessitent un broyage fin pour la mettre sous forme de poudre, typiquement pour qu'elles atteignent une taille comprise entre 30 et 300 microns. Une fine poudre de biomasse, en particulier une biomasse ligno-cellulosique, permet intrinsèquement un temps de séjour court, de l'ordre de la seconde, à l'intérieur du réacteur de gazéification.

Un certain nombre d'études est consacré au broyage fin de particules de biomasse, notamment de plaquettes forestières, pour atteindre des granulométries du millimètre au micron selon les cas. Dans ces études, les effets de la nature de la biomasse, du type de broyeur(s) utilisé(s), de la granulométrie désirée ont été caractérisés sur le coût énergétique de l'opération proprement dite de broyage fin, et/ou les propriétés de la poudre obtenue (distribution granulométrique, forme des particules).

Mais, quel que soit le broyage fin réalisé, une poudre de biomasse présente néanmoins des inconvénients.

Tout d'abord, la poudre de biomasse, en particulier de bois, est cohésive, ce qui implique qu'elle s'écoule difficilement du fait de l'attraction par forces de van der Waals et forces électrostatiques, et de la forme allongée des particules de poudre. En outre, de nombreuses étapes de manipulation d'une poudre de biomasse sont nécessaires en amont du gazéifieur, comme le stockage, la décharge, le convoyage, et enfin l'injection dans le gazéifieur. Du fait du caractère cohésif de la poudre de biomasse, on rencontre des difficultés techniques à chacune de ces étapes.

A ce jour, en partie du fait que le convoyage d'une poudre de biomasse s'heurte toujours à des difficultés, le procédé de gazéification de la biomasse, plus particulièrement de biomasse ligno-cellulosique, n'a pas connu de développement à l'échelle industrielle

La technique de granulation des poudres est connue et maitrisée dans le domaine de l'industrie pharmaceutique, notamment pour la fabrication des comprimés et granulés pour sachets. La granulation a pour fonction de transformer des particules de poudres en agrégats solides plus ou moins résistants et plus ou moins poreux, appelés couramment granulés.

Par rapport à un simple mélange de poudres, des granulés présentent un certain nombre d'avantages dont un meilleur écoulement, en raison de l'augmentation de la densité et de la taille des particules par la formation d'un granulé et à la modification de la forme et de l'état de surface de ces particules.

La granulation par voie humide est particulièrement efficace. Elle consiste en une mise en mouvement et une agitation des particules d'un mélange de poudres ou d'une poudre avec un liant sous la forme d'un liquide de mouillage, afin d'en obtenir leur agglomération. Cette étape d'agitation mécanique est suivie d'une étape de séchage des granulés obtenus. L'étape de séchage permet de diminuer le taux d'humidité à une valeur adaptée pour obtenir la mise en forme.

Plusieurs technologies peuvent être mises en œuvre pour la granulation humide. On pourra se référer aux publications [1] et [2].

Parmi celles-ci, on peut citer les granulateurs à assiette tournante qui ont pour principaux avantages d'être simple à mettre en place de permettre un séchage en même temps que la granulation.

Les granulateurs-mélangeurs à fort taux de cisaillement dont la gamme de géométries disponibles est très variée permettent par leur compacité, d'obtenir des granulés denses et moins sphériques que les autres technologies, mais utilisent moins de liquide de mouillage. Les granulateurs à arbre central d'agitation mécanique peuvent produire des granulés de taille comprise entre 0,5 et 1mm. Les temps de séjour sont de quelques secondes. Les granulateurs à arbre central sont le plus souvent reliés en aval à des mélangeurs à plus long temps de séjour et à faible cisaillement qui permettent de continuer la croissance et la densification des granulés.

L'auteur de la publication [3] s'est intéressé à la granulation humide de particules de biomasse pour une production de granulés à utiliser en tant que combustibles. Les liants utilisés décrits dans cette publication, sont de plusieurs natures différentes : il peut s'agir de déchets d'usine de papier, de lignine, bentonite, huiles de pyrolyse ou encore d'amidon. De cette publication [3], il ressort que l'amidon présente les meilleures performances en termes de capacité à lier les particules, le contenu en cendres après combustion des granulés obtenus, de coût ou encore de disponibilité. L'auteur de cette publication s'intéresse surtout à l'augmentation de la densité des granulés de biomasse ligno-cellulosique, en vue d'améliorer leur manipulation, transport et stockage à des fins exclusivement de combustion.

Il existe donc un besoin général d'améliorer le procédé de gazéification de biomasse, en particulier de biomasse ligno-cellulosique, afin de surmonter les inconvénients actuels liés aux poudres cohésives de biomasse, avant leur injection dans un réacteur de gazéification.

Il existe un besoin particulier d'une solution qui réponde au besoin général, qui soit simple à mettre en œuvre et peu coûteuse, notamment qui puisse être intégrée sans modifications substantielles dans une installation de gazéification en continu.

Le but de l'invention est de répondre au moins en partie à ce besoin.

Exposé de l'invention

Pour ce faire, l'invention concerne, sous un de ses aspects, un procédé de gazéification de biomasse, comprenant les étapes successives suivantes :

a/ séchage d'une biomasse ;

b/ broyage de la biomasse afin d'obtenir une poudre sèche,

c/ granulation humide de la poudre de biomasse pour obtenir des granulés de biomasse sous la forme d'une semoule ;

d/ séchage des granulés de semoule ;

e/ injection de la semoule sèche dans un réacteur de gazéification.

Par « granulés de semoule », on entend ici et dans le cadre de l'invention un produit dont la matière première est de la biomasse et qui est obtenu par mouture grossière de grains humidifiés par granulation humide d'une poudre séchée de biomasse, qui est suivie d'une étape séchage et le cas échéant d'une étape de tamisage.

L'étape e/ est de préférence une injection dans un réacteur de gazéification à flux entraîné (RFE).

La biomasse peut être avantageusement de la biomasse ligno-cellulosique.

Dans le cadre de l'invention, il est possible de réaliser l'étape c/ de granulation humide avec ou sans liant. Dans la plupart des cas, il est préférable d'avoir un liant.

Le liant peut être compris en tant que tel dans la biomasse à gazéifier. Par exemple, lorsque la biomasse est constituée de déchets de canne à sucre, il n'est pas nécessaire de rajouter un liant supplémentaire car les déchets de canne à sucre contiennent déjà un liant qui est le sucre contenu.

En revanche, pour certains types de biomasse, on peut procéder avantageusement à l'ajout d'un liant en supplément de la biomasse.

Ainsi, selon un mode de réalisation avantageux, l'étape c/ de granulation humide est réalisée par ajout à la poudre d'un liant choisi parmi l'amidon, la drêche de féculerie, des déchets agricoles comprenant des déchets de canne à sucre et/ou des pépins de raisin, et/ou des drèches de palmier à huile et/ou des déchets de sorgho et/ou des grignons d'olive et/ou des coques de graines de tournesol, des écorces d'agrumes, des micro-algues, des algues, du lactosérum ou un mélange de ceux-ci.

Les inventeurs ont procédé à différentes analyses de type thermogravimétrique (ATG) : on pourra se reporter à la publication [4] pour les protocoles et appareils d'essais utilisés.

De de ces analyses, ils ont pu en déduire que :

- l'amidon est avantageux à mettre en œuvre, car il se dégrade en même temps que le bois;

- le lactosérum i fonctionne très bien en tant que liant, car il se dégrade avant le bois, sous l'effet de la chaleur. Ainsi, cela permet d'envisager que des granulés de biomasse liés par du lactosérum s'effritent lors de leur injection dans le réacteur de gazéification des températures élevées qui y règnent typiquement entre 1200 et 1600°C, et forment à nouveau une poudre dont les particules présentent un diamètre parfaitement adapté, typiquement inférieur à 1 mm, pour subir la gazéification, et donc avantageusement sans aucune augmentation de leur temps de séjour dans le réacteur. En outre, le lactosérum a pour avantage supplémentaire de ne pas nécessiter de préparation

préalable et ainsi de pouvoir être versé directement en tant que liant liquide sur la poudre séchée de biomasse.

La proportion massique de liant par rapport à celle de la poudre peut être comprise entre 0 et 90%.

Selon une variante avantageuse, un liquide, de préférence de l'eau, est ajouté directement par pulvérisation dans le mélange entre liant et poudre.

Selon une autre variante avantageuse, le liant est mélangé à un liquide, de préférence de l'eau, le mélange étant éventuellement chauffé de sorte à obtenir un gel ajouté par pulvérisation dans la poudre. Lorsque le liant est l'amidon, le chauffage du mélange est nécessaire.

Dans le cas où le liant est l'amidon, sa proportion massique est avantageusement comprise entre 5 et 10% de celle de la poudre.

Le procédé peut comprendre en outre, après l'étape d/, une étape d1/ de tamisage de la semoule séchée. Le tamisage peut être réalisé lorsqu'au moins une partie des granulés obtenus au préalable ont des dimensions qui ne permettent pas de respecter les spécifications de temps de séjour courts pour la réaction de gazéification.

De préférence, les granulés secs obtenus, éventuellement après l'étape d1/ de tamisage, et avant l'étape d'injection e/, ont un diamètre représentatif inférieur à 1 mm.

L'invention a également pour objet, selon un autre de ses aspects, une installation gazéification en continu de biomasse comprenant un réacteur de gazéification et en amont de celui-ci un dispositif de mise en œuvre de la granulation humide de poudre séchée de biomasse, destinée à mettre en œuvre l'étape c/ du procédé décrit précédemment.

L'invention est particulièrement avantageuse à mettre en œuvre dans une installation comprenant un réacteur à flux entrainé (RFE), avec un dispositif constitué par un granulateur à plateau tournant ou un granulateur-mélangeur à fort taux de cisaillement, le réacteur étant un réacteur de type à flux entraîné.

Ainsi l'invention consiste essentiellement à introduire une étape de granulation humide de la poudre séchée de biomasse avant l'étape d'injection dans le réacteur de gazéification.

De par la modification de la forme et l'augmentation de la taille induites par la granulation, les granulés de biomasse formant une semoule ont des propriétés d'écoulement grandement améliorées par rapport à une poudre séchée de biomasse.

Le convoyage de la biomasse est ainsi grandement amélioré ce qui permet d'obtenir une injection aisée et en continu dans le réacteur de gazéification, avec un dosage fin, précis, stable et reproductible.

Description détaillée

D'autres avantages et caractéristiques de l'invention ressortiront mieux à la lecture de la description détaillée d'exemples de mise en œuvre de l'invention faite à titre illustratif et non limitatif en référence aux figures suivantes, parmi lesquelles :

- la figure 1 est une vue d'un organigramme d'enchaînement des opérations et des états de la biomasse ligno-cellulosique qui en résultent dans un procédé de gazéification selon l'invention;

- la figure 2 est une reproduction photographique des granulés de bois formant une semoule obtenue selon l'étape de granulation humide de l'invention;

- la figure 3 montre des courbes de distribution granulométriques d'exemples de semoules de granulés de bois selon l'invention et d'un exemple comparatif d'une poudre du même bois selon l'état de l'art ;

- la figure 4 montre sous forme de courbes les lieux d'écoulement, c'est-à-dire qui traduisent l'évolution des contraintes de cisaillement en fonction des contraintes normales, d'un exemple de semoule de granulés de bois selon l'invention et d'exemples comparatifs de poudres du même bois selon l'état de l'art.

On précise que les termes « amont », « aval », « entrée », « sortie » utilisés en référence avec la figure 1 sont à considérer par rapport au sens de circulation de la biomasse ligno-cellulosique dans une installation de gazéification en continu selon l'invention.

On précise également que les termes d10, d50, d95, dX, désignent les diamètres des particules tels que respectivement 10%, 50%, 95%, X% en volume du matériau solide de biomasse soit de taille inférieure.

On précise également que la mesure de la densité aérée qui est le rapport entre la masse d'un échantillon et le volume initial de l'échantillon, pour les exemples de

poudres séchées selon l'état de l'art et les exemples de semoules de granulés selon l'invention est faite selon une même méthode et avec un même appareil.

Les densités aérées indiquées ci-après ont toutes été mesurées par le rhéomètre commercialisé sous la dénomination « FT4 » par la société Freeman Technology.

On précise également que la mesure de l'angle d'avalanche pour les exemples de poudres séchées selon l'état de l'art et les exemples de semoules de granulés selon l'invention est faite selon une même méthode et un même appareil.

L'angle d'avalanche permet d'évaluer la coulabilité des milieux granulaires.

Les inventeurs ont privilégié cette méthode de mesure, car ils pensent que la mesure de l'angle de rotation du tambour est la seule qui soit indépendante de l'action d'un opérateur. Ainsi, le tambour rotatif en tournant sur lui-même, met le milieu granulaire en mouvement. La coulabilité d'une poudre ou plus généralement d'un milieu granulaire sous contrainte normale nulle peut être déterminée par le biais de l'angle d'avalanche, qui est une mesure dynamique. A ce sujet, on pourra se reporter à la publication [5].

Les angles d'avalanche indiqués ci-après ont été tous mesurés à l'aide de l'analyseur de poudres, commercialisé sous la dénomination « Revolution » par la société Mercury Scientific Inc. Il consiste en un tambour contenant un volume précis de poudre mis en rotation devant une caméra.

L'opérateur peut déterminer la vitesse de rotation du tambour et le temps de préparation de l'échantillon, i.e. le temps pendant lequel le tambour tourne sans mesurer l'angle d'avalanche pour annuler l'effet de l'opérateur qui a versé la poudre. Des algorithmes déterminent l'angle d'avalanche de la poudre à partir des images recueillies par la caméra.

L'angle d'avalanche θ est l'angle que forme la surface libre de la poudre avec l'horizontale juste avant qu'elle ne s'écoule à cause de la rotation du tambour. Ainsi, dans la méthode de mesure mise en œuvre selon l'invention, l'angle d'avalanche θ peut être défini comme l'angle maximal, mesuré en degré, de rotation d'un tambour rotatif autour de son axe à l'horizontal, qu'atteint l'interface entre le milieu granulaire et le milieu ambiant juste avant l'avalanche dudit milieu granulaire.

On précise également que la détermination de granulométrie pour les exemples de poudres séchées selon l'état de l'art et les exemples de semoules de granulés selon l'invention est faite selon une même méthode et un même appareil par analyse vidéo.

Les inventeurs ont ainsi utilisé un appareil de vidéo-granulométrie commercialisé sous la dénomination « Camsizer » par la société Horiba. Cet appareil fournit grâce à l'analyse d'images numériques des informations rapides et précises sur la taille et la forme des particules pour des matériaux solides secs et qui s'écoulent dans une gamme de tailles entre 30 microns jusqu'à 30mm.

Plus précisément, cet appareil collecte de nombreuses images des particules de poudres ou semoules selon l'invention qui passent devant ses caméras, dispersées par un jet d'air. Les images en deux dimensions sont ramenées à des objets tridimensionnels en fournissant des hypothèses à un logiciel. Typiquement pour les poudres de bois, les hypothèses sont que les particules sont assimilées à des cylindres. Le logiciel fournit ensuite les distributions granulométriques des poudres ou semoules, en pourcentages en nombre de particules dont le diamètre est inférieur à une dimension donnée.

On précise enfin que les tests de cisaillement pour les exemples de poudres séchées selon l'état de l'art et les exemples de semoules de granulés selon l'invention est faite selon une même méthode et un même appareil.

Un test de cisaillement permet de tracer le lieu de rupture, (aussi appelé lieu d'écoulement) de la poudre, c'est-à-dire l'évolution de la contrainte de cisaillement en fonction de la contrainte normale appliquée au milieu granulaire.

Un test de cisaillement donne accès à plusieurs paramètres, comme le coefficient de friction statique de la poudre ou sa cohésion. Ce test est mené à l'aide d'une cellule de cisaillement, dont il existe plusieurs types.

Le mode opératoire d'un test cisaillement utilisé par les inventeurs applique la méthode de Jenike telle que décrite dans la publication [6].

Les valeurs de contraintes de cisaillement indiquées ci-après et reportées en figure 4 ont toutes été mesurées par le rhéomètre commercialisé sous la dénomination « FT4 » par la société Freeman Technology.

Dans cet appareil, la cellule de cisaillement qui a été utilisée est de type torsionnelle, avec comme instruments nécessaires aux différentes étapes du test fixés dans

l'appareil puis mis en mouvement automatiquement, une hélice, un piston et une tête de cisaillement structurée.

La figure 1 montre l'enchaînement des étapes du procédé de gazéification selon l'invention, appliqué à du bois en tant que biomasse ligno-cellulosique.

Etape a/: Des plaquettes de bois sont tout d'abord séchées.

Etape b/: A la sortie de l'unité de séchage, ces plaquette séchées subissent un broyage fin de sorte à obtenir une poudre sèche.

Etape c/: Au lieu d'essayer convoyer et d'injecter cette poudre sèche dans un gazéifieur, comme usuellement, les inventeurs ont pensé à introduire une étape de granulation humide qui permet d'obtenir des agrégats de particules, ou granulés, formant une semoule, par ajout d'un liant, et ainsi d'améliorer les propriétés d'écoulement de la poudre, par modification de la forme et augmentation de la taille des particules.

Etape d/: Les granulés humides formant la semoule de bois obtenue sont ensuite séchés en aval.

Etape d1/: Lorsque les granulés séchés ont une taille qui ne permet pas d'envisager de respecter les temps de séjour courts requis par une gazéification, alors on réalise un tamisage desdits granulés.

Ainsi, seuls les granulés, de dimension inférieure à une valeur seuil, seront injectés dans le réacteur de gazéification.

Etape e/: La semoule sèche de bois injectée dans le réacteur produit par gazéification un gaz de synthèse.

Les inventeurs ont procédé à plusieurs essais de granulation humide d'une poudre séchée de bois afin de valider l'obtention de granulés adaptés à une gazéification.

Les exemples de réalisation de semoules de bois selon l'invention sont indiqués ci-après.

Les caractéristiques de la poudre de bois séchée, à partir de laquelle ces exemples de semoule sont obtenus par granulation humide, sont indiquées dans le tableau 1 ci-dessous.

TABLEAU 1

Diamètres (microns)	d10	14,6
	d50	37,7
	d95	104,1
Etalement de la distribution granulométrique	(d90-d10)/d50	2
Autres caractéristiques	Densité aérée (kg/m^3)	206
	Angle d'avalanche θ (°)	72
	Cohésion à 3kPa (kPa)	0,99

Les caractéristiques de cette poudre de bois sèche en font une poudre qui s'écoule difficilement par rapport à des poudres non-cohésives comme la semoule de blé et le sucre en poudre, dont les cohésions à 3kPa sont d'environ 0,01 et 0,05 kPa respectivement, et leur angle d'avalanche autour de 40°.

Exemple 1 selon l'invention :

La poudre de bois sèche est mélangée à de l'amidon, dont la proportion massique est comprise entre 5 et 10% en masse de la poudre.

Le mélange est réalisé dans un bac, puis de l'eau est ajoutée par pulvérisation en petites quantités.

La poudre sèche ne se granule qu'une fois que de l'eau se trouve en surface et forme des ponts liquides entre les particules de poudre.

Ainsi, l'eau ajoutée permet de former des ponts liquides entre les particules. Ces ponts liquides contiennent de l'amidon qui en séchant va former des ponts solides entre les particules de biomasse et donc les lier ensemble.

Le mélange est homogénéisé à la main et le bac secoué de manière circulaire de sorte que la poudre roule sur elle-même. De petits agrégats, de dimensions inférieures au cm se forment.

Le mélange est ensuite mis sur des supports plats en aluminium selon une répartition en couches assez fine pour permettre un séchage efficace.

Puis les supports contenant le mélange sont placés dans une étuve à température ambiante pendant une durée d'environ 8h.

Un séchage efficace est réalisé préférentiellement pour n'évaporer que l'eau libre, c'est-à-dire une quantité d'environ 75% de l'eau ajoutée, qui forme les ponts liquides, et de ne pas évaporer l'eau lié, soit la quantité restante d'eau de l'ordre de 25%. Cette quantité restante d'eau liée, ne change pas les propriétés d'écoulement et requiert en pratique beaucoup d'énergie pour l'évaporer.

La semoule de granulés obtenue est ensuite tamisée avec une grille de maille de l'ordre de 900 microns. Les granulés de moins de 900 microns passent ainsi à travers la grille et constitue l'exemple 1 de semoule selon l'invention. On précise que les granulés au-dessus de 900 microns peuvent être broyés puis recyclés.

Exemple 2 selon l'invention :

Un gel d'amidon est préparé par ébullition d'une poudre d'amidon dans de l'eau.

La poudre de bois sèche est placée dans un bac puis est mélangé avec le gel d'amidon préparé. L'ajout du gel se fait par pulvérisation de petites quantités. La proportion massique finale du gel d'amidon est comprise entre 5 et 10% d'amidon par rapport à la masse de poudre de bois sèche.

Le mélange est homogénéisé à la main et le bac secoué de manière circulaire de sorte que la poudre roule sur elle-même. De petits agrégats, de dimensions inférieures au cm se forment.

Le mélange est ensuite mis sur des supports plats en aluminium selon une répartition en couches assez fine pour permettre un séchage efficace.

Puis les supports contenant le mélange sont placés dans une étuve à température ambiante pendant une durée d'environ 8h.

La semoule de granulés obtenue est ensuite tamisée avec une grille de maille de l'ordre de 900 microns. Les granulés de moins de 900 microns passent ainsi à travers la grille et constitue l'exemple 2 de semoule selon l'invention. On précise que les granulés au-dessus de 900 microns peuvent être broyés puis recyclés.

Exemple 3 selon l'invention:

Une semoule de bois a été fabriquée avec les mêmes conditions et mêmes étapes que celles de l'exemple 1 mais en remplaçant l'amidon par de la poudre issue de tourteau de tournesol séché et broyée, dans une proportion entre 5 et 10% en masse par rapport à la poudre de bois.

Les inventeurs ont procédé à plusieurs observations et analyse des semoules de granulés obtenus.

A l'œil nu, contenues dans un flacon, on constate tout d'abord que les semoules selon les exemples 1 à 3 de l'invention s'écoulent facilement dans le flacon, contrairement à la poudre de bois qui s'écoule par blocs, et il est nécessaire d'incliner fortement le flacon pour voir cette dernière s'écouler.

Des observations de semoules selon les exemples 1 et 3 de l'invention, ont ensuite réalisées à la loupe binoculaire.

La figure 2 montre sous un grossissement de x63, des granulés de l'exemple 1 selon l'invention avec 10% en masse d'amidon, étant précisé que l'échelle est indiquée par le trait en bas de la figure, dont la longueur vaut 100 microns.

Ainsi, il ressort de cette figure 2 que les agrégats ou granulés sont de forme proche de la sphère. Quelques particules pointent en dehors de l'agrégat. La forme générale et l'augmentation de la taille expliquent l'amélioration de l'écoulement par rapport à la poudre sèche de bois selon l'état de l'art.

On a également procédé à l'évaluation de la granulométrie des semoules selon les exemples 1 et 3 de l'invention.

Les différentes distributions granulométriques sont représentées sous forme de courbes en figure 3.

A la lecture de ces courbes, on constate que la granulométrie des semoules de granulés de bois selon l'invention est très différente de celle de la poudre sèche de bois selon l'état de l'art.

Ainsi, les semoules contiennent peu de particules fines et sont donc moins soumises aux forces cohésives et leurs diamètres d50, d90 et d10 sont autour respectivement de 500 microns, 800 microns et 300 microns.

L'étalement de la distribution granulométrique, qui correspond à la valeur (d90-d10)/d50 est environ égal à un pour les semoules selon l'invention, tandis qu'il est de l'ordre de deux pour la poudre sèche de bois selon l'état de l'art.

Or, d'après ce que l'on connaît par la bibliographie sur l'écoulement des milieux granulaires, une distribution plus resserrée améliore l'écoulement.

Autrement dit, la granulation humide des poudres de biomasse, en augmentant le diamètre des particules pour la transformer en semoules de granulés, peut permettre d'obtenir un meilleur écoulement.

Les inventeurs ont validé par d'autres essais, le meilleur écoulement obtenu par les semoules de bois selon l'invention.

Ils ont ainsi procédé à la comparaison des exemples suivants :

- Exemple 1 comparatif selon l'état de l'art : poudre sèche de bois;
- Exemple 2 comparatif selon l'état de l'art : poudre sèche de bois tamisée à 900 µm;
- Exemple 2 selon l'invention : semoule à partir de la même poudre sèche de bois que celle des exemples comparatifs 1 et 2.

Trois paramètres peuvent permettre de déterminer et comparer la coulabilité entre poudres selon l'état de l'art et semoules selon l'invention:

- la position relative des lieux d'écoulement,
- la cohésion,
- l'angle d'avalanche.

Pour caractériser l'aptitude d'un milieu granulaire à s'écouler, les inventeurs ont mis en œuvre un test de cisaillement.

Au préalable, pour déterminer la contrainte normale à laquelle effectuer le test de cisaillement on calcule la contrainte maximale que va subir chaque milieu (poudre séchée, poudre séchée et tamisée) dans un silo de stockage de forme cylindrique de 2m de diamètre, en appliquant la théorie dit théorie de Janssen.

En appliquant cette théorie, la contrainte normale maximale subie par la poudre dans le silo cylindrique est alors donnée pas l'équation suivante :

$$\sigma sat=(g*\rho*R)/(2*K*\mu)$$

avec :

σsat : contrainte normale maximale subie par la poudre (Pa)

g : accélération de la pesanteur (m/s^2)

R : rayon du silo (m)

K : rapport entre les contraintes normale et radiale (-)

µ : coefficient de friction statique (radians).

La valeur de K n'étant pas mesurable directement dans le silo, on la considère ici égale à 0,4 pour faire une estimation de la contrainte, les valeurs typiques de K étant comprises entre 0,3 et 0,6.

Les résultats des différents tests sont présentés dans le tableau 2 ci-dessous.

On précise que les inventeurs ont pensé que la semoule de bois selon l'exemple 2 de l'invention pouvait repartir en poudre lors du test de cisaillement. La contrainte maximale de cisaillement obtenue pour la semoule selon l'invention étant de 1,8 kPa, un test de cisaillement a été également effectué pour un autre exemple comparatif 1, qui a une contrainte à 1,8kPa.

TABLEAU 2

Paramètres	Contrainte maximale (kPa)	Densité aérée (kg/m^3)	Angle d'avalanche θ (°)	Cohésion (kPa)
Exemple comparatif 1 selon état de l'art (poudre à 2,5kPa)	2,5	0,206	72	0,084
Exemple 2 selon l'invention (semoule)	1,8	0,152	55	0,042
Exemple comparatif 2 selon état de l'art (poudre tamisée)	2,1	0,179	65	0,083
Autre exemple comparatif 1 selon état de l'art (poudre à 1,8kPa)	-	0,206	72	0,072

On a reporté sous la forme de courbes, pour chacun des exemples précités, l'évolution de la contrainte de cisaillement en fonction de la contrainte normale appliquée à l'échantillon.

Les courbes sont illustrées en figure 4.

Du tableau 2 et de la figure 4, on constate que :

- le lieu d'écoulement de la semoule selon l'invention est en dessous de celui l'autre exemple comparatif 1 de la poudre de bois, à 1,8kPa de contrainte maximale. Il en va de même avec la cohésion puisque la valeur de cohésion de la semoule vaut 0,042kPa contre 0,072 kPa pour l'autre exemple comparatif 1. On peut en conclure que la semoule de bois selon l'invention ne repart pas en poudre lors du test de cisaillement.

- le lieu d'écoulement de la semoule selon l'invention est en dessous de celui l'exemple comparatif 1 de la poudre de bois, à 2,5 kPa de contrainte maximale. Il en va de même avec la cohésion puisque la valeur de cohésion de la semoule vaut 0,042kPa contre 0,08 kPa pour l'exemple comparatif 1, ainsi que pour la valeur d'angle d'avalanche puisqu'égal à 55° contre 72°.

- le lieu d'écoulement de la semoule selon l'invention est en dessous de celui l'exemple comparatif 2 de la poudre de bois tamisée. Il en va de même avec la cohésion puisque la valeur de cohésion de la semoule vaut 0,042kPa contre 0,082 kPa pour l'exemple comparatif 2, ainsi que pour la valeur d'angle d'avalanche puisqu'égal à 55° contre 65°.

De ces essais, on peut en conclure qu'une semoule de bois obtenue selon l'invention s'écoule mieux que la même poudre sèche de bois dont elle est issue que cette dernière soit ou non tamisée.

De fait, la forme d'un granulé de la semoule selon l'invention, qui est plus proche de la sphère, lui permet de mieux s'écouler que les aiguilles de poudres sèches de bois. De même, la distribution granulométrique d'une semoule selon l'invention est plus resserrée et elle contient moins de fines que les poudres sèches de bois.

D'autres variantes et avantages de l'invention peuvent être réalisés sans pour autant sortir du cadre de l'invention.

L'invention n'est pas limitée aux exemples qui viennent d'être décrits; on peut notamment combiner entre elles des caractéristiques des exemples illustrés au sein de variantes non illustrées.

Références citées

[1]: «*Mise en œuvre des poudres – Techniques de granulation humide et liants*», Techniques de l'ingénieur réf J2254 v1.

[2]: «*Agglomeration technology: Equipment selection*» de B. J. Ennis, Chem. Eng., vol. 117, no. 5, pp. 50–54, 2010.

[3]: « *Granulation of lignocellulosic powders*», V. Yandapalli, University of Georgia, 2013.

[4] : « *Volatiles species release during torrefaction of wood and its macromolecular constituents : part 1- Experimental Study* », T. Nocquet et al., Energy 72, pp 180-187, 2014.

[5] : « *Avalanching flow of cohesive powders* », A. Alexander et al., Powder Technology 164, pp 13-21, 2006.

[6] : « *Powders and Bulk Solids , Behavior, Characterization, Storage and Flow* », Chapter 4 « *Practical determination of flow properties* », pp 75-99, D. Schulze, Springer, 2008.

REVENDICATIONS

1. Procédé de gazéification de biomasse, comprenant les étapes successives suivantes :

a/ séchage d'une biomasse ;

b/ broyage de la biomasse afin d'obtenir une poudre sèche,

c/ granulation humide de la poudre de biomasse pour obtenir des granulés de biomasse sous la forme d'une semoule ;

d/ séchage des granulés de semoule ;

e/ injection de la semoule sèche dans un réacteur de gazéification.

2. Procédé selon la revendication 1, l'étape e/ étant une injection dans un réacteur de gazéification à flux entraîné (RFE).

3. Procédé selon la revendication 1 ou 2, la biomasse étant de la biomasse ligno-cellulosique.

4. Procédé selon l'une des revendications 1 à 3, l'étape c/ de granulation humide étant réalisée par ajout à la poudre d'un liant choisi parmi l'amidon, la drêche de féculerie, des déchets agricoles comprenant des déchets de canne à sucre et/ou des pépins de raisin, et/ou des drèches de palmier à huile et/ou des déchets de sorgho et/ou des grignons d'olive et/ou des coques de graines de tournesol, des écorces d'agrumes, des micro-algues, des algues, du lactosérum ou un mélange de ceux-ci.

5. Procédé selon la revendication 4, la proportion massique de liant par rapport à celle de la poudre étant comprise entre 0 et 90%.

6. Procédé selon la revendication 4 ou 5, un liquide, de préférence de l'eau, est ajouté directement par pulvérisation dans le mélange entre liant et poudre.

7. Procédé selon la revendication 4 ou 5, le liant étant mélangé à un liquide, de préférence de l'eau, le mélange étant chauffé de sorte à obtenir un gel ajouté par pulvérisation dans la poudre.

8. Procédé selon l'une des revendications 4 à 7, le liant étant l'amidon, dont la proportion massique est comprise entre 5 et 10% de celle de la poudre.

9. Procédé selon l'une des revendications précédentes, comprenant en outre, après l'étape d/, une étape d1/ de tamisage de la semoule séchée.

10. Procédé selon l'une des revendications précédentes, les granulés secs obtenus, éventuellement après l'étape d1/ de tamisage, et avant l'étape d'injection e/, ayant un diamètre représentatif inférieur à 1 mm.

11. Installation de gazéification en continu de biomasse comprenant un réacteur de gazéification et en amont de celui-ci un dispositif de mise en œuvre de la granulation humide de poudre séchée de biomasse, destinée à mettre en œuvre l'étape c/ du procédé selon l'une quelconque des revendications précédentes.

12. Installation selon la revendication 11, le dispositif étant un granulateur à plateau tournant ou un granulateur-mélangeur à fort taux de cisaillement, le réacteur étant un réacteur de type à flux entraîné.

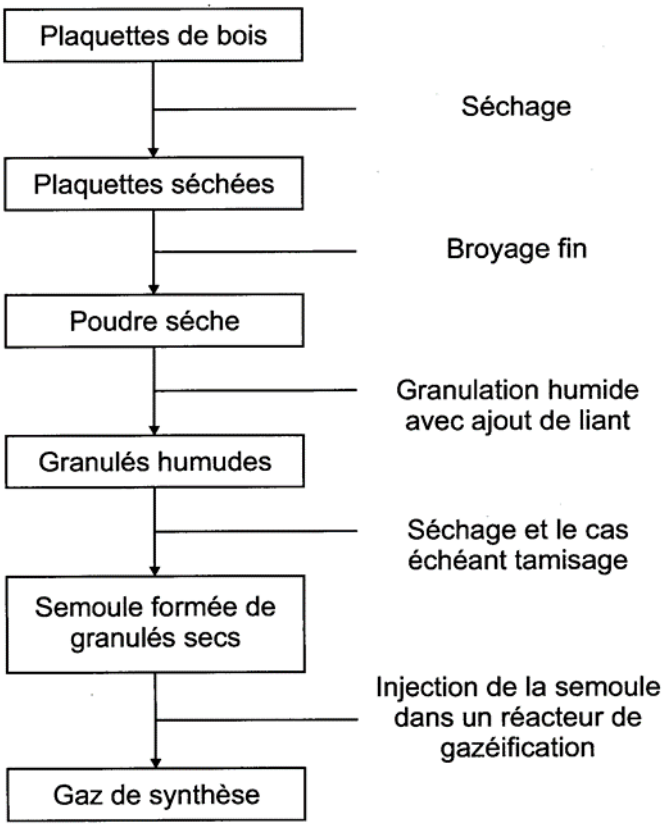
Plaquettes de bois
Séchage
Plaquettes séchées
Broyage fin
Poudre séche
Granulation humide avec ajout de liant
Granulés humudes
Séchage et le cas échéant tamisage
Semoule formée de granulés secs
Injection de la semoule dans un réacteur de gazéification
Gaz de synthèse

Fig. 1

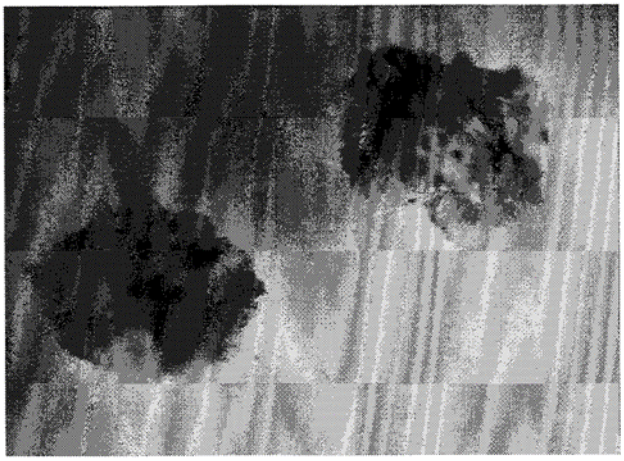

Fig. 2

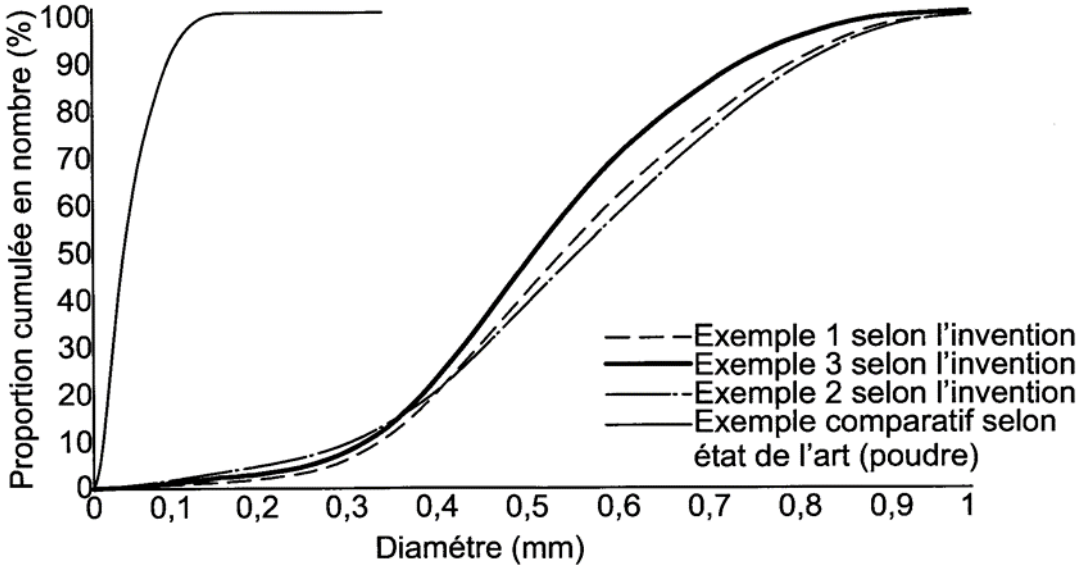
Proportion cumulée en nombre (%)
100
90
80
70
60
50
40
30
20
10
0
0
0,1
0,2
0,3
0,4
0,5
0,6
0,7
0,8
0,9
1
Diamétre (mm)
Exemple 1 selon l'invention
Exemple 3 selon l'invention
Exemple 2 selon l'invention
Exemple comparatif selon état de l'art (poudre)

Fig. 3

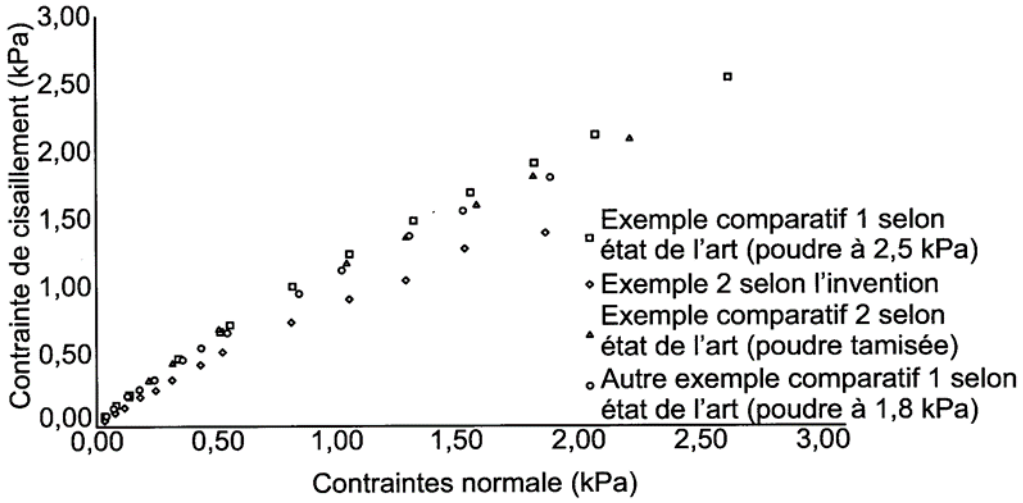
Contrainte de cisaillement (kPa)
3,00
2,50
2,00
1,50
1,00
0,50
0,00
0,00
0,50
1,00
1,50
2,00
2,50
3,00
Contraintes normale (kPa)
Exemple comparatif 1 selon état de l'art (poudre à 2,5 kPa)
Exemple 2 selon l'invention
Exemple comparatif 2 selon état de l'art (poudre tamisée)
Autre exemple comparatif 1 selon état de l'art (poudre à 1,8 kPa)

Fig. 4

RÉPUBLIQUE FRANÇAISE

3059008

INSTITUT NATIONAL DE LA PROPRIÉTÉ INDUSTRIELLE

RAPPORT DE RECHERCHE PRÉLIMINAIRE

établi sur la base des dernières revendications déposées avant le commencement de la recherche

N° d'enregistrement national

FA 830854
FR 1661477

DOCUMENTS CONSIDÉRÉS COMME PERTINENTS		Revendication(s) concernée(s)	Classement attribué à l'invention par l'INPI
Catégorie	Citation du document avec indication, en cas de besoin, des parties pertinentes		
X	DE 10 2013 019090 A1 (TECH UNIVERSITÄT BERGAKADEMIE FREIBERG [DE]) 21 mai 2015 (2015-05-21) * alinéa [0015]; revendications 1,3,4 * -----	1,3,11	C10L5/44 C10B53/02 C10J3/66
X	RU 2 602 150 C2 (FED GOSUDARSTVENNOE BJUDZHETNOE UCHREZHDENIE NATSIONALNYJ ISSLEDOVATEL) 10 novembre 2016 (2016-11-10) * le document en entier * -----	1,3,11	
X	WO 2013/114327 A1 (COMMISSARIAT ENERGIE ATOMIQUE [FR]) 8 août 2013 (2013-08-08) * le document en entier * -----	1-12	
A,D	Vikramaditya Yandapalli: "GRANULATION OF LIGNOCELLULOSIC POWDERS", , 1 janvier 2013 (2013-01-01), XP055339717, Athens, Georgia Extrait de l'Internet: URL:https://getd.libs.uga.edu/pdfs/yandapalli_vikramaditya_201305_ms.pdf [extrait le 2017-01-27] * abrégé * * pages 109-110 * -----	1-11	
			DOMAINES TECHNIQUES RECHERCHÉS (IPC)
			C10L

Date d'achèvement de la recherche	Examinateur
27 janvier 2017	Greß, Tobias

CATÉGORIE DES DOCUMENTS CITÉS

X : particulièrement pertinent à lui seul
Y : particulièrement pertinent en combinaison avec un autre document de la même catégorie
A : arrière-plan technologique
O : divulgation non-écrite
P : document intercalaire

T : théorie ou principe à la base de l'invention
E : document de brevet bénéficiant d'une date antérieure à la date de dépôt et qui n'a été publié qu'à cette date de dépôt ou qu'à une date postérieure.
D : cité dans la demande
L : cité pour d'autres raisons

& : membre de la même famille, document correspondant

3

EPO FORM 1503 12.99 (P04C14)

3059008

ANNEXE AU RAPPORT DE RECHERCHE PRÉLIMINAIRE RELATIF A LA DEMANDE DE BREVET FRANÇAIS NO. FR 1661477 FA 830854

La présente annexe indique les membres de la famille de brevets relatifs aux documents brevets cités dans le rapport de recherche préliminaire visé ci-dessus.
Les dits membres sont contenus au fichier informatique de l'Office européen des brevets à la date du 27-01-2017
Les renseignements fournis sont donnés à titre indicatif et n'engagent pas la responsabilité de l'Office européen des brevets, ni de l'Administration française

Document brevet cité au rapport de recherche	Date de publication	Membre(s) de la famille de brevet(s)	Date de publication
DE 102013019090 A1	21-05-2015	AUCUN	
RU 2602150 C2	10-11-2016	AUCUN	
WO 2013114327 A1	08-08-2013	EP 2809446 A1	10-12-2014
		FR 2986444 A1	09-08-2013
		WO 2013114327 A1	08-08-2013

EPO FORM P0465

Pour tout renseignement concernant cette annexe : voir Journal Officiel de l'Office européen des brevets, No.12/82

FRENCH SUMMARY

Depuis la révolution industrielle, le taux de CO_2 dans l'atmosphère a augmenté, ce qui a mené à une modification du climat. Une augmentation de 0,74°C de la température globale moyenne a été observée depuis l'époque préindustrielle. Les conséquences sont déjà observables : acidification des océans, blanchiment des récifs coralliens et extinction de masse des amphibiens par exemple. Les conséquences du dérèglement climatiques selon le Groupe d'Experts Intergouvernemental sur l'Evolution du Climat (GIEC) sont alarmantes. Si les 2°C d'augmentation de la température sont dépassés, le changement climatique pourrait mener, entre autres, aux conséquences suivantes :

- Disparition de l'habitat naturel de 8% des animaux vertébrés, 18% des insectes et 16% des plantes.
- Fonte totale de la banquise en été une fois par décennie.
- Montée de 10 cm du niveau des océans.

Cette situation est causée par les activités humaines, et l'utilisation de combustibles fossiles en particulier.

Des solutions doivent être trouvées pour diminuer l'utilisation de ces combustibles fossiles, tandis que la demande en énergie risque de doubler d'ici 2050. La sobriété énergétique est un premier aspect à prendre en compte pour atteindre cet objectif. Elle consiste en une diminution de l'énergie consommée par une utilisation appropriée des équipements consommateurs d'énergie (par exemple en réduisant le chauffage domestique ou en utilisant des voitures de plus petite taille). La sobriété énergétique doit aller de pair avec un autre aspect à prendre en compte pour diminuer l'utilisation des énergies fossiles : l'efficacité énergétique, qui permet de diminuer les pertes énergétiques. Enfin, les énergies renouvelables peuvent être envisagées pour atteindre la demande énergétique.

La biomasse est une alternative prometteuse pour remplacer une partie des combustibles fossiles, car elle est abondante, bien distribuée dans le monde, et neutre du point de vue des émissions de gaz à effet de serre (dans un contexte de production gérée de manière durable), et renouvelables dans des échelles de temps courtes. De plus, de nombreuses applications sont disponibles. La biomasse peut être directement brûlée pour produire de la chaleur ou de l'électricité. Elle peut aussi être transformée en biocarburants par traitement

biochimiques ou biologiques. Enfin, elle peut être transformée en chaleur, électricité et biocarburants par voie thermochimique.

La gazéification en réacteur à flux entraîné (RFE) est une des technologies de gazéification les plus prometteuses. Les conditions typiques du procédé sont une température haute (1300-1500°C), une haute pression (20-70 bars) et un temps de séjour de la biomasse dans le réacteur court (quelques secondes). Ses principaux avantages sont de hauts taux de conversion de la biomasse en gaz de synthèse, avec un contenu en goudrons et en hydrocarbures gazeuses faible, et une importante production (plusieurs tonnes de biomasse traitées par heure). Cependant, le développement de la gazéification en RFE fait face à des verrous technologiques. L'un d'entre eux est l'utilisation nécessaire de poudres de biomasse, due aux faibles temps de séjour (la taille des particules doit être petite pour avoir le temps de réagir lors de son temps de séjour dans le réacteur). Les poudres de biomasse ont une faible coulabilité, et les injecter dans un réacteur sous pression est problématique.

Les poudres sont omniprésentes dans les différents domaines de l'industrie : alimentaire, pharmaceutique, ciment, sable, charbon et de nombreux autres. Environ 60% des produits industriels sont des milieux granulaires ou présentent une étape de manipulation de poudres durant leur production. Cependant, en dépit de la forte proportion de poudres dans l'industrie, leur comportement est largement incompris, et des problèmes lors de leur manipulation sont rencontrés par 94% des usines qui les utilisent. Les poudres de biomasse en particulier sont cohésives à cause de plusieurs de leurs caractéristiques : faible densité vrac, polydispersité de la taille des particules, et particules allongées par exemple. Les problèmes de coulabilité sont fréquents (formation d'arches dans les silos par exemple) et peuvent mener à des arrêts de production.

La gazéification en RFE présente de nombreuses étapes de manipulation des poudres (stockage, convoyage, injection…), et les poudres de biomasses sont susceptibles de bloquer à chacune d'elles. L'objectif de cette thèse est de mieux comprendre l'écoulement des poudres de biomasse, et de proposer des solutions pour en améliorer la manipulation dans le contexte de la gazéification en RFE. La caractérisation de la coulabilité des poudres de biomasse est un sujet de recherche récent, et encore peu compris. Ainsi, ce travail inclut

l'étude des poudres de biomasse à la fois à l'échelle du laboratoire et à l'échelle pilote. De plus, plusieurs méthodes de préparation existent pour l'injection de biomasse en RFE (torréfaction, pyrolyse…). Dans ce travail, une méthode innovante de granulation, adaptée au RFE, est proposée.

Le premier chapitre de cette thèse est une étude bibliographique, divisée en trois parties. La première est une description de la biomasse et de sa structure. La seconde s'étend sur le comportement des poudres et leur caractérisation. Enfin, la troisième partie traite de la manipulation des poudres à l'échelle industrielle.

Le second chapitre est dédié à la description du matériel et des méthodes utilisés dans l'étude à l'échelle du laboratoire. Les méthodes de caractérisation incluent des tests en rhéomètre à poudre FT4 et en tambour rotatif Revolution (Mercury Scientifics), des mesures de densité, d'humidité, ainsi que de tailles et de formes de particules.

Dans le troisième chapitre, les résultats expérimentaux à l'échelle du laboratoire sont présentés et discutés. Ce troisième chapitre est organisé en cinq études principales. Premièrement, des études préliminaires ont été menées avec le FT4 pour s'assurer que les particules ne s'orientent pas pendant les tests de cisaillement. En effet, les tests de cisaillement présentant plus de points que de tests classiques, et les particules étant allongées, il semble possible que les particules s'orientent au cours du test. Ensuite, l'effet du nombre d'avalanches dans le tambour rotatif sur des paramètres de coulabilité a été étudié. L'étude suivante s'intéresse à l'influence de l'humidité de la poudre sur les paramètres d'écoulement. Enfin, la dernière étude porte sur une nouvelle méthode de granulation adaptée à la gazéification en RFE.

Les principales conclusions des expériences à l'échelle laboratoire sont les suivantes :

Un test de cisaillement modifié a été étudié : des points mesurés en début de test sont répétés en fin de test sans changer l'échantillon. Les points répétés sont proches des points mesurés

la première fois. Ainsi, s'il y a effectivement un phénomène d'orientation des particules, il n'affecte pas les résultats du test de cisaillement.

Dans le tambour rotatif Revolution, le nombre d'avalanches mesuré n'a qu'une faible influence sur l'angle d'avalanche, et une influence négligeable sur les autres paramètres d'écoulement. 150 avalanches sont suffisantes pour obtenir des paramètres d'écoulement fiables.

Une nouvelle méthode de description des lieux d'écoulement non-linéaires est proposée, basée sur l'équation de Warren-Spring. Elle ne requiert pas la mesure de la traction. Le modèle décrit les points expérimentaux avec précision.

En se basant sur les données expérimentales obtenues avec trente-trois poudres (principalement du bois) à trois préconsolidations (2, 3 et 5 kPa), les paramètres de l'équation de Warren-Spring ont pu être exprimés en fonctions de paramètres simples à mesurer : l'angle d'avalanche et la densité aérée. La cohésion, qui est un paramètre-clef de la coulabilité des poudres, peut être évaluée avec cette méthode. Pour les poudres de biomasses présentant un angle d'avalanche supérieur à 50°, le lieu d'écoulement peut être modélisé. Ce modèle est particulièrement adapté pour déterminer le comportement mécanique des poudres dans le domaine des faibles contraintes. Ce travail permis de mettre en place une méthode d'estimation de la cohésion et de description du lieu d'écoulement de poudres de biomasse cohésives à partir de paramètres simples à mesurer.

L'ajout d'eau dans les poudres de biomasse a une faible influence sur leur densité, à cause d'un phénomène de gonflement qui contrebalance l'accroissement de la masse. La coulabilité des poudres de bois commence à changer quand l'humidité atteint 15% (en base humide), ce qui correspond à la transition vitreuse. Cet effet est plus évident sur des paramètres comme le temps entre deux avalanches, et l'écart-type de la distribution de temps entre deux avalanches. Il y a un effet de l'intensité du broyage sur la coulabilité avec l'augmentation de l'humidité des feuillus (chêne, hêtre). En effet, les feuillus présentent de petits pores qui disparaissent pour un broyage fin. Avec une poudre fine, les ponts liquides (dont l'augmentation du nombre augmente la cohésion) peuvent se former directement sur la surface des particules, alors que pour un broyage grossier, l'eau doit remplir les pores

avant de pouvoir former les ponts liquides entre les particules. Ainsi, la coulabilité des poudres fines commence à décroître pour des humidités moindres que celle des poudres grossières.

La méthode de granulation innovante décrite dans ce troisième chapitre permet de former des granules dont le diamètre est inférieur au millimètre à partir d'une poudre de biomasse brute (dont les particules sont allongées et la distribution de tailles de particules est large) en y ajoutant un liant produit à partir de déchets de biomasse. Les principaux résultats sont :

- Les granulés sont moins allongés que les particules de la poudre brute initiale. Des particules moins allongées sont moins susceptibles de s'entremêler.

- La taille des particules est augmentée. Le contenu en fines (qui a une forte influence sur la coulabilité) est inférieur dans la poudre granulée (presque nul) et la taille moyenne est augmentée.

- L'étalement de la distribution de tailles de particules est très faible pour la poudre granulée, comparé à celui de la poudre brute. Les poudres dont la distribution de tailles est étroite ont une meilleure coulabilité, qui est due à un nombre moins important de points de contact entre les particules.

- L'effet de la granulation sur la coulabilité a été évalué avec des mesures d'avalanches. L'angle d'avalanche, la distribution d'angles d'avalanche, le temps entre deux avalanches et l'écart-type de la distribution de temps entre deux avalanches montrent une forte amélioration de la coulabilité, comparée avec la poudre brute.

- La comparaison de ces résultats avec ceux d'une poudre de bois brute dont la taille est proche de celle de la poudre granulée a montré que les effets de la granulation sur la coulabilité ne sont pas uniquement dus à l'accroissement de la taille des particules, mais aussi à la réduction de la distribution de tailles, la diminution du contenu en fines et la diminution de l'élongation des particules.

Le quatrième chapitre décrit le matériel et les méthodes utilisés dans l'étude à l'échelle pilote. Le pilote d'injection IRIS est présenté, ainsi que les installations expérimentales des tests effectués. De plus, les méthodes de préparation des différentes poudres sont présentées, et la méthode de granulation en particulier.

Le cinquième et dernier chapitre présente les résultats obtenus à l'échelle pilote. Celui-ci est organisé en quatre études principales. En premier lieu, une étude de la trémie d'alimentation et de la vis d'alimentation du pilote d'injection IRIS a été menée. Ensuite, l'accumulation de poudre dans les injecteurs lors de l'alimentation a été étudiée. La poudre granulée selon la méthode précédemment citée a été injectée dans le réacteur de gazéification à flux entraîné Giroflé. Enfin, une étude énergétique du procédé de granulation a été mise en place. Les principales conclusions de ces études à l'échelle pilote sont les suivantes :

- Etude de la trémie d'alimentation et de la vis d'alimentation du pilote IRIS :

La vitesse de la vis varie linéairement avec la vitesse du moteur, ce dernier étant le paramètre qui varie lors des expériences sur le pilote.

Il a été montré que le débit massique est répétable pour la poudre de microbilles à différentes vitesses de la vis. Une répétabilité semblable est supposée pour les poudres de biomasse.

La variation de la contrainte verticale sur la vis avec la hauteur de remplissage de la trémie a été calculée avec le logiciel SiloStressTool, pour la poudre de référence et la poudre de microbilles. La hauteur de remplissage de la trémie a une influence sur la longueur de cohésion et la densité de la poudre de microbilles, et une influence faible pour la poudre de référence. Ces faibles variations n'ont pas d'influence sur le débit massique. Cependant, l'influence de la hauteur de remplissage sur le couple moteur est un sujet qu'il serait intéressant d'étudier.

Le débit volumique théorique a été calculé grâce à la géométrie de la vis. Le débit volumique réel des différentes poudres est inférieur au débit volumique théorique. En effet, l'efficacité volumique décroît avec plusieurs phénomènes (remplissage incomplet des

espaces entre les filets de vis, vitesses axiale différente de la vitesse idéale et espacement entre la calandre et la vis, menant au glissement des particules). La diminution de l'efficacité de l'efficacité volumique est attribuée au glissement entre les particules et la vis pour la poudre de microbilles (dont l'angle de friction avec l'acier est faible) et au remplissage incomplet de la vis par la poudre pour les poudres de biomasse (ces poudres sont compressibles).

- Accumulation dans l'injecteur :

R est un paramètre utilisé pour évaluer le diamètre de l'orifice minimum permettant à une poudre de s'écouler à travers celui-ci. R est le rapport du diamètre à travers lequel la poudre peut s'écouler et de la taille des particules. Les microbilles et la poudre granule ont des particules sphériques, presque monodispersées. Elles présentent des valeurs R au-dessus de la valeur critique (valeur au-dessus de laquelle le blocage est impossible pour des poudres sphériques et monodispersées). Pour celles-ci, l'accumulation de poudre dans l'injecteur n'est pas due à un blocage mais à un débit d'alimentation trop important. Si de la poudre s'accumule pour ces poudres, diminuer le débit d'alimentation (le débit de sortie de la vis) permet de résoudre le problème.

Les poudres de biomasse présentent des particules allongées et de tailles polydispersées. Pour des particules allongées, la valeur de R au-dessus de laquelle le blocage est impossible augmente comparée aux particules sphériques. Une forte polydispersité de taille de particules est supposée augmenter la valeur critique de R comparée à une poudre monodispersée, à cause d'une augmentation du nombre de points de contact entre particules. Cependant, le calcul de cette valeur critique de R est difficile à cause du choix d'un diamètre de particules adapté à une poudre polydispersée. La détermination de l'effet de la polydispersité de la taille des particules est une perspective intéressante. Expérimentalement, le blocage a lieu dans l'injecteur avec toutes les poudres de biomasse. Ainsi, l'élongation et la polydispersité ont un effet significatif sur le phénomène de blocage. Pour ces poudres, si de l'accumulation à lieu dans l'injecteur, le procédé doit être mis à l'arrêt le temps de nettoyer l'injecteur.

Dans la littérature, il est supposé que la nature de la poudre n'a pas d'influence sur le blocage. Ceci est vérifié pour les poudres de bois résineux et la poudre grossière torréfiée. Elles ont une distribution de tailles de particule et des formes de particules comparables, et elles présentent le même comportement dans l'injecteur. L'effet de la torréfaction sur la coulabilité n'est pas observable. Cependant, la poudre torréfiée fine et la poudre de référence (poudre brute fine) ont, elles aussi, des tailles et formes de particules comparables, mais leur comportement dans l'injecteur est très différent. La poudre torréfiée peut passer à travers des orifices plus petits que la poudre de référence. De plus, pour des diamètres d'injecteur plus importants, la poudre torréfiée ne forme pas d'arche, contrairement à la poudre de référence. Ainsi, pour cette taille de particules, il y a un effet observable de la nature de la poudre sur la coulabilité. La torréfaction a un effet positif pour de petites tailles de particules. Ceci pourrait être dû à l'effet de la torréfaction sur la qualité des surfaces, qui a un effet moins important pour des tailles de particules plus importantes (avec la poudre grossière par exemple).

Le paramètre R a été adapté aux particules polydispersées avec le d_{10}, et relié à un paramètre à l'échelle laboratoire : l'écart-type de la distribution de temps entre deux avalanches (ou temps d'avalanche). Cette relation doit être utilisée avec précautions : le faible nombre de points a peut-être conduit à un faux-positif. Cependant, si cette relation est correcte, l'écart-type du temps d'avalanche est lié au R_{10}. Cette relation donne des informations sur l'écoulement dans le tambour rotatif : le contenu en fines, la taille et la forme des particules ont un rôle important dans la régularité de l'écoulement.

- Injection dans le gazéifieur Giroflé :

Les bilans dans le gazéifieur à l'échelle pilote n'ont pas pu être correctement réalisés. Ainsi, il n'est pas possible de conclure sur une meilleure conversion de la poudre granulée en gaz de synthèse par rapport à une poudre brute par exemple. La seule observation possible est que la poudre granulée n'a pas bloqué dans l'injecteur, tandis que la poudre de hêtre qui a été utilisée comme poudre brute pour comparer les résultats a formé une arche dans l'injecteur.

- Evaluation énergétique du procédé de granulation :

Quatre configurations du procédé ont été étudiées : avec une chaleur gratuite ou avec des étapes de combustion des plaquettes de bois pour les étapes de séchage et avec deux tailles de particules, 100 et 500 µm. Les résultats ont été comparés avec le procédé de granulation, une autre méthode de préparation de la biomasse pour la gazéification.

Le broyage à 100 µm mène à une consommation énergétique excessive lors de l'étape de broyage. Cette option doit donc être rejetée.

Broyer à 500 µm mène à des consommations énergétiques moindres, comparable à celle du procédé de torréfaction. Des recherches plus poussées doivent être menées pour évaluer l'impact de granules dont les bords sont saillants sur leur coulabilité.

Avec de la chaleur gratuite pour les étapes de séchage, le procédé de granulation consomme 4% du pouvoir calorifique inférieur (PCI), et aucune matière n'est perdue (contrairement au procédé de torréfaction). Avec des étapes de combustion des plaquettes pour les étapes de séchage, 20% de la masse est perdue.

La quantité d'eau ajoutée pour la granulation n'a pas été optimisée. Utiliser moins d'eau pour la granulation mènerait à un une chaleur requise moindre pour les étapes de séchage, et donc une consommation énergétique moindre. La granulation est une alternative intéressante à la torréfaction d'un point de vue énergétique. Une étude économique est la prochaine étape avant le passage à une échelle supérieure de ce procédé.

Les principales perspectives de ce travail sont les suivantes :

La corrélation entre les paramètres dérivés du test de cisaillement et l'angle d'avalanche a été déterminée à l'aide du FT4. La validité de cette corrélation pourrait être étudiée avec une autre cellule de cisaillement (celles de Jenike et Schulze par exemple). De plus, la densité aérée a été choisie à cause des faibles consolidations auxquelles les poudres de biomasse sont confrontées dans le procédé de gazéification en RFE. Cependant, d'autres densités pourrait-être essayées (densité tapée par exemple).

L’effet de l’humidité a été testé sur six poudres de bois. L’effet de ce paramètre pourrait être évalué pour d’autres essences de bois et d’autres biomasses (résidus agricoles par exemple).

Il a été montré que, d’un point de vue énergétique, le procédé de granulation était intéressant pour des tailles de particules importantes (500 µm). Cependant, les granules formées avec de grosses particules initiales présentent des bords saillants. Ainsi, la coulabilité des granules aux bords saillants doit être évaluée à l’échelle du laboratoire et à l’échelle pilote. D’autres biomasses et liants pourraient être envisagés aussi. De plus, l’intérêt économique du procédé doit être étudié. Enfin, la poudre granulée pourrait être injectée dans la RFE Giroflé dans des conditions adaptées pour que les bilans soient mis en place. Son comportement en gazéification pourrait ainsi être observé.

Le paramètre R pourrait être étendu aux tailles de particules polydispersées, ce qui donnerait des pistes intéressantes quant à la coulabilité des poudres de biomasse à travers des orifices. De plus, un effet de la nature de la poudre (torréfiée et brute) a été mis en évidence pour de petites tailles de particules. Cela pourrait être un effet de la perméabilité du gaz, de la friction entre les particules ou de la cohésion. De recherches plus approfondies doivent être menées sur ce sujet et ces paramètres pourraient être pris en compte dans un paramètre R étendu.

Dans ce travail, le diamètre de Feret minimal a été pris en compte en ce qui concerne la taille des particules. Cependant, le diaamètre de Feret maximal pourrait être intéressant à utiliser, pour les études de blocage lors des écoulements à travers un orifice en particulier.

RESUME

Etude de poudres de biomasse dans le cadre de la valorisation thermique de biomasse

Certains procédés de production d'énergie nécessitent l'utilisation de poudres de biomasse, par exemple la gazéification en réacteur à flux entraîné (RFE). Cependant, les poudres de biomasse ont une mauvaise coulabilité. L'objectif de cette thèse est d'étudier leurs propriétés d'écoulement dans le contexte de la gazéification en RFE, à l'échelle du laboratoire et à l'échelle pilote.
A l'échelle du laboratoire, des mesures en tambour rotatif, des tests de cisaillement et des mesures de densité ont été effectués. D'une part, une corrélation est mise en évidence entre la cohésion (issue des tests de cisaillement), la densité et l'angle d'avalanche (tiré des mesures en tambour). Ainsi, un paramètre difficile à obtenir comme la cohésion peut l'être à partir de mesures simples. D'autre part, l'influence de l'humidité sur la coulabilité des poudres de biomasse a été évaluée. L'humidité n'a pas d'effet significatif sous 15 % (en masse, base humide), car l'eau est adsorbée dans la structure de la biomasse ; les particules gonflent et ne sont pas liées par des ponts liquides.
Un procédé de granulation humide est proposé. Un liant issu de déchets de biomasse est ajouté à la poudre pour former des granulés d'environ 1 mm. Leur forme sphérique diminue l'entrelacement des particules et leur faible polydispersité diminue le nombre de points de contact. Une amélioration de l'écoulement est observée à l'échelle labo. Une étude énergétique montre que la consommation énergétique du procédé peut descendre jusqu'à 12% du pouvoir calorifique inférieur, ce qui suggère une potentielle rentabilité économique du procédé.
Enfin, la caractérisation à l'échelle supérieure est effectuée dans un pilote reproduisant l'injection en RFE. Les résultats montrent le rôle essentiel de la sphéricité et d'une faible polydispersité des particules. L'effet positif de la torréfaction et de la granulation sur la coulabilité est mis en évidence.

Mots-clefs : Poudres, Biomasse, Coulabilité, Granulation, Humidité

ABSTRACT

Study of biomass powders in the context of thermal recovery processes

Some power generation processes require the biomass to be finely ground, such as biomass gasification in entrained flow reactors. However, fine biomass powders are cohesive and present flow issues. This thesis aims to study the biomass powder flowability in the context of the entrained flow gasification process. Biomass powders are characterized both at laboratory scale and pilot scale.
Characterization at lab scale consisted of rotating drum measurements, shear tests and density measurements. First, a correlation is found between the cohesion (derived from shear tests), the powder density and the avalanche angle (derived from the rotating drum measurements). Thus, parameters difficult to get such as the cohesion can be obtained with easy to perform measurements. Then, the influence of moisture content on wood powder flowability has been assessed. No significant effect of the water content is found below 15 wt% (wet basis). Below 15%, as water is adsorbed in the biomass structure, the particles swell without being linked by liquid bridges.
A wet granulation method is proposed. Biomass waste binders are added to the powder to form granules around 1 mm. The spherical shape lowers the interlocking phenomenon. The low size dispersity of the grains decreases the number of contact points between particles. An improvement of the flowability at lab scale is observed. An energetic study of the granulation process is proposed, showing the energy consumption can be as low as 12% of the biomass Lowest Heating Value. Thus, the process is potentially economically profitable.
Finally, characterization at pilot scale is performed with a device mimicking the injection in an entrained flow reactor. The results show the essential roles in the injection step of both the spherical shape and the narrow size distribution of the particles. The positive effect of torrefaction and granulation on the flowability is highlighted.

Keywords: Powders, Biomass, Flowability, Granulation, Moisture content